Characterizing the Final Steps of Chromosomal Replication at the Single-molecule Level in the Model System *Escherichia coli*

For the Degree of

Doctor of Philosophy

King Abdullah University of Science and Technology, Thuwal,

Kingdom of Saudi Arabia

EXAMINATION COMMITTEE APPROVALS FORM

The dissertation of *Mohamed Elshenawy* is approved by the examination committee

Committee Chairperson: Samir Hamdan

Associate Professor, Bioscience
Biological and Environmental Science and Engineering
KAUST, Thuwal 23955, KSA

Committee Member: Pierre Magistretti

Distinguished Professor, Bioscience
Dean, Biological and Environmental Science and Engineering
KAUST, Thuwal 23955, KSA

Committee Member: Satoshi Habuchi

Associate Professor, Bioscience
Biological and Environmental Science and Engineering
KAUST, Thuwal 23955, KSA

Committee Member: Boon Ooi

Professor, Electrical Engineering
Electrical and Mathematical Science and Engineering
KAUST, Thuwal 23955, KSA

Committee Member: Nick Dixon

Director, Centre for Medical and Molecular Bioscience
Distinguished Professor, Biological Chemistry
University of Wollongong, NSW 2522, Australia

ABSTRACT

Characterizing the Final Steps of Chromosomal Replication at the Single-molecule Level in the Model System *Escherichia coli*

Mohamed Elshenawy

In the circular *Escherichia coli* chromosome, two replisomes are assembled at the unique origin of replication and drive DNA synthesis in opposite directions until they meet in the terminus region across from the origin. Despite the difference in rates of the two replisomes, their arrival at the terminus is synchronized through a highly specialized system consisting of the terminator protein (Tus) bound to the termination sites (*Ter*). This synchronicity is mediated by the polarity of the Tus−*Ter* complex that stops replisomes from one direction (non-permissive face) but not the other (permissive face). Two oppositely oriented clusters of five Tus–*Ters* that each block one of the two replisomes create a "replication fork trap" for the first arriving replisome while waiting for the late arriving one. Despite extensive biochemical and structural studies, the molecular mechanism behind Tus−*Ter* polar arrest activity remained controversial. Moreover, none of the previous work provided answers for the long-standing discrepancy between the ability of Tus−*Ter* to permanently stop replisomes *in vitro* and its low efficiency *in vivo*.

Here, I spearheaded a collaborative project that combined single-molecule DNA replication assays, X-ray crystallography and binding studies to provide a true molecular-level understanding of the underlying mechanism of Tus−*Ter* polar arrest activity. We showed that efficiency of Tus−*Ter* is determined by a head-to-head kinetic competition between rate of strand separation by the replisome and rate of rearrangement of Tus−*Ter* interactions during the melting of the first 6 base pairs of *Ter*. This rearrangement maintains Tus's strong grip on the DNA and stops the advancing replisome from breaking into Tus−*Ter* central interactions, but only transiently. We further showed how this kinetic competition functions within the context of two mechanisms to impose permanent fork stoppage. The rate-dependent fork arrest activity of Tus−*Ter* explains its low efficiency *in vivo* and why contradictory *in vitro* results from previous studies have led to controversial elucidations of the mechanism. It also provides the first example where the intrinsic heterogeneity in rate of individual replisomes could have different biological outcomes in its communication with double-stranded DNA-binding protein barriers.

ACKNOWLEDGEMENTS

I would like to thank my supervisor prof. Samir Hamdan for his continuous support, guidance and supervision. His infinite enthusiasm and excitement about research has always inspired me. His inspiration and encouragement made all the difference. Working for him has been a great opportunity for me to grow and develop as a student. I hope I can grow up and be like him one day. I am definitely honored to have worked with Prof. Nick Dixon. It was a great pleasure for me to work in collaboration with him. I am indebted to him for countless and invaluable contributions through up the way up along completion my dissertation. A special thanks to Dr. Slobodan Jergic for his generous support and exceptional efforts. This work would have never seen the light of day without him. I would like also to thank Prof. Aaron Okaley and Dr. Zhi-Qiang-Zu for their valuable assistance and contribution throughout the course of this research. Above all, I would like to sincerely thank KAUST for the generous scholarship that granted me an opportunity to fulfil my dream of developing as a researcher.

I would like to extend my gratitude to all members of DNA replication and Recombination lab for providing a perfect environment, scientifically challenging and pleasant, which contributed importantly to the successful completion of my PhD. In particular, I am grateful to Dr. Mohamed Sobhy and Dr. Masateru Takahashi; it would not be possible to conduct this research without their precious support. Last but not least, I would like to give big cheers to the students in the lab (Manal, Luay, and Fahad); working with them has always been charming and enjoyable and I will absolutely be missing our days.

TABLE OF CONTENTS Page

LIST OF ABBREVIATIONS

E.coli	*Escherichia coli*
ssDNA	Single-stranded DNA
dsDNA	Double-stranded DNA
dNTPs	Deoxnucleotide triphosphates
kbp	Kilo base pair
Mbp	Mega base pair
SSB	Single-strnaded DNA binding protein
Oric	Origin of replication
Pol III HE	DNA polymerase III holoenzyme
CBM	Clamp binding motif
B. subtilis	*Bacillus subtilis*
Tus	Terminus utilization substance
Da	Dalton
RTP	Replication termination protein
Ter	Termination site
NP	Non-permissive
P	Permissive
UV	Ultraviolet
GFP	Green fluorescent protein
SPR	Suface plasmon resonance

SEM	Standard error of mean
SV40	Simian virus 40
ELISA	Enzyme-linked immunosorbent assay
FRET	Förster Resonance Energy Transfer
RNAP	RNA polymerase
SF1	Super Family 1
PNK	T4 polynucleotide kinase
GP5	Gene 5 protein
GP4	Gene 4 protein
trx	Thioredoxin
PAGE	Polyacrylamide Gel Electrophoresis
CCD	Charge Coupling Device
PEG	Poly Ethylene Glycol
PBS	Phosphate-buffered saline
BSA	Bovine Serum Albumin
pN	picoNewton
MSD	Mean Square Displacement
TIRF	Total Internal Reflection Fluorescent
EMCCD	Electron Multiplying Charge Coupled Device
nt	Nucleotide

LIST OF ILLUSTRATIONS Page

LIST OF TABLES Page

Chapter 1

1. General Introduction

1.1 DNA Replication Machinery

DNA is the essence of life that stores the information controlling and directing all cellular activities. The cells therefore acquired elaborate mechanisms to replicate and repair its genetic materials to ensure the accurate passing of traits from one generation to another. The replisome, the multiprotein DNA replication machinery, copies the genomic DNA in an highly efficient and accurate manner by providing a scaffold that coordinates the activities of many cross-interacting proteins and binding partners[1,2]. The replisome functions according to highly conserved activities across all organisms (Figure 1.1)[1-4]. A helicase translocates along single-stranded DNA (ssDNA) on the lagging strand converting the chemical energy of nucleotides hydrolysi into mechanical energy to separate the parental double-stranded DNA (dsDNA)[5-7]. The two exposed ssDNA serve as templates for high fidelity replicative DNA polymerases that utilize deoxynucleotide triphosphates (dNTPs) as building blocks to synthesize the complementary strand[3,8,9]. The unidirectional movement of the DNA polymerization activity (5'−3') and bidirectional polarity of the parental DNA strands permits the leading strand to be copied continuously but compels the lagging strand to be copied discontinuously[10,11]. On the lagging strand, a primosome repeatedly synthesizes RNA primers for their extension by the DNA polymerase into short Okazaki fragments (1-2 kilo base pair (kbp) in prokaryotic systems). A specialized mechanism replaces the RNA primers with DNA and the two consecutive Okazaki

fragments are subsequently sealed by the action of a DNA ligase to generate the contiguous lagging strand[12,13].

The structure and function of the individual replisomal proteins and the interactions that orchestrate their activities have been subject of intensive studies over the past fifty years. This led to many discoveries and sophisticated models on how the system works[4,8,14-16], which was primarily driven by the ability of reconstituting replication systems from purified proteins *in vitro*. I will allocate the next section to present an overview of the structure and function of the *E. coli* replisome (Figure 1.1), one of the early and well-studied systems, and the one that is the primary focus of this study.

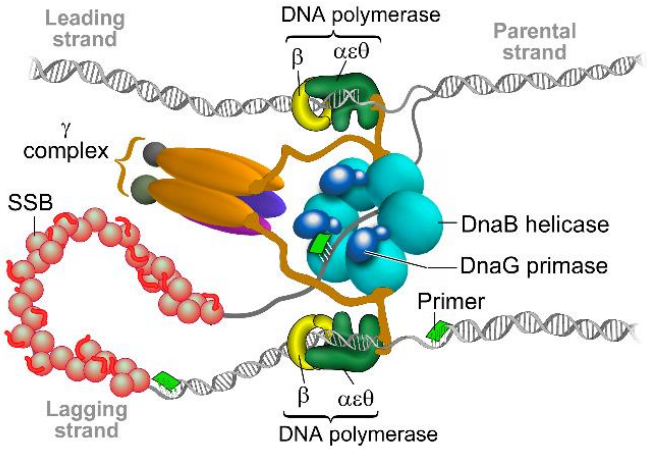

Figure 1.1: A schematic representation of *E. coli* replisome

A fully functional replisome comprises: DnaB helicase, DnaG primase, single-stranded DNA-binding protein (SSB), β_2 sliding clamp, a γ clamp loader complex, and two αƐΘ polymerase cores. DnaB, the front replisome runner, encircles the lagging strand as a hexamer and uses the energy of ATP hydrolysis to translocate on it and displace the complementary leading strand. The two exposed ssDNA strands act as templates for two identical polymerase cores. The β_2 clamp encircles the primer-template strands and tethers the polymerase core to it, enormously improving the processivity of DNA synthesis. The unidirectional nature of DNA polymerization activity (5'−3') and the bidirectional polarity of the parental DNA strands supports a continuous mode of DNA synthesis on the leading strand but forces the lagging strand to frequently initiate DNA synthesis to form short Okazaki fragments. DnaG initiates synthesis of short RNA primers (8-12 nucleotides) along the lagging strand through its direct interaction with the translocating DnaB. Polarity of lagging strand synthesis is aligned with leading strand synthesis by reversing the orientation of the lagging strand through the formation of a DNA replication loop structure that grows and shrinks during each cycle of Okazaki fragment synthesis. Figure is adapted from[47].

1.2 Structure and Function of the *E. coli* Replisome

The *E. coli* replisome copies DNA at an impressive average speed of a 1000 base pairs/s (bp s^{-1}), and with an extremely high accuracy of one mistake for every 10^9 incorporated nucleotides[17,18]. Replication of the 4.6-mega bp (Mbp) circular *E. coli* chromosome initiates at a specific site termed origin of replication (*oriC*). Two replisomes are assembled, fired simultaneously, and move bidirectionally away from *oriC* to meet after nearly 40 minutes in the terminus region across from the origin (Figure 1.2)[19-21]. The innermost part of the terminus region contains the *dif* site where segregation of the two sister chromosomes takes place (Figure 1.2)[21,22]. The cell developed a specialized system that is activated at the end of the "S-phase" of the cell cycle to synchronize the meeting of the two forks in the terminus to coordinate termination of DNA replication with the subsequent steps involved in chromosomal segregation[20,23,24].

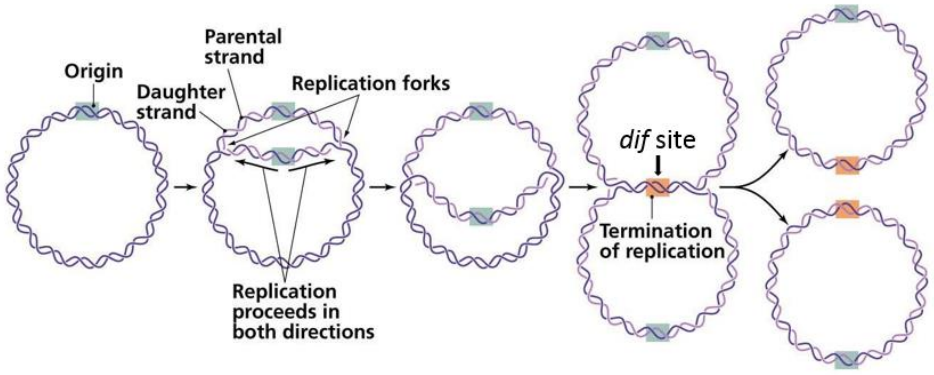

Figure 1.2: Initiation and termination of DNA replication in *E. coli*

Bidirectional replication of the circular bacterial chromosome. Replication starts from a unique origin of replication, *oriC*. Two replication forks fire synchronously to drive DNA synthesis in opposite direction, until they meet at the terminus region located opposite to *oriC*. The resulting two fully replicated chromosomes are then segregated at a specific site near the center of the terminus region termed the *dif* site, prior to cell division.

1.2.1 DnaA Replication Initiation Protein

Initiation of DNA replication is mediated by the binding of the initiation protein DnaA, to five copies of a 9-bp DnaA box sequence (TTATNCACA) in *oriC*[25-27]. DnaA is a member of the AAA+ ATPase superfamily that uses the energy of ATP hydrolysis to locally melt a 13-bp A/T-rich region located at the left border of *oriC*[26,28]. The opening of this region is followed by the recruitment of a preformed complex of the helicase loader DnaC and the replicative helicase DnaB through direct interaction of DnaC with its cognate binding domains on DnaA[29,30], as discussed in the coming section.

1.2.2 DnaBC Helicase and Helicase Loader Complex

DnaB is a ring-shaped hexameric complex that encircles the lagging strand and uses the energy of ATP hydrolysis to translocate on it in the 5'−3' direction and consequently unwind the parental dsDNA[31,32]. Loading of DnaB at the closed ssDNA at *oriC* is topologically forbidden and requires therefore the opening of the hexameric ring by DnaC. DnaC is a monomeric protein in solution and is a member of the AAA+ ATPase superfamily[33-35]. It acts as a DnaB ring breaker by utilizing its N-terminal domain to interact at the interfaces of DnaB in an ATP-binding dependent manner[36,37]. The oligomerization of DnaC *via* the AAA+ domains stimulates the opening and stabilization of DnaB into an open lockwasher conformation[37,38]. This ATP-bound form of DnaC aids the loading of DnaB onto ssDNA and interacts with the N-terminal domain of DnaA at *oriC*[33,39]. ATP hydrolysis and/or binding of accessory proteins stimulates the closure of the DnaB helicase ring and the subsequent binding of the Dna G primase[39-42]. It is not conclusive yet if DnaC dissociates after ATP hydrolysis or remain bound at the fork.

1.2.3 DanG Primase

DnaG primase is a DNA-dependent RNA polymerase that synthesizes short 8-12 nucleotide RNA primers in a sequence dependent manner (5'-CTG-3')[43,44]. DnaG synthesizes primer to initiate the DNA polymerization activity by the replicative DNA polymerase III holoenzyme (Pol III HE) on both leading and lagging-strands at *oriC* and then on the lagging strand during each cycle of Okazaki fragment synthesis[10,45]. The RNA primers provide the 3'-OH group that acts as a nucleophile on the α-phosphate of the incoming dNTPs[9,12,44]. Similar to other primases, the rate of primer synthesis by DnaG is too slow to support robust DNA synthesis[44,46]. The association of DnaG with DnaB increases its activity by nearly 1000-fold presumably by enhancing its inherent low affinity to ssDNA and allowing it to search for its recognition sites on the lagging-ssDNA template that is extruded behind the moving helicase[43,45,47]. The interaction of DnaG with DnaB is also shown to modulate the processivity of leading-strand synthesis, providing a mechanism that could prevent leading-strand synthesis from outpacing lagging strand synthesis during the slow primer synthesis step[47].

1.2.4 Pol III Holoenzyme

PoI lII holoenzyme (Pol III HE) is a large assembly of several subunits that is composed of three subassemblies: a β_2 sliding clamp, a Y clamp loader complex and a polymerase core[48-50]. The latter is a heterotrimer of three subunits: α polymerase, Ɛ exonuclease for proofreading, and Θ for stabilizing ε[9,48-50]. In contradiction to the earlier findings that Pol III HE contains two cores[8,50], recent studies demonstrate the presence of a third core; one acts on the leading strand and two on the lagging strand[51,52]. The second core on the

lagging strand is thought to complete Okazaki fragment synthesis in the case the first Pol III core is released prematurely before reaching the 5' end of the previously synthesized Okazaki fragment[53]. This molecular architecture of three polymerases per active replisome considerably improves the processivity of DNA synthesis[51].

β_2 is a homodimer ring-shaped protein that encircles the primer-template strands and topologically tethers Pol III core to the DNA through direct protein-protein interaction[54,55]. Pol III core has weak affinity to DNA and consequently falls off the primer-template strands after the incorporation of a few nucleotides[12,48]. The association with β_2 enhances its affinity to DNA and improves its processivity to hundreds of nucleotides per single DNA binding event[55-57]. The interactions among β_2 and the core are mediated by a strong interaction between the conserved internal clamp binding motif (CBM) on α and the C-terminal multi-binder motif on β_2[58,59] and a weak interaction between the equivalent site on the second monomer of β_2 and a CBM site on ε[55]. The latter interaction increases the rate and processivity of DNA synthesis by the *E. coli* replicase in the polymerization mode[55].

The five core subunits of the Y clamp loader complex are also all members of the AAA+ ATPase superfamily. The clamp loader opens and loads β_2 at the 3'-terminus of the primed-template strand[60,61]. It is composed of six different subunits: δ, δ', Y, τ, χ, ψ[61-63]. The Y subunit is a C-terminally truncated form of τ that results from a programmed frame-shift mutation during the translation of the τ-encoding dnaX gene[61]. The two forms exist in the cell in 1:1 ratio and are interchangeable components of the clamp loader[62]. The τ

subunit is the form that interacts with the Pol III core and also couples the core with DnaB *via* direct τ/DnaB interaction; both interactions involve the C-terminal domains of τ[64,65]. δ interacts with β_2 and opens it in a process that involves ATP binding to the clamp loader and is modulated by δ'[60,61]. This ternary complex can now interact with the primer-template strand[60,66]. ATP hydrolysis stimulates the dissociation of the clamp loader complex to result in the reclosing of β_2 for its utilization by the core[60,61,66]. The χ and ψ subunits are not essential for clamp loading but enhance its stability through direct physical interactions[67,68]. ψ denotes the only link between Pol III HE and the ssDNA binding protein (SSB) and it is indispensable for primer handoff from the primase to the polymerase subunits, as it is shown to compete with DnaG for SSB binding[69,70].

1.2.5 Single-stranded DNA-Binding Protein (SSB)

SSB binds tightly to ssDNA and in a sequence independent manner[71,72]. Binding of SSB stabilizes and protects ssDNA from cellular stress factors and other cellular DNA damage inducing agents[71-73]. Additionally, SSB prevents or resolves the formation of secondary structures such as hairpins in DNA that are inhibitory for the DNA polymerization activity of Pol III HE[72,74]. SSB binds to ssDNA through its N-terminal domain as a tetramer with the ssDNA making contacts with each monomer and looping around the tetramer in a topology that resembles the seams on a baseball[74,75]. The flexible C-terminal domain of SSB is involved in binding to other DNA-processing enzymes such as Pol III HE[74-76]. There are three distinct binding modes of the SSB tetramer on ssDNA that occlude 35, 56 or 65 nucleotides and are consequently termed SSB35, SSB56 and SSB65 modes, respectively[77-79]. These modes are believed to all exist in the cell and control the activity of many DNA-

processing enzymes through either direct protein-protein interactions or modulating their accessibility to ssDNA[80-83]. The interconversion between these modes is reversible and depends on the type and concentration of salt as well as binding protein partners[80,84].

1.3 Termination of DNA Replication

The bidirectional movement of the replication forks from a single origin in bacteria or multiple origins in archaea and eukaryotes would results in the convergence of two oppositely moving forks and the termination of their DNA synthesis activity[85,86]. In bacteria and in some examples in eukaryotes, termination occurs in a site-specific manner, while in archaea and the majority of the cases in eukaryotes it occurs in zonal regions or randomly between origins (reviewed in [19,85,86]). I will be focusing on termination of DNA replication in bacteria, in particular the model systems *E. coli* and *Bacillus subtilis (B. subtilis)*, as expanding it to the archaeal and eukaryotic systems is beyond the scope of this current research.

When *Jacob et al.*, proposed that initiation of DNA replication in bacteria would involve binding of a *trans*-acting factor to a *cis*-acting element in 1964, they did not anticipate that this theory would be also applicable to other processes such as termination of DNA replication. The initial interest in studying termination of DNA replication started after the discovery of the concept of bidirectional DNA synthesis from an origin. It was clear therefore that in a circular chromosome, the two progressing replication forks would meet in a head-to-head fashion away from the origin. Initial mapping studies of the *E. coli* chromosome supported this proposition by identifying the terminus region to be opposite

to *oriC* and close to the *trp* operon[87,88]. Early models suggested that termination in this region occurs by a simplistic collision mechanism between the two forks, while others proposed a process mediated by sequence-specific sites. The first evidence of sequence-specific termination was shown in the R6K plasmid, which contains at least two replication origins (α and β)[89], with recent studies suggesting the presence of a third replication origin (γ)[90,91]. Examination by electron microscopy showed asymmetric and asynchronous firing of replication forks from the origin with the first fork traveling and stopping at the terminus and the second one moving from the same origin to meet the halted fork[89].

Shortly, the same concept of discrete sequence-specific termination sites was reported in *E. coli* by experiments that followed the termination site under condition where the location of the origin in the *E. coli* chromosome was changed by controlling it through an R-plasmid origin-dependent replication[92]. This was possible by preventing the endogenous *E. coli* initiation mechanism by altering the *dnaA* gene that encodes for the DnaA initiation protein[93]. Interestingly, although the two-replication forks initiated from different *oriC* locations, termination always occurred at the same region opposite to *oriC*, demonstrating that discrete sequence-specific sites direct termination in *E. coli*[92].

The next question was whether the same site-specific termination mechanism operates in both R6K and *E. coli* systems, particularly since their modes of termination with respect to the synchronicity of their initiation process at the origin are rather different[89,92,94,95]. Moreover, the terminus site in R6K-plamsid was assigned to a 200 bp segment of DNA[96], while its location in *E. coli* hinted at a much larger region[92]. Sequencing of the surrounding

region of the replication terminus in the R6K-plasmid was achieved in 1980[96] and surprisingly did not show any regions with 2-fold symmetry (Figure 1.3). This finding argued against a prevailing hypothesis at that time that secondary DNA structures in this region could impose a barrier to stop the replication forks. This provoked a new hypothesis that termination is induced by a *trans*-acting protein element bound to discrete sequence-specific termination sites. Deletion studies at the terminus region, initially aimed to narrow the search for the exact location of the terminus, defined a specific site in the terminus that was able to deactivate replication termination elsewhere[97]. This provided clear evidence for the presence of a terminator protein in the *E. coli* system that is encoded by a gene placed at this site. The presumed gene was named the termination utilizing substance (Tus)[98]. The gene was cloned and a 35,783-Dalton (Da) protein was isolated and shown to bind to the R6K-plasmid terminus (Figure 1.3)[99]. It became clear therefore that the termination sites are not inherent replication stoppage sites but necessitate the binding of a terminator protein.

The study of replication termination in *E. coli* went in parallel with the mechanistically related system in *B. subtilis*. Despite the apparent similarities between the termination modes in the two systems, the structure of the replication termination protein (RTP) in *B. subtilis* is completely distinct from Tus (reviewed in [20,24,86]). In contrast to Tus that binds as a monomer to its termination that displays no inverted sequence symmetry[100,101], RTP binds the termination site as a dimer and cooperatively assembles a second dimer in a symmetric manner[102,103]. I will next introduce the fundamental concept of “polar arrest

activity" that mediates replication termination in *B. subtilis* and *E. coli* before introducing the fine molecular details of the two systems.

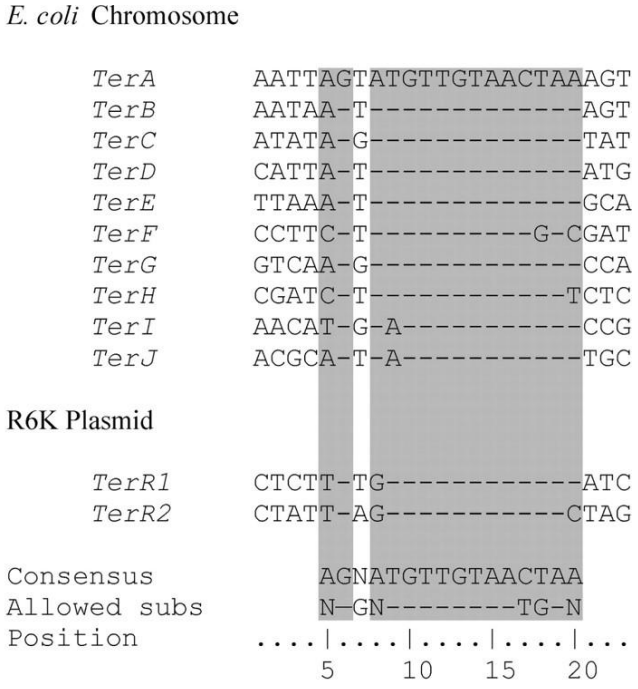

Figure 1.3: Termination sites (*Ter* sites) in the *E. coli* chromosome and R6K plasmid

Nucleotide sequences of *Ter* sites in the *E. coli* chromosome and R6K plasmid. Dashes correspond to conserved nucleotides. Tus protein interacts with the base pairs (bps) indicated in the shaded region. Figure is adapted from[23].

1.4 Replication Fork Trap

The fork trap consists of a series of discrete termination sites that each is able to stop replication forks approaching from only one direction. This "polar fork arrest" activity creates a trap for the first arriving fork by arranging the termination sites into two clusters flanking the halfway mark of the circular chromosome in a manner where each cluster blocks approaching forks from only one direction[20,23,24,86]. The first evidence of the replication fork trap was shown in *E. coli* using a marker frequency assay, which monitors

DNA synthesis by measuring the number of DNA copies at different locations in the *E. coli* chromosome under conditions where replication initiation is controlled by a phage or a plasmid origin[104,105]. These studies showed that despite the different spatial locations of the origins, DNA synthesis by the clockwise traveling replication fork repeatedly terminates in a broad region encompassing one side of the terminus region, while the counter-clockwise traveling fork stops in an equally dispersed region but at the opposite side[104,105]. A more sophisticated marker frequency analysis showed the termination regions of the first arriving fork in both cases to be widely spaced[106,107]. A specific site was subsequently identified in each region leading to the identification of the *TerA* site at the right half cluster terminating the counter-clockwise moving fork and *TerB*/*TerC* sites at the left half cluster terminating the clockwise moving fork[106,107] (Figure 1.4A). Each termination site therefore acts in a polar manner whereby *TerA* in the right cluster allows the passage of clockwise traveling forks while stoping the counter-clockwise traveling fork and the opposite is true for *TerB* and *TerC* in the left cluster.

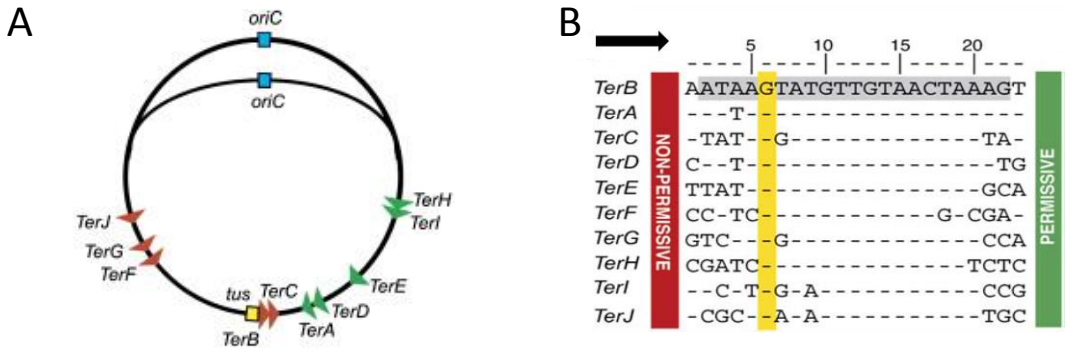

Figure 1.4: Terminus region in *E. coli* and sequences of *Ter* sites

A. *E. coli* circular chromosome showing a total of ten *Ter* sites. *Ter* sites are arranged into two clusters; each cluster acts as a replication trap by allowing the first arriving fork to enter but not to leave the termination site, waiting for the later arrival of the other fork. The region encoding Tus protein is indicated by a yellow square. The tus gene is autoregulated by the binding of Tus to *Ter* sites within the promotor region. Figure is adapted from[130].
B. Sequence alignment of the 10 *Ter* site showing a conserved cytosine residue (C6) at the sixth position (highlighted in yellow), followed by a 13-bp core region that is responsible for the main sequence-specific contacts with Tus. Dashed lines correspond to strictly conserved nucleotides. Replication forks are arrested only at the non-permissive face (NP) of *Ter* sites, indicated by a black arrow, while allowed to pass at the permissive face (P). Figure is adapted from[130].

1.4.1 Physiological Significance of the Fork Trap

Cells lacking the termination system, Δtus in *E. coli* or Δrtp in *B. subtilis*, are indistinguishable from wild-type cells and even do not show any defect in growth rate, morphology, sporulation, or sensitivity to utraviolet (UV) radiation and other DNA damaging agents[108,109]. However, detectable phenotypic changes are observed when deactivation of the fork trap system was combined with other mutations, supporting an important physiological role for the fork trap[110,111]. It is proposed that the main duty of the fork trap is to prevent passage of replication forks over the terminus region in the terminus-to-origin direction. Transcription is also arranged to be mostly in the direction of DNA replication from origin-to-terminus. The fork trap would therefore provide a mechanism that minimizes the deleterious head-to-head collision between the replication and transcription machineries[112]. It is also believed that it would prevent over-

replication and play a role in synchronizing termination of DNA replication with the subsequent steps involved in chromosomal segregation[20,112]. In *E. coli* plasmids, the fork trap is believed to prevent the 3' end of the replicating strand from displacing the 5' end, and consequently promoting rolling circle mode of DNA replication[113]. Inactivation of the fork trap in some plasmids therefore can lead to plasmid instability and generation of multiple plasmid copies per cell[20,113].

1.5 Replication Termination in *B. subtilis*

The study of termination in *B. subtilis* and *E. coli* systems went in parallel since the 1980s. Similar to *E. coli*, the circular *B. subtilis* chromosome contains 10 termination (*Ter*) sites located at the antipode of *oriC*, but in a significantly more confined region relative to *E. coli* and are arranged to create a replication fork trap by means of blocking the first arriving fork. *Ter1* is the strongest blocking site that is utilized with the highest frequency *in vivo* and is located at the innermost of the ten sites (Figure 1.5A)[114,115]. Unlike *E. coli* sites, the sequence of *B. subtilis Ter* site was described as symmetric surrounding two overlapping sequences (Figure 1.5A)[114,116,117]. This raises an interesting paradox as to how it induces termination in a polar manner. The answer became possible from studying the assembly of RTP on *Ter* sites, which identified two overlapping sequences, a core (strong RTP binder) and an auxiliary (weak RTP binder) (Figure 1.5B)[103,116,117].

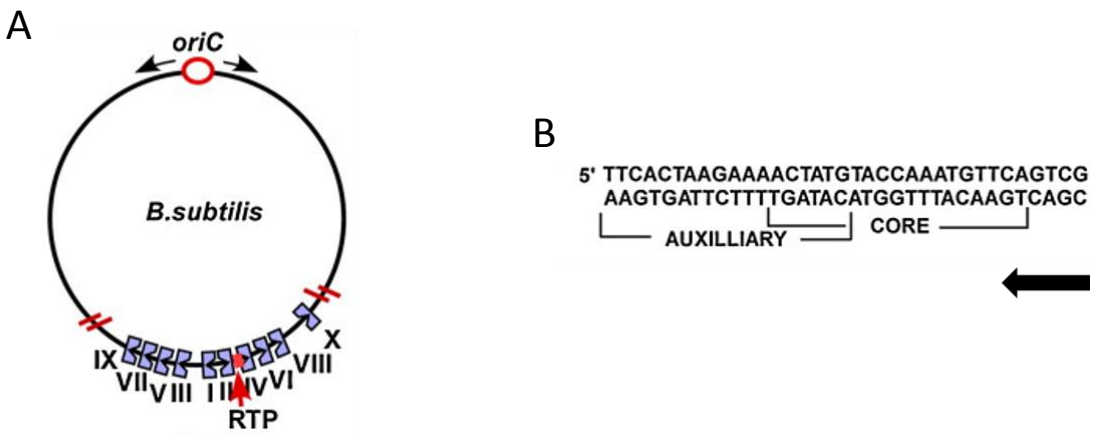

Figure 1.5: Terminus region in *B. subtilis* chromosome and the location of termination sequences

A. The relative locations of *Ter* sites in *B. subtilis* are shown including the region encoding the terminator protein, RTP. The rtp gene is autoregulated by the binding of RTP to *Ter* sites within the promotor region. In *B. subtilis*, the *Ter sites* are clustered in a more confined region towards the center of the terminus region. Note that *TerI* and *TerII* are spatially separated by only ~ 0.1 kb. DNA replication always terminates at *TerI* because of the asymmetric location of *TerI* and therefore the clockwise moving fork has to travel a shorter distance to reach the *TerI* site than the counterclockwise fork to reach *TerII* site. Figure adapted from[86].
B. The sequence of *TerI* showing the overlapping core and auxiliary sequences. The black arrow shows the end that arrests replication forks. Figure adapted from[86].

RTP binds *Ter* sites as a dimer of dimers in a cooperative manner with the first dimer binding to the core sequence followed by the binding of the second dimer to the auxiliary sequence (Figure 1.6A)[116,117], promoting the hypothesis that this binding would solve the asymmetry puzzle. This was further supported by the observation that RTP is not able to bind to the auxiliary sequence in the absence of the core sequence while it binds the core independent of the auxiliary sequence[118,119]. Binding of RTP to DNA causes a slight DNA

bending that is believed to contribute to a better fit between RTP and its binding site (Figure 1.6A)[116,117]. The contribution of this bending for RTP function however is still unknown[120]. The crystal structure of RTP was solved in 1995, and presented a bipartite structure that belongs to the winged-helix family of proteins (Figure 1.6A)[121]. The crystal structure confirmed the biochemical experiments that suggested the asymmetric binding of two dimers of RTP apoprotein to generate an asymmetry upon binding to the core and auxiliary DNA sequences, providing an explanation to its fork polar arrest mechanism. RTP consists of four α helices, three β strands and a flexible N-terminal arm[121]. α3 forms a large antiparallel-coiled coil with its symmetry mate in the homodimer and thus serves as a key element for dimerization (Figure 1.6A)[121]. The main contacts with DNA occur *via* α4 helix and β2 strand, where α4 heavily contacts the major grove of the DNA double helix (Figure 1.6B)[116,117].

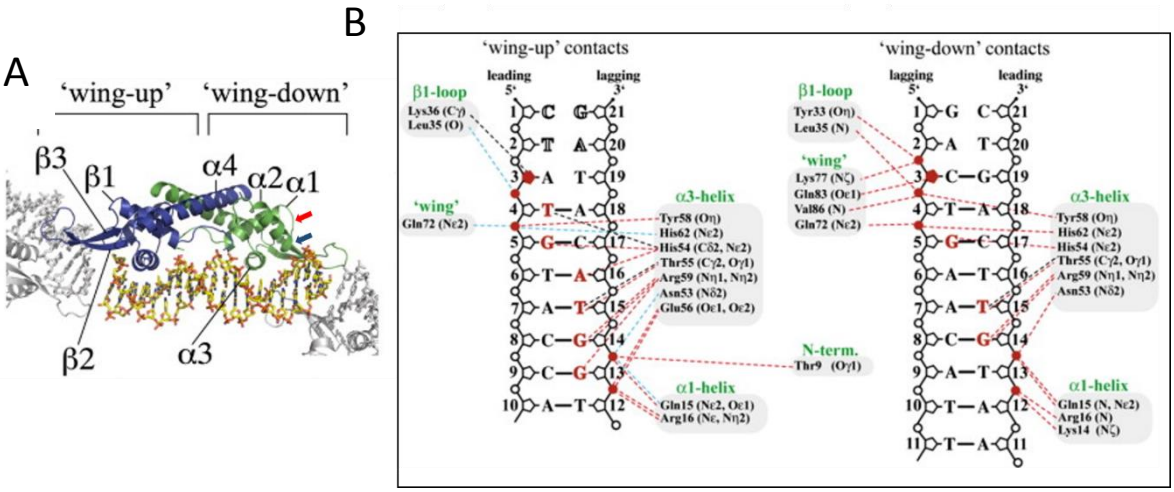

Figure 1.6: Crystal structure of RTP complex with *TerI* sites and protein–DNA contacts

A. Structure of the RTP complex with *TerI* sequence oligonucleotide. Ribbon drawing of RTP-*TerI* complex, showing its winged helix structure (PDB code: 1F4K)[116]. The orientations of the wing-up and wing-down monomers are shown in blue and green colors, respectively. The main sequence-specific interactions with DNA occur *via* α4 helix and β2 strand, where α4 heavily contacts the major groove of the DNA double helix at the wing-down monomer. E30 and Y33 residues that contribute to RTP/helicase interaction are denoted by red and blue arrows, respectively. Figure is adapted from[116].
B. Summary of DNA contacts with the wing-up and wing-down halves of RTP dimer structure. Phosphate groups, sugar moieties and bases are denoted by circles, pentagons and single letter abbreviations, respectively. Dashed black, red and blue lines represent non-bonded contacts, hydrogen bonds, and water-mediated interactions, respectively. Figure is adapted from[116].

Random and site-directed mutagenesis followed by biochemical analysis of the altered proteins for their fork arrest and anti-helicase activities provided valuable insights on the functional regions of RTP. Regions contacting the DNA are important for fork arrest activity, but DNA binding alone was insufficient to account for the fork arrest activity, since correlation was not always observed between defects in DNA binding and arrest activity[122]. Moreover, the crystal structure of RTP shows an unprotected hydrophobic patch at the blocking face that is proposed to be a site for a potential physical interaction with the replicative DnaC helicase[121]. Two specific residues, E30 and Y33 in this region were shown to be defective in fork arrest and counter-helicase activities *in vitro* without altering RTP's DNA binding, dimerization or dimer-dimer interaction properties (Figure 1.6A)[123]. *In vitro* binding studies show that the E30 mutation reduces protein-protein interaction with the heterologous *E. coli* DnaB helicase[123]. The *B. subtilis* RTP-*Ter*

termination system is active in stopping *E. coli* replication forks when it is introduced into the *E. coli* chromosome but with a 3-fold lower activity compared to the cognate *B. subtilis* system[124]. Nonetheless, the RTP–*Ter* system was identified to be unable to arrest other non-replicative helicases such as Rep and UvrD, indicating that RTP has some helicase-blocking specificity[118,125]. A significant role for a physical interaction with the replicative helicase is therefore suggested as an important player in RTP-mediated fork arrest activity *in vivo*. The second line of evidence for this putative interaction was revealed from experiments that fused peptides to the blocking face of RTP in order to block protein-protein interactions with the advancing replisome without altering RTP binding to DNA[126]. Indeed, these peptide-fusion RTPs severely compromise its fork arrest activity *in vivo*[126].

A composite mechanism of DNA binding and RTP-replisome interaction was proposed to induce replication polar arrest in *B. subtilis*[20]. The replication fork traveling towards the auxiliary site would dislodge the dimer binding to that weak site by decreasing the cooperativity of the RTP dimer/dimer interaction, leading to a successful passage through the terminus. In contrast, forks approaching the core site are unable to displace the protein, where the hydrophobic patch of RTP faces the advancing replisome and interacts with the replisomal-helicase and hence induces fork stoppage[20].

1.6 Replication Termination in *E. coli*

1.6.1 Overview of the System

DNA replication in *E. coli* initiates at *oriC* and proceeds bidirectionally until the two forks meet after ~ 40 minutes in the terminus region located nearly opposite the origin (Figure 1.4A)[100,101,127]. In this region, 10 DNA binding sites are located, termed the termination sites (*Ter*) that are arranged into two clusters of five in order to create a trap for the first arriving fork by blocking the progression of the replication forks moving in one direction but not the other[23,86,128]. Since the *Ter* sites have no inverted symmetry of sequence [100,101,129,130](Figure 1.4B), the mechanism that determines the polarity of replication termination became a central question of research (reviewed in [23,24,86,128]).

The components of the replication-termination system involve a *cis*-acting element *Ter* bound to its *trans*-acting factor Tus. The tus gene was isolated in 1989[98]and soon after, the purified protein was shown to bind to *Ter* sites[99]. The gene encodes a 308-amino acid monomeric protein of 35,783 Da that binds extremely tightly to the *Ter* sites[99,131]. The Tus−*Ter* complex has an equilibrium dissociation constant (K_D) of 3.4×10^{-13} M and a dissociation half-life of 550 min at 150 mM potassium glutamate[101,132], making Tus the strongest monomeric sequence-specific binding protein ever to have been identified. This tight binding of Tus−*Ter* complex has been utilized recently in many biotechnology and diagnostic applications[133,134].

The Tus−*Ter* complex impedes the DNA unwinding activity of DnaB helicase, the first replisomal component that is believed to encounter Tus−*Ter*, in an orientation dependent

manner[118,135,136]. A DnaB helicase approaching Tus−*Ter* from the permissive face (P) displaces Tus and continues DNA synthesis, while it is blocked when it encounters the non-permissive face (NP).

Sequence alignment of the ten 23-bp *Ter* sites shows the first 5 bps at the NP face to be AT rich and nonconserved, followed by a strictly conserved cytosine residue at the sixth position and a 13-bp core region that is responsible for the main sequence-specific contacts with Tus (Figure 1.4B)[100,127]. *Ter* sites display heterogeneity in their binding affinities to Tus and in their fork arrest efficiency (Figure 1.7A and B and Table 1.1)[129,137,138]. The strong *Ter* sites (*TerA*, *TerB*, *TerC*) are located innermost in the terminus region while weaker sites are located at its distal regions (Figure 1.7A)[127,129]. The adenosine base at position five is rather conserved in the strong *Ter* sites (Figure 1.4B and Figure 1.7A and B)[100,129,137], suggesting a possible role for this particular AT5 bp in fork arrest efficiency. Recent studies identified four new *Ter* sites (*TerK*, *TerL*, *TerY* and *TerZ*), with two of them (*TerY* and *TerZ*) oriented to block replication forks from the origin-to-terminus direction (Figure 1.8)[137]. Despite the weak binding of *TerY* and *TerZ* to Tus, they still display a much higher fork arrest activity as compared to similarly weak-binding *Ter* sites[137]. This is likely due to the opposite orientation of these newly isolated sites that causes them to encounter all traveling forks including late-fired forks. These sites are therefore being utilized more significantly than other weak sites, which are barely utilized since the strong sites innermost in the termination region stop most of the forks (Figure 1.8).

The tus gene is located very close to the strong *TerB* site and it is reported that binding of Tus to this region causes a negative feedback regulation on Tus transcription (Figure 1.5A)[109,139]. The structure of the Tus−*Ter* complex and the proposed model for its polar arrest activity are reviewed in the following section.

A

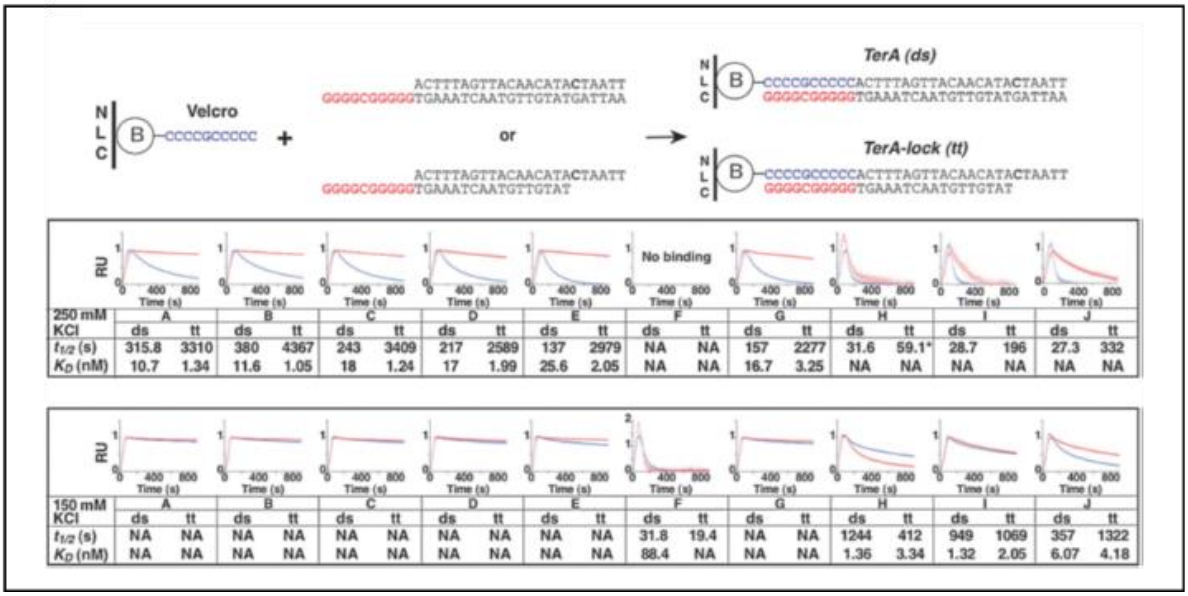

250 mM KCl	A ds	A tt	B ds	B tt	C ds	C tt	D ds	D tt	E ds	E tt	F ds	F tt	G ds	G tt	H ds	H tt	I ds	I tt	J ds	J tt
$t_{1/2}$ (s)	315.8	3310	380	4367	243	3409	217	2589	137	2979	NA	NA	157	2277	31.6	59.1*	28.7	196	27.3	332
K_D (nM)	10.7	1.34	11.6	1.05	18	1.24	17	1.99	25.6	2.05	NA	NA	16.7	3.25	NA	NA	NA	NA	NA	NA

150 mM KCl	A ds	A tt	B ds	B tt	C ds	C tt	D ds	D tt	E ds	E tt	F ds	F tt	G ds	G tt	H ds	H tt	I ds	I tt	J ds	J tt
$t_{1/2}$ (s)	NA	NA	NA	NA	NA	NA	NA	NA	NA	NA	31.8	19.4	NA	NA	1244	412	949	1069	357	1322
K_D (nM)	NA	NA	NA	NA	NA	NA	NA	NA	NA	NA	88.4	NA	NA	NA	1.36	3.34	1.32	2.05	6.07	4.18

B

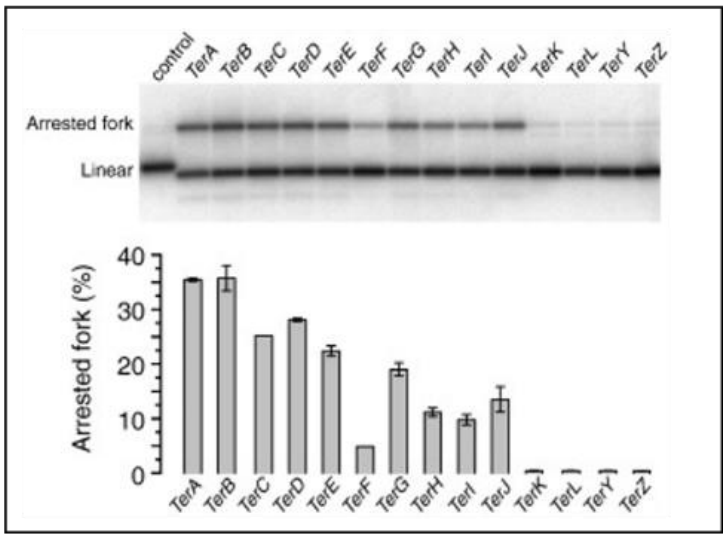

Figure 1.7: *Ter* sites display heterogeneity in their binding affinities to Tus and in their fork arrest efficiencies

A. Surface plasmon resonance (SPR) binding kinetics of DNA to different *Ter* and C6-lock *Ter* sequences. Top panel: principle of the reversible "Velcro" surface to allow for the anchoring of *Ter* sequences into the SPR chip. The complementary sequences of the Velcro oligonucleotides are shown in red and blue colors. Middle and bottom panels: binding kinetics of Tus to different *Ter* structures obtained at 250 mM KCl (middle) and 150 mM KCl (bottom). The blue and red curves represent the senograms of Tus binding to *Ter* and C6-lock *Ter* structures, respectively. Figure is adapted from[129].

B. Fork pausing efficiency of *E. coli Ter* sites. Each *Ter* site was cloned into pACYC184 plasmid so that the unidirectional moving replication fork would approach the *Ter* site towards the NP face. Fork arrest efficiency was determined by quantifying the ratio between the linear and forked DNA structures obtained by Southern blotting. Figure is adapted from[137].

	150 mM KCl		250 mM KCl	
	$t_{1/2\text{-agg}}$ ± SEM (s)		$t_{1/2\text{-agg}}$ ± SEM (s)	
Ter Site	*Ter*	*Ter-lock*	*Ter*	*Ter-lock*
A	7445 ± 2653	2009 ± 436	746 ± 129	1532 ± 138
B	4064 ± 362	3085 ± 694	1271 ± 157	1721 ± 151
C	2484 ± 130	2997 ± 1107	511 ± 46	2250 ± 132
D	1848 ± 69	1305 ± 120	329 ± 36	1045 ± 27
E	799 ± 31	744 ± 35	191 ± 22	523 ± 59
F	68 ± 8	28 ± 1	30 ± 3	24 ± 1
G	2044 ± 519	1299 ± 32	407 ± 23	708 ± 50
H	294 ± 17	144 ± 14	107 ± 5	131 ± 7
I	355 ± 45	103 ± 3	100 ± 9	88 ± 5
J	244 ± 8	178 ± 4	55 ± 2	114 ± 13
OriC	10 ± 1	11 ± 2	25 ± 3	25 ± 3
No DNA	8 ± 0.2		24 ± 0.4	

Table 1.1: Binding kinetics of Tus to *Ter* and C6-lock *Ter* structures using a method based on DNA-induced thermal stabilization of Tus-GFP

Mean and standard error (SEM) values of half-lifetime ($t_{1/2}$) for each *Ter* and C6-lock *Ter* sequences in 150 and 250 mM KCl. Aggregation rate constants (expressed in $t_{1/2}$) of Tus-GFP complexes with either *Ter* or C6-lock *Ter* sequences were measured at 52° in 250 mM KCl and at 58° in 150 mM KCl. Table is adapted from[138].

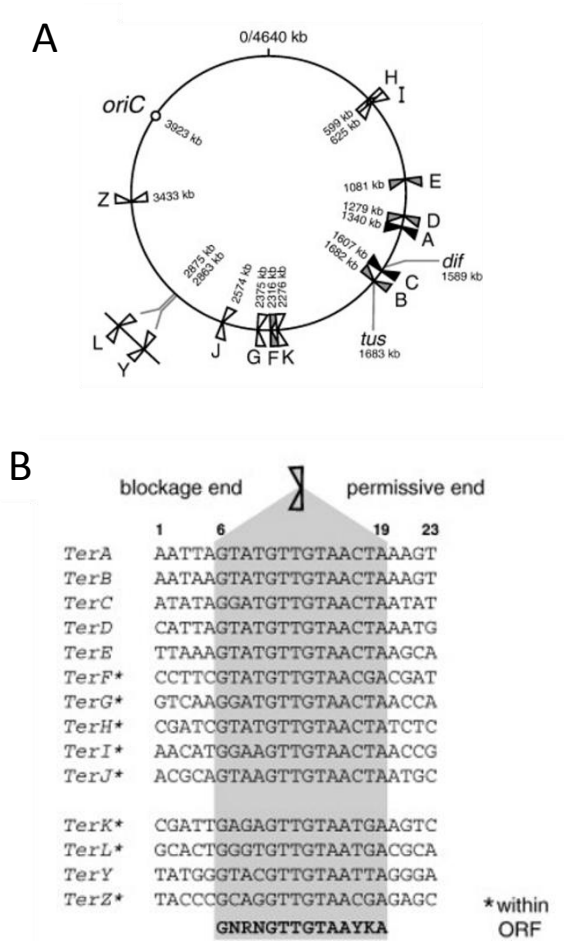

Figure 1.8: Location, orientation and sequences *of E. coli Ter* and *Ter*-like sites

A. Circular map of the 4.6-mega bp (Mbp) *E. coli* chromosome showing the location and orientation of *E. coli Ter* sites in relation to *oriC* and *dif* sites. *Ter* sites are represented by black markers have been previously identified as functional sites in wild-type cells, while grey *Ter* sites have been analyzed under artificial conditions. The unshapped *Ter* sites were identified by sequence similarity. Figure is adapted from[137].

B. Sequences of the 14 *Ter* sites. The orientation of P and NP faces of *Ter* sequences are shown. The core sequences that contribute to the main contacts with Tus are shaded. Figure is adapted from[137].

1.6.2 Mechanism of *E. coli* Replication Fork Arrest

1.6.2.1 Roadblock Model

Despite the extensive biochemical and structural studies of Tus−*Ter*, the precise mechanism that mediates its polar arrest activity remains debatable (reviewed in [23,24,86]). The first model was developed based on the crystal structure of Tus−*Ter* complex that was solved in 1996 (Figure 1.9A)[127]. The overall structure has three distinct regions, two α-helical regions and central β-structures, which jointly form a large central cleft that is positively charged and accommodates the *Ter* DNA (Figure 1.9A). The structural asymmetry observed in the complex from the P and NP faces hinted at a passive 'roadblock' model (Figure 1.9B)[127]. The α-helices are concentrated at the NP face and are proposed to clasp the duplex DNA. This would protect the central interactions with the interdomain β-structure from the direct encounter with a DNA unwinding motor like DnaB (Figure 1.9B). On the other hand, at the P face, there is no steric hindrance to stop the approaching helicase form disrupting these central DNA interactions (Figure 1.9B). This prompted the authors to propose that strength of the Tus−*Ter* complex is sufficient to form a nonspecific barrier, not only to DnaB helicase but also in principle to any protein that would unwind DNA[127].

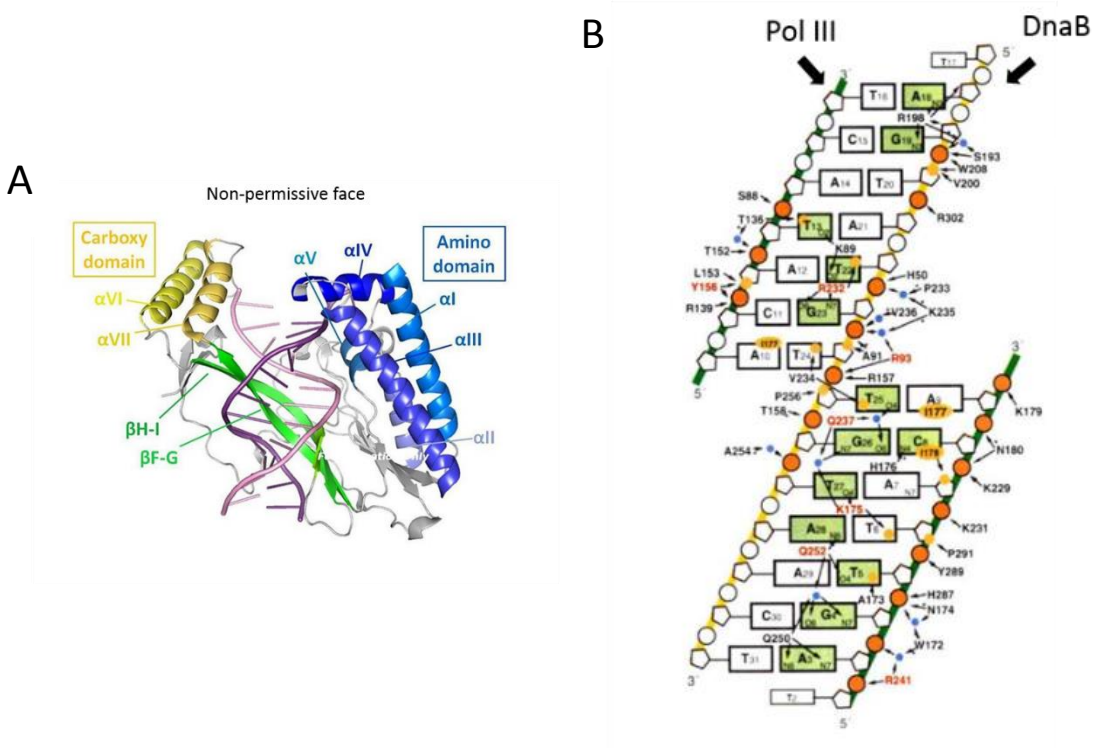

Figure 1.9: A passive road-block model determines polarity of replication fork arrest

A. Crystal structure of the Tus complex with *TerA* sequence oligonucleotide. Ribbon drawing of Tus–*Ter*A complex (PDB code: 1ECR)[127]. α-helices are concentrated on the NP face. The interdomain β-structure forms a central large cleft that accommodates the *Ter* sequence. Polar interactions between the DNA phosphate backbones and the interdomain β-structure form the main contacts with DNA.

B. Polar interactions and van der Waals contacts between Tus and DNA are indicated by arrows. Bases and phosphates making polar interactions are shown in green and red, respectively. The polar interactions between the DNA phosphate backbones and Tus protein are biased towards the lagging strand at the NP face of the complex. The DnaB- and polymerase-translocating strands are indicated by black arrows. Figure is adapted from[127].

Such a basic passive roadblock model was found to be unsatisfactory for several reasons. Firstly, the bacterial chromosome does not exist *in vivo* as naked DNA but is coated with various DNA-binding proteins, some of which bind to DNA with strong affinity. Yet, replication forks pass through these DNA-protein complexes while still being arrested efficiently only at the replication termination region. Secondly, Tus−*Ter* complex shows some helicase specificity in that it arrests helicases such as DnaB, PriA helicase and simian virus 40 (SV40) T-antigen, but not others such as *B. subtilis* DnaC helicase, PcrA, helicase I, and UvrD helicase *in vitro*[136,140-142]. It should be noted however that this specificity is disputed between various studies and results were rather conflicting. Thirdly, no further characterization of the structural asymmetry was performed to identify the specific features that give rise to Tus−*Ter* polar arrest activity. Lastly and most importantly, the different reported mutants of Tus with either enhanced or reduced binding affinities to DNA do not always correlate with their fork arrest activity[143,144]. In summary, neither the helicase specificity nor the polarity issue appeared to be consistent with a passive roadblock model.

1.6.2.2 C6-mousetrap Model

Biochemical and structural studies established two new models that differ on whether a physical interaction between the Tus−*Ter* complex and the approaching replisome, in particular the forefront component DnaB, is required for mediating polar arrest. The first model proposes that strand separation activity of DnaB at the NP face would engineer a new highly stable Tus−*Ter* complex. In particular, melting a *Ter* site past the conserved GC bp at the sixth position (Figure 1.4B) results in flipping of the C6 nucleotide to induce new

interactions with a cytosine-binding pocket on Tus, thus creating what is called a "mousetrap" that blocks the progression of the replication fork[130].

This model is directly supported by a crystal structure showing the C6 moving 14 A° from its normal position to flip into the cytosine-binding pocket when Tus was co-crystalized with *Ter* oligonucleotide that has a forked structure at the NP face (Figure 1.10A)[130]. Binding studies using surface plasmon resonance (SPR) and synthetic oligonucleotides of various structures demonstrate the formation of a highly specific "locked complex" when a fork structure is placed at the NP face of *TerB* site with C6 being unpaired; Tus dissociates 40-folds slower than from ds*TerB* (Figure 1.10B)[130]. The situation is different at the P face where strand separation progressively weakens Tus−*T*er interactions and hence displaces Tus before the C6 is flipped (Figure 1.10C). Since this study did not employ a helicase, the authors reasoned the enhanced stability of Tus−*Ter* interaction at the NP face to the DNA unwinding activity of DnaB and without the involvement of a Tus/DnaB specific interaction[130].

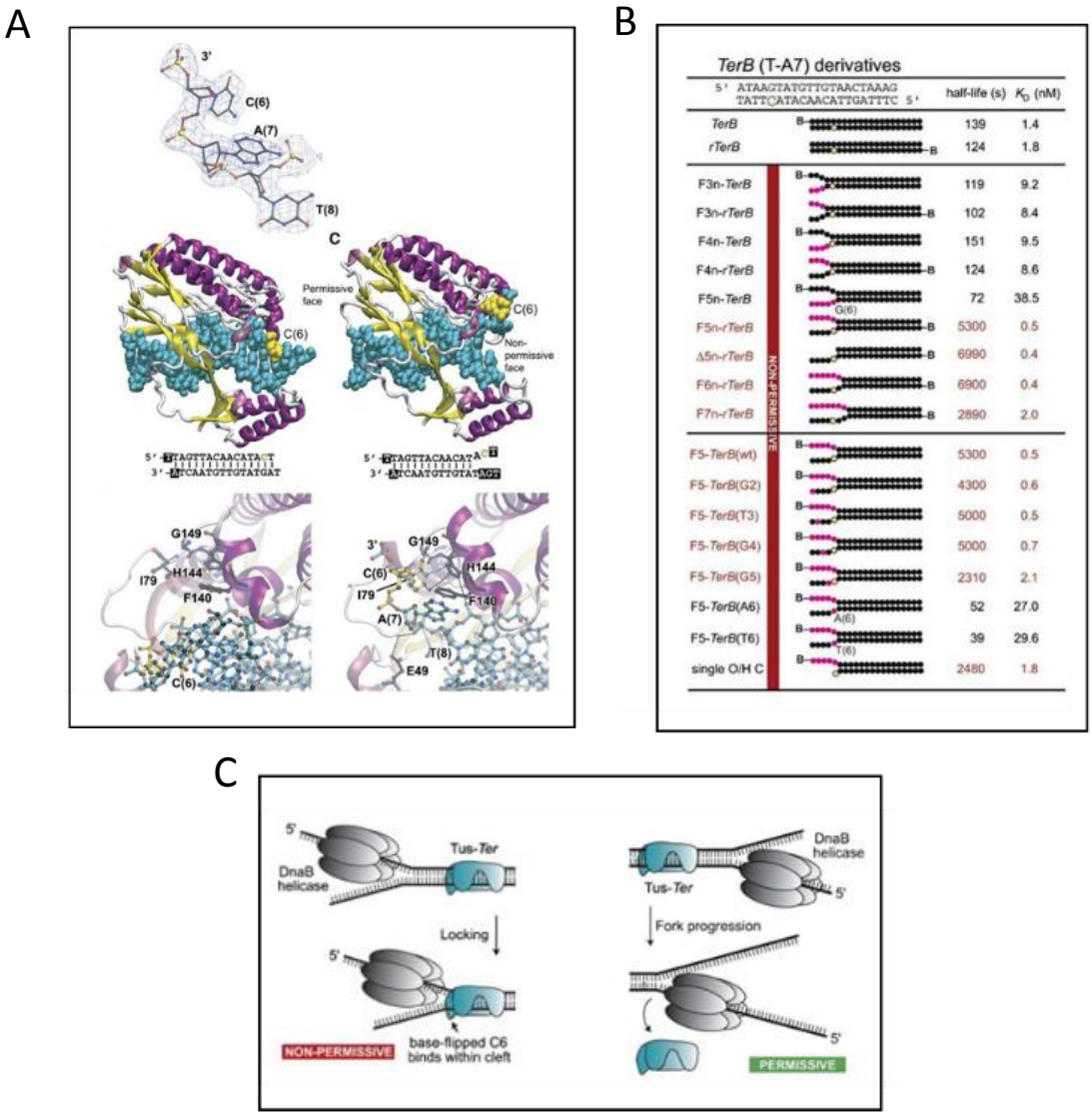

Figure 1.10: A molecular mousetrap determines polarity of DNA replication termination

A. Structure of the Tus–*Ter* C6-lock complex. Top panel: electron density map showing the region of the displaced strand in the Tus–*Ter* lock complex. Middle panel: comparison of structures of complexes of Tus with wild-type *TerA* (PDB code: 2I05, left)[127] and with C6-lock *Ter* complex (PDB code: 2I06, right)[130]; the strictly conserved C6 is highlighted in yellow. Bottom panel: structure of the cytosine-binding pocket, showing the movement of C6 to form a locked structure. Figure is adapted from[130].

B. Dissociation of Tus from complexes with *TerB* oligonucleotides forked at the NP end, measured by SPR. Data from variant *TerB* sites are shown. The locked complex forms when the fork extends far enough to expose C6. Data that showed the locked behavior are in red color. Base substitutions that replace the natural *TerB* sequence are shown in magenta, and the C6 residue is highlighted in yellow. Figure is adapted from[130].

C. Mousetrap model of fork arrest at the NP face (left). Model for dissociation of Tus following DNA mediated strand separation at the P face (right). Figure is adapted from[130].

1.6.2.3 Tus/DnaB Interaction Model

The second model proposes that a specific protein–protein interaction between DnaB and Tus occurs at the NP face and accounts for the Tus−*Ter* polar arrest activity[135]. This model is based on results that mapped the physical interaction between DnaB and Tus *in vivo* using the yeast two-hybrid system (Figure 1.11A,B)[135]. The authors further showed that this interaction occurs *in vitro* using an enzyme-linked immunosorbent assay (ELISA) and with a glutathione *S*-transferase (GST) pull down assay. In ELISA, Tus was immobilized on a microtiter plate and radioactively-labeled DnaB was injected over (Figure 1.11C). While in the GST-pull down assay, Tus was fused in frame to GST and was immobilized onto glutothione-agarose beads. ^{32}P-labeled DnaB was then flowed through the GST affinity matrix (Figure 1.11D). In both assays, audioradiograms confirmed the binding of the ^{32}P-labeled DnaB to the immobilized Tus[135]. An interesting mutant of Tus, E49K, was defective in helicase interaction hinted at the significance of a Tus and DnaB interaction in mediating polar arrest. The glu49 residue is located in the L1 loop of Tus that projects

from the helicase-blocking surface (Figure 1.11A) and contacts the phosphate backbone of the nucleotide at the seventh position when C6 is flipped (Figure 1.10A). Tus(E49K) specifically reduces the interaction with DnaB as shown by yeast-two hybrid analysis (Figure 1.11C,D) and compromises the ability of Tus to mediate polar arrest *in vitro* and *in vivo*. The authors concluded that Tus/DnaB interaction plays a significant role in inducing Tus−*Ter* polar arrest activity[135].

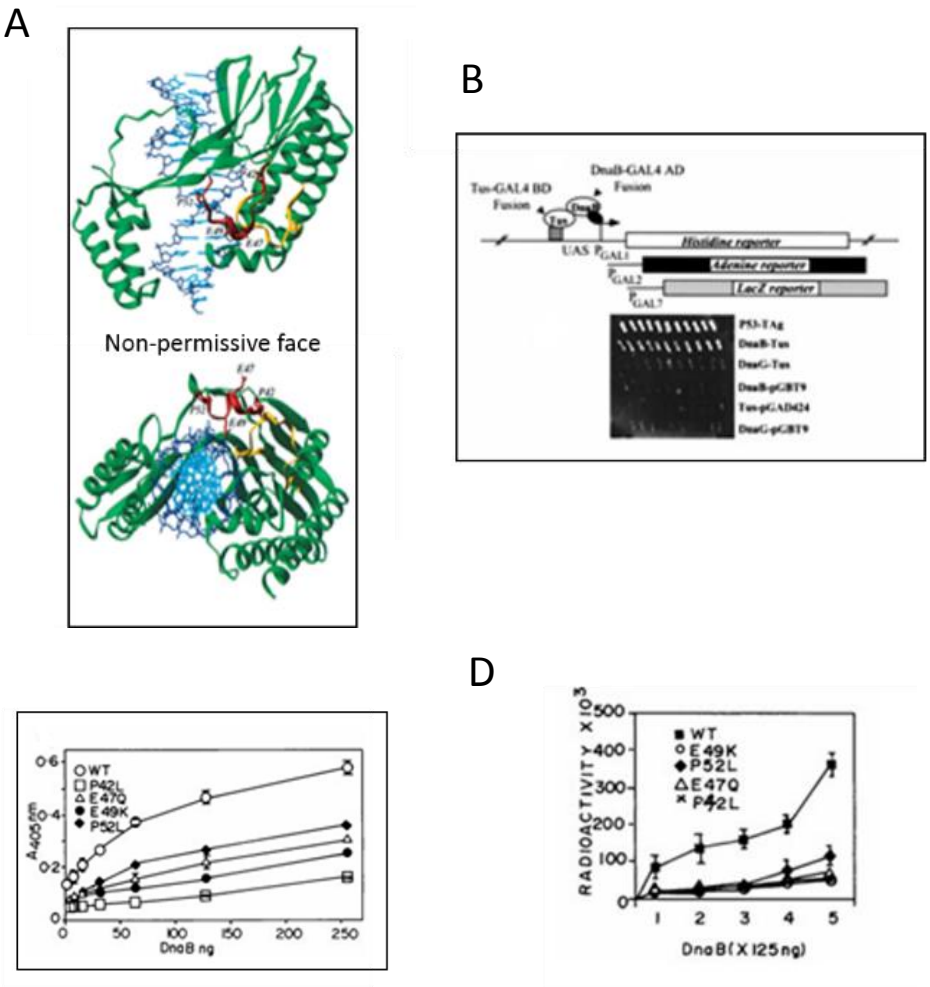

Figure 1.11: A Tus/DnaB interaction determines polarity of DNA replication termination

A. Top panel: crystal structure of Tus–*TerA* complex showing the P and NP faces of Tus[127]. The L1 loop, highlighted in red, is projecting from the NP face and is available for contact with the DnaB helicase. Bottom panel: a cross-sectional view of the DnaB-arresting surface. Figure is adapted from[135].
B. Forward and reverse two-hybrid analysis of Tus/DnaB interaction. Top panel: schematic diagram showing the three separate promoters and reporters that were used in the analysis. Bottom panel: photograph of a His-selection plate showing growth of cells containing Tus and DnaB fusion proteins. SV40 L-Tag and p53 proteins were used as positive controls, while Tus and DnaG proteins were used as negative controls. Figure is adapted from[135].
C. ELISA (enzyme-linked immunosorbent assay) showing the relative binding affinities of immobilized wild-type and the various mutant forms of Tus to DnaB in solution. Wild-type Tus, but not DnaB-interaction defective mutants, interact *in vitro* with DnaB. Figure is adapted from[135].
D. Quantification of GST (glutathione *S*-transferase) pull down assay binding data of labeled DnaB to the wild-type and the mutant forms of Tus. Wild-type Tus but not DnaB-interaction defective mutants, interact *in vitro* with DnaB. Figure is adapted from[135].

In a follow up study[145], a meticulous functional assay was employed to signify the role of this physical interaction in mediating polar arrest and refute the C6-flipping mousetrap model. The helicase activity of DnaB was optimized to translocate along dsDNA; an activity of DnaB that is proposed to resolve the key recombination Holliday junction intermediary structure[146]. In this assay, DnaB encircles the dsDNA to displace dsDNA-bound proteins actively without unwinding the dsDNA. Interestingly, DnaB is still arrested at the NP face of the Tus−*Ter* complex, providing evidence that rules out any role of the mousetrap model in fork arrest (Figure 12A)[145]. The second line of evidence contradicting

the mousetrap model was shown using the same DnaB helicase assay to demonstrate that the NP face of Tus−*T*er stops DnaB under condition where unwinding of the duplex DNA that is adjacent to GC6 was prevented by site-directed covalent interstrand cross-linking at two predetermined sites immediately preceding the C6 base (Figure 12B)[145]. Consistent with the previous mutant studies, DnaB-interaction defective Tus mutant, Tus(E49K), was defective in polar arrest in these assays (Figure 12B), supporting the notion that proper Tus/DnaB interaction is compulsory for fork arrest[145]. Collectively these experiments suggest that neither DNA unwinding nor C6-flipping is a prerequisite for the Tus−*Ter* polar arrest activity.

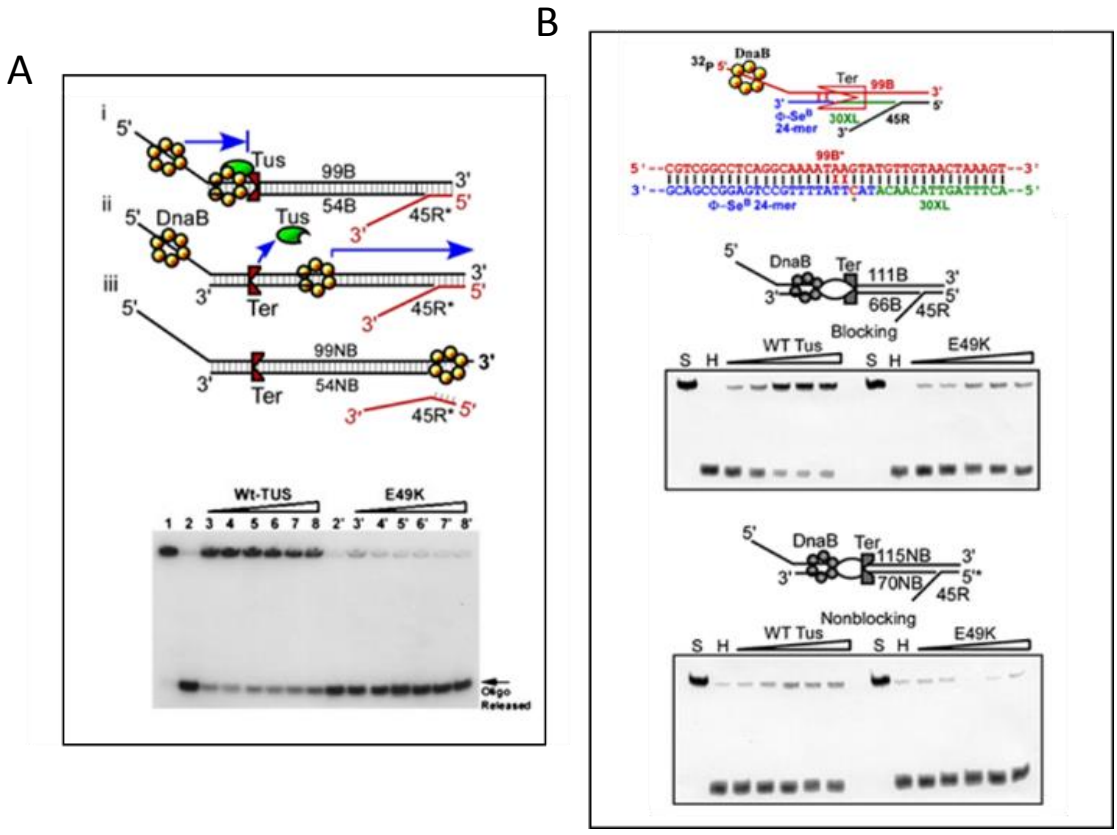

Figure 1.12: Helicase translocation along dsDNA in absence of C6-flipping did not abolish fork arrest activity by Tus–*Ter* complex

A. Top panel: experimental strategy for measuring DnaB translocation on dsDNA and its arrest at a Tus–*Ter* complex. Diagram showing the triplex substrates used for measuring the helicase translocation by the release of the 45R reporter oligo; *(i)*: helicase arrest at the NP face, *(ii* and *iii)*: helicase bypass and release of the 45R reporter oligonucleotide at the P face. Bottom panel: phosphorimagergrams of gels showing arrest of sliding DnaB by the wild-type and the E49K mutant form of Tus at the NP face. Figure is adapted from[145].
B. Top panel: schematic representation and sequences of the cross-linked triplex substrate with *Ter* at the NP face showing the locations of the various oligos and the induced cross-links. The cross-linked triplex is used as a substrate in DnaB helicase translocation reactions; the conserved GC6 bp is shown in red with an asterisk. Middle and bottom panels: phosphorimagergrams of gels showing arrest of sliding DnaB by the wild-type and Tus(E49K) at the NP (middle) and P (bottom) faces. Figure is adapted from[145].

1.6.3 Alternative Hypothesis of Replication Termination at *dif* Sites

XerCD chromosomal segregation complex recognizes the two *dif* sites that are located within the replication terminus region in the two sister chromosomes and induces recombination between them (Figure 1.13)[147]. Relatedly, FtsK is another bacterial protein that acts at the *E. coli* division septum and is essential for coordinating cell division and chromosomal segregation[147,148]. The N-terminus of FtsK is involved in assembly of the cell-division machinery, while its C-terminus functions as a DNA motor in order to travel along dsDNA in an ATP-dependent manner towards the *dif* recombination site[148-150]. Translocation stops specifically at Xer-*dif* sites where FtsK interacts with the Xer recombinase allowing the activation of chromosome unlinking by inducing the formation of Holliday junctions and recombination[151,152]. FtsK is thought to reserve the order of

action of XerCD complex, whereas XerD makes the first pair of strand exchanges to form Holliday junctions that are then resolved by XerC (Figure 1.13)[152,153]. A recent study suggested that the *dif* site is the actual location of termination of replication forks originating from *oriC*, while *Ter* sites are proposed to stop replication forks originating from DNA repair events[154]. The *dif* site hypothesis is based on a well-established observation in prokaryotic genomes of skewness of base composition between the leading-and lagging-strands, which correlates with replication directionality and in turn can be utilized to predict the location where termination occurs[155,156]. The study showed a shift in the skewness near the *dif* site and not the *Ter* sites, and therefore concluded that *dif* is the actual site of termination[154]. However another recent study refuted this hypothesis; a 2D gel analysis of replication intermediates found no detectable pausing near the *dif* site, while a significant fork arrest is observed at *TerC*, clearly supporting the fork trap model[137]. Later computational genome analysis concluded that a finite termination site near the *dif* site is not sufficient to explain the genomic computational bias in the published genome's sequence where fork trap takes place[157].

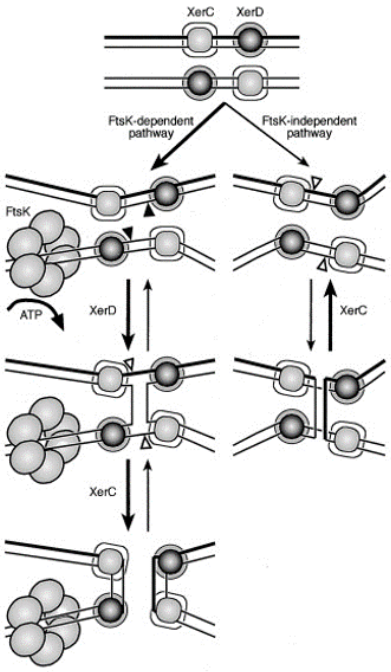

Figure 1.13: Resolving of the two sister chromosomes by FtsK–XerCD–*dif* chromosome dimer resolution machinery

FtsK-dependent and independent pathways of Xer recombination at *dif* site. In the absence of FtsK, the Xer synaptic complex adopts a conformation suitable for XerC-mediated strand exchanges. FtsK can use the energy of ATP to switch the Xer synaptic complex to a conformation suitable for XerD-strand exchanges. Figure is adapted from [147].

1.6.4 Replication Past Termination and Towards the *dif* Sites

During fork traveling, accumulation of positive supercoiling in front of the *E. coli* replisome is resolved by the major cellular decatenase, topoisomerase IV, which is responsible for unlinking of precatenates during replication and after termination[158-160]. It is also reported that FtsK interacts with topoisomerase IV to guide its unlinking activity into the terminus region, where it is needed to decatenate the built-up positive supercoils between the two forks[161]. However, prior to termination, the accumulated positive supercoils between the

two approaching forks are expected to oppose DNA unwinding by the helicase at the final stages of DNA replication in this region. Recently, the first clues as to how this might be resolved was revealed in a study of *in vitro* replication of *E. coli* chromosomes that demonstrated a role for RecQ in unwinding catenates in the late stage of replication and when the two opposed forks are spaced ~ 130 bp apart[162]. Topoisomerases I and III can specifically unlink the resulting ssDNA catenates. Both reactions necessitate the presence of SSB and the resulting chromosomes would contain gaps that require filling[162]. The same study proposes that some nonreplicative polymerases in the cell fulfil this job, in particular Pol I and DNA ligase to form contiguous chromosomes, ready for the late action of XerCD complex at the *dif* site to initiate the chromosomal segregation process[128,162].

1.7 Power of Single-molecule Imaging in Studying Biological Reactions

Understanding the complexity of biomolecules has been a goal for many decades. A wide variety of structural techniques, such as X-ray crystallography, NMR spectroscopy, and electron microscopy, combined with biochemical and molecular biological studies, have led to a quantitative understanding of the molecular details and mechanisms underlying several biological processes. Nevertheless, the static and ensemble averaged view obtained with these techniques limits our understanding the dynamic behavior of biomolecules and the nature of their interactions.

Recent advances in imaging and molecular manipulation techniques have made it possible to observe single molecules and to record molecular movies that provide a true molecular understanding of their dynamics and reaction mechanisms[163-166]. This enables

the observation of short-lived intermediary steps, characterization of the mechanism of intermediary steps within the context of the entire reaction and building of the timing mechanisms of intermediary steps and reactions.

Single-molecule techniques have evolved rapidly and already proven their novelty in studying the activity of a variety of individual enzymes. Nevertheless, many complex biological reactions are driven by a series of orchestrated steps that are carried out by large multi-protein complexes, often comprising many enzymatic activities. DNA replication is at the forefront of these processes that were studied at the single-molecule level including the reconstitution of bacteiophages T4 and T7 and the more complex *E. coli* systems over the past ten years[164,167-169]. This provided mechanistic insights and built the timing mechanisms of key processes and intermediary steps during replication. These systems are now being taken to the next level where complexity of reactions studied at the single-molecule level is advanced to tackle the communication between replication and other process. Studying DNA replication at the single-molecule level contributes to various fields by developing wide range of force- and fluorescence-based single-molecule imaging assays and approaches that are readily available to study the mechanism of large multiprotein complexes acting on nucleic acids[15,164,170-172]. In the following section, I will be presenting examples of studies that utilized single-molecule techniques to unravel the dynamic behavior of several enzymes and provide information on the molecular fine details and action mechanisms of multi-protein complexes.

Fluorescence imaging of individual DNA-binding protein and mechanical manipulation of DNA by flow or magnetic tweezers or optical traps, were typically the common methods used to study nucleic acid enzymes at the single-molecule level (reviewed in [169,173,174]). The assembly of the bacteriophage T4 replisome was studied by single-molecule Förster Resonance Energy Transfer (FRET) and fluorescently labelled replicating proteins[175,176]. The study showed that the assembly of the T4 replisome follows one of four major possible pathways; each is strictly linked to the progress of one phase of the cell-cycle[175]. The unwinding activity of UvrD helicase was studied by manipulating a DNA in magnetic tweezers, taking advantage of the fact that the ssDNA is longer than dsDNA at high stretching forces[177]. The study showed that UvrD shuttles between the two strands, leading to reannealing of the melted DNA as the helicase is translocating away from the fork[177]. Mechanical manipulation of a DNA hairpin substrate by magnetic tweezers allowed for building a detailed timing mechanism of the restart of a stalled T4 bacteriophage replisome, whereas different repair pathways are triggered depending on the nature of the DNA lesion[178,179]. The helicase and nucleolytic activities of RecBCD were studied by flow-stretching a DNA substrate and monitoring the displacement of a fluorescent intercalating dye[180,181]. Study of bacteriophage T7 replisome elongation was achieved by means of flow-stretching the DNA template and monitoring the change of its length during leading-strand synthesis[14,168,182,183]. The study provided novel insights about the exchange of T7 DNA polymerase during catalysis[183,184], as well as the coordination of DNA synthesis between leading and lagging strands[182].

1.8 The Encounter of the *E. coli* Replisome with Transcription Machinery, DNA-Binding Proteins and DNA Lesions

Studying the mechanism of Tus−*Ter* polar arrest activity served as a model system that established several concepts that could govern the communication between DNA replication and dsDNA-binding protein barriers. Here I am dedicating a section to discuss the various conflicts between replication and other process and how the cell manages these conflicts.

The replisome recurrently enters into conflicts with processes that are simultaneously acting on the parental DNA strands including DNA repair, recombination, transcription and high affinity nucleoproteins[185-189]. It is critical for cell viability and stable inheritance of the genetic material to coordinate these conflicts and to be able to restart DNA synthesis in the event they stall the replisome.

The encounter of the *E. coli* replisome and stalled RNA polymerase (RNAP) transcribing genes on either the leading- or lagging-strands is a common incident that could result in either co-directional or head-on-head collisions, respectively[190,191]. Head-on-head collision is more deleterious than co-directional one and is minimized by preferential arrangement of the highly transcribed genes on the leading strand[192,193]. *E. coli* developed several mechanisms to resolve replication-transcription conflicts (reviewed in [190]). (i) At DNA lesions, inhibition of formation of arrays of stalled RNAPs is prevented by the action of RNAP modulators proteins including GreA, GreB, DnaK, DksA, pGpp, and Mfd, which displace RNAP from the lesion and help recruiting UvrABC complex to repair the lesion site. (ii) In bacteria, translation and transcription are coupled events, which provide a

mechanism by which the ribosome displace a backtracked RNAP. In the event of uncoupled transcription and translation, backtracking of the RNAP is prevented or resolved by the RNAP secondary channel-interacting factors DksA, GreA and GreB. (iii) At ribosomal-RNA-encoding (*rrn*) operons, *E. coli* replisome recruits non-replicative helicases (DinG, Rep, and UvrD) to reduce the replication and transcription conflict at *rrn* operons; this accessory helicase-mediated restart will be discussed in the coming section.

The *E. coli* replisome would frequently stall at other kinds of obstacles on the DNA including dsDNA-binding proteins, and many types of DNA lesions[189,194]. A lengthy stalling of the replisome could lead to its dissociation from the fork[195-197]. Accessory helicases such as Rep, UvrD and DinG act by shortening the stalling time to prevent the dissociation of the replisome and the subsequent activation of recombination-restart pathways that could increase the chance of perilous chromosomal rearrangements[197-200]. Among these accessory helicases, Rep is the only helicase that specifically interacts with the replisomal DnaB helicase and its absence increases the chromosomal duplication time as a result of frequent stalling and inactivation of the replisome[201,202]. Nonetheless, *E. coli* viability is compromised only when Rep and UvrD are both lacking, underscoring an interplay mechanism between these two accessory helicases[203]. It is proposed that Rep provides a replisome-specific motor, while UvrD provides a generalized motor that relies on its high cellular concentration to bind to the stalled DNA replication fork[194]. The role of DinG in removing protein–DNA barriers is yet to be confirmed, but it seems to play a specific role in removing the DNA/RNA R-loop structures that form naturally during transcription and have been shown to impose an impediment to the replisome[203]. Rep and UvrD share

significant structural similarities as both belong to the super family 1 (SF1) group of DNA helicases that translocate in the 3'−5' direction[202,204]. DnaB helicase assays and binding studies on short replication forks illustrate that functional coupling of Rep with DnaB requires the availability of at least 6 nucleotides of ssDNA ahead of the leading strand DNA polymerase for Rep binding[202]. This would align Rep and DnaB to cooperate in unwinding dsDNA, thus providing the replisome with two powerful motors to remove protein–DNA barriers ahead of the fork. Rep utilizes its extreme 33 residue C-terminal tail to physically and functionally interact with DnaB[205-207]. UvrD on the other hand does not form a complex with DnaB on these short replication fork constructs[202].

The cell established several recombinant and direct restart pathways to reassemble the replisome outside the origin of replication in the event of dissociating the stalled replisome from the fork (reviewed in [197-199]). Direct restart could be achieved by the action of PriA, PriC and both PriB and Rep, which recognize different intermediary-branched structures at the stalled fork and mediate the reloading of the DnaB helicase. The stalled replisome might mediate fork reversal DNA synthesis activity to result in a four-way Holliday junction structure that serves as an intermediary step for different restart pathways. This include recombination-dependent pathway that relies on the excision reaction of RuvABC helicase/endonuclease to induce a double strand break (DSB) at the fork followed by a homologous strand invasion reaction mediated by RecA and RecBCD to form the D-loop structure, which is then resolved by RuvABC to create a fork structure that is compatible with the aforementioned direct restart mechanisms. A prolonged stalling of the replisome could also result in a spontaneous DSB that is repaired in similar

manner by the action of RecA and RecBCD. Alternatively, the fork structure would be generated from the four-way Holliday junction through either leading strand extension or degradation of regressed DNA to bypass or excise the lesion, respectively. This would result in the formation of replication fork structures that can be rescued by direct restart mechanisms.

1.9 About this Thesis

Although the Tus−*T*er locked complex is extremely stable *in vitro* and is able to permanently stop the replication fork, the efficiency of fork arrest at any *Ter* site *in vivo* does not exceed 50% (Figure 1.7B)[137]. This low efficiency explains why the terminus contains redundant *Ter* sites but it also leaves us with an interesting paradox regarding the discrepancy between the *in vitro* and *in vivo* findings. An earlier study showed that DNA supercoiling attenuates fork arrest activity suggesting a role for the helicase unwinding activity in fork arrest efficiency[208]. Given the discrepancy between the *in vitro* and *in vivo* work and the conflicting models on how the system works (reviewed in [20,23,24,86,128]), it is clear that more definitive experiments conducted under physiological conditions, where DnaB unwinds dsDNA within the context of the replisome as it encounters the Tus−*Ter* complex from the P or NP faces are required. Experiments in the C6-mousetrap model did not use an actual helicase and employed instead mismatch mutations to mimic fork opening[130]. Moreover, detection of the contribution of the C6-flipping to the interaction of Tus with *Ter* required the use of high salt concentrations, ranging from 250 to 400 mM KCl, which is much higher than those *in vivo*. Indeed DNA and RNA synthesis is almost completely inhibited *in vitro* at this range of salt

concentration[209,210]. On the other hand, previously published *in vivo* data showed that a C6-to-A6 transversion in *Ter* did not manifest any loss of arrest activity[131] and another study has reported that the same mutation caused only 3-fold reduction in fork arrest[100]. Additionally, the C6-mousetrap model cannot explain why MCM2–7 helicase is stopped in a polar manner at the Tus−*Ter* complex[211], although it is recognized to translocate in the 3'–5' direction[212,213] and presumably should inhibit C6-flipping. On the other hand, in the experiments that supported the Tus/DnaB interaction model, DnaB was functioning under nonreplicative conditions where it does not mediate DNA unwinding[135,145]. Another serious criticism of the physical interaction model is the inherent ability of Tus−*Ter* to arrest a wide range of helicases such as PriA and SV40 L-Tag in a polar manner[136,140-142,214].

In summary, the main aim of my PhD thesis study is to unravel the molecular mechanism that coordinates and synchronizes termination of DNA replication using the model bacterial replication system from *E. coli* and the heterologous system from bacteriophage T7. A comprehensive and multidisciplinary collaborative effort that combines X-ray crystallography and binding studies with the real-time observation of replication of single DNA molecules was applied to provide a true molecular level understanding of the final steps in DNA replication prior to cell division, a problem that has challenged scientists for several decades.

In the following chapters, I will first discuss results of my work that are already published. Original manuscripts were reformatted and adapted to be a part of the presented work in accordance with the university guidelines. This resulted in redundant information in

the introduction and other part of the thesis. I will next discuss unpublished results followed by a comprehensive discussion that critically integrates the findings of the published and unpublished work.

Chapter 2

2. Materials and Methods

2.1 Materials

2.1.1 General Materials

DNA restriction enzymes (*EcoRI* and *ApaI*), T4 DNA ligase, T4 polynucleotide kinase (PNK), bacteriophage lambda DNA (λ-DNA), and M13mp18 ssDNA were purchased from New England Biolabs (NEB). Biotin-PEG-SVA, MW 5000 and Malemide-PEG-Succinimidyl Valerate, MW 5000 were purchased from Laysan-Bio. (3-Aminopropyl)triethoxysilane and streptavidin were purchased from Sigma-Aldrich. α-digoxigenin Fab antibody solution and Sytox Orange dsDNA-stain were purchased from Invitrogen. Tosyl activated 2.8 μm diameter magnetic beads were purchased from Dynal.

2.1.2 DNA Replication Proteins

E. coli DNA replication proteins were purified in Professor Nicholas Dixon's lab (University of Wollongong). β_2 sliding clamp, Pol III αεΘ core and $\tau_3\delta\delta'\chi\psi$ clamp loader, DnaBC helicase and helicase loader complex, and fork restart proteins (PriA, PriB, and DnaT) were typically prepared according to previously described methods[55,215,216].

Bacteriophage T7 DNA replication proteins were purified at KAUST. Gene 4 protein (gp4) helicase/primase, and gene 5 protein DNA polymerase (gp5) bound to its processivity factor *E. coli* thioredoxin (trx) (the complex is termed gp5/trx) were prepared as described previously[217-220].

2.1.3 Tus Proteins

N-terminally His_6-tagged Tus and its mutant derivatives Tus(E49A), Tus(E49K), Tus(I79A), Tus(F140A) and Tus(H144A), Tus(R198A) were purified in Professor Nicholas Dixon's lab (University of Wollongong), as described previously[101,130]. Tus-GFP fusion protein was a generous gift from Professor Patrick Schaeffer (James Cook University)[138].

2.1.4 Oligonucleotides

All oligonucleotides were purified by Polyacrylamide Gel Electrophoresis (PAGE) and purchased from Integrated DNA Technologies (IDT) or Sigma-Aldrich. The sequences of the primers used for constructing DNA templates for single-molecule DNA replication assays are displayed in Table 2.1.

Substrate	Sequence (5' – 3')
λ phage Leading-strand tail	GGGCGGCGACCTGGACAGCAAGTTGGACAATCTCGTTCTATCACTAATTCACTAATGCAGGGAGGATTTCAGATATGGCA
λ phage Leading-strand primer	TGCCATATCTGAAATCCTCCCTGCATTAG
λ phage Lagging strand biotinylated arm	Biotin-AAAAAAAAAAAAAAAAAGAGTACTGTACGATCTAGCATCAATCACAGGGTCAGGTTCGTTATTGTCCAACTTGCTGTCC
λ phage digoxigenin-modified arm	AGGTCGCCGCCCAAAAAAAAAAAA-digoxigenin
M13 Bitinylated primer	Biotin- TTTTTTTTTTTTTTTTTTTTTTTTTTTTTTTTTTTTAATTCGTAATCATGGTCATAGCTGTTTCCT
NP*TerB* (leading strand)	AACGCGCCATAATATTAACCACTTTAGTTACAACATACTTATTTTATAGCACAGTCGTGGTGACTTG
NP*TerB* (lagging strand)	AATTCAAGTCACCACGACTGTGCTATAAAATAAGTATGTTGTAACTAAAGTGGTTAATATTATGGCGCGTTGGCC
P*TerB* (leading strand)	CAAGTCACCACGACTGTGCTATAAAATAAGTATGTTGTAACTAAAGTGGTTAATATTATGGCGCGTT
P*TerB* (lagging strand)	AATTAACGCGCCATAATATTAACCACTTTAGTTACAACATACTTATTTTATAGCACAGTCGTGGTGACTTGGGCC
5-mismatch C6 - NP*TerB* (leading strand)	AACGCGCCATAATATTAACCACTTTAGTTACAACATACTTATTTTATAGCACAGTCGTGGTGACTTG
5-mismatch C6 - NP*TerB* (lagging strand)	AATTCAAGTCACCACGACTGTGCTATAAAAACCTCATGTTGTAACTAAAGTGGTTAATATTATGGCGCGTTGGCC
5-mismatch G6 - NP*TerB* (leading strand)	AACGCGCCATAATATTAACCACTTTAGTTACAACATAGTTATTTTATAGCACAGTCGTGGTGACTTG
5-mismatch G6 - NP*TerB* (lagging strand)	AATTCAAGTCACCACGACTGTGCTATAAAAACCTCATGTTGTAACTAAAGTGGTTAATATTATGGCGCGTTGGCC
CG(6) - NP*TerB* (leading strand)	AACGCGCCATAATATTAACCACTTTAGTTACAACATAGTTATTTTATAGCACAGTCGTGGTGACTTG
CG(6) - NP*TerB* (lagging strand)	AATTCAAGTCACCACGACTGTGCTATAAAATAACTATGTTGTAACTAAAGTGGTTAATATTATGGCGCGTTGGCC
TA(6) - NP*TerB* (leading strand)	AACGCGCCATAATATTAACCACTTTAGTTACAACATATTTATTTTATAGCACAGTCGTGGTGACTTG
TA(6) - NP*TerB* (lagging strand)	AATTCAAGTCACCACGACTGTGCTATAAAATAAATATGTTGTAACTAAAGTGGTTAATATTATGGCGCGTTGGCC
Swapped F5n GC(6) - NP*TerB* (leading strand)	AACGCGCCATAATATTAACCACTTTAGTTACAACATACAATAATTATAGCACAGTCGTGGTGACTTG
Swapped F5n GC(6) - NP*TerB* (lagging strand)	AATTCAAGTCACCACGACTGTGCTATAATTATTGTATGTTGTAACTAAAGTGGTTAATATTATGGCGCGTTGGCC
Swapped F4n GC(6) - NP*TerB* (leading strand)	AACGCGCCATAATATTAACCACTTTAGTTACAACATACTATAATTATAGCACAGTCGTGGTGACTTG
Swapped F4n GC(6) - NP*TerB* (lagging strand)	AATTCAAGTCACCACGACTGTGCTATAATTATAGTATGTTGTAACTAAAGTGGTTAATATTATGGCGCGTTGGCC
TA(5) - NP*TerB* (leading strand)	AACGCGCCATAATATTAACCACTTTAGTTACAACATACATATTTTATAGCACAGTCGTGGTGACTTG
TA(5) - NP*TerB* (lagging strand)	AATTCAAGTCACCACGACTGTGCTATAAAATATGTATGTTGTAACTAAAGTGGTTAATATTATGGCGCGTTGGCC
NP*TerH* (leading strand)	AACGCGCCATAATATTAACCGAGATAGTTACAACATACGATCGTTATAGCACAGTCGTGGTGACTTG
NP*TerH* (lagging strand)	AATTCAAGTCACCACGACTGTGCTATAACGATCGTATGTTGTAACTATCTCGGTTAATATTATGGCGCGTTGGCC

Table 2.1: Sequences of the primers used for constructing various DNA templates for single-molecule DNA replication assays

2.1.5 Bacterial Plasmids

pTH931, pTH102, and pBAD30 plasmids used in the *in vivo E. coli* growth assay of fork arrest activity were provided by Professor Thomas Hill[208,221] and the assays were performed in Professor Nicholas Dixon's lab (University of Wollongong).

2.2 Methodology

2.2.1 Flow-stretching Single-molecule Leading-strand DNA Synthesis Assay

This section describes the flow stretching single-molecule assays used to observe replication of individual DNA molecules mediated by the replisomes of *E. coli* and its bacteriophage T7.

2.2.1.1 Microfluidic Flow Cell

Flow cell was constructed by cutting a double-forked 3 mm-wide channel out of a nonreactive double-sided sticky tape (~ 100 µm thick) (Secure-Seal, Grace BioLabs). The channel was fixed to a glass slide and to the functionalized coverslip. Tubing (Intramedic PE60, Becton Dickinson) was inserted through holes drilled into the glass and sealed with epoxy, creating a sealed chamber that is used for the single-molecule experiments (see the schematic in Figure 2.1A). The tubing was used to flow and exchange buffer, reagents and proteins into the flow cell. A permanent magnet positioned above the flow cell exerts a magnetic force upwards in order to prevent the nonspecific interaction of the beads with the surface (illustrated in Figure 2.1B).

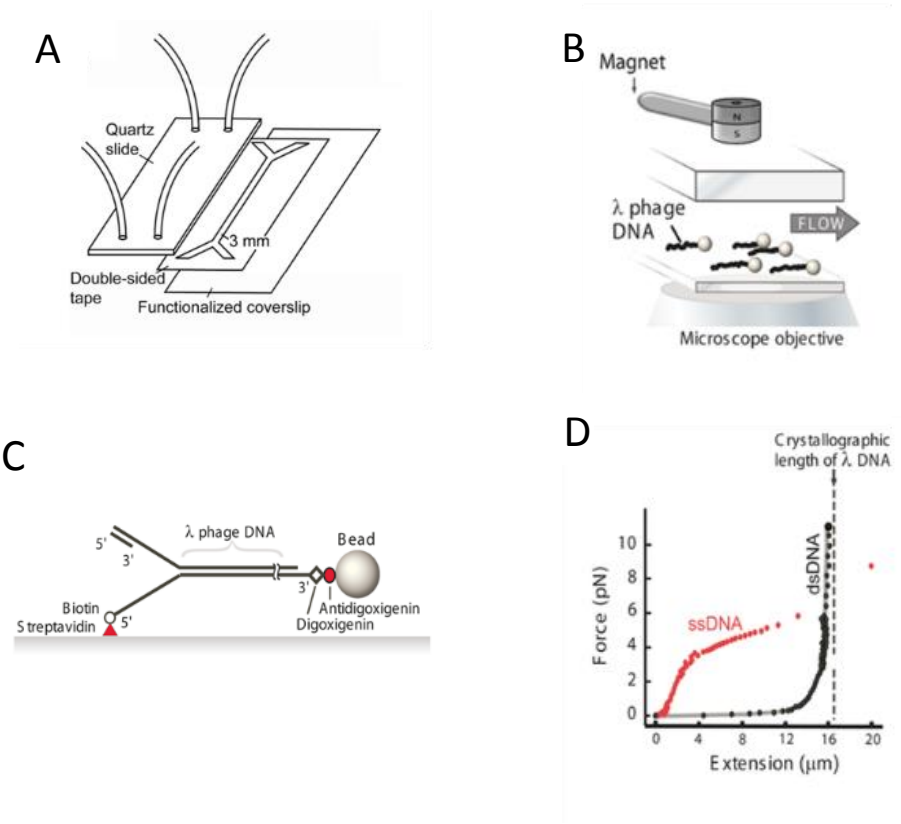

Figure 2.1: Experimental design of flow stretching single-molecule assay for observing leading-strand DNA synthesis

A. Flow cell is constructed by cutting 3 mm-wide channel out of a non-reactive double sided adhesive table. The channel is affixed to a glass slide and the functionalized coverslip. Tubings were inserted in holes drilled in the quartz slide and sealed with epoxy creating a sealed chamber that is used for single-molecule experiments.

B. Schematic representation of the experimental arrangement. The surface-tethered DNA molecules are stretched by a drag force on the beads that is exerted by a laminar flow of buffer over the surface. A magnet placed above the flow cell exerts a magnetic force upward and prevents the nonspecific interaction of the beads with the surface. The flow cell is positioned on the stage of a wide-field optical microscope and a Charge Coupling Device (CCD) camera is used to image the beads. The length of individual DNA molecules is monitored in real time by tracking the centroid positions of the beads.

C. DNA construct, duplex λ-phage DNA (~ 48.5 kilobase (kb)) is modified by attaching a biotinylated replication fork to one of its ends and a digoxigenin oligonucleotide to the other end. The replication fork contains a primer to initiate the DNA polymerization activity and ssDNA to enable the loading of the helicase on the lagging strand. The lagging strand is attached to the surface of a glass coverslip *via* the 5' end of the fork using a biotin/streptavidin linker and to a paramagnetic bead *via* its 3' end using a digoxigenin/antidigoxigenin linker.
D. Extension of λ-phage double-stranded (dsDNA) (black circles) and single-stranded (ssDNA) (red circles). The dashed vertical line at 16.3 μm corresponds to the crystallographic length of λ-phage dsDNA. This figure is adapted from[226].

2.2.1.2 Coverslip Surface Functionalization

Described methods were used to functionalize the surface of coverslip and allow for subsequent tethering of DNA molecules[222,223]. Briefly, to minimize non-specific interaction between the proteins and the glass surface, a high molecular weight Poly Ethylene Glycol (PEG) polymer was covalently linked to the surface. This was achieved by firstly coupling alkoxy groups of amino-silane ((3-Aminopropyl)triethoxysilane) to leave the surface functionalized with amino groups. Secondly, a mixture of biotinylated and non-biotinylated (Biotin-PEG-SVA, MW 5000 and Malemide-PEG-Succinimidyl Valerate, MW 5000) was used to coat the amino-functionalized glass surface and passivate the coverslip with a thin layer of PEG displaying a mixture of biotin and PEG groups. Biotin was used to bind tightly to free streptavidin for the subsequent coupling of biotinylated DNA molecules to the glass surface.

2.2.1.3 Beads Functionalization

Described methods were used to coat the paramagnetic polystyrene beads with α-digoxigenin Fab fragments *via* an amino-coupling reaction[222-224]. Briefly, the suspended beads were cleared from the supernatant by placing the tube in a magnetic separator (Dynal). To allow for the antibody coupling reaction to proceed, the beads were mixed with the antibody solution for 16-24 h at 37 °C. The uncoupled Fab fragments were removed by washing with buffers and then BSA was used to block the free tosyl groups on the beads. The beads were then resuspended in storage buffer containing 1X phosphate-buffered saline (PBS) (mM NaCl, 2.7 mM KCl, 10 mM Na-phosphate, pH 7.4), 0.1% w/v Bovine Serum Albumin (BSA). The suspended beads are then aliquoted and stored at 4 °C for daily usage.

2.2.1.4 Templates for Single-molecule Tethered Bead Assay

Bacteriophage λ-DNA (~ 48.5 kilobase (kb)) was linearized by heating and manipulated by attaching modified oligos to its 12-bases ssDNA overhangs, 5' AGGTCGCCGCCC 3'. A biotinylated forked DNA structure was constructed from three oligos and then attached to one end of the λ-DNA and a digoxigenin-modified oligonucleotide was attached to the other end, using standard DNA annealing and ligating techniques as described previously[222-224]. The biotinylated oligonucleotides allow for the immobilization of the DNA to a streptavidin-functionalized surface of a coverslip, while the digoxigenin moiety allows for the binding of paramagnetic bead *via* digoxigenin/anti-digoxigenin interaction (α-digoxigenin Fab antibody solution) (see the schematic in Figure 2.1C). The sequences of the primers used for constructing the λ-DNA template are shown in Table 2.1.

2.2.1.5 Constructing DNA Templates Containing Termination (*Ter*) Sites (~ 13.7 kb)

Engineered λ-DNA, which contains a biotinylated-fork at one end and a digoxigenin on the other end, was digested with *EcoRI* restriction enzyme to generate a 3.6 kb fragment from the forked end and with *ApaI* restriction enzyme to generate a 10.1 kb fragment from the digoxigenin end (Figure 2.2A). A 59 base pair (bp) oligonucleotide containing a single copy of *TerB* site, or a modified version of it, and a ssDNA overhangs that are complementary to the overhangs in the *EcoRI* and *ApaI* digested fragments, was first phosphorylated only at the 5' end of the *EcoRI* site to prevent self-ligation at the *ApaI* site, and then ligated to the 3.6 kb *EcoRI* λ-DNA DNA digest. The ligation product was gel purified to remove excess unligated oligos. The purified fragment was phophorylated (T4 PNK) at the *ApaI* site and then ligated to the 10.1 kb *ApaI* λ-DNA digest (Figure 2.2A). The final product was sequenced to ensure that only a single copy of *TerB* site was inserted. The sequences of the primers used to generate different constructs containing wild-type and various altered alleles of *Ter* sites are shown in Table 2.1.

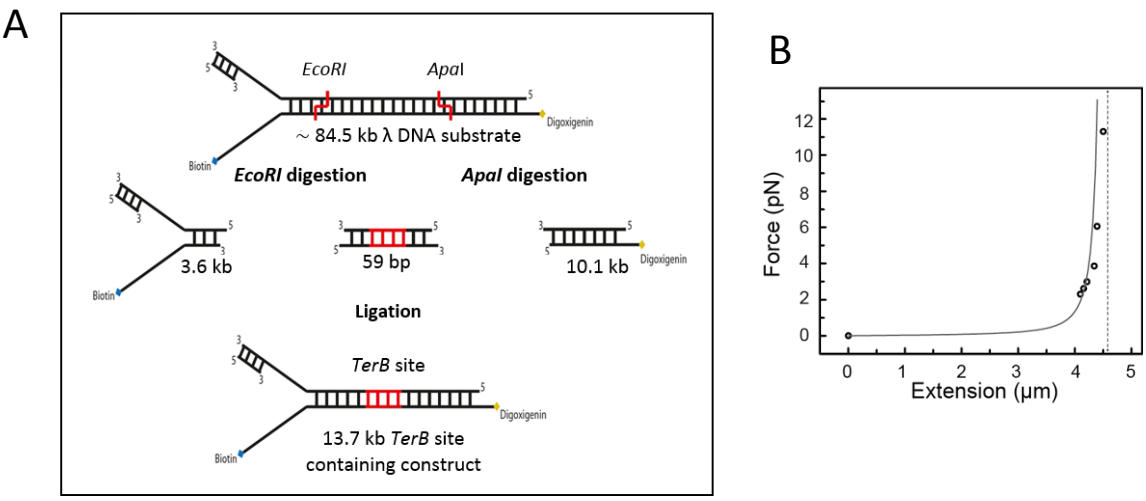

Figure 2.2: Constructing DNA templates containing termination (*Ter*) sites

A. Experimental strategy for constructing DNA templates containing *Ter* sites. λ-DNA molecules were digested by *EcoRI* and *ApaI* restriction enzymes to generate 3.6 and 10.1 (kb) fragments, respectively. The forked 3.6 kb fragment is ligated to a 59-basepair oligonucleotide containing *TerB* sequence. Excess unligated oligonucleotides are removed by running an agarose gel. The gel-purified 3.6 kb fragment containing a single-copy of *TerB* site is ligated to the 10.1 kb fragment, generating a 13.7 kb *TerB* site containing DNA construct for single-molecule leading-strand DNA synthesis experiments.
B. Force-extension curve of the 13.7 kb dsDNA substrate as a function of applied stretching force. The curve was constructed by measuring the length of individual DNA molecules at different stretching forces. The force was calculated based on the equipartition theorem equation[225]. The dashed vertical line at 4.6 µm represents the estimated crystallographic length of the 13.7 kb dsDNA substrate.

2.2.1.6 Force Calibration of the 13.7 kb DNA Construct

A force extension curve was plotted by measuring the length of the individual flow-stretched DNA molecules at different stretching forces. The exerted drag force was calculated using the equipartition theorem equation and according to the following formula[225,226]:

$$F = K_B T L / \langle \Delta X^2 \rangle$$

F is stretching force, K_B is Boltzmann constant, T is temperature in Kelvin, L is DNA length, $\langle \Delta X^2 \rangle$ is Mean Square Displacement (MSD). MSD was obtained from the Brownian motion of the bead in the transverse direction to the flow, and L was measured by reversing the flow direction and observing the position of the bead bound to the end of DNA molecules. The calculated force extension curve of the 13.7 kb substrate is shown in Figure 2.2B.

Fluctuation of the laminar flow during DNA synthesis will result in an error in estimating the length of the individual DNA molecules and consequently in determining the position of the *TerB* site. At an applied stretching force of 2.61 picoNewton (pN) (the force regime in our experiment), the standard error in force calculation from 7 DNA molecules was 0.21 pN. The conversion between ss- and ds-DNA at 2.4 and 2.8 pN, estimated from the force extension curve of λ- DNA (Figure 2.1D), are 3.85 and 3.67 nucleotide/nm, respectively. Therefore, the error in length measurement if the entire λ- DNA molecule was converted from ds- to ss-DNA was estimated to be ± 1.1 (kb), and consequently the error in defining the location of *TerB* at 3.6 kb relative to the site of fork assembly was reduced proportionally to ± 0.1 kb.

2.2.1.7 Data Acquisition and Processing

The experiments were performed at a stretching force of ~ 3 pN, which consists of the horizontal drag force against the bead exerted by the laminar flow and the vertical upward force exerted by the magnet. The beads were imaged with a Charge Coupling Device (CCD) camera (Q-imaging Rolera-XR) with a time resolution of 500 millisecond for an average acquisition time of 30 min. The centroid positions of the beads during each acquisition time point were determined by fitting 2-D Gaussian distributions of bead intensities using Diatrack particle-tracking software (Semasopht). The leading-strand DNA synthesis was monitored by relying on the difference in the elastic properties of ssDNA and dsDNA, which acquire different lengths at different applied stretching forces (Figure 2.1D). For data analysis, after particle tracking, the traces were corrected for residual instabilities in the flow by subtracting traces corresponding to tethered DNA molecules

that were not enzymatically altered. Displacements of the beads, due to the conversion of the lagging strand from ds- to ss-DNA during leading-strand synthesis, was converted into numbers of synthesized nucleotides using a conversion factor (3.76 b/nm) that was derived from the difference in the length between ss- and ds-DNA at the specified applied stretching force (Figure 2.1D) [226]. Fitting a linear regression of a single-molecule trace will report on the rate of the process, while the length of the DNA molecule from the start to the end of the shortening event will report on the processivity. Pausing of DNA synthesis represents points where a minimum of 3 s of no change in DNA length was detected. For increased accuracy and precision, rate and processivity distribution measurement from many traces were fitted with Gaussian and single exponential decay, respectively. Pausing of DNA synthesis represents points where a minimum of 3 s of no change in DNA length was detected.

2.2.1.8 Reconstitution of Bacteriophage T7 Leading-strand Synthesis at the Single-molecule Level

For continuous flow leading-strand DNA synthesis experiments, 20 nM gp4 (hexamer) helicase and 20 nM gp5/trx were continuously present in the flow cell in a replication buffer containing (40 mM Tris-HCl pH 7.5, 50 mM K-glutamate, 10 mM $MgCl_2$, 100 µg/ml BSA, 10 mM DTT, 600 µM dNTPs). For preassembly conditions, gp4 and gp5/trx proteins were assembled at the surface-anchored DNA molecules by flowing them at 5 nM and 40 nM respectively in a replication buffer containing (40 mM Tris-HCl pH 7.5, 50 mM K-glutamate, 100 µg/ml BSA, 10 mM DTT, 600 µM dNTPs). The excess proteins was washed with replication buffer and DNA synthesis was triggered by introducing $MgCl_2$ to the

replication buffer. Experiments were performed at 22˚C and at regime force of ~ 3 pN, as described in the section above.

2.2.1.9 Reconstitution of *E. coli* Leading-strand Synthesis at the Single-molecule Level

E. coli replication proteins were continuously present in the flow cell in the replication buffer (50 mM HEPES-KOH pH 7.9, 80 mM KCl, 12 mM $Mg(OAc)_2$, 2 mM $MgCl_2$, 5 mM DTT, 0.1 mg/mL BSA, 760 μM dNTPs, and 1 mM ATP) at concentrations of 30 nM clamp loader $\tau_3\delta\delta'\chi\psi$ 30 nM preassembled helicase/loader complex $DnaB_6$ $(DnaC)_6$, 30 nM clamp β_2, 60 nM core polymerase αεΘ, and fork restart proteins at 20 nM PriA, 40 nM PriB and 480 nM DnaT. Experiments were performed at 32˚C by placing a heater over the flow cell to maintain the temperature during the course of experiment. Data acquisition and processing were as described above.

2.2.2 Fluorescence Imaging of Single DNA Molecules for Monitoring Coordinated DNA Replication

This section describes control fluorescence-based DNA replication assays, results are not shown, used to assess the activity of the *E. coli* and T7 replisomes in a coordinated leading- and lagging-strand DNA synthesis in a rolling circle replication reaction of M13mp18 DNA template.

2.2.2.1 Constructing DNA Templates for Single-molecule M13 Rolling Circle Assay

A biotinylated-forked M13mp18 DNA rolling circle substrate was prepared as described previously[227,228]. Briefly, a biotinylated primer with 5' ssDNA overhang (Biotin- TTTTTTTTTTTTTTTTTTTTTTTTTTTTTTTTTTTTAATTCGTAATCATGGTCATAGCTGTTTCCT) was annealed to M13mp18 ssDNA. T7 DNA polymerase was used to extend the 3' end of the

primer and fully copy the M13mp18 ssDNA template by only one round of DNA synthesis. The reaction included 40 nM T7 DNA polymerase and 70 nM M13mp18 ssDNA and was carried out at 32˚C in a buffer containing (40 mM Tris-HCl pH 7.5, 50 mM K-glutamate, 10 mM $MgCl_2$, 100 µg/ml BSA, 10 mM DTT, 600 µM dNTPs). The biotinylated-forked M13mp18 DNA template was then purified by running through Amicon 50K centrifugal filter for DNA concentration (Millipore). The substrate was tethered to a streptavidin-coated coverslip at 0.5 nM in a buffer containing (20 mM Tris pH 7.5, 2 mM EDTA, 50 mM NaCl, 0.2 mg/mL BSA, 0.005% Tween-20), followed by washing the excess of unbound DNA molecules. M13mp18 DNA substrates were replicated extensively by continuous flowing of 20 nM gp4, 40nM gp5/trx and 1 µM gp2.5 in a buffer containing (40 mM Tris-HCl pH 7.5, 50 mM K-glutamate, 10 mM $MgCl_2$, 100 µg/ml BSA, 10 mM DTT, 600 µM dNTPs) at 22˚C (Figure 2.3). The experiment was performed in a mounted flow chamber constructed with a functionalized coverslip, adhesive tape and drilled glass slide; similar setup to what has been previously described for the flow stretching experiment.

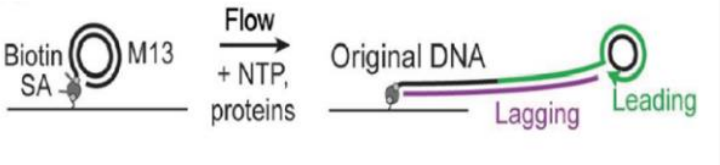

Figure 2.3: Single-molecule rolling-circle DNA replication assay

A schematic representation of single-molecule M13 rolling-circle replication assay. Leading strand synthesis is displaced from the circle as the replisome rolls around the template. The emerging DNA from the circle acts as a temple for lagging-strand synthesis. The replicated lagging strand increases in length as a function of time and extended by flow. The figure is adopted from[227].

2.2.2.2 Data Acquisition and Processing

The newly synthesized dsDNA is extended by laminar flow and stained using a Sytox Orange interchelating dye that specifically bind and stain dsDNA (Figure 2.3). A Total Internal Reflection Fluorescent (TIRF) microscope was used to image the stained DNA molecules. The Sytox Orange was excited continuously at 520 nm wavelength and fluorescence signal was collected using Electron Multiplying Charge Coupled Device (EMCCD) camera (Rolera-XR). Plotting kymographs for positions of the newly growing DNA end versus time enables the precise measurement for the rate of coordinated replication, while measuring the length of the completely replicated molecule reported on the processivity of the reaction; a dsDNA with known length is used to calibrate the length of the replicated molecule.

2.2.3 Imaging of Fluorescently Labeled Tus-GFP Bound to DNA

This section describes protocol used to track fluorescently-labeled Tus-GFP and flow stretched λ-DNA molecules, results are not shown. In this assay, fluorescently-labeled Tus-GFP protein molecules were imaged near the surface by introducing it into a flow cell containing many surface-anchored single-tethered λ-DNA molecules. A TIRF microscope was used to image single molecules of Tus-GFP by restricting the depth of illumination into an evanescent wave that is ~ 100 nm above the surface of the coverslip[229]. Tus-GFP was introduced to the flow chamber at 80 nM concentration in a buffer containing (20 mM Tris-HCl pH 7.6, 10 mM $MgCl_2$, 0.5 mM EDTA, 50 mM NaCl). Tus-GFP was excited continuously at 470 nm wavelength and fluorescence signal was collected on EMCCD camera. Tus-GFP binding displayed a strong salt dependency where apparent coating

filaments on the DNA was observed at low salt and well-resolved fluorescence spots were observed at higher salt. Tracking the movement of Tus-GFP on DNA on both X- and Y-directions was used to determine diffusion of Tus along the DNA.

Chapter 3

3. Replisome Speed Determines the Efficiency of the Tus–*Ter* Replication Termination Barrier*

3.1 Abstract

In all domains of life, DNA synthesis occurs bidirectionally from replication origins. Despite variable rates of replication fork progression, fork convergence often occurs at specific sites[1]. *Escherichia coli* sets a "replication fork trap" that allows the first arriving fork to enter but not to leave the terminus region[23,100,112,230]. The trap is set by oppositely oriented Tus-bound *Ter* sites that block forks on approach from only one direction[23,24,100,112,130]. However, the efficiency of fork blockage by Tus–*Ter* does not exceed 50% *in vivo* despite its apparent ability to almost permanently arrest replication forks in *vitro*[137,208]. Here we use data from single-molecule DNA replication assays and structural studies to show that both polarity and fork arrest efficiency are determined by a competition between rates of Tus displacement and rearrangement of Tus–*Ter* interactions that leads to blockage of slower moving replisomes by two distinct mechanisms. Thus we provide the first example where intrinsic differences in rates of individual replisomes have different biological outcomes.

---

*This chapter contains data published in "Mohamed M. Elshenawy, Slobodan Jergic, Zhi-Qiang Xu, Mohamed A. Sobhy, Masateru Takahashi, Aaron J. Oakley, Nicholas E. Dixon, Samir M. Hamdan. Replisome speed determines the efficiency of the Tus–*Ter* replication termination barrier. *Nature*. 2015 Sep. 17;525(7569)

3.2 Introduction

In the circular *E. coli* chromosome, two replication forks move from the replication origin to converge opposite in a region that contains ten 23-base pairs (bp) *Ter* (termination) sites and the *dif* site for chromosome segregation(Figure 3.1A)[23,24,100,112,130]. The *Ter* sites are arranged in two oppositely oriented groups[100,230], and each of them is tightly bound to the monomeric protein Tus[130,132]. The lack of symmetry in *Ter* sequences fixes the orientation of the Tus−*Ter* complex such that forks are blocked at its non-permissive (NP) face, but allowed to pass from the permissive (P) end[127,130]. The two *Ter* clusters thus form a trap from which the first arriving fork can enter but not leave, awaiting arrival of the other[23,100,112,230].

The mechanism determining polarity of Tus−*Ter* action serves as a model for communication between replication forks and double-stranded (ds) DNA-binding proteins, but it is also controversial. Strand separation by the DnaB helicase at the NP face can engineer a new structure, the “locked” complex of the mousetrap model (Figure 3.1B)[130]. Cytosine(6) of *Ter* flips out of the DNA helix to form new interactions in a pocket on Tus that markedly prolongs the lifetime (>40-fold) of the Tus−*Ter* complex, protecting the central interactions from the trailing polymerase. Conversely, strand separation at the P face rapidly dissociates Tus.

Despite the stability of the locked complex *in vitro*, at any sampling time in reporter plasmids *in vivo*, even when Tus is overproduced, ~ 50% of forks moving towards the NP face displace Tus[137,208]. This could be due either to the fork block being transient or to its

low efficiency of formation. The K_D of the Tus–*TerB* locked complex is only threefold lower than Tus–ds*TerB* while its lifetime is much longer[130], so we tested the hypothesis that the efficiency of lock formation is kinetically controlled, that is, that NP fork arrest efficiency is determined by competition between lock formation and Tus displacement, dependent on the rate of fork approach. Inherent inefficiency of fork arrest would also explain the presence of backup *Ter* sites in the chromosome.

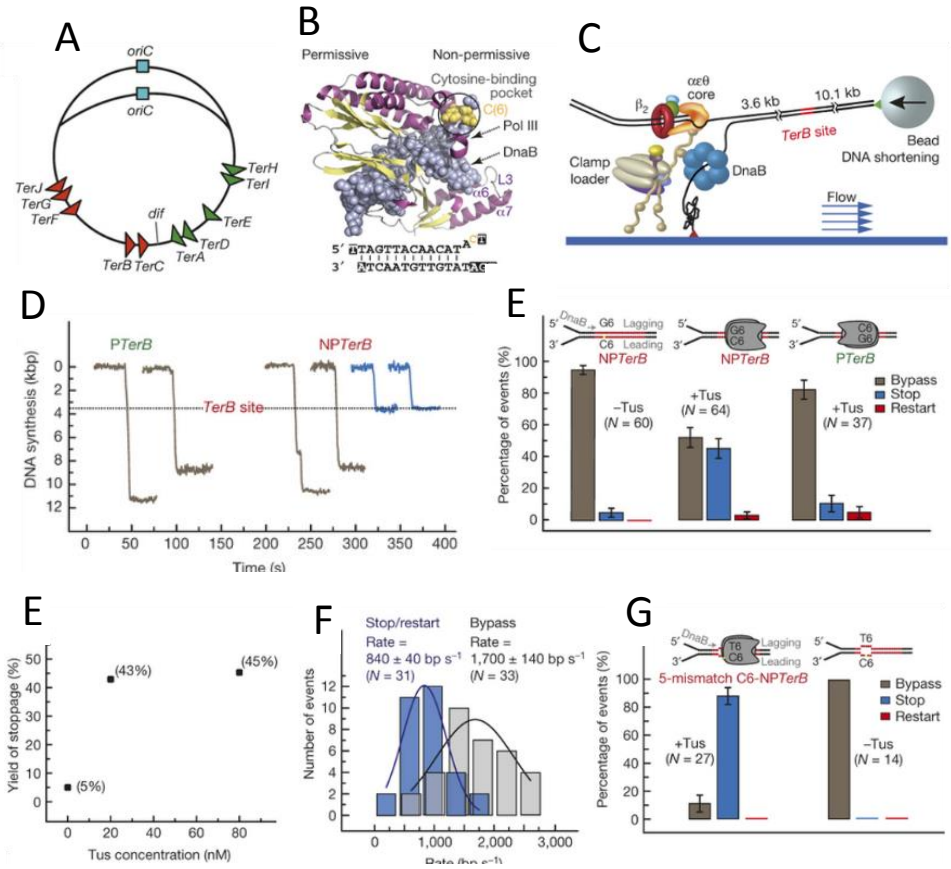

Figure 3.1: Fate of the *E. coli* replisome upon encountering Tus–*TerB*

A. Polarity of the replication fork trap. Replication occurs bidirectionally from a unique origin of replication (*oriC*). Each fork passes through the first five permissive (P) *Ter* sites, but is arrested on encounter with one of the next five non-permissive (NP) sites.
B. Structure of the Tus–*Ter* locked complex[130]. Strand separation of C6 (yellow) at the NP face induces its flipping into a specific binding pocket on Tus.
C. Schematic of the single-molecule setup for observing leading-strand synthesis, which converts the tethered double-stranded (dsDNA) (long) to single-stranded (ssDNA) (short), displacing the bead opposite the flow.
D. Representative synthesis trajectories upon encountering Tus–*TerB* oriented to the P (P*TerB*, left) or NP (NP*TerB*, right) faces.
E. Percentages of forks bypassed, transiently or fully stopped at the P or NP face. Error bars corresponds to standard deviations of binomial distributions; *N* = 60, 64 and 37 for NP*TerB* (−Tus), NP*TerB* (+Tus) and P*TerB* (+Tus), respectively.
F. Effect of Tus concentration on arrest activity at the NP face. Tus was present continuously with the replication proteins. Washing excess DNA-unbound Tus (80 nM) before introduction of replication proteins resulted in 38% stoppage.
G. Rate dependence of replication stalling at the NP face. Rate distributions of events that bypassed (grey; *N* = 33) or stopped/restarted (blue bars; *N* = 31) were fit with Gaussian distributions. Fit lines are shown; the uncertainty corresponds to the standard error.
H. Percentages of forks that bypassed, transiently or fully stopped at Tus bound to the NP*TerB* site containing a bubbled-DNA structure in place of base pairs (bps) 3−7 of *TerB*, while keeping C6 (5-mismatch C6-NP*TerB*). Error bars correspond to standard deviations of binomial distributions; *N* = 14 and 27 in absence and presence of Tus, respectively.

3.3 Results

We used single-molecule imaging to monitor the fate of the *E. coli* leading-strand replisome as it approaches Tus−*TerB* from either direction. Real-time synthesis trajectories were derived from multiplexed arrays by monitoring the length of individual DNA molecules[47,55,182]. The forked primer–template DNAs, each with a single *TerB* site 3.6 kilobase (kb) from the site of fork assembly, were tethered between the surface of a coverslip and a magnetic bead (Figure 3.1C and Figure 3.2A) and extended by a laminar flow exerting a 2.6 picoNewton (pN) drag force on the beads. The trajectories (Figure 3.1D) show DNA shortening through its conversion from dsDNA (long) to single-stranded (ss) DNA (short) during leading-strand synthesis. The position of *TerB* could be defined to ± 0.1 kb under this force regime (see the methods). Consistent with previous single-molecule studies of DNA replication[14,47,55,182,185], rates of DNA synthesis vary among replisomes (Figure 3.3), reflecting the *in vivo* situation[231]. Work using several *in vitro* single-molecule DNA replication assays has reported similar findings of a wide distribution in fork rates[47,55,182,185,227]. Furthermore, a Gaussian distribution of forks rates was also reported *in vivo*[231]. The underlying mechanism behind this heterogeneity in rates is unknown. The replisome is a multi-protein complex that is kinetically stabilized at the fork, but it is also dynamic, as is manifested in both its ability to exchange some of its components, including its replicative DNA polymerases, with those from solution and its reliance on a significant number of transient physical interactions to coordinate its various activities. It would be surprising, therefore, if every replisome would have and/or maintain these variables consistently to achieve a perfectly uniform rate. For example,

we recently characterized a weak interaction between the proofreading subunit of Pol III (ε) and its processivity clamp (β_2) that significantly increased both the rate and processivity of the *E. coli* replisome, and in another example, showed how the stoichiometry of DnaB helicase and its loader DnaC strongly influences rate and processivity of the replisome[55].

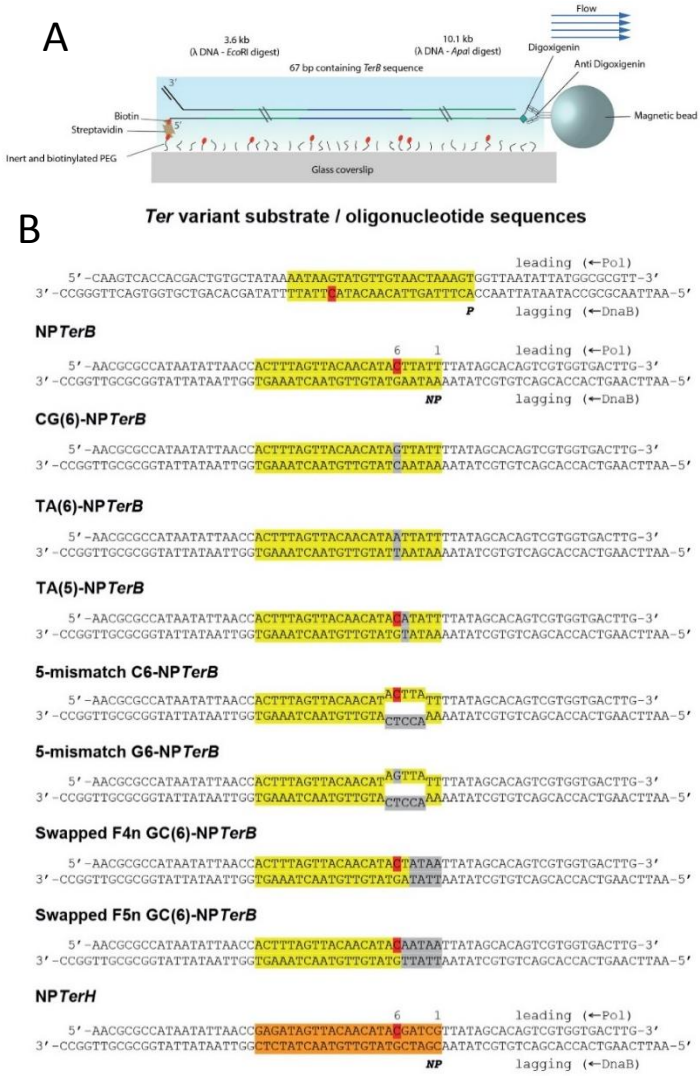

Figure 3.2: Setup for leading-strand replication assays

A. A schematic representation of the 13.7 kilo base (kb) DNA substrate construct. The substrate contains a biotinylated fork at one end to attach it to the streptavidin-coated glass coverslip and a digoxigenin moiety at the other end to attach it to a 2.8 µm diameter anti-digoxigenin-coated paramagnetic bead. A single insert of *TerB* site is located at 3.6 kb from the biotinylated fork.

B. Oligonucleotides used to assemble wild-type and variants of *TerB* substrates for their ligation to the 3.6 kb *EcoRI* and 10.1 kb *ApaI* λ-DNA fragments. Native *TerB* residues are highlighted in yellow except C6 that is in red. Non-native (modified) residues in *TerB* are highlighted in grey. Native *TerH* residues are highlighted in orange. Leading and lagging DNA strands as well as P and non-permissive NP faces of *Ter* when bound to Tus are denoted. Directionality of translocation of DnaB that encircles the lagging strand as it unwinds dsDNA during leading strand DNA synthesis by Pol III holoenzyme is denoted by arrows.

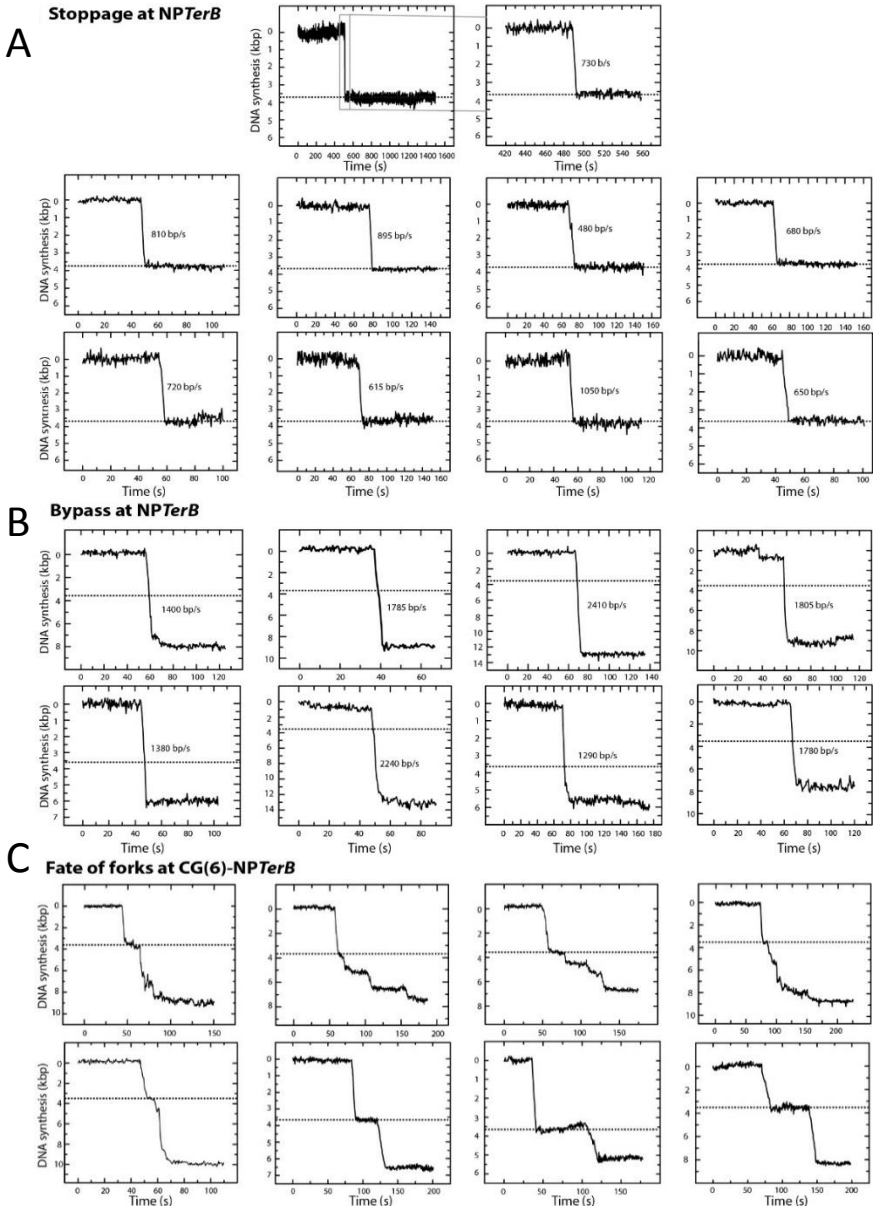

Figure 3.3: Examples of trajectories for leading-strand synthesis upon encountering Tus bound to NP *Ter* sites

The location of the *TerB* site at 3.6 ± 0.1 kb is indicated by the dashed lines. The rates of leading strand synthesis were calculated by fitting the slopes of the trajectories by linear regression using a least-squares approach. The replisomes displayed heterogeneity in rates of DNA synthesis.

A. Trajectories where forks stopped at the NP*TerB* site. The average stoppage time captured within our acquisition time was 9.7 ± 1 min (uncertainty is the standard error) as illustrated for the top trajectory.
B. Trajectories where forks displaced Tus and bypassed the NP*TerB* site without displaying any transient stoppage.
C. Fate of the replication fork upon encountering CG6-NP*TerB*. Examples of trajectories for leading-strand synthesis upon encountering Tus bound to CG6-NP*TerB* showing transient stoppage at CG6-NP*TerB*, followed by resumption of DNA synthesis; 56% of the restarted events displayed DNA synthesis with disrupted behavior (top row) while 44% showed normal behavior (bottom row). We attributed the disrupted restart of DNA synthesis in some of the trajectories to the replisome losing some components other than DnaB during stalling.

3.3.1 Setting and Monitoring Individual Traps

In the absence of Tus, 5 ± 3% of forks that reached the *TerB* site stopped there by chance (Table 3.1, Figure 3.1E, Figure 3.4A,B). DNA synthesis stops near the *TerB* site in the absence of Tus as a result of the randomness of processivity of DNA synthesis rather than any peculiar effect of the *TerB* sequence. This is confirmed by the random probability of termination of DNA synthesis at 0.2 kb intervals (spatial resolution of the assay) along the 13.7 kb substrate in the absence of Tus (Figure 3.4A) and the fact that processivity of DNA synthesis followed a single exponential decay distribution (Figure 3.4B). In our data analysis, we ignored events where DNA synthesis stopped before reaching the *TerB* site; i.e. the total number of events (summing to 100%) corresponds only to those that reached or passed the *TerB* site, with or without pausing. The processivity of DNA synthesis was 5.5 ± 1.2 kb on these short DNA constructs (Figure 3.4B); the DNA shortening trajectories in these assays are only observed when both dNTPs and Pol III are present[47,55]. The probability of stoppage would therefore decrease from 5% to 3% if we were to include events that did not reach the *TerB* site (Figure 3.4A). With Tus−*TerB* oriented with its P face towards the fork (P*TerB*), this frequency increased to 11 ± 5% (including the 5% random stoppage), presumably owing to forks encountering a strong protein–DNA roadblock (Figure 3.1E). The interactions of Tus with *Ter* are asymmetric − they are more intensive with the leading strand on the P face and with the lagging strand on the NP face. In a supportive study[232] discussed in the following chapter, we showed using the heterologous T7 replication system that these asymmetric interactions act in a differential manner in stopping the polymerase and the helicase. The T7 helicase and T7 replisome

are stopped more effectively at the NP face while the T7 polymerase is stopped more effectively at the P face. Nonetheless, consistent with our findings in the *E. coli* system, we also observed residual permanent stoppage of the T7 replisome at the P face. Furthermore, our results on the *E. coli* replisome also showed that the clasping mechanism at the P face acts in a dynamic manner since we observed that slower moving replisomes tend to stop more frequently than faster ones at the P face (Table 3.1). Transient stoppage followed by resumption of synthesis occurred in 5% of trajectories, and in the remaining 84% of replication forks displaced Tus and continued synthesis without stopping, even transiently (Figure 3.1D,E). The average rate of DNA synthesis was otherwise unaffected by Tus (Figure 3.4C).

In contrast, when the fork approached the NP face (NP*TerB*), permanent stoppage (9.7 ± 1 min) of DNA synthesis occurred in 45% of trajectories, and restart in only 3% (Figure 3.1D,E and Figure 3.3A,B). The remaining 52% showed no sign even of transient stoppage. All *TerB* sites were Tus-bound under our experimental conditions (Figure 3.1F), indicating they have an inherently low efficiency of fork arrest. We are thus able for the first time to distinguish between the two different mechanisms that could explain the *in vivo* data[137,208].

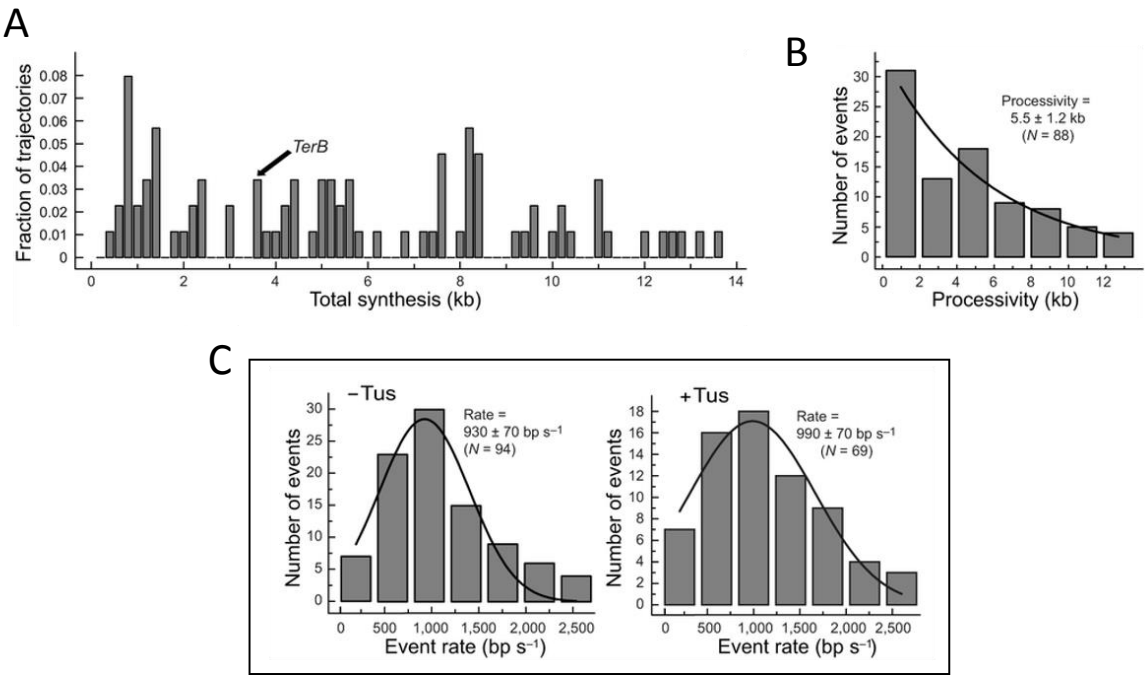

Figure 3.4: Effect of *TerB* site alone and nonspecifically DNA-bound Tus on DNA synthesis

A. Probability of termination of DNA synthesis at 0.2 kb intervals (spatial resolution of the assay) along the 13.7 kb NP*TerB* in the absence of Tus, showing stops at *TerB* (3.5–3.7 kb, denoted by black arrow) occur randomly with a 3% probability when all events were considered, in contrast to 5% when only events that reached *TerB* (≥ 3.5 kb) were taken into account.

B. Processivity of DNA synthesis on the NP*TerB* substrate in the absence of Tus. The processivity distribution is fit with an exponential decay (*N* = 88) and uncertainty corresponds to the standard error, illustrating the random stoppage behavior of the replisome during synthesis.

C. Rate of leading strand synthesis using the 13.7 kb force-calibrated DNA construct (NP*TerB* in this case) in the absence (left panel; *N* = 94) or presence of Tus (right panel; *N* = 69). The rate distributions were fit with a Gaussian distribution. The fit lines are shown and the uncertainties correspond to the standard error. The rate agrees with our previously reported rate using force-calibrated λ-DNA constructs[55], demonstrating the accurate force calibration of the 13.7 kb substrate.

Ter 5′-AATAAGTATGTTGTAACTAAAGT P NP TTATTCATACAACATTGATTTCA-5′	Tus	Stop (%)	Bypass (%)	Restart (%)	Pause time (s)	Stop/restart rate (bp s^{-1})	Bypass rate (bp s^{-1})
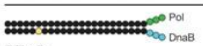 PTerB	WT Tus	11 ± 5	84 ± 6	5 ± 4	31 ± 24	330 ± 30	1,300 ± 110 (1,250 ± 120)
 NPTerB [GC(6)-NPTerB]	No Tus	5 ± 3	95 ± 3	0	–	800 ± 100	1,160 ± 70 (930 ± 70)
	WT Tus	45 ± 6	52 ± 6	3 ± 2	146 ± 31	890 ± 70 (840 ± 40)	1,690 ± 100 (1,700 ± 140)
	H144A	27 ± 8	55 ± 9	18 ± 7	33 ± 5	840 ± 120 (740 ± 10)	1,520 ± 130 (1,520 ± 120)
	R198A*	5 ± 5	77 ± 9	18 ± 8	14 ± 4	400 ± 40	1,300 ± 140 (1,310 ± 70)
 CG(6)-NPTerB	WT Tus	8 ± 4	47 ± 8	45 ± 8	29 ± 6 (37 ± 6)	820 ± 70 (720 ± 80)	1,810 ± 110 (1,740 ± 60)
	WT Tus†	18 ± 9	41 ± 11	41 ± 11	56 ± 13	800 ± 80 (790 ± 70)	1,820 ± 180
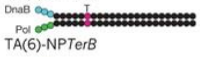 TA(6)-NPTerB	WT Tus	7 ± 4	73 ± 7	20 ± 6	22 ± 5 (24 ± 2)	380 ± 60 (360 ± 40)	1,350 ± 110 (1,310 ± 50)
 5-mismatch C6-NPTerB	WT Tus	89 ± 6	11 ± 6	0	–	1160 ± 130 (1030 ± 130)	1,230 ± 310
	R198A*	86 ± 7	14 ± 7	0	–	1130 ± 120 (950 ± 170)	1,200 ± 270
 5-mismatch G6-NPTerB	WT Tus	8 ± 5	15 ± 7	77 ± 8	111 ± 18 (177 ± 20)	1130 ± 140 (960 ± 170)	1,230 ± 170
 TA(5)-NPTerB	WT Tus	32 ± 9	68 ± 9	0	–	390 ± 70 (360 ± 40)	1,480 ± 140 (1,320 ± 60)
 Swapped F4n GC(6)-NPTerB	WT Tus	41 ± 9	59 ± 9	0	–	880 ± 110 (860 ± 90)	1,480 ± 120 (1,550 ± 110)
 Swapped F5n GC(6)-NPTerB	WT Tus	22 ± 7	75 ± 7	3 ± 3	186	400 ± 60 (310 ± 70)	1,260 ± 100 (1,260 ± 60)
 NPTerH	WT Tus	19 ± 6	70 ± 8	11 ± 5	180 ± 26	400 ± 60 (350 ± 20)	1,320 ± 100 (1,300 ± 60)

Table 3.1: Fate of replisomes and fork rate dependencies of events at Tus-bound *Ter* sites

The *TerB* site and its alterations are depicted in cartoon with the native nucleotides in black except that C6 is in yellow and substituted nucleotides are in magenta. The directionality of the replication fork is shown with the strands on which Pol III holoenzyme and DnaB translocate. The nucleotides in native *TerH* that differ from *TerB* are also shown in magenta. The sequences of oligonucleotides used to assemble the variants of *TerB* substrates are given in Figure 3.2B. Stop, bypass and restart events were quantified as a percentage of all events that reached or bypassed *TerB*, as described in the methods. Uncertainties correspond to standard deviations of binomial distributions. The mean of the rates and pause durations are shown either as their arithmetic averages or, in parentheses, by fitting their histograms with Gaussian or exponential decay distributions, respectively (see Figure 3.6A and Methods). The uncertainties correspond to standard errors. Each experimental condition represents results from three or four technical replicates and the number of derived molecules (N) is specified in the corresponding figures.

*Concentration of Tus(R198A) was 250 nM versus the standard 80 nM.

† Reaction from which the restart proteins PriA, PriB and DnaT were omitted.

3.3.2 Faster Forks Avoid the Trap

Fork arrest is attenuated *in vivo* by DNA supercoiling, suggesting that it is affected by the rate of strand separation[208]. To test this proposition, we separated the trajectories that showed full or transient stoppage from those that did not and found the rate of DNA synthesis and fork bypass were correlated (r = 0.62; Figure 3.5A); fast forks were arrested less often than slower ones. In fact, there was a twofold difference in average rates of synthesis at forks that stopped and those that bypassed *TerB* (Figure 3.1G). DNA synthesis at individual forks before stoppage at *TerB*, or in full trajectories where they bypassed it, progressed at nearly constant rates under our spatial and temporal resolution (Figure 3.5B-E). As we showed previously[55], the overall average rate reproduces the average *in vivo* rate ($\sim$ 950 bp s^{-1})[231]. This underscores the importance of our ability to achieve the *in vivo* rate of DNA synthesis to reproduce the $\sim$ 50% efficiency of fork arrest *in vivo*.

The rate dependence of stoppage supports the hypothesis that strand separation competes with inefficient C6-flipping. To demonstrate this, we pre-formed the locked complex before replisome assembly using *TerB* with a mismatched bubble in place of bps 3-7 while keeping an unpaired C6 (Figure 3.1H and Table 3.1)[130]. The yield of fork arrest increased to 89%; thus, once the lock is established, it is a very effective fork block.

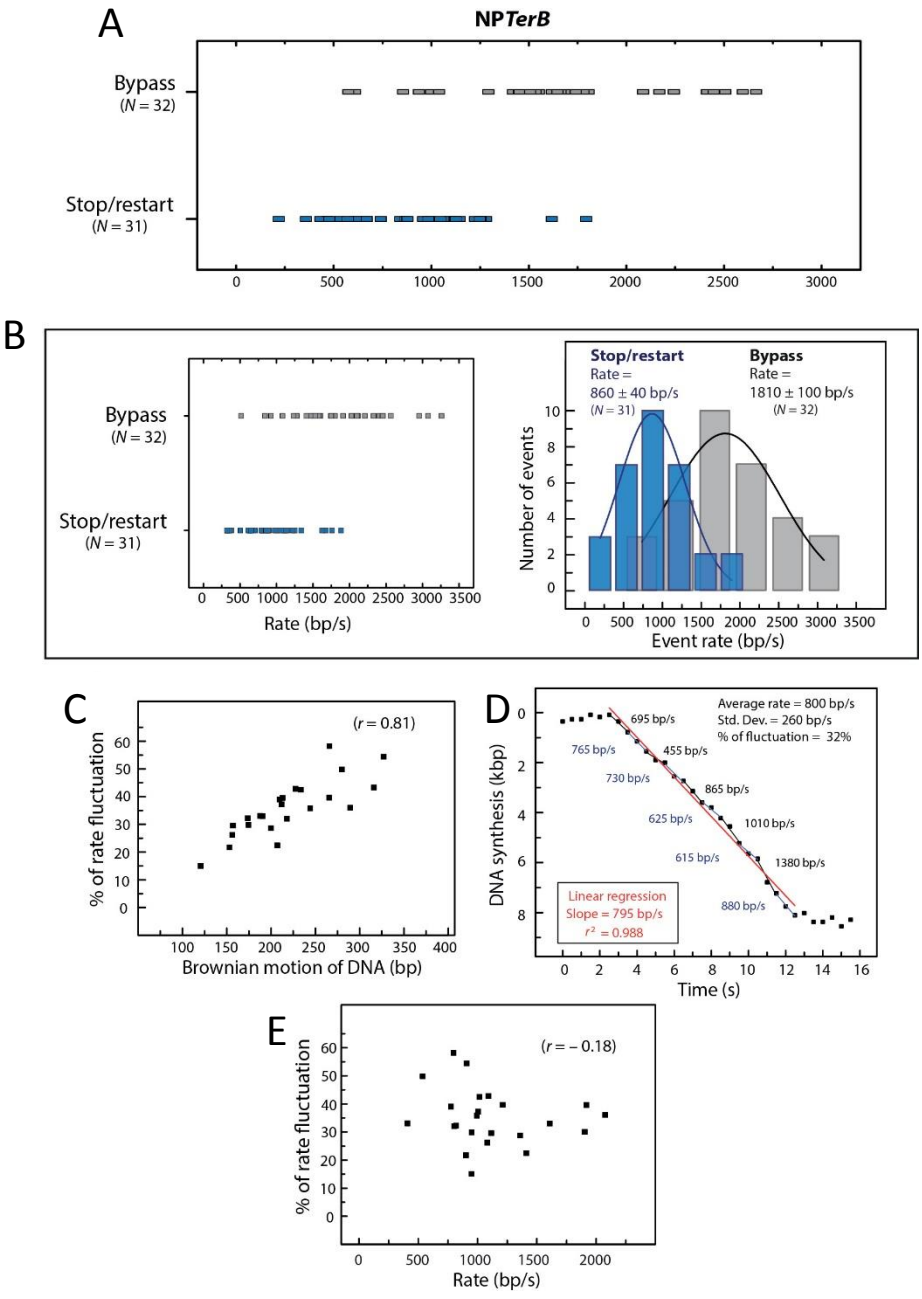

Figure 3.5: Linear fitting of the rate of leading-strand synthesis is appropriate for deriving the correlation between rate of DNA synthesis and stalling activity at the NP *TerB* site

A. Rate dependence of fork arrest at NP*TerB.* A scatter plot of forks that stopped (*N* = 31) or bypassed (*N* = 32) Tus bound to NP*TerB*; rates were calculated by fitting the DNA shortening phase of the entire trajectory in cases of events that bypassed and up to the stoppage point in events that stopped/restarted (histograms are shown in Figure 3.1gG). A significant correlation between fork progression rate and fork bypass at NP*TerB* is observed using a one sided Pearson's correlation test at the 0.05 level of significance (the calculated correlation coefficient (*r*) was 0.62). The Pearson's correlation coefficient was calculated using the equation:

$$r = \frac{\sum_{i=1}^{n}(x_i - \bar{x})\left(y_i - \bar{y}\right)}{\sqrt{[\sum_{i=1}^{n}(x_i - \bar{x})^2][\sum_{i=1}^{n}\left(y_i - \bar{y}\right)^2]}}$$

B. Scatter plot (top panel) and rate distributions (bottom left panel) of leading-strand synthesis for events that bypassed (grey bars) (*N* = 32) or stopped/restarted (blue bars) (*N* = 31) at NP*TerB* when the rate was estimated from fitting the slope of the three data points before the *TerB* site (acquisition time is 0.5 s per data point). The rates were fit with a Gaussian distribution and uncertainty corresponds to the standard error. The calculated average rates for events that bypassed or stopped/restarted at NP*TerB* are similar to those calculated when the rates were fit using the DNA shortening phase of the entire trajectory in cases of events that bypassed and up to the stoppage point in events that stopped/restarted (see Figure 3.1G), underscoring the suitability of linear fitting of the rate.

C. The correlation between apparent fluctuation in rate of DNA synthesis within individual DNA molecules and their corresponding Brownian motion (*N* = 23). The percentage of apparent fluctuation in rate of individual DNA molecules displayed a strong positive correlation with their corresponding Brownian motion when analysed by two-sided Pearson's correlation test at the 0.05 level of significance (*r* = 0.81).

D. r^2 from linear regression fits was 0.95 ± 0.05. Individual trajectories displayed apparent fluctuation in rate of DNA synthesis as illustrated in a representative trajectory where we zoomed in at the DNA shortening phase and fit the rate linearly to intervals of three consecutive data points. The percentage of apparent fluctuation in rate of DNA synthesis within individual DNA molecules was calculated by dividing the standard deviation of the average of interval rates over the average rate. The standard deviation of the average of Brownian motion of each individual DNA molecule was calculated from the fluctuation of the DNA before and after being replicated.

E. The correlation between the percentage of apparent fluctuation in rate and the average rate of individual molecules. The percentage of apparent fluctuation in rate of individual molecules for the same 23 replisomes. There was no correlation between the average rate of individual DNA molecules and their corresponding percentage of apparent fluctuation in rate; the Pearson's correlation coefficient was –0.18. These results demonstrate that one strong factor behind the apparent fluctuation in rates within our individual 13.7 kb molecules under our spatial and temporal resolution is the Brownian motion of the DNA and that this apparent fluctuation in rate does not bias the estimates of speed of the replisomes.

3.3.3 How the Trap is Triggered

We next interrogated the role of lock formation with C6-defective *TerB* mutants[130]. Surprisingly, the GC6 to CG substitution did not lead to ~ 95% bypass. Instead, it resulted in transient (for 37 ± 6 s) rather than permanent blockage, again in ~ 50% of trajectories (Figure 3.6A,B and Figure 3.3C). Moreover, the fork rate dependence of pausing was similar to the normal lock (Figure 3.6C). DnaB remained at the fork during transient arrest since DNA synthesis could restart in the absence of helicase reloading proteins (Table 3.1). The crystal structure of a Tus complex with a forked *Ter* containing an unpaired G

replacing C6 showed that the substituted G6 base neither bound in the cytosine pocket nor formed any new specific interaction with Tus (Figure 3.6D and Table 3.2). This remained the case even when the fork was extended to also disrupt the TA7 bp (Figure 3.7A-C). Thus the fork-rate-dependent step producing transient stoppage must precede engagement of C6 in its binding pocket.

In the Tus crystal structures, the α6/L3/α7 region has extensive interactions with the lagging strand (Figure 3.1B) before and after C6-lock formation[127,130], providing a paradox about how the lagging-strand-translocating DnaB in fast-approaching replisomes disrupts these interactions without even pausing. The main sequence-specific contact this region makes with the first 6 bps of ds*Ter* are *via* Arg198 in L3 with the A5 and G6 bases on the lagging strand and T5 on the leading strand (Figure 3.7E)[127], but these interactions are not present in the locked complex, where Arg198 makes a new salt bridge to the phosphate between lagging strand nucleotides 6 and 7 (Figure 3.7A)[130]. We suggest that the Arg198 side chain forms transient interactions with G6, the TA5 bp and the lagging-strand phosphate, holding the two DNA strands together before strand separation reaches GC6 (Figure 3.7E). Moreover, comparison of the structures of Tus with the wild-type[127] and CG6 mutant ds*Ter* sites (Table 3.2) suggests rearrangement of lagging strand interactions with Arg198 (Figure 3.7E,F). We propose that Arg198–DNA contacts rearrange substantially during strand separation. This provides a window of opportunity for the fast-moving DnaB to break into the Tus−*Ter* central interactions before Arg198 rearrangement or C6 base flipping occurs.

To test this proposition, we used a bubble substrate with altered C6 (5-mismatch G6-NP*TerB*) to eliminate lock formation[6] but allow rearrangement of interactions on the separated strands before arrival of DnaB. We observed efficient transient stoppage that reached 77% with a long duration of 177 ± 20 s (Figure 3.6E and Figure 3.8). The fivefold increase in pause duration compared to CG(6)-NP*TerB* (Table 3.1) is probably owing to the interactions of the unpaired seventh nucleotide as in the locked complex structure[130]. Thus, strand separation beyond GC6 in the absence of the C6 lock would impose only transient fork stoppage.

We next altered A5 and T5 alone and in the context of the first 5 bps of *TerB* (Table 3.1); this resulted in the largest decrease in yield of stoppage and shift in the rate-dependence of arrest to lower values, underscoring that A5 and/or T5 are the primary contributors in this region to the rate dependence (Figure 3.9A-C). To investigate the effect of A5 and T5 of *TerB* on fork arrest activity, we altered them alone and within the context of the first five bps of *TerB*. When AT5 was swapped to TA5 (in TA(5)-NP*TerB*), the yield of stoppage reduced to 32% and the range of rate-dependent fork arrest shifted to lower values (Table 3.1 and Figure 3.9A). The first four bps make unidentified contacts with Tus that contribute to a 7-fold reduction in K_D of the Tus−*TerB* complex when unpaired, suggesting that they impose an energy barrier to DnaB's strand separation activity[130]. Swapping the first four bps (swapped F4n GC(6)-NP*TerB*) versus the first five (swapped F5n GC(6)-NP*TerB*) showed a minor accumulative effect for melting the first four bps (Table 3.1 and Figure 3.9B,C); the primary contribution by the first five bps of *Ter* to rate-dependent fork arrest thus comes from A5 and/or T5. AT5 is conserved in strong *Ter* sites but not at

weaker ones like *TerH*[137]. We also found that the NP Tus−*TerH* complex stops the forks with a similarly low rate dependence to TA(5)-NP*TerB* (Table 1). However, one-third of the stopped forks restarted synthesis after a pause of 180 ± 26 s (Figure 3.9G,H), which we attribute to other alterations in *TerH* that weaken its binding in its locked form[129].

Substitution of wild-type GC6 with CG has a modest effect on Tus binding to ds*TerB* in comparison to an AT or TA[100]. We observed that, relative to CG(6)-NP*TerB*, the TA substitution resulted in transient fork stoppage with decreased yield (Table 3.1, Figure 3.6A-C, Figure 3.9D-F), demonstrating the importance of the specific interaction of Tus with the native G6 for transient stoppage.

We then altered Arg198 itself. The R198A mutant interacts with ds*TerB* with a 140-fold increased K_D, but only a 2-folds shorter lifetime[101]. We showed by surface plasmon resonance (SPR) that R198A can form a lock (Figure 3.10A-D), but it was very defective in fork arrest (Table 3.1); stoppage was inefficient (18%) and transient (pauses of 14 ± 4 s; N = 4). Nevertheless, preforming the locked complex with R198A on the 5-mismatch C6-NP*TerB* substrate restored efficient stoppage (Table 3.1), consistent with lock formation. These results suggest that C6 flipping cannot occur unless Arg198 interactions slow down or transiently stop the fork beforehand.

So we have by now revealed two separate processes, one leading to a transient stoppage preceding but probably on the pathway to C6 lock formation, and one that leads directly to bypass and Tus dissociation. Previous results have suggested the operation of an uncharacterized C6-lock-independent arrest mechanism[100,145]. Our study shows that this

mechanism must be invoked before or as GC6 is melted, because permanent stoppage was not achieved when the GC6 was melted in the absence of the C6 lock (Figure 3.6E).

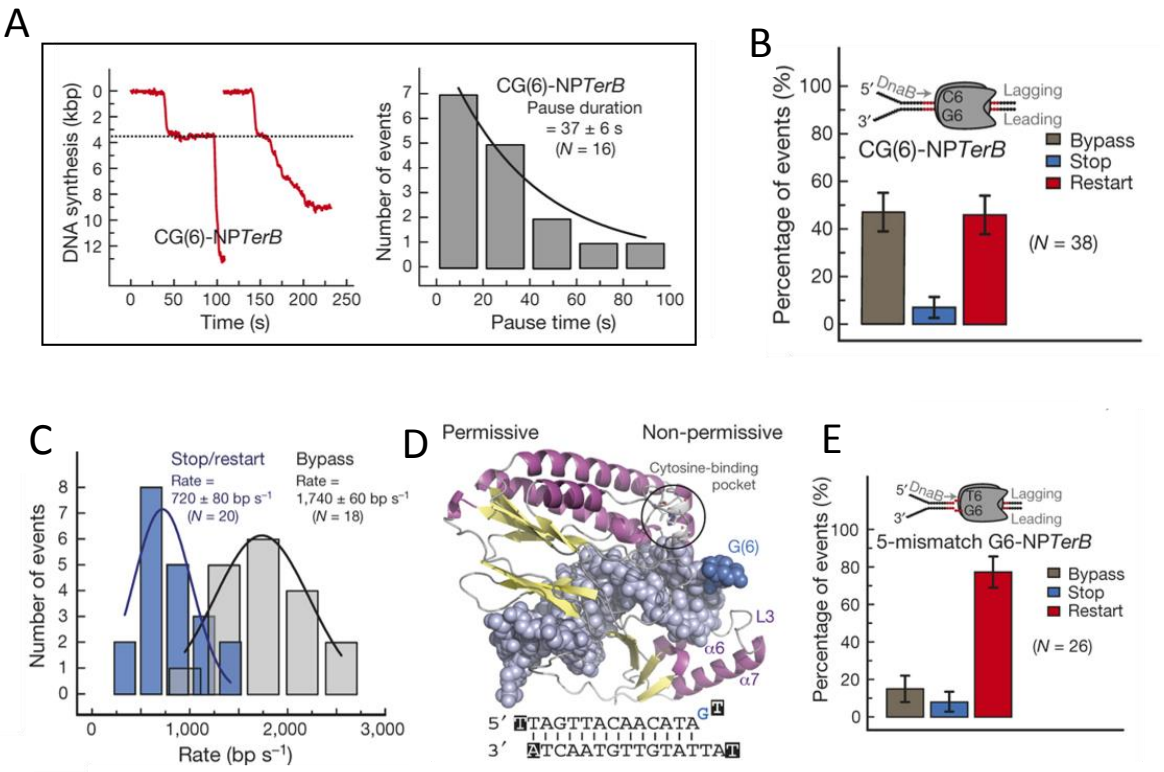

Figure 3.6: Characterization of transient stoppage of the replication fork at the NP face of Tus–*TerB* before C6 base flipping

A. Representative trajectories of restart of DNA synthesis after transient stoppage at a Tus-bound *TerB* site where the GC6 bp was swapped to CG6 (CG(6)-NP*TerB*). The distribution of pause durations was fit with a single exponential decay; the fit line is shown and uncertainty corresponds to the standard error (*N* = 16).

B. Percentages of the populations of replication forks that bypassed, transiently stopped or fully stopped at CG(6)-NP*TerB*. Error bars correspond to standard deviations of binomial distributions (*N* = 38).

C. Rate dependence of replication restart at CG(6)-NP*TerB.* The rate distribution of leading-strand synthesis for events that bypassed (grey; *N* = 18) or stopped/restarted (blue bars; *N* = 20) at CG(6)-NP*TerB* are presented as in Figure 3.1G.

D. Crystal structure of Tus with a forked *Ter* sequence that has a substituted G base in the C6 position in the locked complex (see Figure 3.7B) (PDB code: 4XR0). The G base, highlighted in blue, was neither docked into the cytosine-binding pocket nor forming any new interactions with Tus. Highlighted nucleotides (at bottom) were not visible in the structure.

D. Fates of replication forks at Tus bound to the *NP* face of a *TerB* site containing a bubbled-DNA structure in place of bps 3−7 in *TerB* and with G replacing C6 (5-mismatch G6-NP*TerB*). Error bars correspond to standard deviations of binomial distributions (N = 26).

	wt Tus / forked *Ter*-UGLT [C6 to G mutant]	wt Tus / forked *Ter*-TGTA [C6 to G, T7 to A mutant]	Tus(H144A) / wt forked *Ter*	wt Tus / ds*Ter*-UGLC [GC(6) to CG(6) mutant]
Data collection				
Space group	$P4_12_12$	$P4_12_12$	$P4_12_12$	$P4_12_12$
Cell dimensions				
a, *b*, *c* (Å)	64.5, 64.5, 248.3	64.8, 64.8, 246.7	64.5, 64.5, 250.9	64.1, 64.1, 249.3
α, β, γ (°)	90, 90, 90	90, 90, 90	90, 90, 90	90, 90, 90
Resolution (Å)	75–2.80 (2.90–2.80)	75–2.40 (2.50–2.40)	75–2.35 (2.43–2.35)	75–2.70 (2.80-2.70)
R_{sym}	11.1 (74.0)	12.0 (71.1)	8.0 (85.6)	10.6 (84.1)
$I/\sigma I$	39.5 (6.6)	24.0 (3.3)	26.7 (2.0)	27.2 (3.6)
Completeness (%)	99.8 (99.6)	99.9 (100)	99.6 (100)	99.8 (100)
Redundancy	22.1 (18.9)	9.7 (10.8)	6.6 (7.5)	13.6 (13.4)
Refinement				
Resolution (Å)	45–2.80 (2.86–2.80)	63–2.40 (2.46–2.40)	62–2.35 (2.41–2.35)	62–2.70 (2.77–2.70)
No. reflections	12,822 (901)	20,288 (1,521)	21,819 (1,658)	14,304 (1,086)
R_{work} / R_{free}	21.7 / 29.6	19.8 / 26.9	22.0 / 26.6	20.7 / 28.4
No. atoms				
Protein	2,504	2,530	2,509	2,503
Nucleic acid	577	574	592	612
Ligand/ion	13	14	14	12
Water	31	96	69	32
B-factors				
Protein	25.3	43.3	39.3	61.3
Nucleic acid	26.5	45.1	38.4	57.4
Ligand/ion	28.7	50.3	58.1	61.4
Water	35.7	57.2	48.1	61.3
R.m.s deviations				
Bond lengths (Å)	0.016	0.017	0.013	0.013
Bond angles (°)	2.16	2.13	1.71	1.97

Table 3.2: Data collection and refinement statistics for Tus–*Ter* complexes

A single crystal was used in each case.

Numbers in parentheses refer to the highest resolution bin.

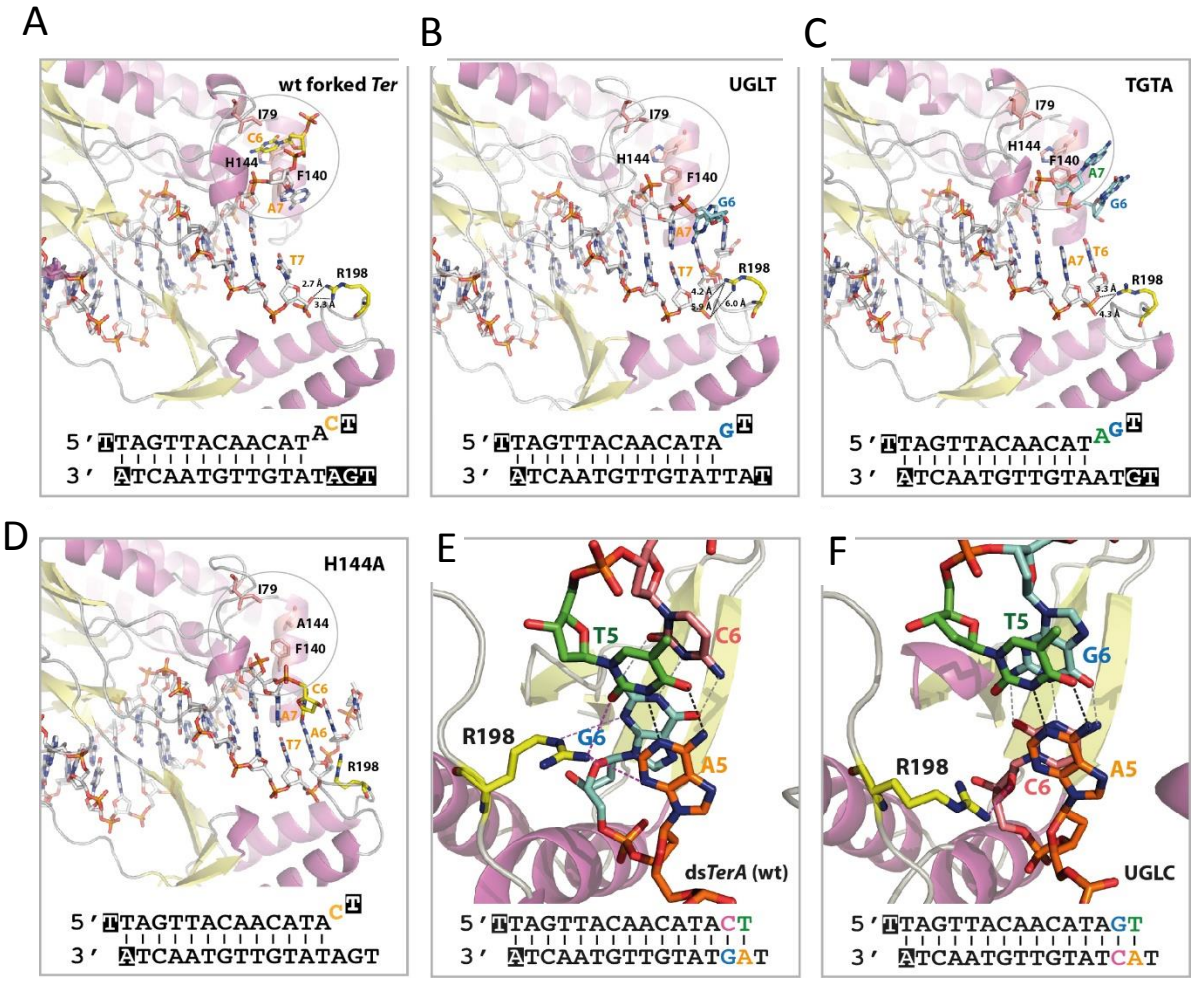

Figure 3.7: Crystal structures of Tus complexes with *Ter* oligonucleotides

The sequences of oligonucleotides used for each complex are shown at the bottom of each panel; nucleotides for which electron density could not be interpreted are highlighted. **A–D**, Complexes of Tus proteins with forked *Ter* sites. The C6-binding pocket is shown in the circle, with key residues Ile79, Phe140 and His144 in the binding pocket, and Arg198 shown in stick form. **A**, The wild-type Tus–*Ter* lock[144], with C6 located in the binding pocket, and the TA7 bp melted. Arg198 is positioned to interact with the 5′-phosphate of T7. **B**, Complex of wild-type Tus with a forked oligonucleotide that has C6 substituted by a mispaired G (UGLT: upper G, lower T; PDB code: 4XR0); G6 does not occupy the pocket nor does it make any new specific interactions with Tus, and Arg198 no longer interacts with the 5′-phosphate of T7.

C, Further extension of the mismatched region in **B** to include A7 (TGTA: mispaired TGTA on the lower strand; PDB code: 4XR1) does not enable G6 to occupy the C6-binding pocket or form any new specific interactions. **D**, Tus(H144A) in complex with the normal Tus–*Ter* lock oligonucleotide (PDB code: 4XR2), showing the mispaired C6 does not occupy the cytosine-binding pocket or form any new interactions with Tus.**E**, **F**, Potential interactions of Arg198 in crystal structures of Tus complexes with fully base-paired *Ter* oligonucleotides. Only nucleotides in bps 5 and 6 are shown, and they are color-coded to match the stick representations of them in the figures. Arg198 is shown in yellow stick representation. **E**, Structure of the wild-type Tus–*TerA* (GC6) complex. Arg198 is positioned potentially to make H-bonding interactions with the A5, G6 and T5 bases and the deoxyribose ring oxygen of G6, as well as electrostatic interactions with the 5'-phosphate of A5, as suggested previously[144] and demonstrated by molecular dynamics simulations (unpublished observations). **F**, Structure of the complex with a GC6-flipped version of the *TerA* oligonucleotide (UGLC: upper G, lower C; PDB code: 4XR3) showing an alternate major conformation of the Arg198 side-chain that has lost all base-specific interactions; only the interaction with the sugar ring oxygen of the substituted C6 is maintained.

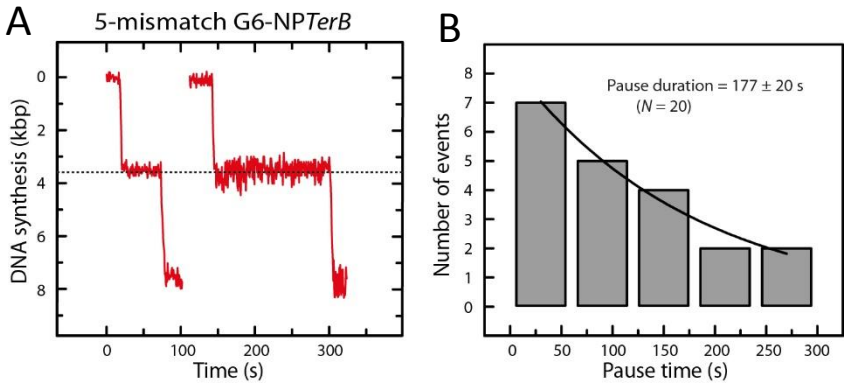

Figure 3.8: Fate of the replication fork upon encountering 5-mismatch G(6)-NP*TerB*

A. Examples of trajectories of replication forks that transiently stopped at Tus bound to the bubble template with C6 switched to G6 (5-mismatch G6-NP*TerB*).

B. The distribution of the pause durations fit with a single exponential decay. The fit line is shown in black and the uncertainty corresponds to the standard error (*N*= 20).

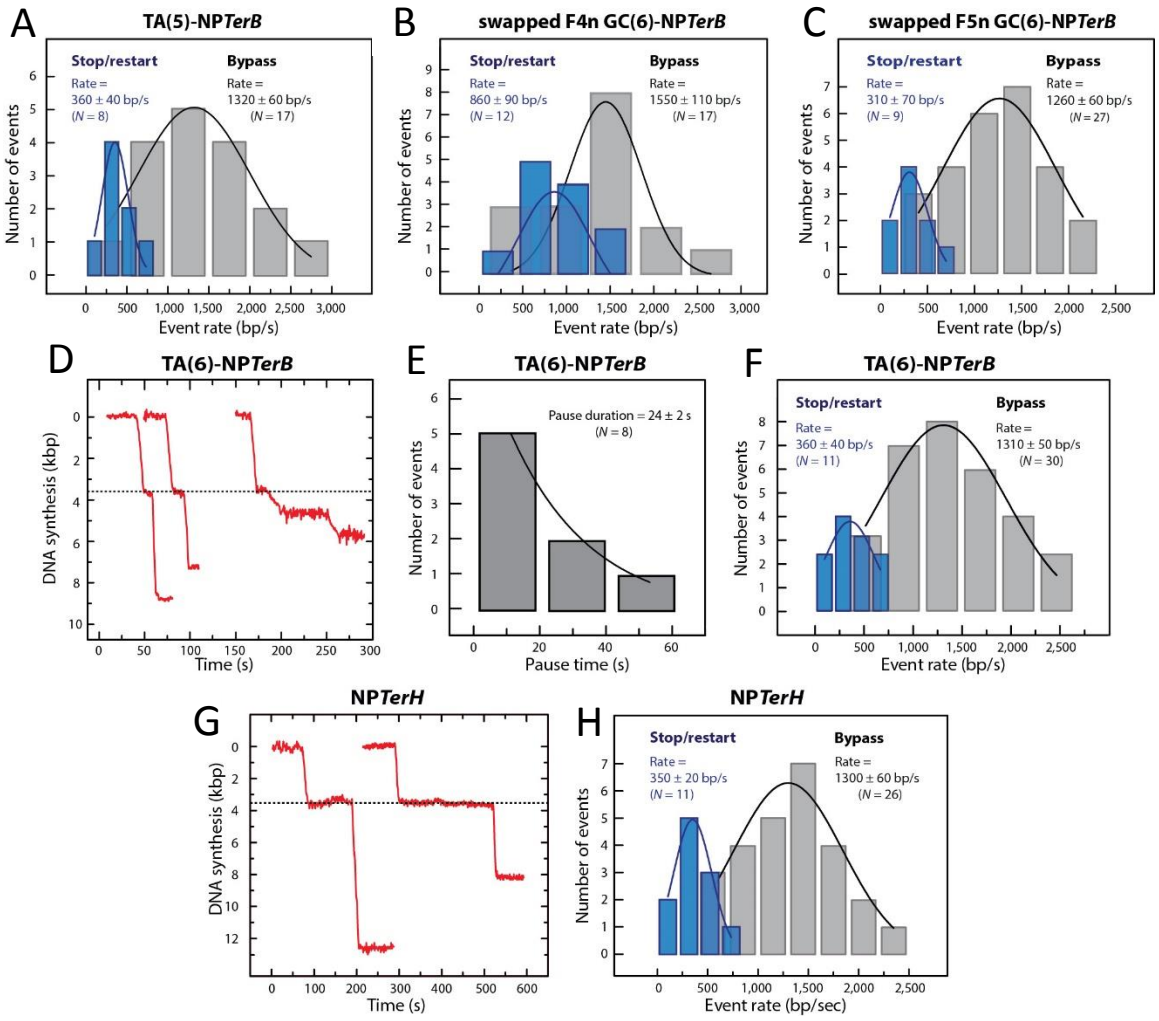

Figure 3.9: Fate of the replication fork upon encountering NP*TerB* sites with swapped sequences in the first five bps, TA(6)-NP*TerB* and NP*TerH*

Rate dependence of replication fork arrest at Tus bound to: **A**, TA(5)-NP*TerB* (*N* = 25); **B**, swapped F4n GC(6)-NP*TerB* (*N* = 29); **C**, swapped F5n GC(6)-NP*TerB*(*N* = 36). The rate distributions of leading-strand synthesis for events that bypassed (grey bars) or stopped/restarted (blue bars) at these sequences.

D. Examples of trajectories of leading-strand synthesis that transiently stopped at Tus bound to TA(6)-NP*TerB*. 75% of the restarted events displayed DNA synthesis of normal behavior (left traces), while 25% showed disrupted behaviour (right trace).

E. The distribution of the pause durations at TA(6)-NP*TerB* fit with a single exponential decay (*N* = 8).

F. The rate distribution of events that bypassed (*N* = 30; grey bars) or stopped/restarted (*N* = 11; blue bars) at TA(6)-NP*TerB*.

F. Examples of trajectories of leading-strand synthesis that transiently stopped at Tus bound to NP*TerH*. The average pause duration was 180 ± 26 s (*N* = 4). The uncertainty is the standard error.

G. The rate distribution of leading-strand synthesis for events that bypassed (*N* = 26; grey bars) or stopped/restarted (*N* = 11; blue bars) at NP*TerH*.

The histograms in **A–C**, **E**, **F** and **H** were fit to Gaussian distributions, the fit lines are shown, and the uncertainties correspond to the standard error.

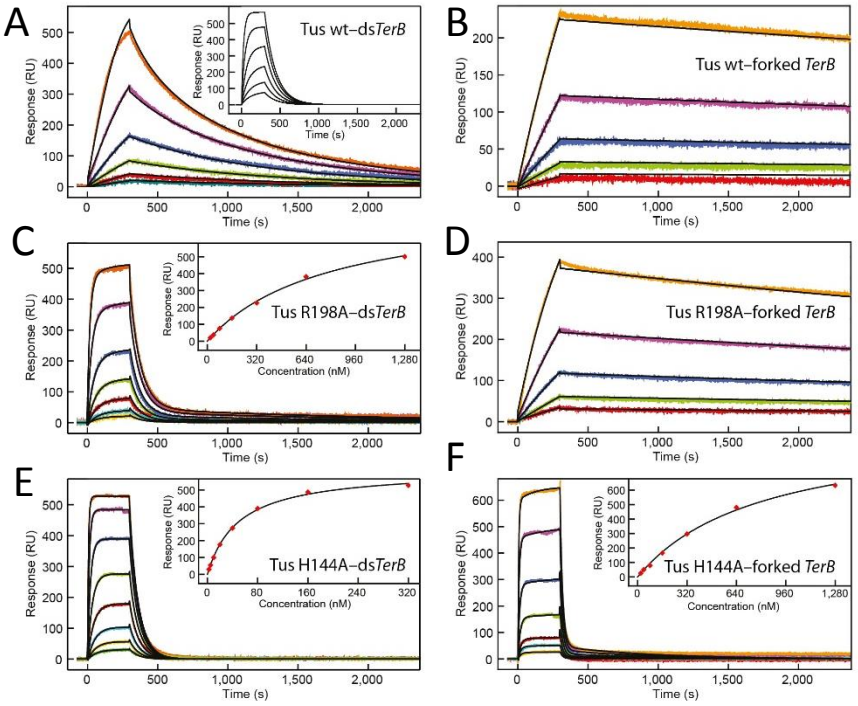

G

Panel	Interaction	[Tus] (nM)	K_D (nM)	k_a ($M^{-1}s^{-1}$)	k_d (s^{-1})	$t_{1/2}$ (s)
a	Tus–ds*TerB*	0.25–8	1.86 ± 0.08	(3.78 ± 0.08) x 10^6	(7.04 ± 0.15) x 10^{-3}	98
a inset	Tus–ds*TerB* simulated	0.25–8	1.86	3.78 x 10^6	7.04 x 10^{-3}	98
b	Tus–forked *TerB*	0.25–4	0.212 ± 0.002	(2.89 ± 0.00) x 10^5	(6.12 ± 0.07) x 10^{-5}	11,320
c	Tus-R198A–ds*TerB*	20–1,280	441 ± 10	(2.99 ± 0.00) x 10^4	(1.32 ± 0.03) x 10^{-2}	53
c inset			782 ± 60	—	—	—
d	Tus-R198A–forked*TerB*	2.5–40	1.80 ± 0.01	(5.52 ± 0.00) x 10^4	(9.95 ± 0.03) x 10^{-5}	6,970
e	Tus-H144A–ds*TerB*	2.5–320	39.3 ± 1.0	(3.92 ± 0.02) x 10^5	(1.54 ± 0.03) x 10^{-2}	45
e inset		2.5–320	49.5 ± 2.3	—	—	—
f	Tus-H144A–forked *TerB*	20–1,280	598 ± 8	(9.09 ± 0.07) x 10^4	(5.44 ± 0.03) x 10^{-2}	13
f inset		20–1,280	805 ± 69	—	—	—

Figure 3.10: SPR assessment of Tus–*TerB* interactions: whereas Tus and Tus(R198A) are capable of forming a lock, Tus(H144A) is not

ProteOn sensorgrams show association and dissociation phases of Tus−*TerB* interactions at ranges of Tus concentrations (as specified in **G**) of serially-diluted samples of Tus proteins. Curves, shown in colors, were fit simultaneously (black curves) to various binding models, as described in the methods.

A. Wild-type Tus and ds*TerB.* Considering that the $k_a > 1 \times 10^6$ $M^{-1}s^{-1}$ suggests significant mass transport limitations, the LMT model was used to fit the data with R_{max} constrained to 700 RU. The derived kinetic parameters were used to simulate sensorgrams devoid of mass transfer limitation using the L model (inset).

B. Wild-type Tus−forked *TerB* interaction; R_{max} was constrained to 775 RU. The fit k_d is in good agreement with the value of $(5.20 \pm 0.00) \times 10^{-5}$ s^{-1} obtained from an independent experiment where dissociation was monitored over 50,000 s (not shown).

C. Tus(R198A)−ds*TerB* interaction. Binding kinetics parameters were obtained using the HLPR model. The sum of fit R_{max1} (543 ± 9) and R_{max2} (54 ± 5 RU) values were in reasonable agreement with the expected value of ~ 700 RU. Only the relevant k_a and k_d values of the predominant (based on R_{max1}) interaction are presented in **G**. For assessment of the fitting procedure, responses at equilibrium were fit using the L model (inset). The derived K_D was within the factor of two of the calculated K_D obtained from kinetic parameters (k_d/k_a). TheR_{max} value of 816 ± 32 RU was slightly higher than theoretical (700 RUs), probably owing to some non-specific binding in the high range of Tus concentration.

D. Tus(R198A)−forked *TerB* interaction. The L model was used to fit the data with R_{max} constrained to 775 RU. The fit k_d was within a factor of two of the value, $(5.70 \pm 0.00) \times 10^{-5}$ s^{-1}, derived from an independent experiment where dissociation was monitored over 50,000 s (not shown).

E. Tus(H144A)−ds*TerB* interaction. Binding kinetic parameters were obtained using the HLPR model. The sum of fit R_{max1} (537 ± 1) and R_{max2} (31 ± 0 RU) values were in reasonable agreement with the expected value of ∼ 700 RU. Only the relevant k_a and k_d values of the predominant interaction (R_{max1}) are presented in **G**. For assessment of the fitting procedure, responses at equilibrium were fit using the L model (inset). The derived K_D was within a factor of 1.5 of K_D obtained from the kinetic parameters. In addition, the fit R_{max} value of 621 ± 10 RU compares reasonably to the expected value of ∼ 700 RU.

F. Tus(H144A)−forked *TerB* interaction. Binding kinetics parameters were obtained using the HLPR model. The sum of fit R_{max1} (879 ± 4) and R_{max2} (65 ± 1) values were somewhat high compared to the expected value of ∼ 775 RU. Only the relevant k_a and k_d values of the predominant reaction are presented in **G**. Responses at equilibrium were fit using the L model (inset). Derived K_D was within the factor of 2 of the calculated K_D obtained from (k_d/k_a). In addition, fit R_{max} value of 1,040 ± 50 RU was slightly higher than theoretical.

G. Summary of binding parameters for Tus–*Ter* interactions. All uncertainties are standard errors in parameters from fitting of complete data sets to appropriate binding models, as described in the methods. Data are representative of those from two technical replicates using different instruments (BiaCore T200 and ProteOn XPR-36).

3.3.4 A second Mechanism of Fork Arrest

To explore whether the interactions of R198 with AT5 and G6 contribute directly to this alternate mechanism, we maintained these interactions using the *TerB* sequence and deactivated the C6 lock using Tus(H144A), the key residue in the binding pocket. This mutation completely eliminated lock formation as shown by SPR (Figure 3.10E,F) and

confirmed by its structure (Figure 3.7D). However, we still observed a high level (27%) of permanent fork arrest, confirming existence of a lock-independent process leading to permanent stoppage. There were also substantial restarts (18%; Table 3.1) after short pauses (33 ± 5 s; N = 6). Pausing must result from a mechanism additional to permanent arrest, since restarts would otherwise be randomly distributed over the full 10 min period of observation. The rate-dependence of arrest was similar to wild-type Tus (Table 3.1 and Figure 3.11).

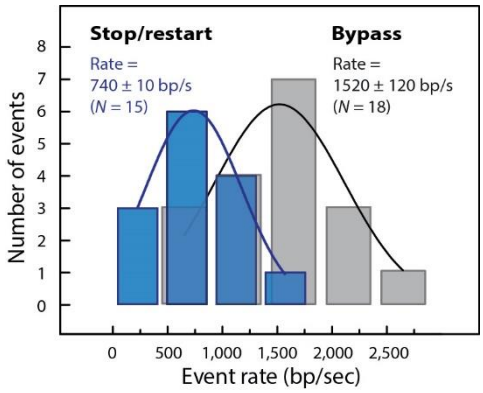

Figure 3.11: Fate of the replication fork upon encountering Tus(H144A) bound to NP*TerB*

Rate dependence of fork arrest. The rate distribution of leading-strand synthesis for events that bypassed (*N* = 18; grey bars) or stopped/restarted (*N* = 15; blue bars) at NP*TerB* fit with Gaussian distributions. The fit lines are shown and the uncertainties correspond to the standard error.

3.3.5 Mechanisms of Fork Arrest

Collectively, our results show that interactions of Arg198 of Tus with G6, A5 and/or T5 act to protect Tus−*Ter* central interactions from the first arriving DnaB. Nevertheless, these gatekeeping interactions are dynamic during separation of the first 6 bps and their rearrangement occurs in competition with strand separation. We suggest that faster forks

have higher probability to separate GC6 before rearrangement of Arg198 interactions, displacing Tus without pausing (Figure 3.12, probability A). Slower forks are either stopped permanently before GC6 melting (probability B) or transiently if GC6 is melted and Arg198 succeeds in rearranging (probability C). The inefficient C6 mousetrap is a terminal step, enabled by transient stoppage to impose permanent fork arrest (probability C). These results provide an explanation of why, in helicase assays, the slowly moving DnaB (35-390 bp s^{-1})[233,234] is efficiently stopped at the NP face without requiring C6 flipping[145].

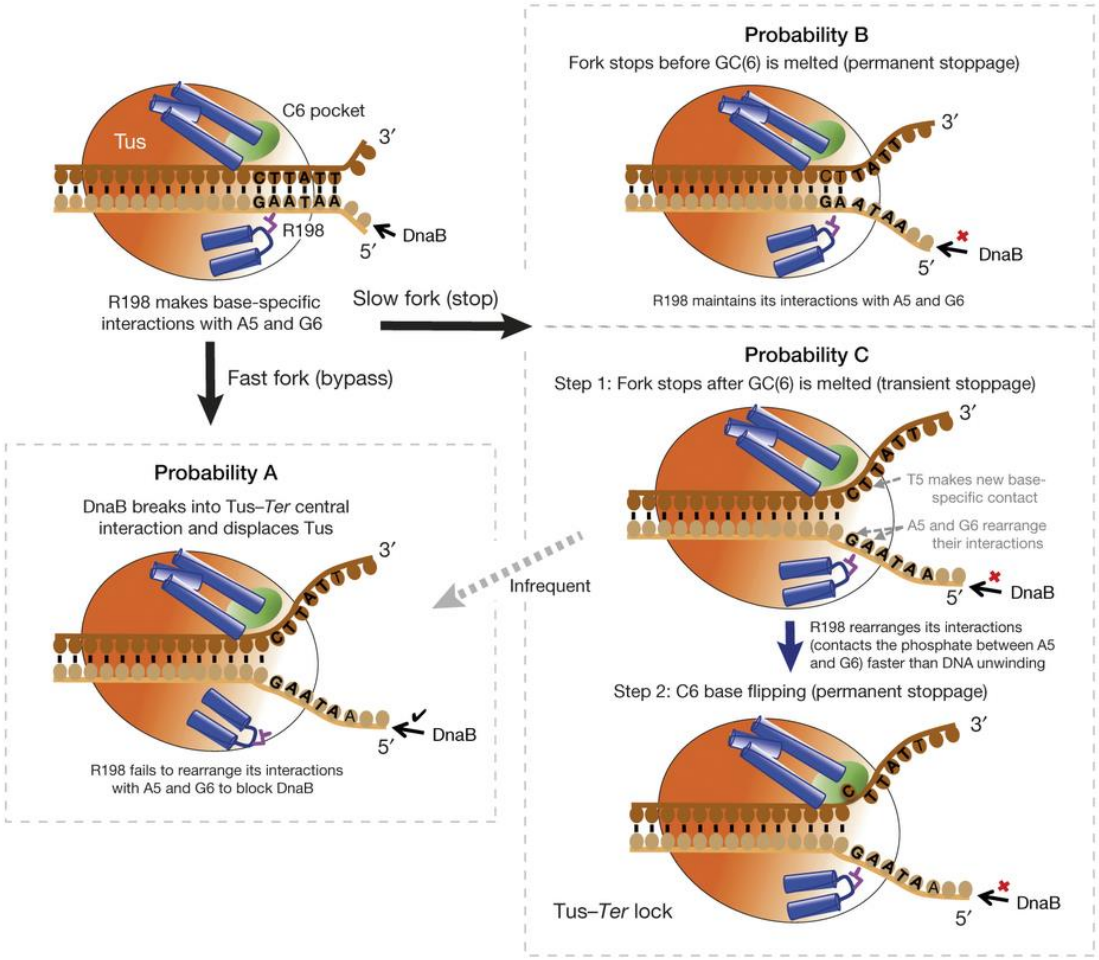

Figure 3.12: Model of Tus–*Ter* polar arrest activity at the NP face

Prior to strand separation, Arg198 makes base-specific contacts with A5 and G6 on the lagging strand to protect Tus–*Ter* central interactions from the DnaB helicase. After separation of the first 6 bps, Arg198 maintains contacts with the lagging strand by rearranging its interactions to make a new salt bridge to the phosphate between A5 and G6 and a new unidentified base-specific interaction is induced with T5. Competition between rates of strand separation and rearrangement of Arg198 interactions determines Tus–*Ter* efficiency. Faster moving forks have higher probability to separate GC6 before rearrangement of Arg198 interactions, leading to effective displacement of Tus (probability A). The slower forks are either stopped permanently before or during GC6 melting (probability B) or transiently if GC6 is melted and Arg198 succeeds in rearranging its interactions (probability C, step 1). The C6 mousetrap acts as a terminal step that is enabled by the transient stoppage to impose permanent fork arrest (probability C, step 2).

3.4 Conclusions

Thus, we refine the mousetrap model and redefine the efficiency of Tus−*Ter* polar arrest to depend on collective contributions of intrinsic affinity of Tus for *Ter*, stability of the flipped C6 in its binding pocket, and rate-dependent induction of fork stoppage that fully or temporarily protects Tus−*Ter* central interactions from DnaB. Our observations also raise a question about how weaker *Ter* sites evolved to block slower forks. Redundant *Ter* sites with different affinities for Tus in the two clusters have evolved to progress from weaker to stronger as they approach the *dif* site (Figure 3.1A). Nevertheless, despite high affinity, only a low level of residual fork blockage was detected at the Tus−*TerB* complex oriented towards the P face (Table 3.1), suggesting that such an arrangement will minimize early blockage of replication and hindrance to other processes such as transcription. The encounter of dsDNA-binding proteins with motor proteins like helicases

and polymerases is a common feature in replication, repair, recombination and transcription and where conflict among these processes arises (reviewed in [235]). We show for the first time that intrinsic heterogeneity in rates of individual molecular motors can have different biological outcomes as they communicate with dsDNA-binding proteins and other barriers. Our study prompts an interesting question regarding the impact of the intrinsic heterogeneity in rates of enzymes on biology. Demonstration that the rates of individual enzymes fluctuate during catalysis and that rates are heterogeneous among presumably identical enzyme molecules are two findings that are considered among the most novel contributions of single-molecule imaging to biology. However, it has not yet been shown how these intrinsic properties of enzyme molecules actually impact on biology. Our study shows this for the first time and also resolves long standing controversies about a well-studied protein–dsDNA interaction.

3.5 Methods

3.5.1 Protein Expression and Purification

Described methods were used to prepare N-terminally His_6-tagged Tus[101] and its mutant derivatives TusR198A[101] and Tus(H144A)[130], as well as the following *E. coli* DNA replication proteins: the β2 sliding clamp[215], the Pol III $\tau_3\delta\delta'\chi\psi$ clamp loader and $\alpha\varepsilon\theta$ core[47], the $DnaB_6(DnaC)_6$ helicase/loader complex[55], and the fork restart proteins PriA, PriB and DnaT[216].

3.5.2 Crystallization of Tus–*Ter* Complexes and Data Collection

Four crystal structures of Tus–*Ter* complexes are reported (Table 3.2); the oligonucleotide sequences and proteins used are given in Figure 3.7. All complexes (finally at 4–5 mg/ml protein) were prepared with a slight excess of DNA in 10 mM Bis-Tris, pH 6.5, 1 mM EDTA, 2 mM dithiothreitol, and excess DNA was removed by using a centrifugal ultrafiltration device, as described previously[130]. Crystals were grown using the vapour diffusion (hanging drop) method at 23 °C. The protein–DNA complex (3µl) was mixed with an optimized reservoir solution (3µl) consisting of 8–12% PEG 3350, 0.1–0.2 M NaI, 50 mM Bis-Tris, pH 6.2–6.8. Crystals appeared after 2 days and reached maximum size after 10 days. The pH was measured using 1 M stock solutions of buffer before addition to the reservoir. Optimized reservoir solutions for the four crystals contained: for Tus–UGLT fork (forked *Ter* with C6 to G change), 12% PEG 3350, 0.2 M NaI, 50 mM Bis-Tris pH 6.2; for Tus–TGTA fork (forked *Ter* with C6 to G change and the fork extended to position 7), 9% PEG 3350, 0.2 M NaI, 50 mM Bis-Tris pH 6.8; for Tus(H144A)–WT fork ("wild-type" forked *Ter* with Tus(H144A)), 8% PEG 3350, 0.1 M NaI, 50 mM Bis-Tris pH 6.2; for Tus–UGLC (ds*TerA* with GC6 to CG flip), 12% PEG 3350, 0.2 M NaI, 50 mM Bis-Tris pH 6.5.

3.5.3 Structure Determination and Refinement

All X-ray data were collected at the Australian Synchrotron beamline MX-1 (X-ray wavelength, 0.95370 Å) using an Oxford cryostream to maintain the crystal temperature at 100 K. Prior to cooling, crystals were transferred stepwise into artificial mother liquors finally containing 15% (v/v) MPD (2-methyl-2,4-pentanediol) in 3% increments of MPD (3 min per step). Data were collected using an ADSC Quantum 210r area detector, using

BLU-ICE for remote data acquisition and processing[236]. Data reduction and scaling was achieved with the HKL2000 package[237].

All structures were solved by molecular replacement in MOLREP[238] using a previously solved Tus−*Ter* lock (PDB code: 2I06) or Tus−*TerA* structure (2I05) as starting model. REFMAC[239,240] was used for structure refinement and calculation of map weighting factors. COOT[241] was used to interpret electron density maps and for model building. Figures were prepared using PyMOL.

3.5.4 Assessment of Tus−*TerB* Interactions by Surface Plasmon Resonance (SPR)

Methods were essentially as used previously[101,130], except that all experiments were carried out at 20 °C (instead of 25 °C) and a 6 × 6 multiplex BioRad ProteOn XPR-36 system was used instead of a Biacore 2000 instrument; dissociation rate constants (k_d) of Tus proteins from immobilized biotinylated *TerB* showed an unusual temperature dependence (high activation energy), which accounts for lower values of k_d and the dissociation constant (K_D) compared to previously reported values (where they are available[101,130]).

All measurements used SPR buffer (50 mM Tris pH 7.6, 250 mM KCl, 0.25 mM EDTA, 0.5 mM dithiothreitol, 0.005% surfactant P_{20}), with a ProteOn NLC (neutravidin-coated) sensor chip for immobilization of 5'-biotinylated *TerB* oligodeoxyribonucleotides (oligos). These were either (1) 5'-bio–(pD)10–ATAAGTATGTTGTAACTAAAG, oligo-1, or (2) 5'-bio–(pD)10–*GGGGC*TATGTTGTAACTAAAG, oligo-2, each containing a 10-unit abasic deoxyribosephosphate spacer (pD)10 to move the *TerB* molecule away from the chip

surface[101], as well as a common lagging strand *TerB* sequence (underlined)[101]. Hybridization of oligo-3: 5'-CTTTAGTTACAACATA***C****TTAT* (C6 of *Ter* in bold) to oligo-1 produces a full ds*TerB* site, while its hybridization to oligo-2 produces a forked *Ter* where C6 is unpaired and exposed (mismatched sequences in oligos-2 and -3 are in italics)[130].

All 36 interaction spots of the sensor chip were activated with three sequential injections of 1 M NaCl, 50 mM NaOH across six vertical (ligand) flow paths (40 s each at 40 µl min^{-1}) and six horizontal (analyte) flow paths (40 s each at 100 µl min^{-1}). The surface was further stabilized by two injections of 1 M $MgCl_2$ in each direction, with the same contact times and flow rates. Oligos-1 and -2 were diluted to 200 nM in SPR buffer and immobilized separately onto the six interaction spots of the vertical flow path (100 µl min^{-1} for 15 s). The chip was then rotated 90° and simultaneous assembly of ds*TerB* and forked *Ter* templates[130] on the chip surface was achieved by hybridization of oligo-3 (300 nM), made to flow across all six horizontal (analyte) channels at 25 µl min^{-1} for 400 s. The sensorgram verified that hybridization went to completion. After subsequent injection of a concentration series of Tus, the surface was regenerated; remaining proteins and hybridized DNAs were removed by two injections of 1 M NaCl, 50 mM NaOH over the six analyte channels at 50 µl min^{-1} for 40 s, followed by re-hybridization of oligo-3 as above. Measured stoichiometries of Tus binding to both templates were close to 1:1 at saturation, as reported previously[101,130].

Tus, Tus(R198A) and Tus(H144A) interactions with *TerB* and forked *Ter* templates were carried out by sequential injections in the analyte direction of one or two appropriate

concentration series in SPR buffer (zero and five concentrations of serially-diluted samples) at 40 µl min^{-1} for 300 s, followed by dissociation in the same buffer over 2,000 s. The final sensorgrams were interspot and unmodified ligand flow path subtracted using ProteOn Manager Software (v. 3.1.0.6) and then zero subtracted and normalized based on the highest response of hybridized oligonucleotide within the discrete ligand flow path using BIAevaluation software (v. 4.0.1; Biacore AB, Sweden). Equilibrium (dissociation constant, K_D) and kinetic (rate constants, k_a and k_d) parameters for the binding of Tus proteins to the *Ter* fragments were determined by global (simultaneous) fitting of at least five sensorgrams per measured interaction from the optimized concentration range using BIAevaluation software and the appropriate interaction model(s): (Langmuir) 1:1 binding with mass transfer model (LMT, for Tus–ds*TerB* interaction; as previously done[101]), (Langmuir) 1:1 binding model (L, for Tus - and Tus(R198A) - forked *Ter*), and 1:1 steady state affinity (LSS) and heterogeneous ligand-parallel reactions (HLPR) binding models for fitting sensorgrams that reached an equilibrium response (Tus(R198A)-ds*TerB*, Tus(H144A)-ds*TerB* and Tus(H144A)-forked *Ter*).

Global best fits were used when LSS and HLPR models were used. When L and LMT models were used, the fitting was constrained by setting the Rmax to a global constant value (response at saturation of ligand binding sites was set to 700 responce units (RU) for bindings to ds*TerB* and 775 RU for forked *Ter*). These values, calculated theoretically as a product of the highest measured response of hybridized oligo-3 (molecular weight 6,354; used as a normalization unit) onto oligo-1 (120 RU) and oligo-2 (134 RU) and the factor 5.8 (molecular weight of His_6Tus/molecular weight of hybridized oligo-3 = 36,737/6,354),

were compared with experimentally determined values obtained by flowing Tus at a saturating concentration (1.024 μM) over the two DNA templates (not shown). In addition, due to slow dissociation, experimentally determined k_d values for Tus- and Tus(R198A)-forked *Ter* interactions using the L model were assessed by comparison with the k_d values determined from the experiment where dissociation was monitored over 50,000 s (not shown). To generate as reliable as possible values for kinetic parameters using the HLPR model, k_a and k_d were estimated in the first approximation based on complete association phase and only an initial phase of dissociation where the rate of change is the greatest. These obtained values of kinetic parameters were sometimes used as initial iterative values; otherwise, the iterations could slip into local minima without reaching a sensible solution. Only the fit kinetic parameters of the prevalent (dominant) reaction using HLPR model were finally presented in Figure 3.10G. For assessment, K_D values calculated from obtained kinetic parameters (k_d/k_a) were compared with K_D values directly obtained using the LSS model (Figure 3.10G).

3.5.5 Single-molecule Flow Stretching Assays

3.5.5.1 DNA Substrate Constructs

Bacteriophage λ-DNA was modified by ligating a biotinylated fork on one end and a digoxigenin moiety at the other end as described previously[55]. This ligated product was digested with either *EcoRI* or *ApaI* to generate 3.6 and 10.1kb fragments from the forked and digoxigenin ends, respectively. An oligonucleotide sequence containing a single copy of wild-type or variants of the *TerB* site was ligated to the digested ends of the 3.6 and

10.1kb fragments as described previously[232] to generate DNA constructs with variant *TerB* sites that are listed in Table 3.1 and Figure 3.2B.

3.5.5.2 Force Calibration

A force extension curve was constructed by measuring the length of individual 13.7 kb DNA molecules and calculating the hydrodynamic drag force at different flow rates using the equipartition theorem equation as described previously[225,226]. The force extension curve was fit using Worm-like chain model[225,232]. The fluctuation in the laminar flow causes an error in estimating the force and consequently the length of individual DNA molecules, which results in an error in estimating the location of the *TerB* site relative to the fork. At the applied stretching force of 2.6 pN in our experiments, the error in estimating the force, derived from the standard deviation between seven DNA molecules in the same field of view, results in an error of ± ~ 85 bp in estimating the position of the *TerB* site at 3.6 kb from the site of fork assembly[232]. Consequently, we treated any replication event ending between 3.5 and 3.7 kb as being stopped at the *TerB* site.

3.5.5.3 Single-molecule Leading-strand Synthesis Assay

The leading strand DNA synthesis and data analysis were performed as described previously[47,55] with the variation of adding Tus to the reaction. Briefly, Tus was first introduced under continuous flow at 80 nM in buffer containing 30 mM Tris-HCl pH 7.6, 50 mM NaCl, 0.5 mM EDTA, 5 mM dithiothreitol and 10 mM MgCl2 for 30 min to ensure the binding of Tus to *TerB*. The excess DNA-unbound Tus was removed by washing with 15 times flow cell volume with replication buffer containing 50 mM HEPES-KOH pH 7.9,

80 mM KCl, 12 mM $Mg(OAc)_2$, 2 mM $MgCl_2$, 5 mM dithiothreitol and 0.1 mg/ ml BSA. Tus was then reintroduced with the replication proteins under continuous flow in the replication buffer supplemented with 760 μM of each dNTP, 1 mM ATP and proteins as follows: 80 nM Tus, 30 nM $\tau_3\delta\delta'\chi\psi$, 30 nM $DnaB_6(DnaC)_6$ helicase–loader complex, 30 nM β_2 clamp, 60 nM $\alpha\varepsilon\theta$ core Pol III, and fork restart proteins, 20 nM PriA, 40 nM PriB and 480 nM DnaT. Experiments were carried out at 32 °C.

For data analysis, the picked particles were first corrected for their Brownian motion using unreplicated tethered DNA molecules. Pausing of DNA synthesis was considered when the amplitude fluctuations of a minimum of six data points (acquisition rate was 2 Hz) was less than three times the standard deviation of the noise. Bead displacement was converted into numbers of nucleotides synthesized using the known length difference between ss- and ds-DNA in λ-DNA[226] (3.76 nucleotides per nm at our applied stretching force of 2.6 pN). Total experimental time was 30 min. In the study of the effect of Tus concentration on Tus−*TerB* polar arrest activity (Figure 3.1F), Tus was first pre-incubated with the DNA at 80 nM and excess Tus was washed out as described above for our standard experimental condition. This was followed by the introduction of either 20 or 80 nM of Tus with the replication proteins. Tus(H144A) was used at concentration of 80 nM while TusR198A was used at 250 nM throughout the reaction. Multiplexed single-molecule experimental results were derived from three or four technical replicates for each experimental condition.

The portion of leading-strand synthesis trajectories that randomly terminated before reaching the position of the *Ter* site at 3.6 ± 0.1 kb (Figure 3.4A) were excluded from analysis. Those that reached the *Ter* site were separated into three categories: (1) those that continued unimpeded through the *Ter* site ("bypass"), (2) those that were "permanently" arrested for all of the period of observation (9.7 ± 1.0 min; "stop"), and (3) those that paused (for ~ 3 s, see above) and then resumed ("restart").

Chapter 4

4. Two Mechanisms Coordinate Replication Termination by the *Escherichia coli* Tus−*Ter* Complex*

In this study, we collaborated with Professor Smita Patel (Rurtgers University) to show that the heterologous T7 replication system is arrested at the Tus−*Ter* Complex in a polar manner. The study showed that C6-mousetrap is active under physiological conditions and provided evidences against Tus/DnaB physical interaction model in mediating polar arrest activity. The findings of this study will be discussed within the context of the results from the *E. coli* systems in a comprehensive discussion in Chapter 7.

4.1 Abstract

The *Escherichia coli* replication terminator protein (Tus) binds to *Ter* sequences to block replication forks approaching from one direction[20,23,24,86,128]. Here, we used single-molecule and transient state kinetics to study responses of the heterologous phage T7 replisome to the Tus−*Ter* complex. The T7 replisome was arrested at the non-permissive end of Tus−*Ter* in a manner that is explained by a composite mousetrap and dynamic clamp model. An unpaired C6 that forms a lock by binding into the cytosine-binding pocket of Tus was most effective in arresting the replisome and mutation of C6 removed the barrier. Isolated helicase was also blocked at the non-permissive end, but unexpectedly the isolated polymerase was not, unless C6 was unpaired. Instead, the polymerase was blocked at the permissive end.

---

*This chapter contains data published in "Pandey M, Elshenawy MM, Jergic S, Takahashi M, Dixon NE, Hamdan SM, Patel SS. Two mechanisms coordinate replication termination by the *Escherichia coli* Tus−*Ter* complex. *Nucleic Acids Res*. 43, 5924–5935 (2015)"

This indicates that the Tus−*Ter* mechanism is sensitive to the translocation polarity of the DNA motor. The polymerase tracking along the template strand traps the C6 to prevent lock formation; the helicase tracking along the other strand traps the complementary G6 to aid lock formation. Our results are consistent with the model where strand separation by the helicase unpairs the GC6 base pair and triggers lock formation immediately before the polymerase can sequester the C6 base.

4.2 Introduction

In the circular *Escherichia coli* chromosome are clusters of specific replication termination (*Ter*) sequences, whose function is to trap the first-arriving replication fork in the terminus region to prevent its over-replication[242,243]. The replication terminator protein, Tus, forms a tight complex (pM K_D) with the *Ter* sequences[101,129,130,137,244,245]. It is remarkable that the Tus−*Ter* complex preferentially blocks the *E. coli* replisome arriving from one direction (at the non-permissive face (NP)) but not the other (permissive face (P)). High affinity binding of Tus to *Ter* sequences is important for efficient replication fork arrest, but high affinity by itself does not explain why the replisome is blocked in a polar manner[243]. Three mechanistic models (that are not mutually exclusive) have been proposed to explain polar arrest of the replisome: *(i)* in the helicase interaction model, the replicative helicase DnaB interacts physically with the NP face of the Tus−*Ter* complex to stop fork progression[124,135,221,246,247]. *(ii)* In the dynamic clamp model, there is an intrinsic difference in the interactions of the Tus protein at the two ends of *Ter*, which leads to facile dissociation of Tus by the DnaB helicase arriving at the P, but not the NP face[101,127]. *(iii)* The mousetrap model proposes a highly specialized mechanism that involves a strictly

conserved cytosine residue C6 in the *Ter* sequence[130]. In this mechanism, DnaB helicase unwinds the DNA toward the NP face, exposing the conserved C6 residue out of the double-stranded (ds)DNA to enable its binding into a specific cytosine-binding pocket in the Tus protein, forming a 'lock' that effectively blocks the replication complex (Figure 4.1A).

To probe these mechanisms, we used the heterologous bacteriophage T7 replication proteins for two reasons: firstly, if DnaB helicase–Tus interactions play a dominant role in polar replication fork arrest, then a helicase or helicase–polymerase that could not have co-evolved might not be arrested in a polar manner. Secondly, unlike with the *E. coli* replication protein system where helicase loading is inefficient, T7 DNA replication on short DNA templates can be used to follow DNA synthesis with single base spatial resolution and on millisecond time scales, as described below. The mechanisms of coupled DNA unwinding by the T7 helicase and DNA synthesis by the T7 polymerase have been studied in detail[14,248-252]. The T7 helicase is a ring-shaped member of the DnaB family that uses the energy of nucleotide triphosphate (NTP) hydrolysis to unwind dsDNA. Like DnaB, it translocates in the 5' to 3' direction on one strand and unwinds dsDNA by a strand exclusion mechanism[250,252-254]. Thus, it separates the strands of ds*Ter* DNA upon approach to the NP face by encircling the lagging strand containing G6 and excluding the leading strand that includes C6. On the other hand, the T7 DNA polymerase binds on the leading strand template and translocates in the 3' to 5' direction to elongate a primer to copy the newly unwound DNA. The separated T7 helicase and polymerase have DNA unwinding and synthesis activities, respectively; however, strand displacement DNA synthesis is

most efficiently promoted by the two enzymes working together at the replication fork[249,255]. In work reported here, this fast and processive DNA synthesis has been measured at single base resolution on synthetic fork DNA substrates[256], and also at more limited resolution in real-time using a single-molecule tethered-bead assay[55,182].

We show, using both of these DNA synthesis assays, that the T7 helicase–polymerase complex is effectively blocked by Tus−*Ter* in a polar manner at the NP, but not at the P face, just like the *E. coli*replication fork *in vivo*. Furthermore, mutation of C6 has clear effects on the duration (transient versus permanent) and extent of replication arrest. We found that the isolated T7 DNA polymerase, uncoupled from the helicase, is not blocked permanently at the NP face of the termination complex, but is surprisingly blocked instead at the P end. On the other hand, isolated T7 helicase is blocked at the NP but not the P face. These results indicate that polar arrest by Tus−*Ter* involves a strand-specific mechanism that is sensitive to the polarity of the DNA motor. We discuss these results in terms of the Tus−*Ter* interactions with the two strands of the DNA at the P and NP faces and for the first time deduce the roles that two of the three mechanistic models play in polar replication fork arrest and the operation of the mousetrap mechanism under conditions of physiological ionic strength. The Tus−*Ter* block is also a great tool to probe the coupling between helicase and polymerase progressing at the replication fork.

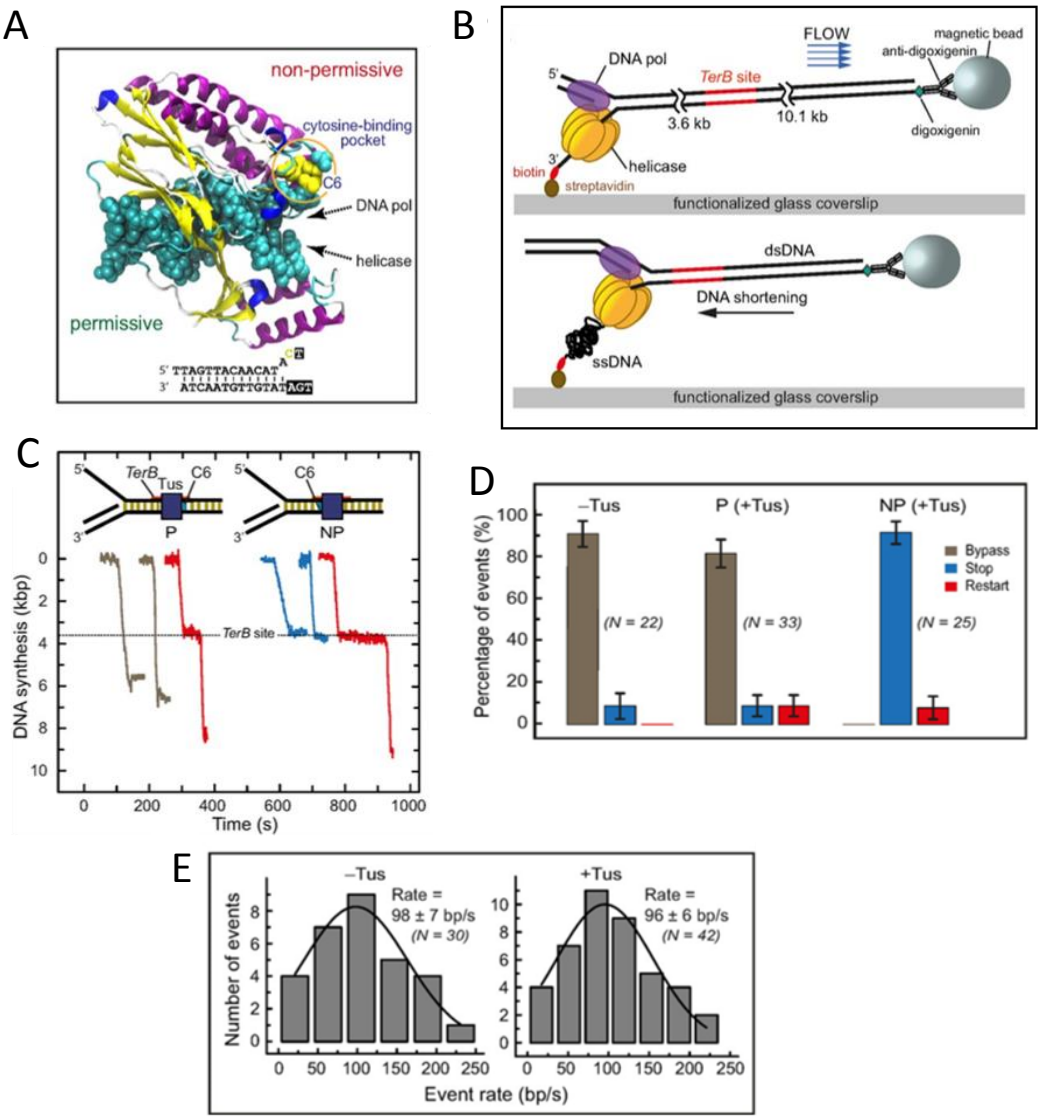

Figure 4.1: Single-molecule DNA synthesis by T7 helicase–polymerase upon encountering the P or NP face of the Tus–*TerB* complex

A. Crystal structure of the locked Tus–*Ter* complex shows the flipped C6 base at the NP face[130].

B. A schematic representation of the single-molecule tethered-bead experimental setup for observing DNA synthesis by the T7 helicase–polymerase. DNA synthesis converts the surface-tethered double-stranded (ds) DNA to single-stranded (ss) DNA, which at a regime force of 2.6 picoNewton (pN) results in shortening of the DNA and displacement of the bead in the opposite direction to the flow.

C. Representative trajectories of DNA synthesis upon encountering Tus–*TerB* complexes. The fork primarily bypassed Tus–*TerB* complex on arrival at the permissive (P) face (left), while it fully stopped at the non-permissive (NP) face (right). Trajectories show permanent stoppage (in blue), unimpeded bypass (gray) or restart (red) at P or NP Tus–*TerB*. The location of the *TerB* site is indicated. Traces have been offset on the time axis for clarity.

D. The percentage of populations of replication forks that bypassed, transiently stopped or fully stopped at P *TerB* and NP *TerB* are shown. A control experiment in the absence of Tus is shown for NP *TerB*. Error bars correspond to the standard deviation of binomial distributions.

E. Rate of leading strand synthesis using forked λ-DNA in the absence (left) or presence of Tus (right). The rate distributions were fit (lines in black) with a Gaussian distribution. The uncertainties correspond to the standard error of the distribution. Leading-strand replication reactions were carried out in the presence or in the absence of Tus protein in buffer containing 50 mM potassium glutamate.

4.3 Results

4.3.1 DNA Synthesis by the T7 helicase–polymerase Is Arrested by Tus–*Ter* in a Polar Manner

We first used single-molecule imaging to investigate the encounter of the T7 helicase–polymerase complex with Tus–*Ter* in both the P or NP orientations. DNA synthesis was measured by monitoring the length of individual DNA molecules in real-time as described previously[55,182]. Briefly, a 13.7 kb primed-forked DNA contained a single copy of the 22-base pair (bp) *TerB*, one of the strongest of the *Ter* sites, at a distance of 3.6 kb from the fork. It was attached in a microfluidic flow cell to the surface of a glass coverslip *via* one end and tethered to a magnetic bead at the other (Figure 4.1B). The DNA molecules were

stretched by a laminar flow that exerted a 2.6 picoNewton (pN) drag force on the beads. Synthesis by the helicase–polymerase converts the surface-tethered dsDNA (long) to single-stranded (ssDNA) (short) and the bead moves in the direction opposite to the buffer flow (Figure 4.1B) to generate real-time trajectories (Figure 4.1C, Figure 4.2A,B, Figure 4.3). The position of the *TerB* site at 3.6 kb could be determined with an accuracy of ±0.1 kb at 2.6 pN (Figure 4.2C). We ignored events (~ 50%) where DNA synthesis terminated before reaching the *TerB* site; under these conditions of continuous presence of all reagents in the flow, synthesis in the absence of Tus appeared to terminate at random positions (Figure 4.2D) and the average processivity of the T7 replisome was 3.7 ± 0.6 kb (Figure 4.2E). The remaining events (~ 50%) where synthesis reached *TerB* were categorized into three classes: *(i)* those that were blocked permanently at the *Ter* site (Figure 4.2B), where permanent stoppage ('stop' in Figure 4.1D) is defined as surviving until the end of data acquisition (10 ± 1 min); *(ii)* those that continued unimpeded through the *Ter* site ('bypass' in Figure 4.1D and Figure 4.2A); and *(iii)* those that paused at the *Ter* site and then resumed synthesis ('restart' in Figure 4.1D and Figure 4.3). Note that percentages of events in each class were calculated relative to the total numbers of events that reached or passed the *Ter* site, with or without pausing and standard deviations were estimated assuming binomial distributions.

In the absence of Tus, 9% (2 of 22) of the replicated molecules that reached *TerB* displayed full stoppage of DNA synthesis at or near *TerB*; we attributed this to random fork collapse in this 0.2 kb window (Figure 4.1D and Figure 4.2D). We next introduced Tus by pre-incubating it alone with the template and also including it in the reaction with T7 DNA

polymerase and T7 helicase. The Tus concentration (80 nM) was well above the reported K_D values of Tus−*Ter**B* of 3.4×10^{-13} M in 150 mM potassium glutamate[244] to 3.1×10^{-9} M in 300 mM KCl[101]; hence, the *TerB* site should always be fully saturated by the Tus protein. With Tus bound to *TerB* in the P orientation, the fork bypassed the Tus−*Ter* barrier just as if Tus were not present (Figure 4.1C,D). However, in a further 9% of the molecules, there was a brief stop before the barrier was bypassed by the helicase–polymerase to continue DNA synthesis. We attributed this bypass to the high affinity of binding of Tus to *TerB* acting as a temporary roadblock to DNA synthesis. In the remaining 82% of molecules, the helicase–polymerase displaced Tus without displaying even transient stops (Figure 4.1C,D and Figure 4.2A). Furthermore, the rate of DNA synthesis on a 48.5 kb λ-DNA template[182] was unaffected by the presence of Tus, suggesting that the helicase–polymerase can effectively displace any Tus that is non-specifically bound to DNA (Figure 4.1E).

In contrast, when the helicase–polymerase encountered Tus−*TerB* oriented to display the NP face, full arrest of DNA synthesis was observed at *TerB* in 92% of the molecules and restart after pausing in the remaining 8% (Figure 4.1C,D and Figure 4.2B). The 100% efficiency in arresting DNA synthesis at Tus−*TerB* confirms that Tus is bound to all *TerB* sites.

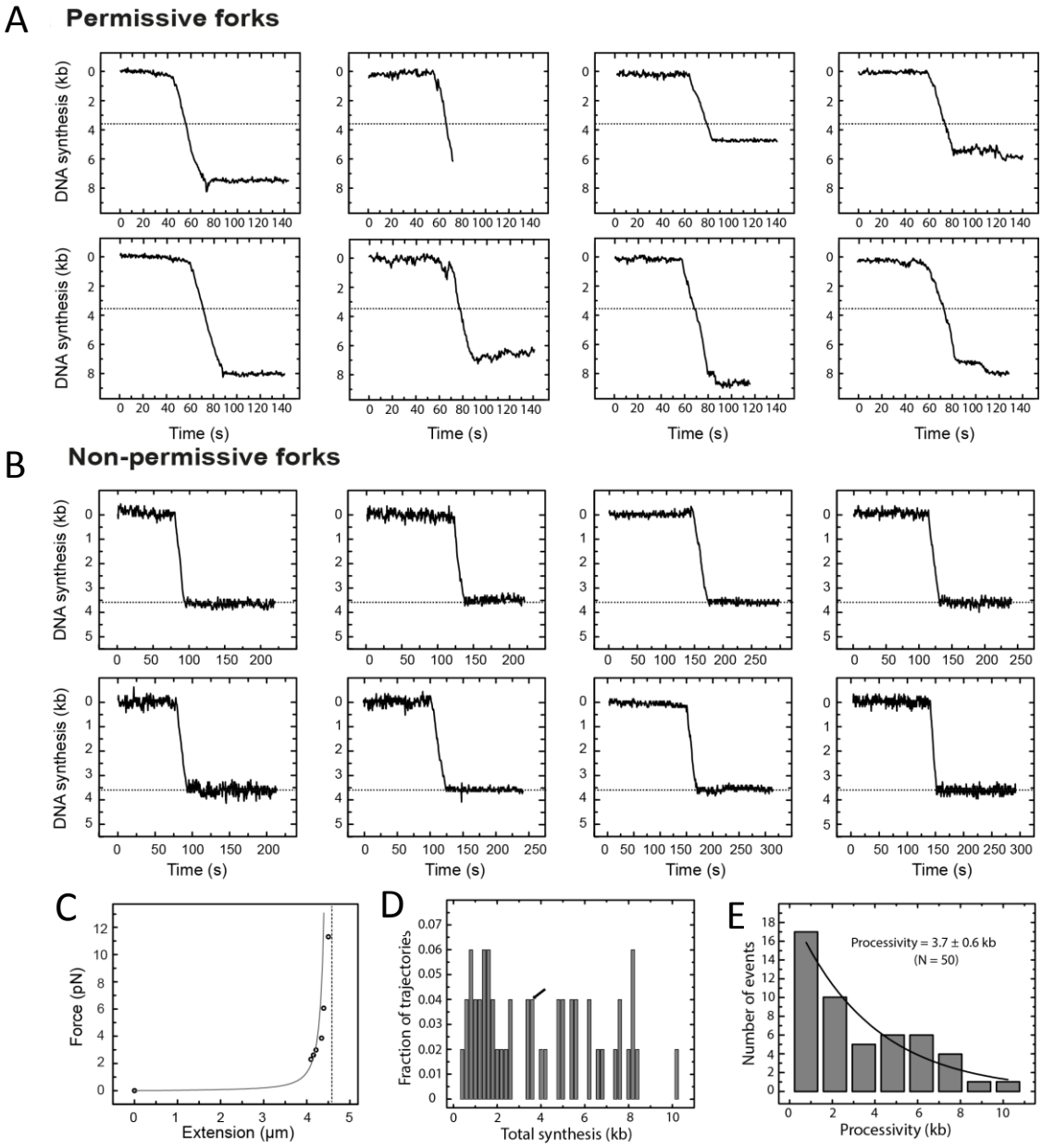

Figure 4.2: Single-molecule tethered bead trajectories

A. Examples of helicase–polymerase synthesis bypass trajectories where forks displace Tus from *TerB* oriened at the P face.
B. Examples of helicase–polymerase synthesis stoppage trajectories where forks are arrested at Tus bound to *TerB* oriened at the NP face. The location of the *TerB* site is indicated by dashed lines.

C. Force extension curve of the 13.7 kilobase (kb) dsDNA substrate as a function of applied stretching force. The curve was constructed by measuring the length of individual DNA molecules at different stretching forces. The force was calculated based on the equipartition theorem equation. Fluctuation of the laminar flow during DNA synthesis will result in an error in estimating the length of the individual molecules, and a corresponding error in estimation of the location of *TerB* relative to the site of fork assembly. At an applied stretching force of 2.61 pN (the force regime in our experiment), the standard error in force calculation from seven DNA molecules was 0.21 pN. The conversion factors between ss- and ds-DNA at 2.4 and 2.8 pN, estimated from the force extension curve of λ-DNA, are 3.85 and 3.67 nucleotide/nm, respectively. Therefore, the error in length measurement if the entire 13.7 kb construct was converted from ds to ssDNA was estimated to be ± 300 bp, which is proportionately reduced to ± 100 bp for conversion of the initial 3.6 kb fragment of the construct. Consequently, we treated any replication event ending between 3.5 kb and 3.7 kb as being stopped at the *TerB* site.

D. Probability of termination of bacteriophage T7 replisome synthesis at 0.2 kb intervals (spatial resolution of the assay) along the 13.7 kb NP*TerB* substrate in absence of Tus showing a random stoppage behavior at *TerB* (3.5–3.7 kb, denoted by black arrow).

E. Processivity of the bacteriophage T7 replisome derived from synthesis of the NP*TerB* substrate in the absence of Tus. The processivity distribution is fit with an exponential decay (uncertainty corresponds to the standard error), illustrating random stoppage behavior of the replisome along the DNA.

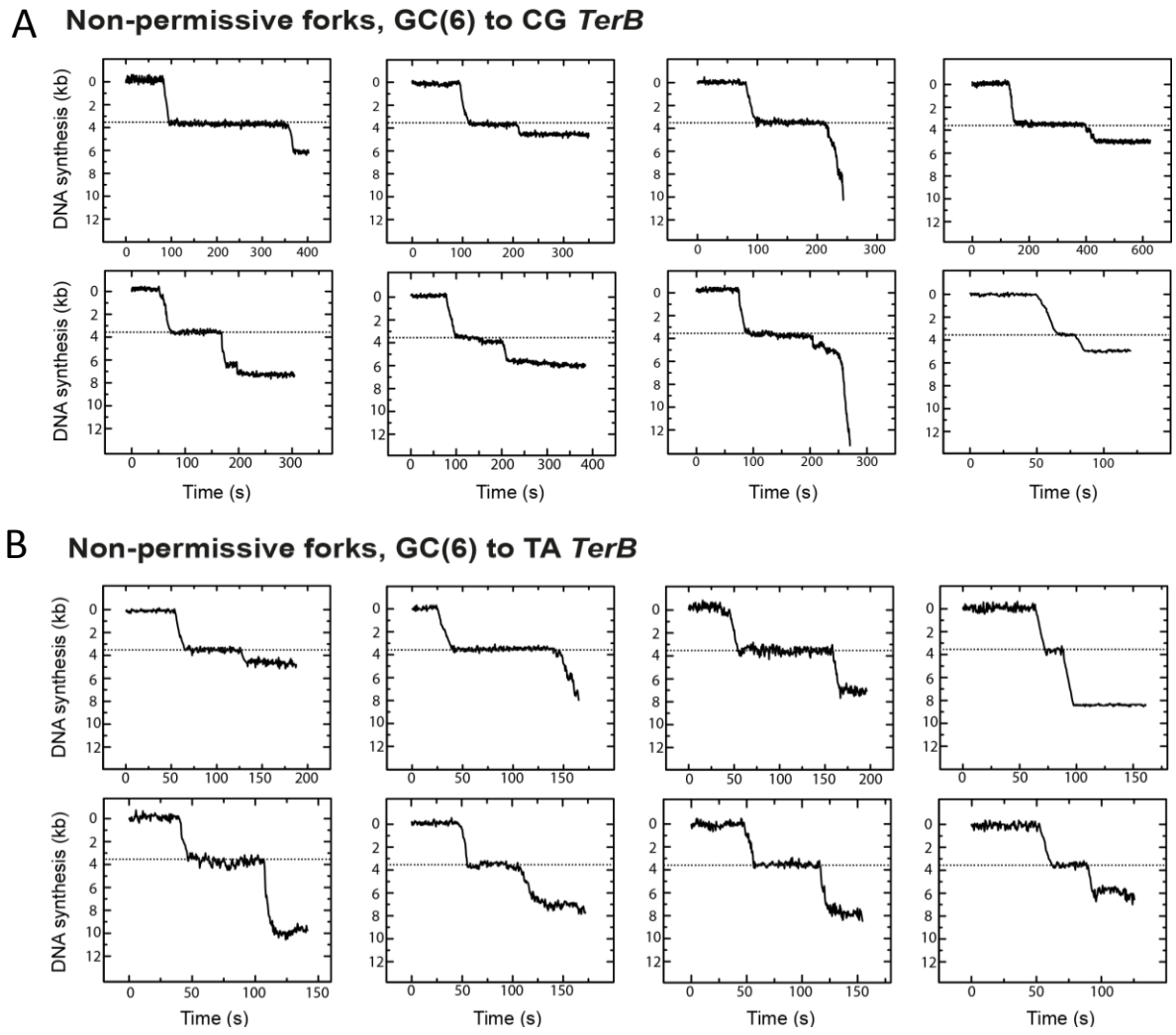

Figure 4.3: Transient stoppages in single-molecule tethered bead trajectories with GC6 mutant *TerB*s

Examples of helicase–polymerase synthesis trajectories showing transient stoppage at the location of the *TerB* site, followed by resumption of DNA synthesis. The location of the *TerB* site is indicated by the dashed lines.

A. Restart trajectories where forks encounter Tus bound to the GC6 to CG mutated *TerB* site.

B. Restart trajectories where forks encounter Tus bound to GC6 to TA mutated *TerB* site. Note the different time scales in **A** and **B**, reflecting the longer duration of pauses in **A**.

We next used a rapid quenched flow assay to follow progressive DNA synthesis at single base resolution, allowing us to study the encounter of the T7 helicase–polymerase with Tus−*TerB* at high spatial and temporal resolution. The 22-bp *TerB* sequence was introduced in either the P or NP orientation at a specific position in the middle of a 60-bp dsDNA region of the synthetic replication fork substrate (Figure 4.4). The replication fork contained a 35-nt 5′-tail for loading of the helicase and a 24-bp primer/template for loading the polymerase (Figure 4.5A,B). The replication fork was pre-incubated with Tus (380 nM) and the T7 DNA polymerase and helicase in the presence of dTTP, but without Mg^{2+}. These conditions promote preassembly of the replication proteins on the DNA and allow synchronization of the DNA unwinding/synthesis reactions initiated with Mg^{2+} and dNTPs. The components were mixed in a chemical quenched-flow instrument and quenched after 0.004 to 600 s before analysis of primer extension at single base resolution on a DNA sequencing gel (Figure 4.5C).

Without Tus, the helicase–polymerase completed strand displacement DNA synthesis of the 60 bp DNA within 1 s at 150 mM KCl without any significant pauses (Figure 4.5C). However, with Tus bound in the NP orientation, 24 nucleotides were incorporated up to T3 of the*TerB* sequence within 0.2–0.4 s, without pausing. After incorporating T3, DNA synthesis slowed as A4 was added and it was effectively and permanently blocked within ~ 2 s at A4, which is two nucleotides before the GC6. At longer times (60 s), some synthesis of A5 was also seen, perhaps from restart as observed in the single-molecule studies (Figure 4.1C). Overall, there was about 10% run-off synthesis of products beyond the *TerB* sequence on the template DNA in 60 s, resulting from displacement of Tus, which

is in agreement with the efficiency of fork arrest estimated from the single-molecule tethered bead experiments (Figure 4.1D). There were no intermediate products between A5 and the run-off products. These results indicate that the highest barrier to the progression of the T7 helicase–polymerase occurs two to three nucleotides before GC6. Similar stalling behavior was observed at 40 mM NaCl (Figure 4.6) and at 50 or 300 mM KCl, even at ten times higher dNTP concentration (Figure 4.5D and Figure 4.7). The only difference was in the amount of run-off products. At 300 mM KCl, run-off synthesis at 60 s was ~ 24% as compared to ~ 10% at 50 mM KCl (Figure 4.5D). This salt dependence is most likely due to the greater ease of Tus displacement at higher ionic strength[101,130].

In contrast, similar experiments with Tus−*Ter* in the P orientation did not exhibit significant stalling or pausing of DNA synthesis by the helicase–polymerase, apart from minor pausing of some replicated molecules at the *TerB* site (Figures 4.8-11), which is consistent with observations of the Tus−*Ter* P orientation in the single-molecule experiments (Figure 4.1D). Thus, like the *E. coli* replisome, the heterologous T7 helicase–polymerase is arrested by Tus−*Ter* in a polar manner. These results argue against the necessity for a co-evolved DnaB–Tus interaction to determine polarity (i.e. the helicase interaction model).

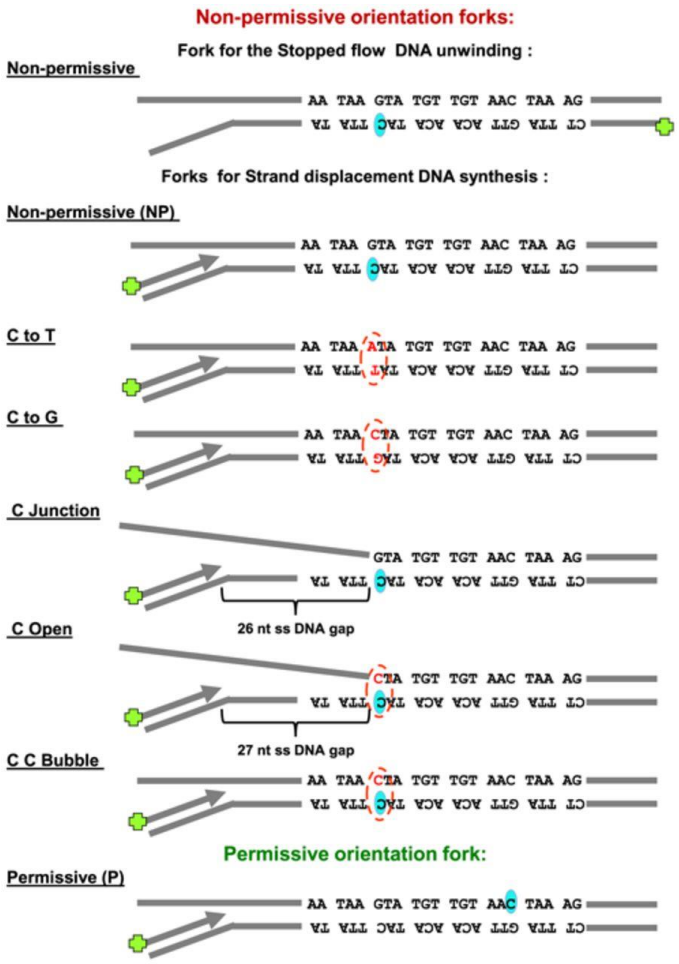

Figure 4.4: Single-molecule DNA synthesis by T7 helicase–polymerase upon encountering the P or NP face of the Tus–*TerB* complex

Schematic representation of the DNA fork substrates used in the bulk studies. *TerB* sequence orientation is shown pertaining to the DNA synthesis direction on primer. C6 base (shaded oval shape) on *TerB* sequence and any mutation of GC6 is indicated (broken line oval shape).

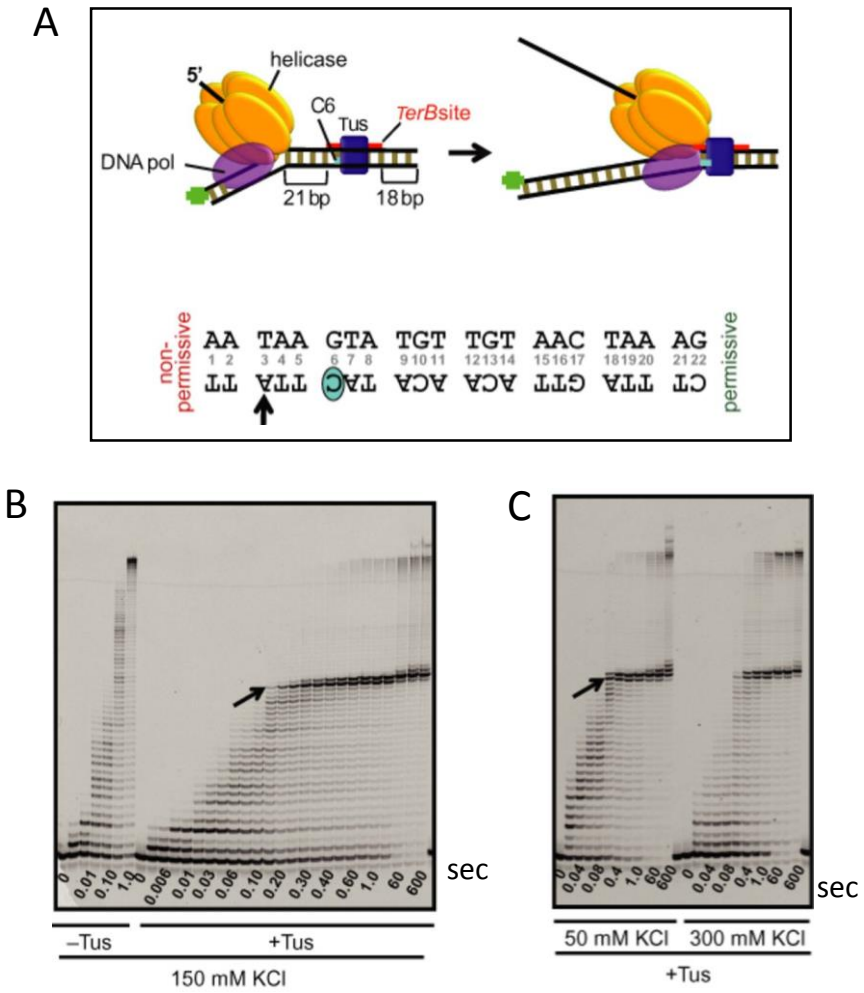

Figure 4.5: Tus–*TerB* arrest of DNA synthesis by T7 helicase–DNA polymerase at single-nucleotide resolution

A. Top panel: Schematic of the experimental design to study replication arrest of T7 helicase-polymerase by Tus–*TerB* at single-nucleotide resolution using the chemical quenched flow assay. Bottom panel: The *TerB* sequence and the C6 base. The *TerB* sequence numbering is followed throughout *TerB* site.

B. High resolution DNA sequencing gel shows progressive strand displacement DNA synthesis by the T7 helicase–polymerase on a fork DNA containing *TerB* in the NP orientation. Arrows indicate the first arrest position band corresponding to the arrow on the *TerB* sequence in (A). These reactions were carried out in the quenched flow apparatus (QF) in the presence or in the absence of Tus protein at 150 mM KCl at 0.1 mM dNTPs and 1 mM dTTP.

C. Sequencing gel shows the QF reactions in the presence of Tus at 50 and 300 mM KCl, with all dNTPs at 1 mM. Each time point shown here is an independent reaction. Another QF experiment is also shown in Figure 4.6 and extended time scale experiments are shown in Figure 4.7 and Figures 4.9-10.

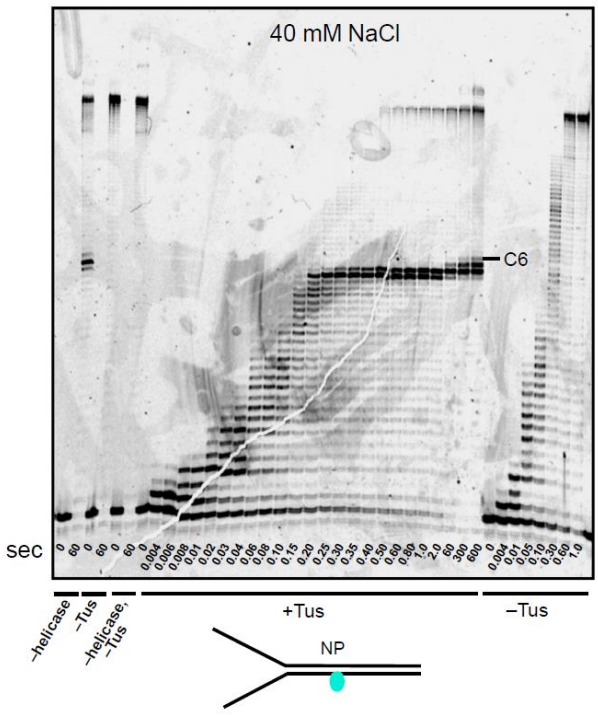

Figure 4.6: Strand displacement DNA synthesis by T7 helicase–DNA polymerase on the NP fork DNA substrate

Reactions in the presence or absence of Tus at 40 mM NaCl and 0.1 mM dNTPs and 1 mM dTTP. Reactions were carried out at 18˚C in the quench flow apparatus. The DNA sequencing gel shows the resolved reaction products on quenching at various time points. Controls lanes without helicase or Tus are indicated. The C6 base position on *TerB* is marked.

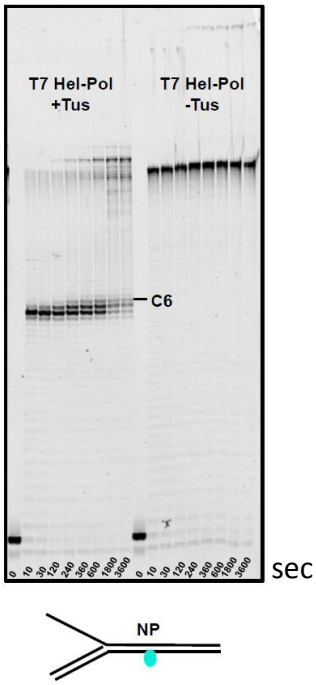

Figure 4.7: Strand displacement DNA synthesis by T7 helicase–DNA polymerase in the presence and absence of Tus on NP fork DNA

The DNA sequencing gel shows the resolved reaction products after quenching at various time points. Reactions were carried out at 18˚C at 50 mM KCl. The C6 base position in *TerB* is marked.

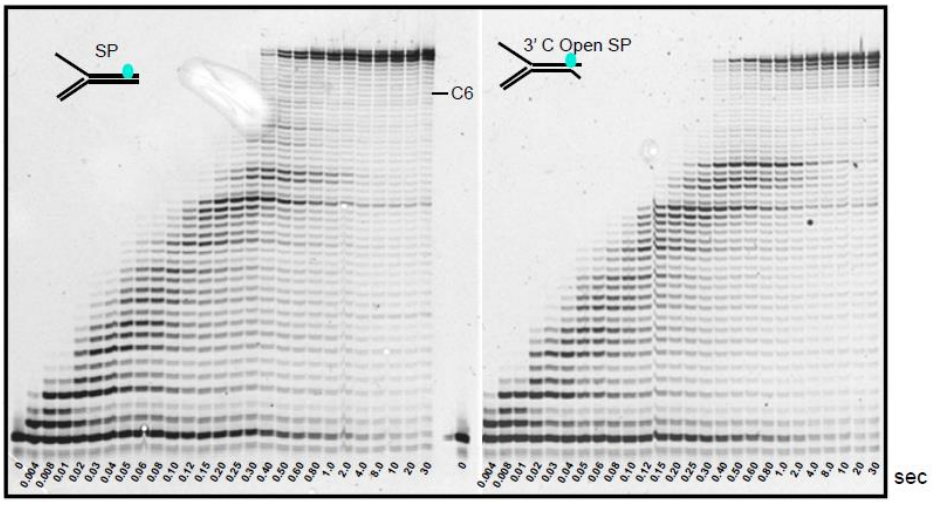

Figure 4.8: Strand displacement DNA synthesis by T7 helicase–DNA polymerase on P fork DNAs SP and 3' C Open SP in the presence of Tus

The DNA sequencing gel shows the resolved reaction products after quenching at various time points. Reactions were carried out at 18˚C at 50 mM KCl in the quench flow apparatus. The C6 base position on *TerB* is marked.

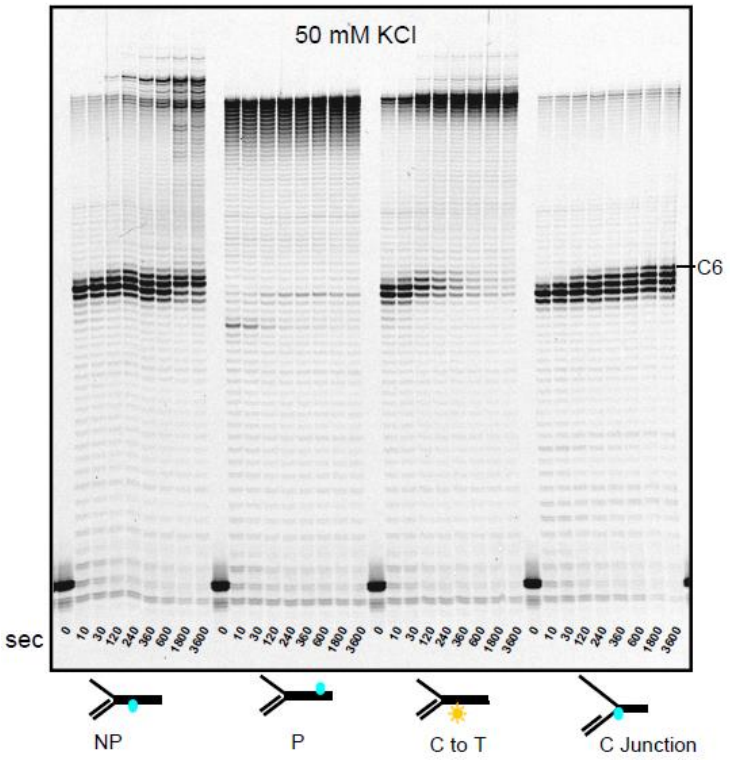

Figure 4.9: Strand displacement DNA synthesis by T7 helicase–DNA polymerase in the presence of Tus on fork DNAs with the *TerB* sequence in NP and P orientations or with mutation in the NP orientation at 50 mM KCl

The DNA sequencing gel shows the resolved reaction products after quenching at various time points. Reactions were carried out at 23˚C at 50 mM KCl. The C6 base position on *TerB* is marked.

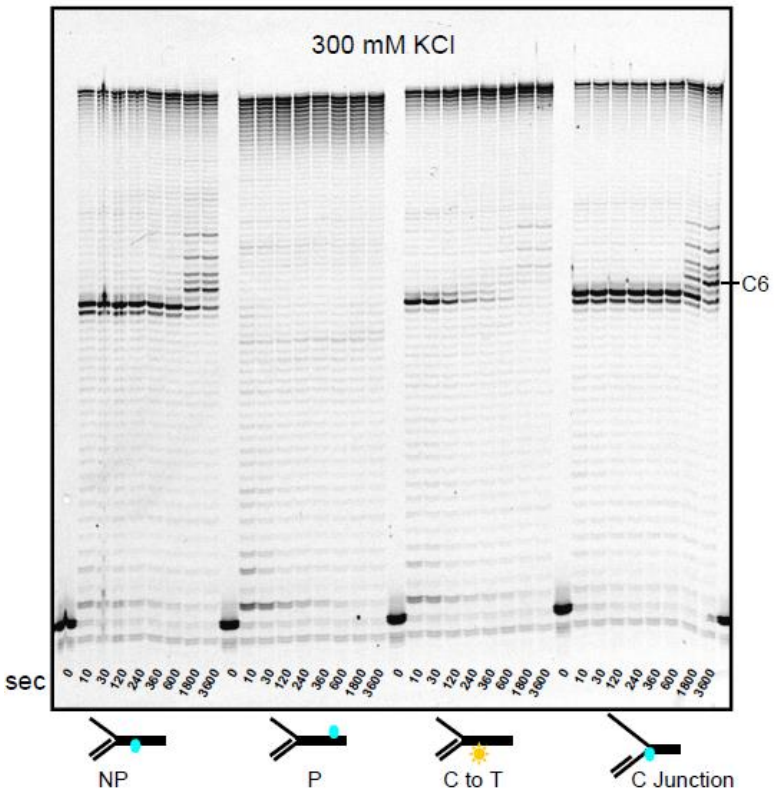

Figure 4.10: Strand displacement DNA synthesis by T7 helicase–DNA polymerase in the presence of Tus on fork DNAs with the *TerB* sequence in NP and P orientations or with mutation in the NP orientation at 300 mM KCl

The DNA sequencing gel shows the resolved reaction products after quenching at various time points. Reactions were carried out at 23˚C at 300 mM KCl. The C6 base position on *TerB* is marked.

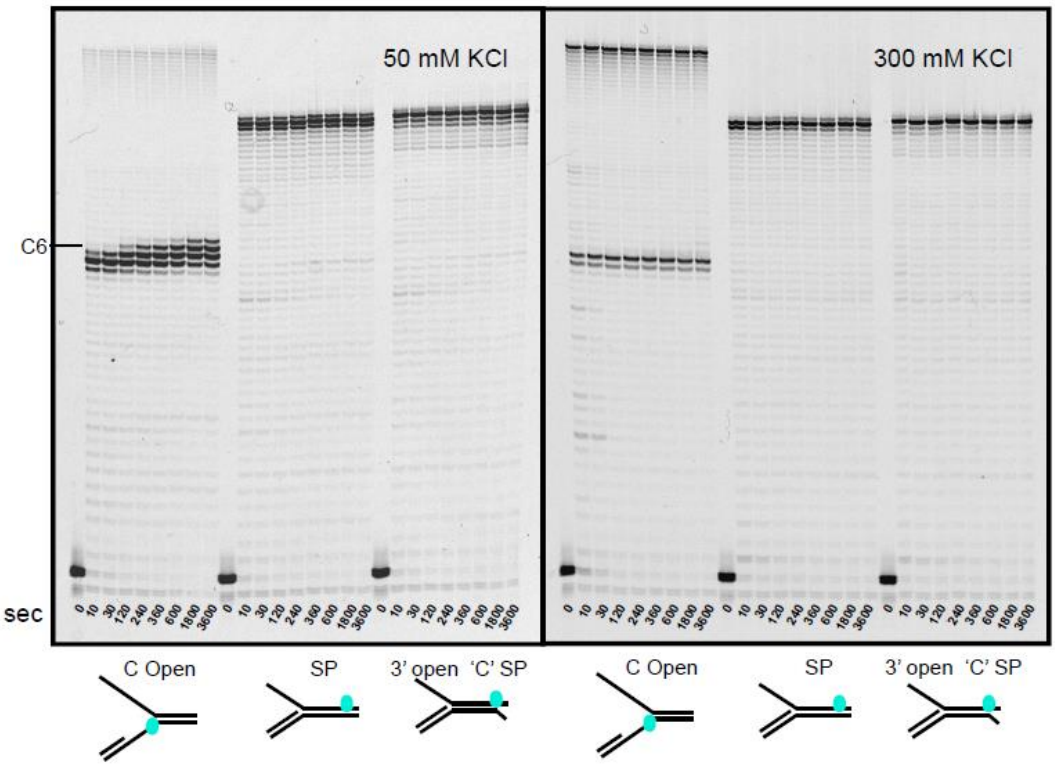

Figure 4.11: Strand displacement DNA synthesis by T7 helicase–DNA polymerase in the presence of Tus on fork DNAs with the *TerB* sequence in NP and P orientations or with mutation in the NP orientation

The DNA sequencing gels show the resolved reaction products after quenching at various time points. Reactions were carried out at 23˚C at 50 and 300 mM KCl. The C6 base position on *TerB* is marked.

4.3.2 Importance of GC6 of *Ter* in Replication Arrest

To investigate the role of the GC6 bp in the operation of the mousetrap, we prepared similar fork templates containing mutant NP *TerB* sequences (Figure 4.4). In one set, the GC6 bp was replaced with AT6 or CG6 (C to T/G). In a second, the *Ter* sequence was unpaired (pre-melted) at the NP end either up to AT5 (C Junction) or GC6 (C Open). In contrast to the GC6 wild-type *TerB*, DNA synthesis by helicase–polymerase was no longer

permanently arrested on the AT6 or CG6*Ter*s (C to T/G) (Figure 4.12A); instead, synthesis paused for 20–30 s at A4 and A5 and then Tus was displaced. Three times more run-off products (~ 70%) were observed with these mutant forks in comparison to the GC6 forks (~ 10–20%) in 4 min (Figure 4.12B).

Similar results were obtained in tethered bead experiments. The GC6 to CG6 (C to G) mutant *TerB* resulted in five-fold increased run-off (Figure 4.12C,D) after a pause duration of 135 ± 15 s (Figure 4.12E). However, 54% of the molecules still exhibited full stoppage at *TerB* (Figure 4.12C and Figure 4.3A). We attribute the lower percentage of run-off and the longer pause duration in the single-molecule assay to the differences in composition of the replication buffers in the two experiments; the Tus–ds*TerB* complex is known to have a much lower K_D in buffers containing potassium glutamate than KCl[101,130,244]. In the case of the TA6 substitution (C to A), we observed an eight-fold increase in run-off (Figure 4.12C and Figure 4.3B) after a pause duration of 60 ± 5 s (Figure 4.12E). The GC6 to TA6 substitution (C to A) allows more run-off synthesis in comparison to GC6 to CG6 (C to G) substitution and this is consistent with a binding study that showed a modest effect on Tus binding to ds*TerB* when GC6 was replaced with a CG6 (C to G) in comparison to a TA6 (C to A). Note that although we used TA6 (C to A) rather that the AT6 (C to T) *TerB* mutant described above, we expect the behavior of these to be similar because their affinity for Tus in both the ds*Ter*[257] and locked[130] complexes is essentially identical, and their (reduced) efficiency of fork arrest *in vivo* are the same[257]. Although none of these three GC6 mutations was reported to produce more than a four-fold increase of the K_D of the Tus–ds*TerB* interaction, they all led to a very significant reduction of fork

arrest *in vivo*, consistent with the importance of the C6 base in operation of the mousetrap[257]. In our single-molecule experiments, the GC6 to TA6 (C to A) substitution resulted in less frequent permanent stoppage and more frequent restart after shorter pauses compared to the GC6 to CG6 (C to G) mutation (Figure 4.12C,D). This is not completely consistent with the *in vivo* data of[257], who showed that the GC6 to CG6 (C to G) mutation resulted in a more serious defect in fork arrest compared to the GC6 to TA6 or AT6 (C to A/T) substitutions. There are clearly subtle aspects that will be resolved in future experiments. The 100% efficiency of transient pausing or stoppage of DNA synthesis in the CG6 and AT6 *TerB* sequences (C to G/T) demonstrates that the run-off DNA synthesis detected in the quenched flow assay primarily occurs after transient pausing of DNA synthesis in all of the replicated DNA molecules.

Interestingly, the histograms of the pause duration in the single-molecule assays followed a Gaussian distribution (Figure 4.12E), indicating that the underlying mechanism of pausing and restart of DNA synthesis involves at least two steps; a single exponential decay is predicted for a single-step process. This is consistent with the observation of multiple stoppages and slow rates of DNA synthesis during the incorporation of T3–A5 (Figure 4.5C,D). Collectively, these results indicate that the conserved GC6 bp is critical for permanent arrest of the helicase–polymerase fork by the mousetrap, but they also suggest contribution of a preceding dynamic clamping process that is independent of GC6.

Unpairing the NP end of *TerB* up to A5 (so GC6 is at the fork junction, C Junction) or up to C6 (so C6 is melted, C Open) was highly effective in completely arresting DNA synthesis.

On these pre-melted *Ter* templates, DNA synthesis paused at A4 for 30 s, but was completely blocked at A5 and G6 (Figure 4.12A, Figures 4.9-11, Figure 4.13); only 6–8% run-off synthesis was observed in 4 min as compared to ~20% in the paired *Ter* sequence (Figure 4.12B). This is consistent with the expectation of the mousetrap model that a pre-melted *Ter* sequence with the C6 base already bound in its pocket in Tus would present the strongest barrier to Tus displacement by replisomes[130]. To narrow down the role of the C6 base, we prepared a fork with a CC6 mispair (C C Bubble). This single base mispair was as effective at arresting DNA synthesis as the pre-melted forks (Figure 4.12A,B).

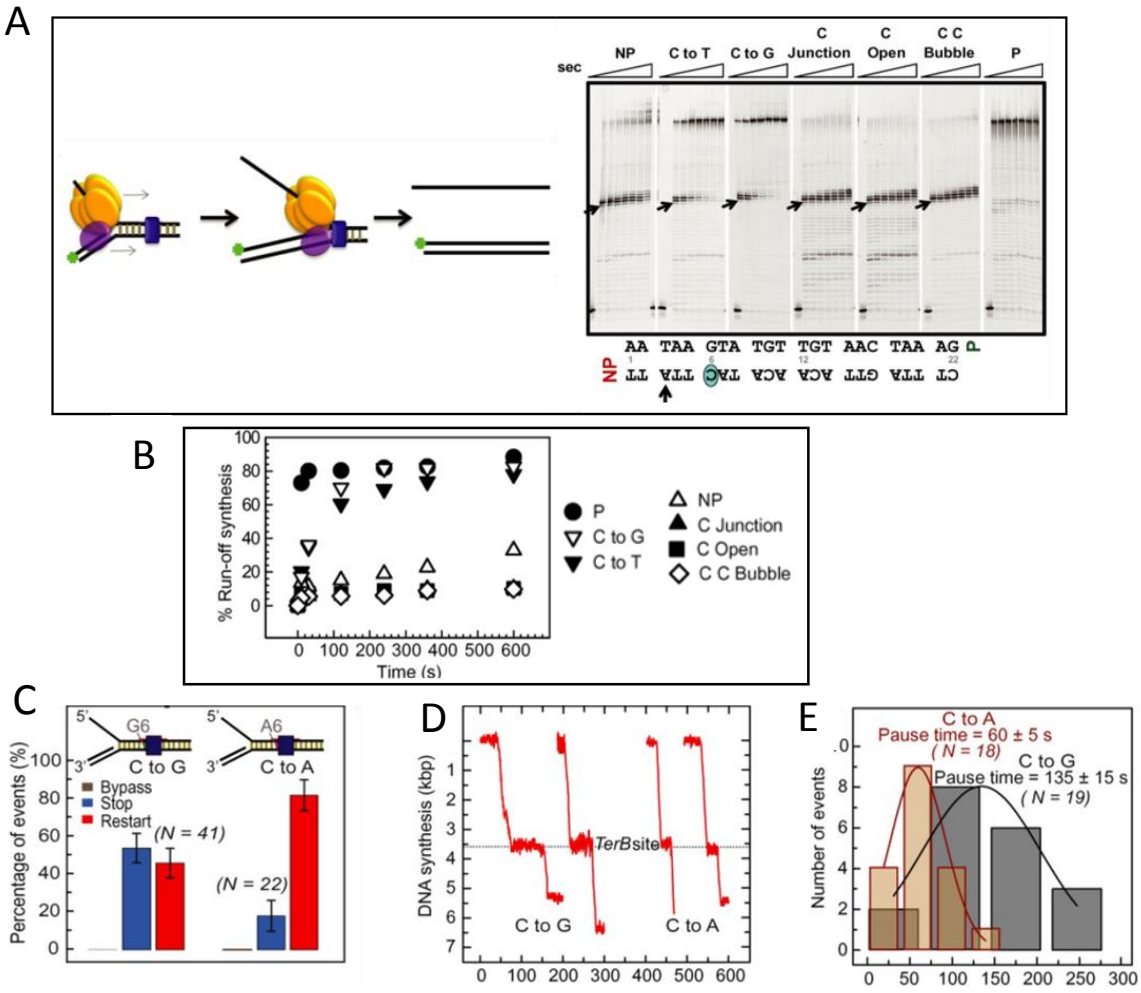

Figure 4.12: Strand displacement DNA synthesis by T7 helicase–polymerase on variant Tus–*Ter* fork DNAs

A. T7 helicase and T7 DNA polymerase were preincubated with the preformed replication fork substrate and reacted with 1 mM dNTPs. DNA forks: NP, GC6 to AT mutation (C to T), GC6 to CG mutation (C to G), GC6 at the junction (C Junction), C Open, C C Bubble and P. Reactions were quenched at 0, 10, 30, 120, 240, 360, 600, 1800 s and products were resolved in sequencing gels. Arrows indicates the first arrest position band corresponding to the arrow on the *TerB* sequence below.

B. Plot showing '% run-off synthesis' against time, quantified from the gels in (A), as described in the methods.

C. Percentages of the populations of replication forks that bypassed (gray), transiently stopped (red) or fully stopped (blue) at Tus bound to *TerB* sites bearing the GC6 to CG (C to G; left) or GC6 to TA mutation (C to A; right). Error bars correspond to the standard deviation of binomial distributions.

D. Representative single-molecule trajectories of the restart of DNA synthesis after transient stoppage at CG6-NP and TA6-NP *TerB* are shown.

E. The pause durations for events that restarted at CG)-NP or TA6-NP *TerB* were fit with Gaussian distributions (black and red lines, respectively). The repeat experiments carried out at 23°C are shown in Figures 4.9-11 and 4.13.

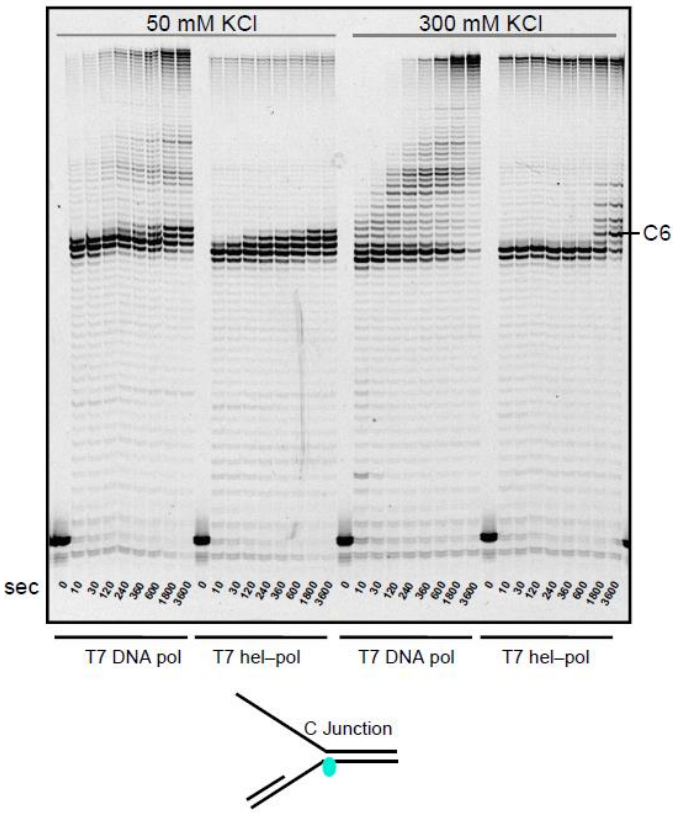

Figure 4.13: Strand displacement DNA synthesis by T7 helicase–DNA polymerase and DNA polymerase alone in the presence of Tus on "C Junction" fork DNA

The DNA sequencing gel shows the resolved reaction products after quenching at various time points. Reactions were carried out at 23˚C at 50 and 300 mM KCl. The C6 base position in *TerB* is marked.

4.3.3 The Isolated DNA Polymerase Is Not Permanently Arrested at the NP Face but Is Arrested at the P Face

T7 DNA polymerase promotes limited strand displacement DNA synthesis in the absence of the helicase[248]. We next probed if the Tus−*Ter* complex could stall the polymerase in the absence of the helicase. There are several scenarios here that depend on the relative power of the polymerase and helicase motors and whether strand separation occurs in a way that allows the C6 base of the displaced strand to access its binding site in Tus.

We found that the isolated polymerase is *not* permanently arrested at the NP face of Tus−*Ter**B*. DNA synthesis paused at T3 but mostly at A4, two nucleotides before the GC6, but within 2–4 min the polymerase overcame the Tus barrier to make ∼ 55% run-off products (Figure 4.14A,B and Figure 4.15). The strand displacement synthesis beyond the Tus barrier is not very processive as indicated by accumulated DNA products below the run-off product and this is because of the absence of helicase. The GC6 to AT6 or CG6 (C to T/G) mutant*TerB* sequences behaved very similarly, showing long pauses at A4 but no permanent arrest. The pre-melted *Ter* sequences, on the other hand, completely arrested the isolated T7 DNA polymerase, but at A5, which is just one nucleotide before GC6 (Figure 4.14A, Figure 4.13, Figure 4.15). The completely open C6 base was most effective, permitting only ∼5% run-off in 4 min (Figure 4.14B). When the GC6 is premelted, then polymerase stops one nucleotide before the C6 base, which is similar to T7 DNA polymerase arrest one nucleotide before the interstrand crosslink in dsDNA[248]. Thus, the C6 base in the premelted forks is most likely flipped into the Tus binding pocket to form a tight barrier before polymerase approaches it.

Although T7 DNA polymerase alone was not arrested at the NP end, we observed pausing of DNA synthesis at the P end at A(23) and G(22) and a complete block at A(20) and A(19) within 10–30 s (Figure 4.14A). This was unexpected and indicates that arrest by Tus−*Ter* depends both on the polarity of the DNA motor and the strand that it occludes as it approaches the Tus−*Ter* complex. As corroborated below, the 5′–3′ helicase is arrested at the NP but not the P face, whereas the 3′–5′ polymerase motor is arrested with the reverse polarity by a mechanism independent of C6 base flipping.

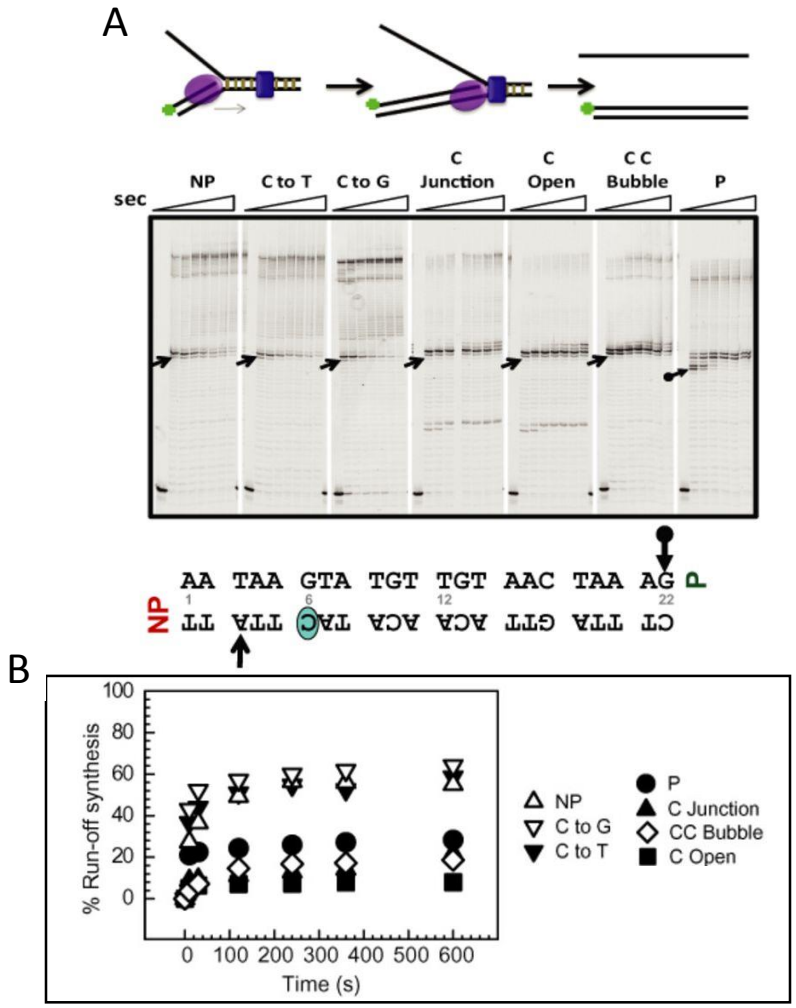

Figure 4.14: Strand displacement DNA synthesis by T7 DNA polymerase alone on various Tus–*Ter* fork DNAs

A. T7 DNA polymerase was preincubated with the preformed replication fork substrate and reacted with 1 mM dNTPs. The DNA forks used here were as follows: NP, GC6 to AT mutation (C to T), GC6 to CG mutation (C to G), GC6 at the junction (C Junction), C Open, C C Bubble and P. Reactions were quenched at 0, 10, 30, 120, 240, 360, 600, 1800 s and products resolved in sequencing gels. Arrows indicates the first arrest position band corresponding to the arrows on the *TerB* sequence below.

B. Plot showing '% run-off synthesis' against time, quantified from the sequencing gels in (A). The duplicate sets of experiments are shown in Figure 4.15 and also those conducted at 23°C in Figure 4.13.

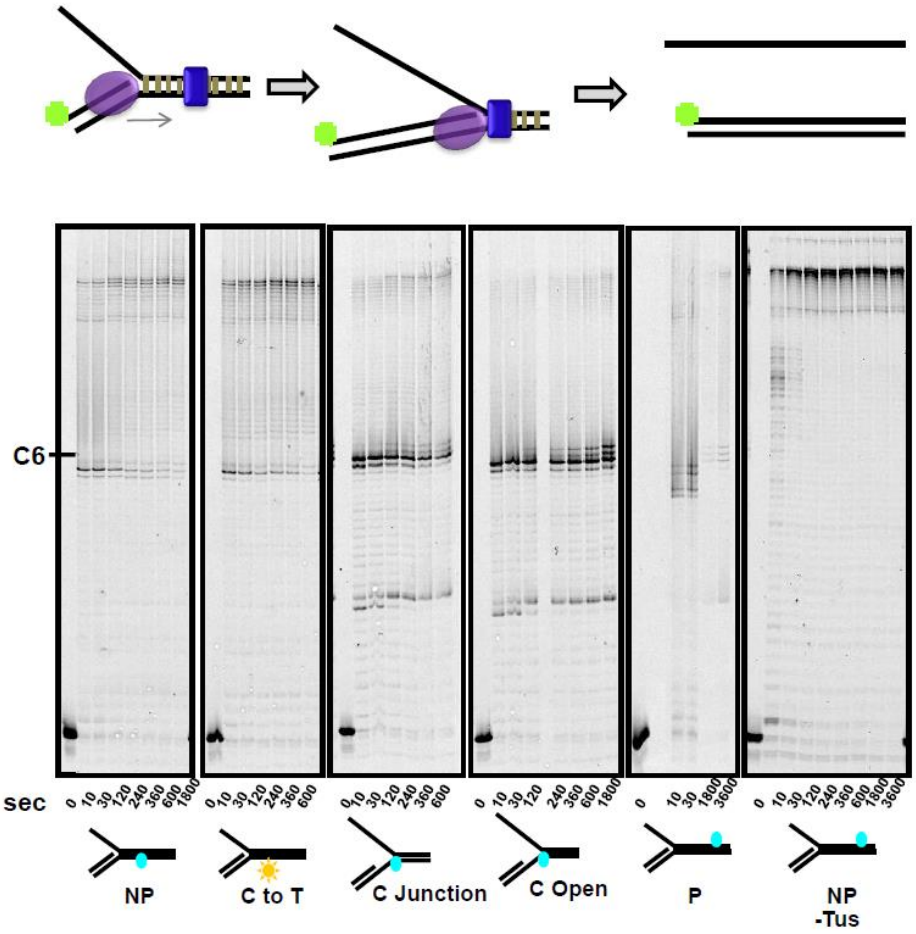

Figure 4.15: Strand displacement DNA synthesis by T7 DNA polymerase alone on various Tus–*Ter* fork DNAs

Cartoon depiction of the strand displacement assay design (Top panel). T7 DNA polymerase was preincubated with the preformed replication fork substrate and reacted with 1 mM dNTPs. The DNA forks used here were as follows: NP, GC6 to AT mutation (C to T), C at the junction (C Junction), C Open and P. Reactions were quenched at 0, 10, 30, 120, 240, 360, 600, 1800 s and products resolved in sequencing gels. Reactions were carried out at 18ºC at 50 mM KCl. The C6 base position on *TerB* is pointed out.

4.3.4 The Isolated T7 Helicase is Arrested at the NP but not the P Face

We used a real-time fluorescence-based DNA unwinding assay on a stopped flow instrument to monitor fork separation by the T7 helicase[253,256,258]. The helicase unwinds the NP fork within 2.5 s in the absence of Tus, but strand separation is completely blocked when Tus is present (Figure 4.16A and Figure 4.17). A radiometric strand separation assay[218,256] showed similar results. T7 helicase unwinds the NP fork without Tus, but not with Tus present (Figure 4.16B,C). The P fork, on the other hand, is unwound by the helicase with or without Tus. The pre-melted fork bound to Tus is slightly more effective in blocking the helicase. Thus, unlike the 3'–5' translocating DNA polymerase motor, the 5'–3' translocating helicase is arrested at the NP, but not the P, face of Tus–*Ter* (Figure 4.16D).

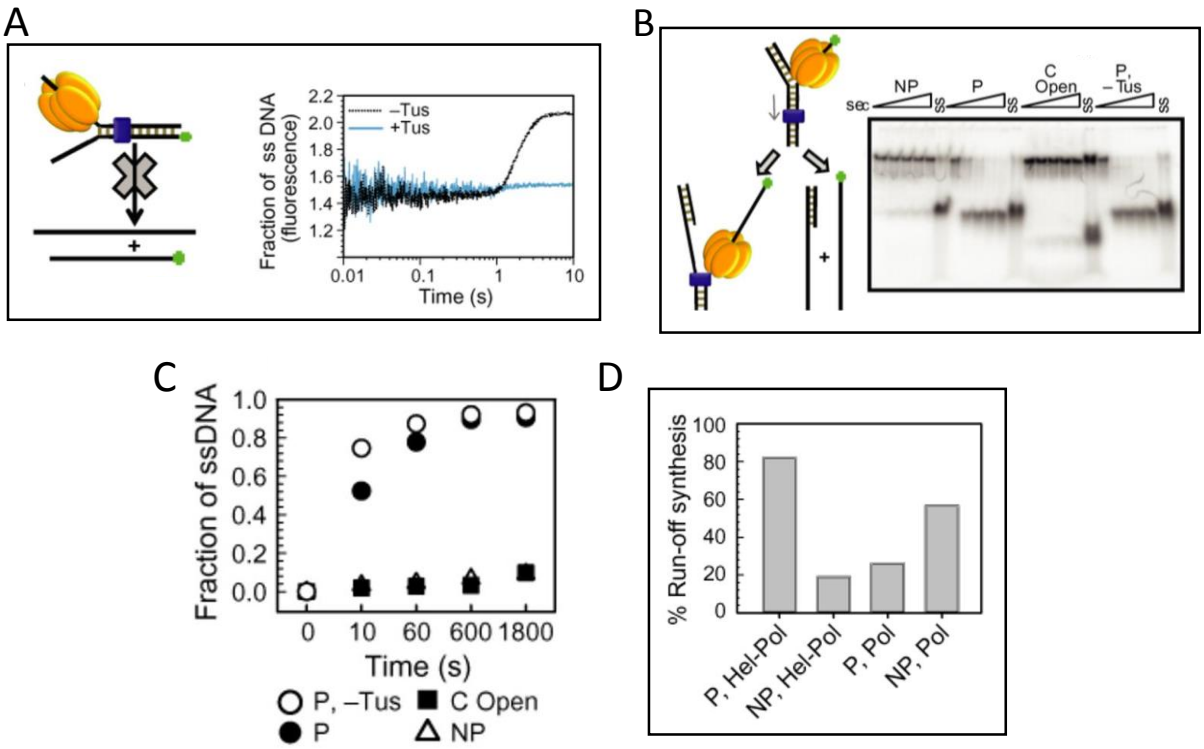

Figure 4.16: DNA unwinding by T7 helicase alone on various Tus–*Ter* fork DNAs

A. Cartoon depiction of the stopped-flow fluorescence unwinding assay design (left). Fluorescence intensity traces represent the unwound ssDNA fraction as the result of DNA unwinding activity of T7 helicase on a NP fork in the presence and absence of Tus (right), plotted against time. The plots are average of at least five reactions.

B. Radiometric gel unwinding assay showing helicase unwinding activity in the presence of Tus on NP, C Open, permissive P forks and on permissive P DNA forks in the absence of Tus. Reactions were quenched at 0, 10, 60, 600, 1800 s and then resolved in a non-denaturing PAGE gel. Lanes marked 'ss' represent single-stranded labeled DNA.

C. Plot showing unwound ssDNA fraction against time, quantified, as described in the methods.

D. Comparison of run-off synthesis by helicase–DNA polymerase and DNA polymerase on fork DNAs with ds*TerB* in the NP and P orientations. The duplicate sets of experiments are shown in Figure 4.17.

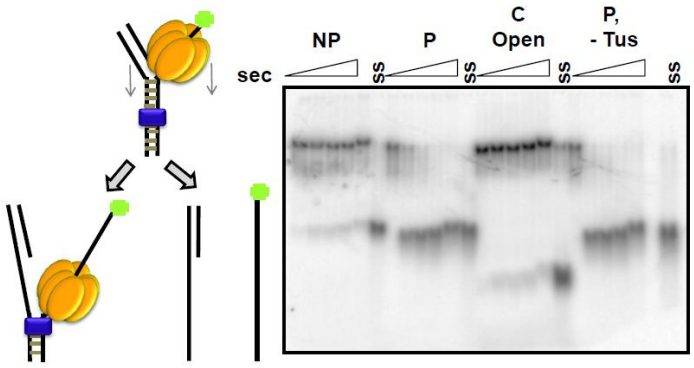

Figure 4.17: DNA unwinding by T7 helicase alone on various Tus–*Ter* fork DNAs

Cartoon depiction of the unwinding assay design (left panel). Radiometric gel unwinding assay showing helicase unwinding activity in the presence of Tus on NP, C Open, P forks and on P DNA forks in the absence of Tus. Reactions were quenched at 0, 10, 60, 600, 1800 seconds and then resolved in a non-denaturing PAGE gel. Lanes marked 'ss' represent single-stranded labelled DNA.

4.4 Discussion

How DnaB helicase and the *E. coli* replisome are arrested on their approach to the NP face of the Tus−*Ter* complex, but manage to displace Tus on approach to the P face, has been a subject of many studies. Despite evidence for several proposed fork arrest mechanisms, answers to this fundamental question are still controversial[86]. Three models of polar arrest include the helicase interaction, mousetrap and dynamic clamp models. Our results showing that the heterologous T7 helicase is arrested in a polar manner by the *E. coli* Tus−*Ter* complex argues against obligatory Tus/DnaB interaction in determining polarity[221,246]. Since T7 DNA contains no *Ter* sites, it seems unlikely that the heterologous T7 helicase would have evolved to show highly specific interactions with Tus and our results confirm that there is an intrinsic mechanism of replication arrest that is independent of protein–protein interactions. Nevertheless, because the T7 helicase is related to DnaB, it is plausible that there may be conserved structural features that facilitate Tus–helicase interactions in events that precede those detectable in our assays, and it is also possible that the putative Tus–DnaB interaction has an ancillary non-essential role in arrest of the *E. coli* replisome. Over the past decade, we have sought using sensitive surface plasmon resonance (SPR) methods in a variety of formats to detect a direct physical interaction between Tus and DnaB, but have so far been unsuccessful in doing so. Moreover, recent work showing that Tus−*TerB* provides a weaker, but still polar, replication fork barrier in yeast[221,246] is also inconsistent with a necessary role for Tus–helicase interactions.

The alternative models for polar fork arrest do not require protein–protein interactions. The mousetrap model postulates that when the helicase unwinds the GC6 bp of *Ter*, the unpaired C6 binds in a specific binding pocket on Tus to create a tight binding interface that permanently blocks a replication complex arriving at the NP face[130]. The dynamic clamp model proposes that there is an intrinsic difference in the interactions of the Tus protein with the *Ter* site at the P versus the NP face[101,127]. Despite the elegance of the mousetrap mechanism for fork arrest at Tus-bound *Ter* sites, its pivotal role in replication termination has remained controversial, because of the diversity of results of *in vitro* strand displacement assays with various 3′–5′ and 5′–3′ helicases with different mechanisms and structures approaching Tus−*Ter* complexes from either direction (reviewed in [243]). In particular, reported polar arrest of DnaB sliding over dsDNA toward the NP face (i.e. without strand separation)[246] is inconsistent with the mousetrap model, but is explained by the dynamic clamp. Most of these studies can now be reconciled with the operation of a dynamic clamp and/or mousetrap mechanism, depending on the inherent polarity and structure of the helicase to produce a free rather than trapped C6, combined with an assessment of the relative power of the helicase motor under the conditions of the particular assays.

The evidence for a composite mousetrap and dynamic clamp model is the observation that the T7 replisome slows at A4, a few nucleotides before GC6 (dynamic clamp) even when the GC6 is mutated to AT6 and CG6 (C to T/G), but permanent fork arrest only happens with the wild-type GC6 sequence, where the C6 base flips into its specific binding pocket (mousetrap). It should be noted that mutation of GC6 to AT6, TA6 or CG6 (C to

T/A/G) severely compromises replication termination *in vivo* in *E. coli*, but has only a slight effect on the affinity of Tus for ds*TerB;* thus permanent fork blockage *in vivo* depends on the GC6 bp, likely involving the ultimate operation of the mousetrap.

It is notable that the K_D of the locked form of Tus−*TerB* is only three-fold lower than the Tus−*TerB* duplex, but the half-life of the locked form is 40-fold longer[130]. This comparison indicates that induction of C6 base flipping may be a slow and inefficient process, but once formed the complex is kinetically stable. We showed that Tus−*TerB* pauses DNA synthesis by the T7 replisome for 20–30 s at A4 and the single-molecule tethered bead experiments showed that all replicated DNA molecules pause, at least transiently, even when the GC6 bp was mutated (Figure 4.1D and Figure 4.12C). This indicates Tus−*Ter* interactions slightly upstream of GC6 transiently stop the replisome and the run-off synthesis within the first 20–30 s is due to failure of C6 base flipping in some of the replicated molecules. However, premelting the C6 base converts the transient pause to a complete arrest of DNA synthesis just before the C6 base. Indeed, even a single mismatched CC6 bubble was sufficient to do this. We showed previously[130] using SPR that this structure in an otherwise fully ds*TerB* does not lead to formation of a locked complex with Tus. However, here the situation is quite different; pausing of the replisome (Figure 4.12A) or the polymerase alone (Figure 4.14A) at A4 would leave only one bp of dsDNA before the bubble, which would be expected to readily separate thermally to facilitate entry of C6 into its binding pocket. These results are all consistent with the critical involvement of C6 in the mousetrap mechanism of polar arrest, operating under physiological conditions of ionic strength. We propose that transient pausing of the fork

before C6 provides a mechanism that enables Tus−*Ter* to deal with the inefficient base flipping process.

DNA unwinding by T7 helicase alone was arrested by Tus−*Ter* in the NP but not the P orientation. However, the Tus−*T*er complex failed to permanently arrest T7 DNA polymerase at its NP face when the helicase was absent. Thus, the Tus−*Ter* mediated blockage of DNA motors depends on whether the motor approaching the NP face is traveling along the 5′-non-template strand (as is the T7 helicase) or the 3′-template strand (the polymerase). The 5′–3′ translocating helicase motor is effectively blocked at the NP face, but the 3′–5′ translocating polymerase motor is not effectively arrested. We rationalize these results as follows: the polymerase moves on its template 3′-strand that contains the C6 base and traps the C6 nucleotide within its template binding channel[259]. This prevents flipping and binding of C6 into the cytosine-binding pocket of Tus. On the other hand, the helicase moves on the opposite 5′-strand, trapping G6 within its central DNA binding channel and effectively excluding C6 so that it is free to bind to Tus. Thus, at the NP end, helicase alone is arrested but polymerase alone is not. Only the pre-melted C6 base that can bind in the template binding pocket of the DNA polymerase can effectively arrest the polymerase coming toward the NP face. That the polymerase alone is blocked efficiently when C6 is premelted further reinforces the argument that specific helicase–Tus interactions are unnecessary to provide an effective block to motor proteins, and indicate that the C6 in normal ds*Ter* is exposed by the T7 helicase before it is trapped by the polymerase.

Nevertheless, the very close proximity of the polymerase active site that can approach to within a few nucleotides of the strand separation 'pin' of the helicase–polymerase is evident from our single base resolution assays that show that DNA synthesis proceeds without impediment to two nucleotides before the conserved GC6 bp of the *Ter* sequence. This is consistent with our recent study which showed that the T7 helicase and polymerase move together at the fork to unwind and copy the DNA in single-nucleotide steps and the 'pin' of strand separation by the helicase–polymerase[248], which is the leading subunit of the helicase hexamer[251], is within two nucleotides of the polymerase active site[248] as shown in Figure 4.18. Polymerase and helicase proximity was apparently also observed with the *E. coli* replisome, which was arrested at the fourth bp before GC6[260,261]. While the *E. coli* studies were at much lower time resolution and may have been complicated by completion of synthesis occurring after dissociation of the helicase[243], this is clearly not the case here where the polymerase reaches at least to TA3 without any sign of pausing. The helicase must normally be involved in this pre-melting step to explain the effective arrest of the helicase–polymerase complex at the NP face. The helicase, a few nucleotides ahead of the polymerase can capture the G6 nucleotide of *Ter* within its central channel, while pausing of the replisome upon encounter with the dynamic clamp provides time for the exposed complementary C6 base of *Ter* to flip and lock into the cytosine-binding pocket of Tus to spring the mousetrap. The helicase thus promotes permanent arrest of the replication fork just before the polymerase is able to capture the exposed C6 by DNA synthesis; this would otherwise lead to displacement of Tus. Thus, a kinetic competition between trapping of C6 by lock formation and DNA

synthesis dictates the efficiency of fork arrest. On the other hand, an isolated DNA polymerase, although slowed by the dynamic clamp, can eventually trap C6 by DNA synthesis, thus disabling the mousetrap mechanism and dissociating Tus for continued DNA synthesis.

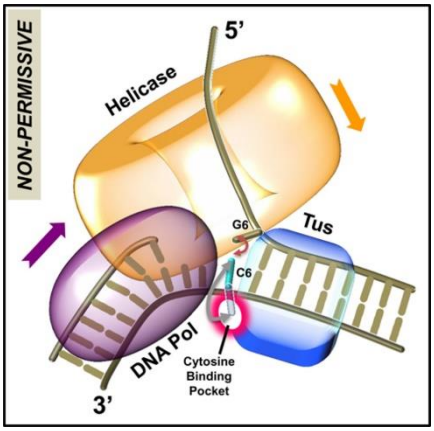

Figure 4.18: Model for replication fork arrest

The helicase ring and DNA polymerase are bound at the fork junction containing the Tus–*Ter* complex. After the *Ter* sequence is unwound up to the GC6 base pair, the unpaired C6 base can flip out and bind into the cytosine-specific pocket on Tus to form the C6 Tus–*Ter* lock, or reanneal back with its complementary base G6, or become base-paired through DNA synthesis. The 'pin' for strand separation occurs when C6 on the template strand is already within three or fewer nucleotides of the polymerase active site. When the helicase-polymerase complex unwinds DNA, the helicase traps the G6 base to prevent reannealing of GC6 base pair, aiding formation of the locked complex. If GC6 base pair is unwound by the strand displacement activity of the isolated polymerase, the C6 is captured by the polymerase through DNA synthesis, which prevents the formation of the locked complex.

Another unanticipated observation was that the isolated T7 DNA polymerase was arrested when arriving at the other (P) end of the termination complex, before significant

strand separation at the NP end of *Ter*. This result is not explained by the mousetrap model, since DNA synthesis is arrested many nucleotides away from the GC6 and in this situation the GC6 bp would still be intact. Examination of the Tus−*Ter* crystal structures[127,130] shows that even though protein–DNA interactions are distributed throughout the length of the *Ter* sequence, the Tus protein interacts extensively and preferentially with the 5′-end at the P face, i.e. the lagging strand template (Figure 4.19). These interactions preferentially slow the isolated polymerase at the P end because the motor is traveling on the 3′-strand and hence less effective at breaking interactions that are mainly with the 5′-strand it is displacing. Essentially, the polymerase traveling along the 3′-strand cannot compete directly with the Tus interactions with the 5′-strand. On the other hand, the helicase traveling along the 5′-strand would be able to compete directly with and break Tus−*Ter* interactions at the P end, as observed. These results are consistent with a previous study that also observed partial arrest of T7 DNA polymerase at the P face of Tus−*Ter*[141]. These findings imply that the Tus−*Ter* mechanism blocks the 3′–5′ directionality motors such as polymerases or helicases arriving at the P face and prevents them from colliding with the stalled replication fork, but interestingly allows the 3′–5′ directionality motors to disable the mechanism at the NP end.

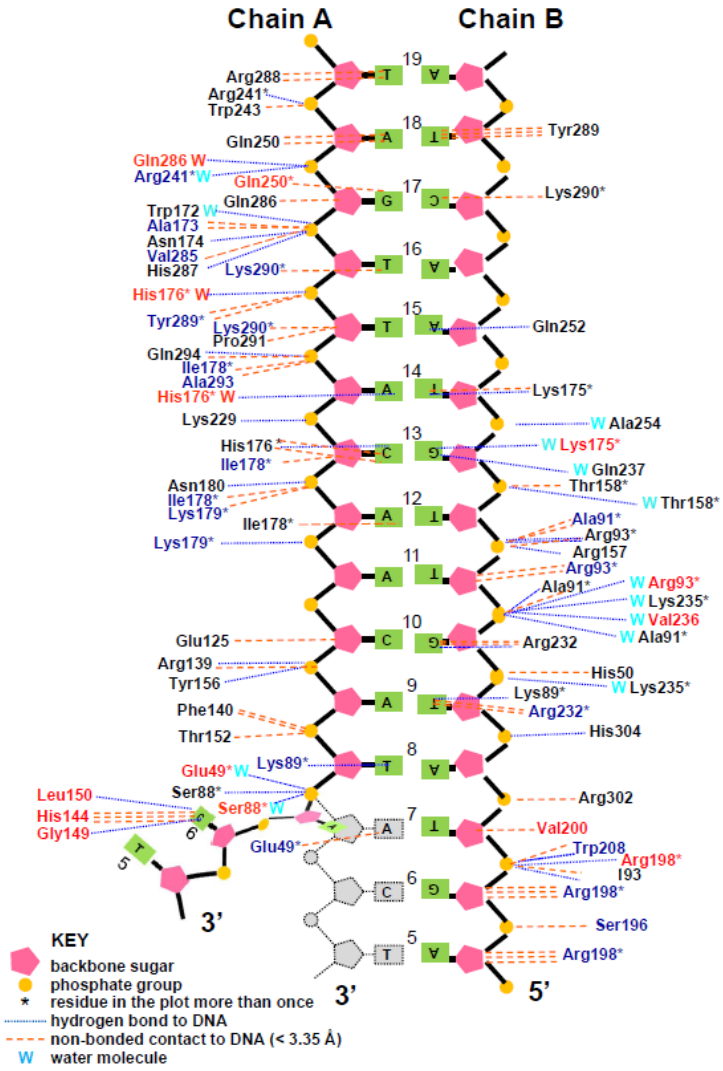

Figure 4.19: A schematic summary of the Tus–DNA contacts in Tus–*Ter* complexes

Contacts are derived from reported crystal structures with and without C6 Tus–*Ter* lock formation[130]. The positions of the bases 5–7 (NP; bottom) are flipped out from the original position shown in grey shade on lock formation. All interactions shown here are within 3.6 Å distance, and putative water mediated H-bonds are included. Interactions with amino acids shown in blue are observed only in the unlocked structure and those in red only in the locked structure. The T7 helicase translocates on Chain B (right) as it approaches the NP face, while the template strand for the polymerase is Chain A (left).

4.5 Materials and Methods

4.5.1 Proteins

T7 gp4 (gp4A'), T7 gp5 Exo$^-$ (D5A, D7A) and T7 gp5/ thioredoxin wild-type proteins were purified using published protocols[217-220]. *E. coli* thioredoxin was purchased from Sigma Life Sciences. His_6Tus protein was purified as described[101]. Protein concentration was calculated by UV absorption (in 8 M guanidine.HCl) using the extinction coefficients at 280 nm of 0.0836 $\mu M^{-1}cm^{-1}$ for gp4, 0.13442 $\mu M^{-1}cm^{-1}$ for gp5 and 0.0397 $\mu M^{-1}cm^{-1}$ for Tus.

4.5.2 Quenched Flow DNA Substrates

Oligodeoxynucleotides were purchased from Integrated DNA Technologies (IDT) and polyacrylamide gel electrophoresis (PAGE) purified (Figure 4.4 and Figure4.2). The concentration of purified oligonucleotides was determined from their absorbance and extinction coefficients at 260 nm after digestion with snake venom phosphodiesterase I[253,262,263]. For quenched flow DNA synthesis assays, a 24-nucleotide primer was labeled with fluorescein [(5/6)-FAM, SE: 5-(and-6)-carboxyfluorescein, succinimidyl ester, mixed isomers]. The 5'- and 3'-strands were mixed in equal proportions with 24-nucleotide primer in the annealing buffer (50 mM Tris–Cl, pH 7.6, 50 mM KCl, 10% glycerol) and fork annealing was carried out at 95°C for 10 min followed by slow cooling to room temperature. For the helicase unwinding assay, the 5' or 3' strand of the fork substrate was end labeled with fluorescein or was radiolabeled with γ-[^{32}P]-ATP (Perkin Elmer) using T4 polynucleotide kinase (New England Biolabs).

4.5.3 Kinetics of DNA Synthesis

Strand displacement DNA synthesis kinetics were measured in a rapid quenched-flow instrument (Kin Tek Instruments, Austin, TX, USA) at 18°C[249,256]. T7 helicase was assembled on the fork DNA substrate (with a labeled primer) on ice for 15 min in the presence of 1 mM dTTP. T7 DNA polymerase was prepared by mixing *E. coli* thioredoxin and T7 gp5 Exo$^-$ (mutated in two positions D5A, D7A) (5:1) in replication buffer containing 5 mM dithiothreitol (DTT) at 22°C for 5 min. The DNA polymerase was added to the helicase and fork DNA template and further incubated for 15 min on ice followed by 10 min at the reaction temperature in the presence of the Tus protein. The protein–DNA mixture from one syringe was rapidly mixed with Mg.dNTP mixture from the second syringe. The final mixture contained the four dNTPs (1 mM each, unless specified), $MgCl_2$ (free 4 mM), 190 nM forked DNA template, 375 nM T7 helicase hexamer, 375 nM T7 DNA polymerase, 375 nM Tus, 2 µM bovine serum albumin (BSA), 1 mM dithiothreitol and 1 mM ethylenediaminetetraacetic acid (EDTA) in the replication buffer (50 mM Tris-Cl, pH 7.6, 50–300 mM KCl, 10% glycerol). After desired time intervals the reactions were stopped with 300 mM EDTA. The quenched samples were mixed with bromophenol blue/formamide loading dye, boiled and then resolved in a 24% acrylamide/7 M urea sequencing gel with 1.5× Tris/Borate/EDTA pH 8.4 buffer (TBE buffer). The gel was imaged on a fluorescence imager and the DNA band intensities were analyzed by ImageQuant software. The percent runoff synthesis was estimated from ratio of runoff products (DNA intensity beyond the *TerB* sequence on template) to total DNA intensity in each lane using the following equation, which takes into account the background correction.

% runoff DNA synthesis = [−(D×Ro)+(R×Do)][Do×(D+R)]×100

where *R* is nascent DNA intensity beyond the *TerB* sequence, *D* is nascent DNA intensity up to the *TerB* sequence, 'o' designates intensities at time zero.

4.5.4 Kinetics of DNA Unwinding

The kinetics of DNA unwinding were measured both by real time fluorescence-based and radiometric assays as described in[256]. The fluorescence-based assay was carried out in a stopped-flow instrument (Kin Tek) at 18°C. Fork DNA labeled with fluorescein on the 3'-strand was preassembled with T7 helicase and dTTP with or without Tus in the replication buffer and rapidly mixed with $MgCl_2$ and a dT_{90} ssDNA trap. The final reaction mixture contained 2 mM dTTP, 5 nM DNA substrate, 100 nM T7 helicase hexamer, $MgCl_2$ (free 4 mM), 3 mM EDTA, 6 µM dT_{90}, 2 µM BSA, 20 nM Tus. The fluorescence at >515 nm (cut-off filter at 515 nm) was monitored after excitation with 480 nm light.

In the radiometric assay, the 5'-strand was radiolabeled and assembly with the helicase and Tus was as described above. The final reaction components were 5 nM forked substrate, 100 nM T7 helicase hexamer, 50 nM Tus, 1 mM dTTP and 4 mM $MgCl_2$ in replication buffer. Reactions were quenched with EDTA and sodium dodecyl sulphate and resolved on a non-denaturing PAGE gel in 1.5 × TBE buffer, exposed to the phosphorscreen, and imaged on a phosphorimager. The DNA bands were analyzed using ImageQuant software. A background correction was applied to each unwound fraction value as shown in the equation used to calculate the unwound DNA strand fraction at each time point:

Fractionun wound = [−(DS×SSo)+(SS×DSo)][DSo×(DS+SS)]

where DS is double-stranded DNA fraction, SS is single-stranded DNA fraction and 'o' designates fractions at the zero time point.

4.5.5 Templates for Single-molecule Tethered Bead Assay

Bacteriophage λ-DNA was modified by ligation of a biotinylated fork on one end and a digoxigenin moiety at the other as described previously[182]. The engineered λ-DNA molecules were digested with *EcoRI* to generate a 3.6 kb fragment from the forked end and with *ApaI* to generate a 10.1 kb fragment from the dig end. A 59-bp ssDNA oligonucleotide containing a single copy of wild-type or variants of the 22-nt *TerB* site (in italics for the wild-type NP example, below) and ends complementary to the overhangs in the *EcoRI* and *ApaI* digested fragments (underlined) (5'-AATTCAAGTCAC CACGACTGTGCTATAA*AATAAGTATGTTGTAACTAAAG*TGGTTAATATTATGGCGCGTTGGCC-3') was first 5'-phosphorylated with T4 polynucleotide kinase. It was then annealed to the complementary oligonucleotide (5'-AACGCGCCATAATATTAACCA*CTTTAGTTACAA CATACTTATT*TTATAGCACAGTCGTGGTGACTTG-3'), ligated to the 3.6 kb λ-fork fragment, and the product was gel purified. The fragment was then 5'-phosphorylated at the *ApaI* site and ligated to the 10.1 kb *ApaI* fragment of λ. The final product was gel purified and sequenced to ensure that only a single copy of *TerB* site had been inserted.

The oligonucleotides used for generating the DNA template containing the P *TerB* substrate were 5'-AATTAACGCGCCATAATATTAACCA*CTTTAGTTAC AACATACTTATT*TTATAGCACAGTCGTGGTGACTTGGGCC-3' and

5′-CAAGTCACCACGACTGTGCTATAA*AATAAGTATGTTGTAACTAAAG*TGGTTAATATTAT GGCGCGTT-3′.

4.5.6 Single-molecule Leading-strand Synthesis Assay

Leading strand DNA synthesis and data analysis were carried out as described previously[182] with some variation. Briefly, Tus (80 nM) was first introduced into the flow cell in 30 mM Tris–HCl pH 7.6, 50 mM NaCl, 0.5 mM EDTA, 5 mM DTT, 10 mM $MgCl_2$ for 30 min to ensure saturation of *TerB*. Excess DNA-unbound protein was removed by washing with 15 flow cell volumes in replication mixture [40 mM Tris–Cl pH 7.6, 50 mM potassium glutamate, 0.1 mg/ml BSA, dNTPs (760 µM each), 2 mM DTT, 5 nM T7 helicase (hexamer) and 40 nM T7 DNA polymerase (purified 1:1 complex of gp5 and *E. coli* thioredoxin)]. These conditions allow the assembly of T7 proteins at the fork and synchronize the start of DNA synthesis on introduction of 10 mM $MgCl_2$ and 80 nM Tus in replication mixture. For data analysis, after particle tracking, the traces were corrected for residual instabilities in the flow by subtracting traces corresponding to tethered DNA molecules that were not enzymatically altered. Pauses were defined as a minimum of six data points (at acquisition rate of 2 Hz) with amplitude fluctuations less than three times the standard deviation of the noise. The displacements of the beads were converted into numbers of synthesized nucleotides using a conversion factor (3.76 base/nm) derived from the difference in the length between ss- and ds- λ-DNA[226] at the applied stretching force of 2.6 pN. Total experimental time was 30 min. To obtain statistically significant numbers of events in these multiplexed assays, experiments were repeated two or three times under each experimental condition.

Chapter 5

5. DNA Replication Fork Arrest by *Escherichia coli* Tus−*Ter* Involves Mechanisms that are Independent of the C6-mousetrap Model*

5.1 Abstract

The *Escherichia coli* replication terminator protein (Tus) bound to its termination sites (*Ter*) blocks replication forks approaching from the non-permissive (NP) face, while allows forks approaching from the permissive (P) face to pass[20,23,24,86,128]. Three models were proposed to decipher the molecular mechanism that specifically blocks the fork at the NP face: a dynamic clamping that stops the first-arriving DnaB helicase in the replisome by an asymmetric interactions between Tus and *Ter*[127], a physical interaction between Tus and DnaB[135,145], and lastly a locking mechanism in which strand separation beyond the GC6 base pair flips the conserved cytosine(6) to create a new contact with a cytosine-binding pocket on Tus[130]. The latter "C6-mousetrap" model proposes that the enhanced stability of Tus−*Ter* complex is sufficient to mediate its polar arrest activity. Here we altered various residues in the cytosine-binding pocket and showed using data from *in vitro* single-molecule replication experiments, *in vivo* replication assays and binding studies that the C6-mousetrap mechanism accounts for only half of the fork arrest activity at the NP face of Tus. These results refine the role of the C6-mousetrap mechanism and support the presence of other independent mechanisms.

---

*This chapter contains unpublished data writtein in a format of a manuscript for consistency with the published work in previous chapters

5.2 Introduction

Replication of the circular *E. coli* chromosome initiates at the unique origin sequence (*oriC*) by assembling two replisomes that drive DNA synthesis in opposite direction at a rate approaching 1000 base pairs/s ((bp) s^{-1}) (Figure 5.1A)[19,21,53,115]. Each replisome copies approximately half of the chromosome and stops at the terminus region located roughly across *oriC* (Figure 5.1B)[20,23,86,128]. Despite the differences in rates of the replisomes, their arrival in the terminus is synchronized through a site-specific "replication fork trap" system that halts the first arriving fork and waits for the late arriving one[23,24,128].

The trap consists of ten 23-bp DNA termination sites (*Ter*) each bound tightly to the terminator protein Tus (K_D = of 3.4 × 10^{-13} M in 150 mM potassium glutamate)[23,132]. Tus−*Ter* complexes are arranged into two clusters of five that are spatially located on opposite halves of the chromosome (Figure 5.1B,C). Tus−*Ter* acts in a polar manner by allowing replication forks approaching from the permissive (P) face to proceed but blocks those approaching from the non-permissive (NP) face [20,23,86]. Each cluster orients the NP face of Tus−*Ter*s to block the fork that replicates the opposite half of the chromosome. This sets up the trap for the first arriving fork from either direction[23,24,86]. The role of the trap is to avoid head-to-head collisions between replication and transcription machinery, prevent over replication and genomic instability and coordinate replication termination with the subsequent chromosomal segregation steps at the nearby *dif* site[20,24].

The structure of a Tus–ds*Ter* complex shows a DNA-binding cleft between two α-helical protein domains, and β-strands that make base-specific contacts with the central 13 bp

of *Ter* (Figure 5.1D)[127,130]. The protruding α6/L3/α7 region at the NP face makes asymmetric contacts with the lagging strand DNA that protect the central interactions from the DnaB helicase, which translocates on that strand and is the first replisomal component to arrive (Figure 5.1D). On the other hand, the polymerase-bound leading strand, containing the conserved cytosine base (C6) (Figure 5.1C), is widely exposed (Figure 5.1D)[23,127,232].

This structure prompted a dynamic clamping model to account for Tus−*Ter* polar arrest activity, where the α6/L3/α7 region clasps the lagging strand and imposes a steric hindrance that blocks the approaching DnaB (Figure 5.1D)[127]. The second model proposes a physical interaction between DnaB and the NP face of Tus and identified specific residues in the L1 loop of Tus that are believed to be the first to encounter DnaB[135,145]. However, this model is strongly challenged by the wide range of helicases that are blocked by Tus−*Ter* in polar manner[118,136,140-142,214,232]. The last model proposes a specialized molecular mousetrap mechanism, where the conserved C6 base (Figure 5.1C) flips out from the DNA helix upon melting of the GC6 bp to make several new interactions in a specific cytosine-binding pocket on Tus leading to a 40-fold enhancement of the kinetic stability of the Tus−*Ter* complex (Figure 5.1D,E)[130]. C6 does not make contacts with Tus when *Ter* is in duplex form and consequently its flipping would create the primary interactions of Tus with the leading strand, providing a mechanism that would also clasp the leading strand from the late arriving polymerase[130].

Although the Tus−*Ter* C6-locked complex is very stable *in vitro*[130,232], the mousetrap model fails to explain the *in vivo* data that shows the blockage efficiency at NP face of Tus−*Ter* not to exceed 50% even at the strongest *Ter* sites (*TerA*, *TerB*, *TerC*); up to 50% of the replication forks replicate past *Ter* and do sp without even stopping transiently[137,208]. The K_D of the C6-locked complex is only 3-fold lower than Tus–ds*TerB*, while its lifetime is much longer, suggesting that efficiency of lock formation is kinetically rather than thermodynamically controlled[130]. We showed recently using single-molecule DNA replication assays that the efficiency of fork stoppage by Tus−*Ter* is determined by kinetic competition between rates of strand separation by DnaB and rearrangement of Tus−*Ter* interactions during the separation of the first 6 bp of *Ter*, *i.e.* faster moving forks tend to displace Tus and continue DNA synthesis while slower ones are effectively blocked[264]. A preformed C6-locked complex however is able to stop both fast and slow moving forks demonstrating that C6-lock formation is an inefficient process but once formed is able to permanently arrest the fork[264].

The rearrangement of Tus−*Ter* interactions during the separation of the first 6 bp are mediated by changing the interactions of the R198 residue in the L3 loop with the AT5 and GC6 bps from base-specific to phosphate backbone-mediated interactions. This rearrangement is required to maintain the clasping of Tus onto the lagging strand to prevent DnaB from advancing into Tus−*Ter* central interactions and displacing Tus. It also imposes transient stoppage that enables the inefficient C6-flipping process[264]. Similar observation of transient stoppage preceding C6-lock formation is also reported in the case of blocking the heterologous T7 replisome at the NP face of Tus−*Ter*[232]. These results

suggest the operation of a composite mechanism that involves dynamic clasping and the C6-mousetrap to impose fork arrest[232,264].

The triggering of the C6-mousetrap however becomes compulsory for permanent fork stoppage only in the event the replisome succeeds in melting the GC6 bp. This scenario accounts for a portion of the fork arrest activity at the NP face of Tus−*Ter*. On the other hand, it has been shown that the interactions of R198 among others are able to stop the replisome before it melts the GC6 bp and this scenario accounts for a significant yield of fork stoppage[264]. These results challenge the significance of the C6-moustrap model as an indispensable mechanism in Tus−*Ter* fork arrest activity.

Other inconsistencies of the mousetrap model lie in the fact that Tus−*Ter* displays some helicase specificity in its blockage activity[118,136,140,142,182,214]. Nonetheless, the effect of the orientation of the helicase translocation activity on its blockage by NP Tus−*Ter* was never carefully studied, and many of the results on the specificity of some helicases were disputed (reviewed in [23]). The role of the C6-flipping is further downplayed by the minor effect of C6 to A6/T6 transversion on Tus−*Ter* fork arrest activity[100,131]. Additionally, Tus−*Ter* blocked DnaB helicase in a polar manner under condition where DnaB translocates on dsDNA and therefore no melting of GC6 bp is induced[145]. Finally, yeast MCM2−7 replicative helicase that translocates in the 3'−5' orientation and consequently is believed to inhibit the C6-mousetrap by sequestering the C6 base was also shown to be blocked in a polar manner by Tus−*Ter*[211].

Collectively, several studies argued against the notion of the C6-mousetrap being the primary mechanism mediating Tus−*Ter* polar arrest activity, while others proposed it to act as a fail-safe mechanism in case the fork bypassed early blockage and managed to restart DNA synthesis[24,86,145]. In this study, we used data from *in vitro* single-molecule and *in vivo E. coli* plamid replication assays, combined with binding studies of several Tus derivatives with mutations in the cytosine-binding pocket to show that some of the C6-lock defective mutants were still able to impose significant polar arrest activity. Nevertheless, there is strong evidence for a role of the C6-mousetrap mechanism as seen by the reduced fork arrest activity of some of the C6-lock-defective mutants. Our results support the presence of other mechanisms acting side-by-side with the mousetrap model rather than the mousetrap being the primary mechanism.

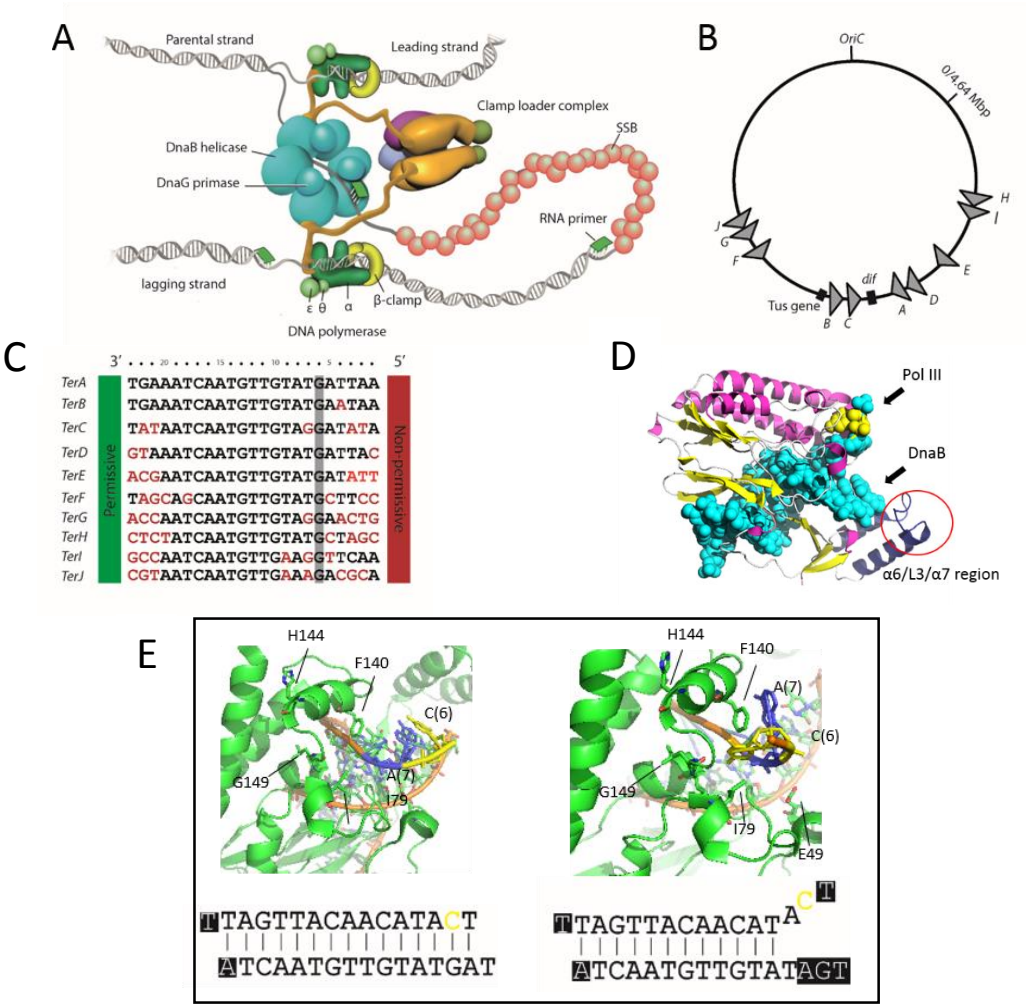

Figure 5.1: Polarity of termination of DNA replication in *E. coli*

A. A schematic representation of the *E. coli* replisome. A fully functional replisome comprises: DnaB helicase, DnaG primase, single-stranded DNA-binding protein (SSB), β_2 sliding clamp, a γ clamp loader complex, and αƐΘ polymerase core. DnaB first unwinds the double-stranded DNA (dsDNA) into two single-stranded DNA (ssDNA) strands. For each of the exposed strands, a new complementary sequence of DNA is synthesized by the action of the replicative Pol III holoenzyme (Pol III HE). The unidirectional movement of the DNA polymerization activity (5'−3') and bidirectional polarity of the parental DNA strands permits the leading strand to be copied continuously but forces the lagging strand to be copied discontinuously. DnaG intermittently synthesizes short (8-12 nucleotide) fragments of RNA along the lagging strand that are extended by Pol III HE to Okazaki fragments.

Figure is adopted from[47].

B. Polarity of the bidirectional replication fork trap. Assembly of two replication forks at the unique origin, termed *oriC*, starts bidirectional replication, where the two forks move at a rate of 1 kb s^{-1} and each replicates one replichore (one half of the chromosome) until they meet across from the origin at the terminus region. Each replication fork will pass through a set of five *Ter* sites from the permissive (P) direction, and is arrested upon encounter with one of the next *Ter* sites from the non-permissive (NP) direction. At the center of the terminus region, the *dif* site is located where segregation of the two sister chromosomes takes place. The region containing the gene encoding for Tus protein is shown.
C. Sequence alignment of the ten *Ter* sites, showing the strictly conserved G6 highlighted in a gray bar. The non-conserved bases are shown in red color.
D. Structure of Tus–*Ter* C6-locked structure, showing the flipping of the C6 base out of the DNA helix upon unpairing of the sixth bp[130]. It is proposed that strand separation by DnaB melts GC6 bp and induces C6 flipping into a specific cytosine-binding pocket in Tus (C6-mousetrap model). The flipped C6 is colored in yellow. The lagging strand on which DnaB translocates and the template leading strand for Pol III are indicated by black arrows. The α6/L3/α7 region that clasps the lagging strand at the NP face to prevent the advancing helicase from breaking into Tus–*Ter* central interactions is shown in a red circle.
E. Structure of C6 binding pocket before and after base flipping, showing the movement of C6 to form the locked structure. The flipped C6 interacs specifically with the following residues H144, F140, I79, G149, and E49.

5.3 Results

The flipped C6 base interacts with the residues I79, F140, H144, G149 and L150 in the cytosine-binding pocket of Tus and E49 that is located outside the pocket (Figure 5.1E)[130]. E49 forms a water-mediated hydrogen bond with the 5’-phosphate of the displaced A7

base[130]. H144 forms a hydrogen bond with the separated NP 5'-strand, where the rotation of its imidazole ring allows the NH group to interact with the N3 of the C6 base and position it close enough to form a hydrogen bond with the 5'-phosphate of the T8 base[130]. The side chains of F140 and I79 forms a hydrophobic batch that sandwiches the C6 base ring (Figure 5.1E)[130]. We sought therefore to test the significance of the C6-mousetrap model by characterizing the effect of mutating some of the residues in the cytosine-binding pocket on Tus−*Ter* polar arrest activity.

5.3.1 Mutations in the Cytosine-binding Pocket Weaken the C6-locked Complex

We first examined the effect of mutating E49, I79, F140 and H144A to alanine on the binding of Tus to ds*TerB* and *TerB*-locked sequences by surface plasmon resonance (SPR) binding studies, conducted in Professor Nicholas Dixon's lab (University of Wollongong). In the locked sequence, mismatches were introduced at the NP face of *TerB* to keep the C6 base unpaired for its binding into the cytosine-binding pocket, as described previously[130]. Increasing concentrations of wild-type Tus or its mutated variants were injected over surface-immobilized 5'-biotinylated ds*TerB* or *TerB*-locked DNA coupled to a ProteOn NLC (neutravidin-coated) sensor chip[130,264]. The equilibrium dissociation binding constant (K_D) was calculated by fitting the steady state response units (RU) of the binding curves from each Tus concentration using a 1:1 steady state binding model. The dissociation (k_d) and association (k_a) rate constants were derived by global fitting of the dissociation and association phases of the response curve by either a 1:1 Langmuir binding model or 1:1 Langmuir binding model with mass transfer correction, as described previously[101].

With wild-type Tus, the half-lifetime ($t_{1/2}$) of the *TerB*-locked complex increased by 115-fold relative to ds*TerB* ($t_{1/2}$ = 16300 and 140 s, respectively), while the K_D decreased by 9-fold (Table 5.1), reflecting the dramatic enhancement of the kinetic stability of Tus−*Ter* upon C6-flipping[130]. Tus(E49A) displayed the least defect in binding to ds*TerB* and *TerB*-locked as compared to the wild-type Tus; $t_{1/2}$ for complexes with ds*TerB* and *TerB*-locked structures were 2-fold slower and 3-fold faster than wild-type, respectively, while K_D increased by only 2-fold in the case of the *TerB*-locked sequence (Table 5.1). A more pronounced effect was seen when E49 was altered to lysine with $t_{1/2}$ of Tus(E49K) bound to the *TerB*-locked structure decreasing by 27-fold and its K_D increasing by 16-fold relative to wild-type Tus (Table 5.1). Tus(F140A) was the only tested mutant showing a remarkable enhancement of binding to the ds*TerB* site; $t_{1/2}$ was 23-fold longer and K_D was reduced by 12-folds relative to wild-type Tus (Table 5.1). Tus(F140A) binding to the *TerB*-locked sequence however displayed a defect of 19-fold faster $t_{1/2}$ and 28-fold higher K_D relative to wild-type Tus (Table 5.1). The I79A mutation reduced $t_{1/2}$ of the Tus−*TerB*-locked complex by 41-fold and increased the K_D by 71-fold (Table 5.1). Tus(I79A) bound to ds*TerB* with comparable K_D and $t_{1/2}$ to wild-type Tus (Table 5.1). The H144A mutation was the most defective in binding to the *TerB*-locked sequence; $t_{1/2}$ was reduced by 89-fold and its K_D increased by 2820-fold. The increased K_D of Tus binding to the ds*TerB* lock sequence in these mutants is primarily due to a defect in their k_d with the exception of Tus(H144A) that displayed also a marked increase in its k_a (Table 5.1). It is remarkable to add here that H144A was the only mutation that displayed a drastic reduced binding to ds*TerB* with K_D increasing by 21-fold relative to wild-type Tus due to defects in both k_a and k_d (Table 5.1).

Interaction	K_a ($M^{-1}S^{-1}$)	K_d (S^{-1})	K_D (nM)	$t_{1/2}$ (sec)
Wild-type Tus–*Ter*	3.78×10^6	7.04×10^{-3}	1.86	142
Wild-type Tus–forked *Ter*	2.89×10^5	6.12×10^{-5}	0.212	16340
Tus(E49A)–*Ter*	2.76×10^6	4.47×10^{-3}	1.62	224
Tus(E49A)–forked *Ter*	4.45×10^5	1.83×10^{-4}	0.412	5465
Tus(I79A)–*Ter*	3.27×10^6	8.36×10^{-3}	2.56	120
Tus(I79A)–forked *Ter*	1.26×10^5	2.53×10^{-3}	15.1	395
Tus(F140A)–T*er*	2.03×10^6	3.09×10^{-4}	0.152	3236
Tus(F140A)–forked *Ter*	1.93×10^5	1.14×10^{-3}	5.90	877
Tus(E49K)–*Ter*	3.21×10^6	5.17×10^{-3}	1.61	193
Tus(E49K)–forked *Ter*	4.78×10^5	1.66×10^{-3}	3.49	602
Tus(H144A)–*Ter*	3.92×10^5	1.54×10^{-2}	39.3	65
Tus(H144A)–forked *Ter*	9.09×10^4	5.44×10^{-3}	598	184

Table 5.1: SPR assessment of binding of wild-type Tus and its mutants to ds*TerB* or C6-locked *TerB* DNA

Summary of binding parameters of wild-type Tus and its mutants to ds*TerB* and C6-locked *TerB* sequences. Fitting of binding parameters to appropriate binding models was carried out as described in the Methods in Chapter 3.

5.3.2 Significance of the C6-lock in Replication Fork Arrest Activity

We next tested the effect of the aforementioned C6-defective Tus mutants on the ability of the NP face of Tus to arrest an approaching *E. coli* fork using single-molecule DNA replication assays, as described previously[55,182,232,264]. Briefly, we engineered a 13.7 kilo base (kb) substrate containing a single copy of the *TerB* site between a 3.6 kb biotinylated forked region and a 10.1 kb digoxigenin (dig)-modified region, as described previously[232,264]. The biotin allows for the tethering of the DNA to a streptavidin-coated surface of a coverslip, while the dig modification on the other end enables its attachment

to a 2.8 µm magnetic bead. A flow exerts a well-defined drag force on the bead that is distributed evenly along the DNA (Figure 5.2A). Multiplex trajectories are derived from the simultaneous monitoring of the length of tens to hundreds of individual DNA molecules over time (Figure 5.2B and Figure 5.3). At the applied regime force of 2.6 picoNewton (pN), leading-strand synthesis converts the surface-tethered lagging strand DNA from double-stranded (ds) long form to single-stranded (ss) short form to result in an overall shortening of the length of the DNA molecule (Figure 5.2A). Location of the inserted *TerB* site can be defined with an accuracy of 0.1 kb, as described previously[232,264].

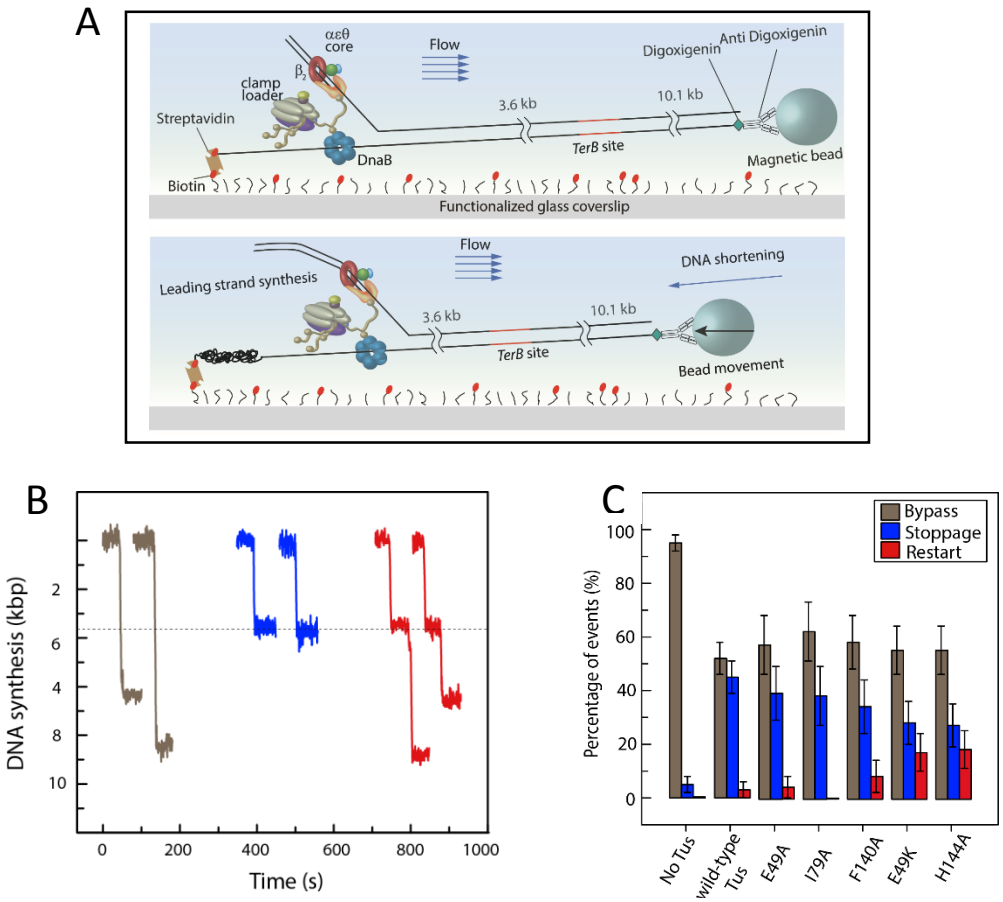

Figure 5.2: Fate of the *E. coli* replisome upon encountering Tus–*TerB*

A. A schematic representation of the single-molecule assay and the 13.7 kilobase (kb) DNA construct containing a *TerB* site. DNA shortening during leading-strand synthesis results from conversion of the surface-tethered lagging strand from the long double-stranded (dsDNA) to the short single-stranded (ssDNA) forms. The movement of the bead is analysed and converted to numbers of nucleotides synthesized, as described in Methods in Chapter 2.
B. Examples of trajectories for the three fates of *E. coli* replisome (bypass, stoppage, restart) upon encountering the NP face of the Tus−*Ter* complex. Two representative trajectories are shown for the restart behavior observed with Tus(E49K) (left) and Tus(H144A) (right) (see also Figure 5.3).
C. Percentages of events that bypassed or permanently or transiently stopped upon encountering the NP face of the Tus−*TerB* complex in the absence and presence of wild-type or mutant derivatives of Tus. Error bars correspond to the standard deviation of binomial distributions.

In the absence of Tus, only 5% of the observed replication forks that reached 3.6 ± 0.1 kb stopped there, while the other 95% replicated past the inserted *TerB* site that is oriented to meet the fork through its NP face; we attributed the observed 5% stoppage to random collapse of the fork due to processivity limitation (Figure 5.2C and Table 5.2)[264]. In the presence of Tus, only 45% of the trajectories displayed permanent stoppage (for 9.7 ± 1 min on average), while in 52% of trajectories the replisome displaced Tus without stopping even transiently (Figure 5.2C and Table 5.2). These results are in agreement with the *in vivo* fork arrest efficiency at *TerB* on a reporter plasmid[137,208]. Rare restart of DNA synthesis was detected in 3% of the trajectories after a long pausing of 146 ± 31 s (Table 5.2). As discussed in Chapter 3, the rate of approaching replisomes is correlated with the efficiency of Tus−*TerB* fork arrest activity, where faster moving forks tend to displace Tus

more effectively than slower ones[264]. The average rate of forks that stopped/restarted at *TerB* was 2-fold slower than those that bypassed it: 890 ± 70 versus 1690 ± 100 bp s^{-1}, respectively (Table 5.2). The 50% bypass events is a result of the inefficient triggering of the C6 flipping upon the separation of the GC6 bp due to failure of R198 to rearrange its interactions with the AT5 and GC6 bps; a step that is required to impose transient fork stoppage in order to enable the inefficient C6-flipping process[264].

	Stop (%)	Bypass (%)	Restart (%)	Pause time (s)	Rate of stop/restart (bp s^{-1})	Rate of bypass (bp s^{-1})
No Tus	5 ± 3	95 ± 3	0	-	800 ± 100	1160 ± 70
Wild-type Tus	45 ± 6	52 ± 6	3 ± 2	146 ± 31	890 ± 70	1690 ± 100
E49A	39 ± 10	56 ± 11	5 ± 4	204.5	730 ± 80	1700 ± 190
I79A	38 ± 11	62 ± 11	0	-	740 ± 130	1720 ± 170
F140A	34 ± 10	58 ± 10	8 ± 6	147 ± 18	690 ± 70	1600 ± 180
E49K	28 ± 8	55 ± 9	17 ± 7	36 ± 4	740 ± 100	1440 ± 140
H144A	27 ± 8	55 ± 9	18 ± 7	33 ± 5	840 ± 120	1520 ± 130

Table 5.2: Fate of the replisome and its rate dependency at the NP face of *TerB* bound to wild-type Tus or its mutant derivatives

Stop, bypass and restart events were quantified as a percentage of all events that reached or bypassed *TerB*, as described in Methods in Chapter 3. Uncertainties correspond to standard deviations of binomial distributions. The arithmetic averages of the rates and pause durations are shown. The uncertainties correspond to standard errors.

We next tested the Tus−*TerB* fork arrest activity when the cytosine-binding pocket was altered. Tus(E49A) and Tus(I79A) did not show a notable effect as compared to wild-type Tus; fork stoppage was reduced by 13% and 15%, respectively (Figure 5.2C and Table 5.2). Tus(F140A) showed a rather modest negative effect of 24% reduced stoppage as compared to wild-type Tus (Figure 5.2C). Restart of DNA synthesis was observed in

Tus(E49A) and Tus(F140A) in 5 and 8% of the trajectories relative to 3% in wild-type Tus, after a rather long pause durations of 2.5−3.5 min that is also similar to that observed in the restart trajectories for the wild-type (Table 5.2 and Figure 5.3).

The strongest effect on fork arrest activity was observed in Tus(E49K) and Tus(H44A), where fork stoppage was reduced by nearly 40% as compared to wild-type Tus (Figure 5.2C and Table 2). Interestingly, a significant percentage of fork restart was observed in ~ 20% of the trajectories, with nearly similar short pausing in both mutations of ~ 35 s (Figure 5.2B,C and Figure 5.3). Unexpectedly however, 60% of permanent fork arrest activity was maintained in the cases of Tus(H144A) (Figure 5.2C and Table 5.2), although this mutation has severe defects in C6-lock formation (Table 5.1). These results demonstrate the ability of Tus to stop the replication fork in a C6-lock independent mechanism and that this mechanism accounts for ~ 60% of its total fork arrest activity. In fact, analysis of the pause duration in events that restarted in Tus(H144A) and Tus(E49K) showed a relatively short pausing of ~ 35 s (Table 5.2). On the other hand, a longer duration of pausing was observed in the restart events in case of wild-type Tus, Tus(E49A) and Tus(F140), reflecting distinct mechanisms mediating pausing of DNA synthesis (Figure 5.2C, Figure 5.3, Table 5.2).

We next investigated the rate-dependence of fork arrest activity of these mutants by comparing the rate of DNA synthesis prior to encountering Tus−*Ter* in the events that stopped/restarted or bypassed relative to that in the wild-type Tus (Table 5.2). The mutants maintained their rate-dependent fork arrest activity but with a slight decrease in

the average rate of the stopped forks relative to the wild-type; the shift was maximal in Tus(F140A) and least in Tus(H144A) (Table 5.2). These results are consistent with our previous study[264], which demonstrate that Tus−*Ter* fork arrest efficiency is determined by a transient stoppage step prior to the triggering of C6 flipping, rather than the C6-locking mechanism itself. Nonetheless, they suggest that interactions of the C6 base with residues in the cytosine-pocket might have a minor contribution to the Tus−*Ter* rate-dependent fork arrest activity in the C6-lock independent mechanism.

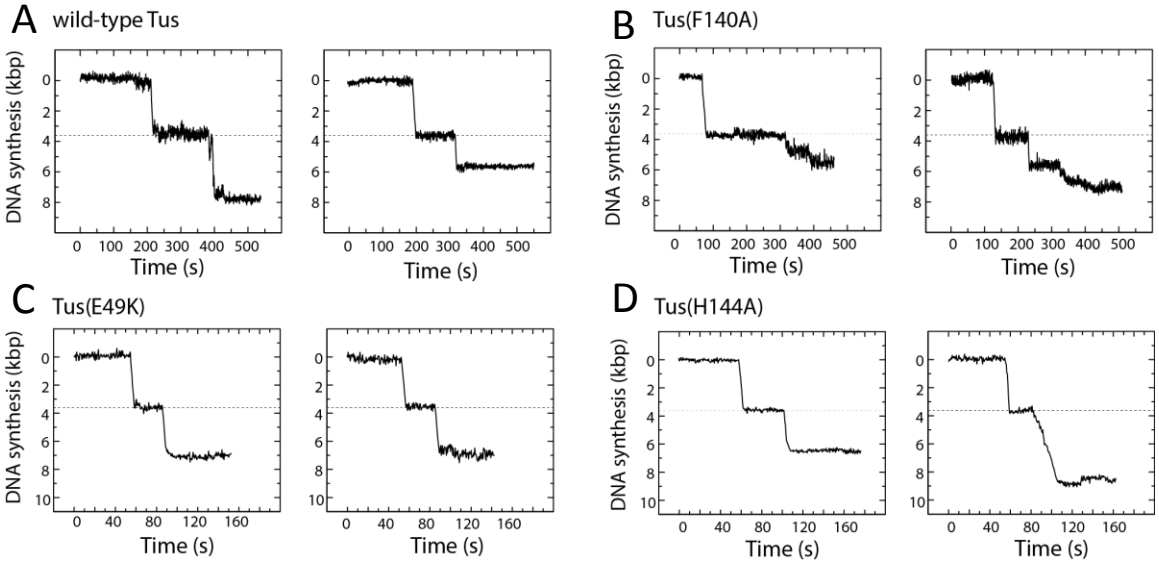

Figure 5.3: Transient stoppages in single-molecule replication assay trajectories using wild-type and mutant derivatives of Tus

Examples of helicase–polymerase synthesis trajectories showing transient stoppage at the location of the *TerB* site, followed by resumption of DNA synthesis. The location of the *TerB* site is indicated by the dashed lines.

Restart trajectories where forks encounter wild-type Tus (**A**), Tus(F140A) (**B**), Tus(E49K) (**C**) and Tus(H144A) (**D**). Note the different time scales in **A**, **B**, **C** and **D**, reflecting the longer pause duration in the cases of wild-type Tus and Tus(F140A).

5.3.3 *In vivo* Fork Arrest Activity of C6-defective Tus Mutants

The only *in vivo* characterization of some of the cytosine-pocket mutants of Tus was performed in yeast[211]. Tus(F140A) is able to arrest MCM2−7 helicase, consistent with its behavior in our *in vitro E. coli* replication assays, but Tus(H144A) failed to arrest MCM2−7[211]. This was attriuted to Tus(H144A)'s reduced binding to ds*Ter* rather than the effect on lock formation. These results contradict the *in vitro E. coli* replication experiments that reported a significant residual fork arrest activity by Tus(H144A)[264]. Two possibilities could be the cause of this discrepancy: either the mode of translocation of MCM2−7 occurs on dsDNA or the power stroke of strand separation by MCM2−7 is significantly stronger than DnaB in displacing Tus(H144A)[265]. The latter possibility is supported by the ability of MCM2−7 to bypass a biotin-streptavidin road block[266]. We sought therefore to characterize *in vivo* the effect of the cytosine-pocket mutants in fork arrest activity *in E.coli*.

In vivo fork arrest activity was characterized in Professor Nicholas Dixon's lab (University of Wollongong) using a growth assay, as described previously[208,221]. Briefly, the TH860 *E. coli* strain containing a deletion of the *recA* gene and an Inv*Ter::spcr* cassette in the chromosome that is flanked on both sides by a *Ter* site oriented to block replication of the *spc* gene, is grown in arabinose medium (Figure 5.4A). The chromosomal tus gene is deleted enabling the examination of Tus alterations through its overexpression from a plasmid under the control of arabinose-inducible promoter. In this assay, the plating efficiency and colony sizes are reduced significantly in cases of overexpression of an active

form of Tus. In order to further reduce the plating efficiency of TH860 strain, a pTH102 plasmid that contains a *Ter* site to block unidirectional replication, was also introduced.

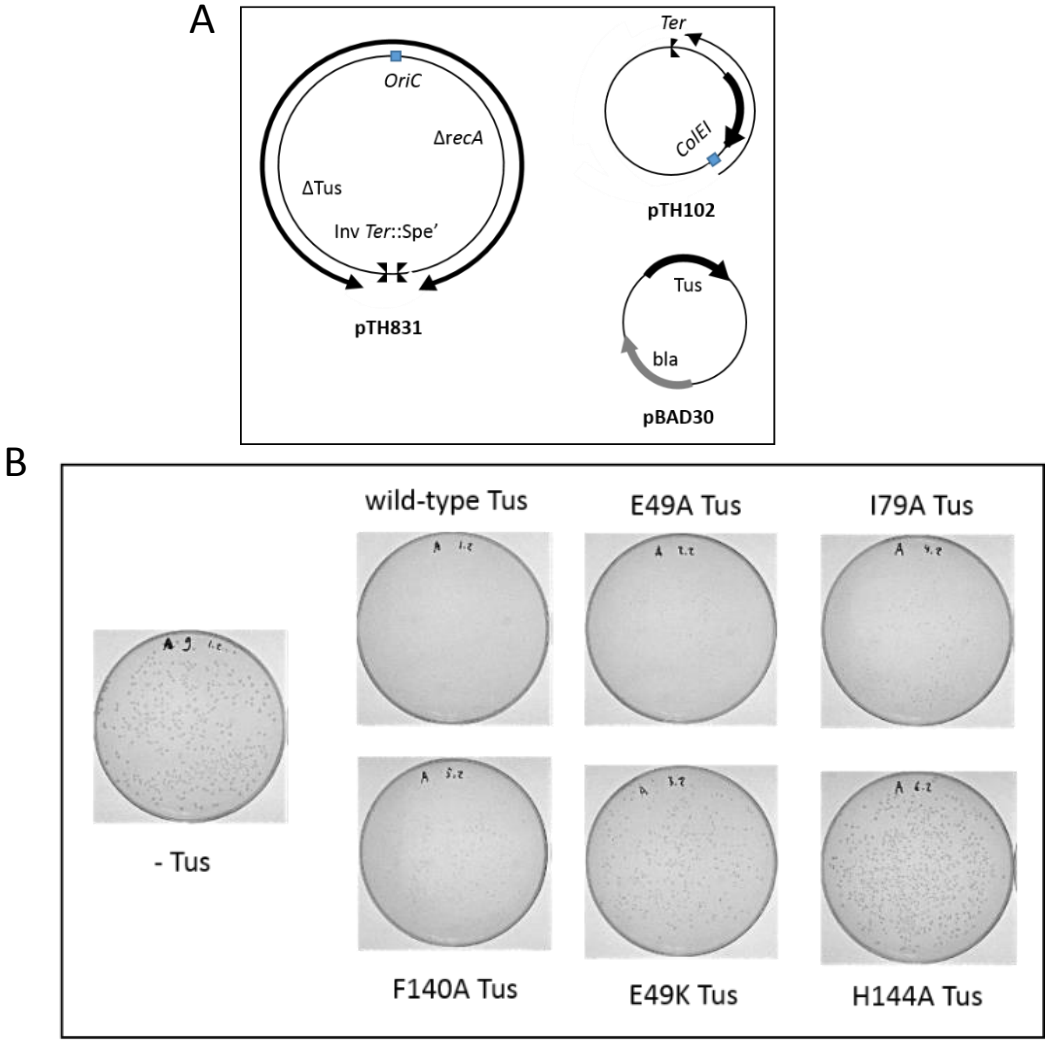

Figure 5.4: *In vivo* fork arrest activity of the C6-binding defective Tus mutants

A. A scheme for selecting cells with altered replication arrest activities. pTH831 contains a deletion of both tus and recA genes and has InvTer::spcr cassette to block DNA replication. Tus is provided from a pBAD30Tus that contains an arabinose-inducible wild-type or mutants derivatives of Tus genes. Another level of selection is implemented by pTH102, which contains a *Ter* site to block unidirectional replication from the *ColEI* origin.

B. Growth assay for pTH860 on LB plates containing antibiotics and glucose (-Tus plate), or arabinose to induce Tus expression (+ Tus plates).

Fork arrest activities of the cytosine-pocket mutants from the *in vivo* growth assay was in perfect agreement with those from our *in vitro* single-molecule assays, underscoring the suitability of the single-molecule replication assay to report on Tus−*Ter* fork arrest activity. Tus(E49A) and Tus(I79A) were the least defective mutants showing barely any weakness in fork arrest activity (Figure 5.4B). Tus(F140A) was marginally defective with only 10% loss of wild-type arrest activity (Figure 5.4B). Tus(E49K) and Tus(H144A) were nearly equivalent and they were the most defective Tus mutants with each mutation abolishing more than 50% of the wild-type Tus activity (Figure 5.4B).

5.4 Discussion

In this study we used *in vitro* single-molecule DNA replication and *in vivo* growth assays, combined with SPR binding studies to assess the efficiency of fork arrest activity of cytosine-binding pocket mutants of Tus, to investigate the significance of the mousetrap model in Tus−*Ter* polar arrest activity.

Recent studies using *E. coli* and the heterologous T7 replication systems showed that a preformed C6-locked complex is able to permanently block these replisomes[232]. More importantly, the efficiency of this blockage is significantly enhanced relative to that when the C6 lock was induced under active strand separation conditions[232]. These results demonstrate that the C6-locked complex is able to permanently block the replication fork once induced but its triggering is an inefficient process. Deactivation of the C6-lock formation by altering the GC6 bp resulted in transient stoppage of the fork at the NP face in both T7 and *E. coli* systems, but without attenuating Tus−*Ter* efficiency[232,264]. These

results, together with the rate dependent fork arrest activity, served as a basis for the model that Tus−*Ter* efficiency is determined by a kinetic competition between rate of strand separation by the helicase and transient stoppage of the fork prior to triggering the C6 lock. This transient pausing is believed to enable the inefficient C6-flipping process[232,264]. It also shows that these mechanisms are intrinsic to Tus−*Ter* activity and system independent, arguing against a Tus/DnaB mediated mechanism[232,264]. Here we show that deactivation of the C6-lock mechanism by altering the cytosine-binding pocket resulted in different outcome from those when the GC6 bp was mutated.

According to the crystal structure of the C6-locked complex (Figure 5.1D,E), the flipped C6 forms three hydrogen bonds with H144, G149, and L150 near α4 at the NP face of Tus. Additionally, the flipped C6 is sandwiched between the side chains of F140 and I79[130]. All these residues are strictly conserved except I79 that is conservatively substituted to leucine in some *Yersinia* species, and L150 is substituted with valine in some plasmid-encoded Tus variants[130]. E49 is located outside the cytosine-pocket boundaries but it forms a water-mediated hydrogen bond with the 5'-phosphate of the displaced A7 base[130]. We showed by SPR that the C6-locked complex was eliminated in the case of Tus(H144A), while it was severely affected in the cases of Tus(E49K), Tus(F140A) and Tus(I79A) and barely affected in the case of Tus(E49A) (Table 5.1). Analysis of the fork arrest activity of these mutants by *in vitro* and *in vivo* replication assays showed that attenuating/deactivation of the C6 lock complex in some mutants did not necessarily abrogate the Tus−*Ter* fork arrest activity (Figure 5.2C and Table 5.2). Tus(H144A)'s results were particularly the most revealing since this mutation maintained nearly 60% of the

Tus−*Ter* permanent stoppage capability relative to the wild-type (Figure 5.2C and Table 5.2), despite the fact that it completely deactivated C6-lock formation (Table 5.1). The remaining 40% of the stopped forks were able to resume DNA synthesis after a short pause of ∼ 35 s (Figure 5.2C, Figure 5.3, Table 5.2). The short pause duration demonstrates that these restart events resulted from an independent mechanism rather than failure of the one(s) that stopped the fork permanently since the later possibility would result in a transient pause that is distributed over the 10 minute period of observation. Collectively, these results demonstrate that Tus−*Ter* is able to stop the fork in the absence of the C6- lock mechanism.

Consistent with our previous findings that Tus−*Ter* efficiency is determined by C6-lock independent mechanisms[264], the rate-dependent fork arrest activity of the cytosine-pocket mutants was found to be largely unaffected. However, we observed some minor shift in the average rates of stopped forks to a slower range (Table 5.2), suggesting a possible involvement of the interactions of the C6 base itself with the cytosine-binding pocket in contributing to the rate-dependent fork arrest activity. Recent magnetic tweezers experiments characterized the kinetics of C6 flipping under conditions where the dsDNA is unwound by force in the absence of active strand separation by the helicase[267]. Three different C6-lock states are identified and shown to progressively strengthen with the third state representing the full C6-locked complex. The probability of the three lock states in some of the tested C6 pocket mutants that include Tus(H144A), Tus(E49K) and Tus(F140A) are affected but to different degrees. The full lock state is observed in the case of Tus(E49K) and Tus(F140A) but with severely reduced probability,

while it cannot be detected in Tus(H144A)[267]. The probabilities of the other two C6 lock forms are also affected to different degrees. The magnetic tweezers experiments suggest that C6 makes interactions with the cytosine-pocket that do not necessarily lead to full C6-locked complex; we consider such interactions to be part of the C6-lock independent mechanism. The minor effect of some of the tested Tus mutants on the rate-dependent fork arrest activity in our replication assays suggests that the C6-lock independent mechanism might involve some minor contribution from the interactions of the C6 base with the cytosine pocket.

A clear correlation between the efficiency of fork arrest and the ability to form the C6-lock could not be observed in some of the tested mutants. Interestingly, Tus(H144A) was severely defective in forming the C6-locked complex, while Tus(E49K)'s deficiency was very similair to that of Tus(I79A) and Tus(F140A) (Table 5.1). Both Tus(I79A) and Tus (F140A) however were less defective in fork arrest activity, prompting a question with respect to the source of the defect observed in the case of Tus(E49K) particularly (Figure 5.2C, Table 5.2, Figure 5.4). E49K is the mutation that was suggested to be defective in the interaction of Tus with DnaB[135,145]. The crystal structure of the *TerB*-locked complex of Tus(E49K) shed light on a potential source of the defect in Tus(E49K) (unpublished results from Professor Nicholas Dixon's lab (University of Wollongong)). The C6 is flipped into the cytosine-binding pocket, demonstrating that Tus(E49K)'s reduced ability to form a C6-locked complex cannot alone account for its defect in polar arrest activity. Interestingly, part of the α6/L3/α7 region including the key residue R198 is apparently unstructured, suggesting that the E49 residue could be involved in maintaining the

clasping of Tus on the DNA during strand separation. This could provide an explanation for its reduced ability in arresting faster moving forks (Table 5.2).

Tus(F140A) had a 23-fold enhanced half-life time of disscociation from ds*TerB* and forms a 2-fold more stable locked complex than Tus(I79A) (Table 5.1). Nonetheless it was more defective in fork arrest activity than Tus(I79A) (Figure 5.2C, Table 5.2, Figure 5.4). The reason behind the enhanced binding of Tus(F140A) to ds*Ter* is puzzling. F140 is strictly conserved among bacterial species, and therefore if the affinity of Tus binding to ds*Ter* sequence is the deterministic factor in its fork arrest activity, this particular mutation would have been selected for by evolution for increasing the efficiency of the process[130]. The results with Tus(F140A) demonstrate that a simple model comprising binding affinities to ds*Ter* and C6-locked sequences cannot explain Tus−*Ter* fork arrest activity and that additional mechanisms are playing a role in its mechanism. To this point, we attributed the defect in fork arrest activity in the case of Tus(F140A) to its reduced ability to form the C6-locked complex in addition to some minor effect on its ability to arrest faster moving forks (Table 2).

The interactions of R198 in loop L3 are key in mediating both the C6-lock dependent and independent mechanisms[264]. Alteration of R198 results in a severe defect in Tus fork arrest activity *in vivo*[23,143,144]. Single-molecule replication assays also show that Tus(R198A) is severely defective in fork arrest activity with permanent fork stoppage reaching the basal background level without Tus[264]. Furthermore, the rate-dependent fork arrest activity is shifted drastically to 2-fold slower range than the wild-type[264] or the

cytosine-pocket mutants in this study. The interactions of R198 are therefore the key factor that determines Tus−*Ter* fork arrest efficiency. Tus(R198A) is able to form the C6-locked complex, demonstrating that stopping and/or slowing the fork by R198 interactions is required for triggering the formation of the C6-locked complex[264].

Our current understanding of the mechanism of Tus−*Ter* polar arrest activity is centered on the interactions of R198 that play significant roles in both C6-lock dependent and independent mechanisms[264]. R198 interacts with the AT5 and GC6 bps in a dynamic manner shifting from base-specific contacts in the case of ds*Ter* to interactions with the phosphate backbone in the C6-locked complex[130,264]. This rearrangement during strand separation provides a window of opportunity for a head-to-head kinetic competition between rates of strand separation and rearrangement of Tus−*Ter* interaction during the separation of the first 6 bps of *Ter*. This rearrangement is a key to maintain the clasping of the lagging strand to prevent DnaB from breaking into Tus−*Ter* central interactions[264]. In the event the replisome advances to melt the GC6 bp, the successful rearrangement of R198 interactions will stop the replication fork but only transiently and then C6-lock formation becomes compulsory. This scenario however accounts for no more than 50% of the permanent fork arrest activity. The other half of the forks are stopped by mechanisms that are also mediated by the interactions of R198 among others that are able to stop the replisome before it melts the GC6 bp[264].

Collectively, our results suggest that Tus−*Ter* fork arrest activity is mediated by the actions of more than a single mechanism, which cooperate to maintain the clasping on the lagging

strand and prevent the approaching helicase from breaking into the Tus−*Ter* central interactions. The C6-mousetrap mechanism functions as one of these mechanisms and cannot alone account for Tus−*Ter* polar arrest activity.

Chapter 6

6. Reconstitution of a Rep-associated *Escherichia coli* Replisome at the Single-molecule Level*

6.1 Abstract

The replisome often enters into conflicts with protein–DNA barriers that are associated with processes acting simultaneously on DNA including repair, recombination, transcription and binding of high affinity nucleoproteins[185-189]. It is crucial to coordinate these conflicts and be able to restart DNA synthesis if the protein–DNA barrier stalls the replisome. The replisome's two powerful motors, the helicase that melts the parental DNA strands and the polymerases that copy them, remove a significant amount of protein–DNA barriers[15,19,268]. Nonetheless, the replisome often stalls and recruits accessory helicases to provide an additional motor that cooperates with its helicase to quickly remove the protein–DNA barriers[194,200,207]. A longer stalling could lead to dissociation of the replisome and subsequent activation of the mutagenic recombination-based pathways for its reassembly (reviewed in [191,197,199]). Our understanding of the recruitment mechanisms of accessory helicases at the fork and their cooperation with the replisomal helicase in removing protein–DNA barriers is largely undeveloped. Here, I will describe preliminary experiments where we reconstituted *E. coli* single-molecule DNA replication assays under conditions that favor the association of the Rep accessory helicase at the fork and showed that it was able to assist the replisome to bypass the non-permissive face of Tus−*Ter* protein–DNA barrier.

---

*This chapter contains unpublished preliminary data

This reconstituted reaction provides a powerful system to characterize the mechanisms that recruits Rep at the fork and how it assists the fork in removing protein–DNA barrier.

6.2 Introduction

It is crucial that the replisome is able to bypass or remove protein–DNA barrier activities that could potentially stall its activity or even lead to its dissociation if the stall exceeds the lifetime of the helicase at the fork [189,195-197,199]. The cell developed recombination-based pathways to reassemble the replisome outside the origin of replication, but such steps are toxic since they increase the chance of perilous chromosomal rearrangements[196,197,199]. A less severe recombination-independent pathway involves the recruitment of accessory helicases to the stalled replisome to increase its stroke power and enhance the chance of removing the protein–DNA barriers before they lead to the dissociation of the helicase[194,204,207,269].

E. coli utilizes Rep, UvrD and DinG accessory helicases to overcome protein–DNA barriers[194,203]. Rep is the only helicase that specifically interacts with the replisomal DnaB helicase and its absence results in frequent stalling and inactivation of the replisome[201,202]. Nonetheless, either Rep or UvrD is required for the *E. coli* viability, suggesting that Rep provides a replisome-specific motor, while UvrD provides a generalized motor[194,207]. In this model, UvrD relies on its high cellular concentration to bind to the stalled DNA replication fork[194,203]. DinG helicase on the other hand, plays a specific role in removing the DNA/RNA R-loop structures that form naturally during transcription[203].

Rep and UvrD share significant structural similarities since both belong to the super family 1 (SF1) group of DNA helicases that translocate in the 3'−5' direction[202,204]. Rep binding at the fork requires at least 6 nucleotides (nt) of single-stranded (ss) DNA ahead of the leading strand DNA polymerase and it utilizes its extreme 33 residue C-terminal tail to physically and functionally interact with DnaB[202,205,206]. UvrD on the other hand is able to bind the ssDNA at the fork but cannot form a complex with DnaB[202]. These studies provided basic information as to how Rep interacts with DnaB at the replication fork and therefore served as a foundation for our goal of reconstituting a Rep-containing *E. coli* fork at the single-molecule level.

In the coming section, I will discuss preliminary results of a collaborative project with Professor Nicholas Dixon's lab (University of Wollongong) combining single-molecule replication assays and conventional biochemical and biophysical techniques to characterize the mechanisms that restart stalled replication forks at protein–DNA barriers by the replisome-specific Rep helicase. I conducted a series of single-molecule experiments aiming to probe the activity of Rep within the context of a stalled *E. coli* replisome at the Tus−*Ter* protein-DNA barrier. The preliminary results provide promising findings on the mechanism of recruitment of Rep helicase to the *E. coli* replisome and thus set up groundwork for this project in the lab. Our ultimate goal is to extend this study to understand how the replisome-nonspecific accessory helicases restart DNA synthesis using the model protein UvrD.

6.3 Results

In vivo results show that chromosomal duplication time in *E. coli* lacking Rep or containing a helicase-deficient Rep increases by 2-fold[201]. This prompted the conclusion that Rep interaction with DnaB does not influence the rate of DNA synthesis and that the apparent increase in chromosomal duplication time in the absence of Rep results from the increased frequency of replication fork stalling and dissociation of the replisome[198,204]. To test this proposition, we reconstituted single-molecule *E. coli* DNA replication assay using the flow-stretching experimental approach described in the Methods in Chapter 2 and studied the effect of Rep recruitment on both rate and processivity of the replisome.

Protein binding studies and DnaB helicase assays on short replication fork substrates demonstrate that functional coupling of Rep with DnaB requires Rep binding to at least 6 nt of ssDNA ahead of the leading strand polymerase[202]. Taking advantage of these studies, we engineered substrates containing a fork that either inhibits or enables Rep binding on the leading strand by controlling the length of the ssDNA gap ahead of the primer-template region (Figure 6.1).

In the first experiment, we restricted Rep access to the fork by designing a fork containing only a 2-nt ssDNA gap on the leading strand. We observed that the average rate (~ 975 base pairs/s (bp s^{-1})) and processivity (~ 8.8 kb) of the *E. coli* replisome in the presence of an excess amount of Rep in solution were similar to those reported[55] in the absence of Rep (Figure 6.1A). We next allowed Rep to bind at the fork by extending the 2-nt ssDNA gap to 19 nt. The rate of DNA synthesis was reduced to ~ 250 bp s^{-1} and processivity was

slightly reduced to ~ 5.1 kb (Figure 6.1B). These results demonstrate for the first time that 1) Rep binding at the fork attenuates rate and processivity of the replisome and 2) Rep can form a long-lived complex with the replisome.

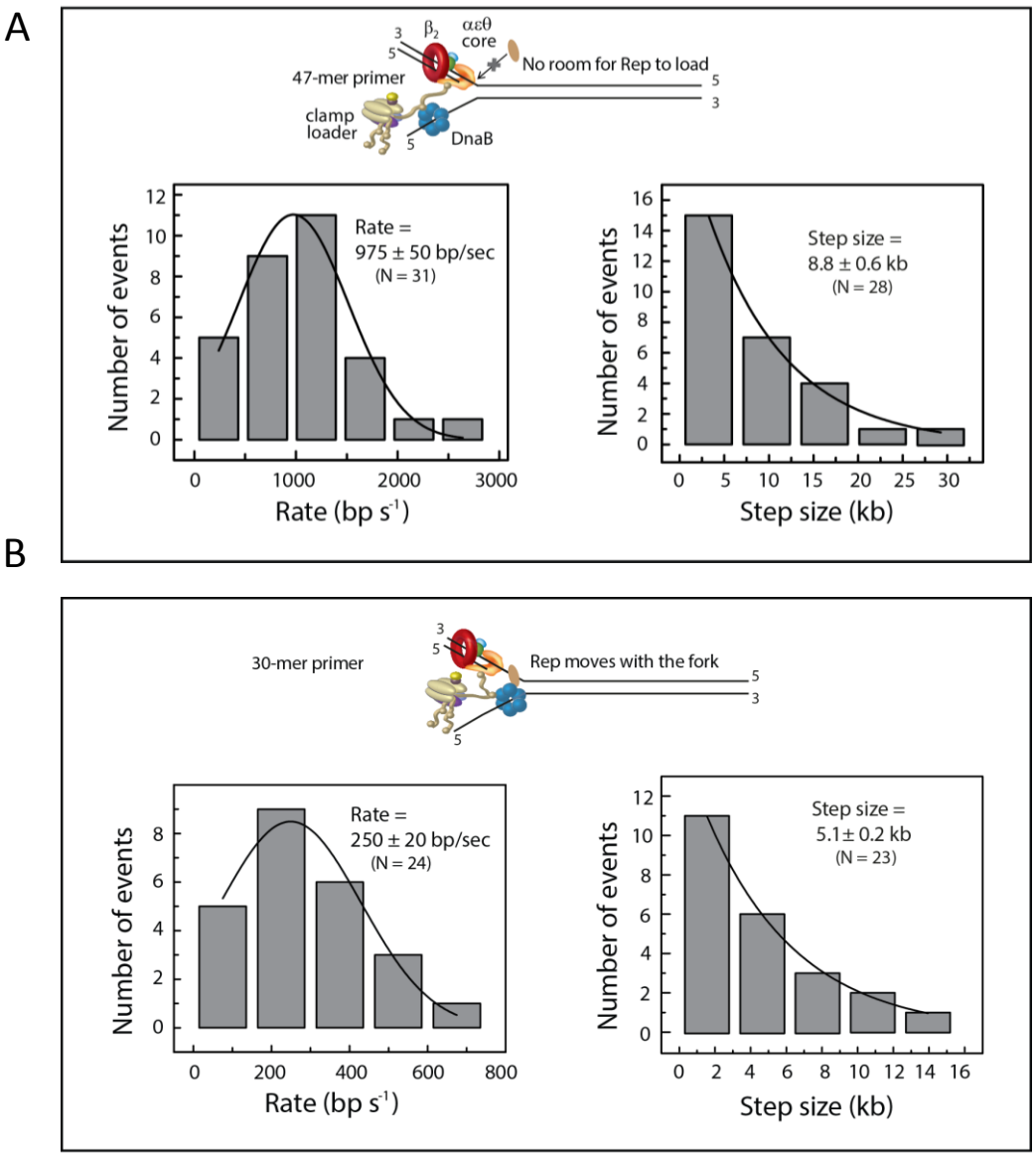

Figure 6.1: Effect of Rep binding at *E. coli* fork on the rate and processivity of leading-strand DNA synthesis

A. Top panel: a modified design of replication fork containing only a 2 nucleotides (nt) single-stranded DNA (ssDNA) gap ahead of the primer−template region in the leading strand to prevent loading of Rep at the fork. Bottom left panel: distribution of rate of leading-strand synthesis *(N = 31)*, fitted with a Gaussian distribution. Bottom right panel: distribution of processivity of leading-strand synthesis *(N = 29)*, fitted with single exponential decay. Fit lines of distributions of rates and processivity are shown and uncertainties correspond to the standard error.
B. Top panel: a design of replication fork containing 19-nt ssDNA gap enables Rep loading ahead of the leading strand polymerase. Rep loading resulted in attenuation of rate and processivity of DNA synthesis. Bottom left panel: distribution of rate of leading-strand synthesis *(N =24)*. Bottom right panel: distribution of processivity of leading-strand synthesis *(N = 23)*. Rate and processivity were fit and presented as in **A**.

6.3.1 Rep Assists the *E. coli* Replisome to Overcome the Tus−*Ter* Protein−DNA Barrier

The reconstituted Rep-associated *E. coli* replisome is a powerful system to address questions related to post-barrier bypass steps. To address the mechanism that loads Rep at the stalled replication fork, we reconstituted the entire process of *E. coli* stalling at a protein–DNA barrier and its restart by Rep. We utilized our ability to stall the *E. coli* replisome at the Tus−*Ter* protein–DNA barrier (discussed in Chapter 3) and the established conditions of loading Rep at the fork by introducing a long ssDNA gap on the leading strand (Figure 6.1), to reconstitute the displacement of Tus from *Ter* by a Rep-containing *E. coli* replisome. Briefly, we constructed a 13.7 kb primed-forked DNA containing a single copy of the 21-bp *TerB* site oriented to encounter the *E. coli* replisome at the non-permissive (NP) face, as described in Methods in Chapter 2 (Figure 6.2A). In

this assay, we showed that replisomes moving at an average rate of 1700 bp s^{-1} displaced Tus without any transient pausing, while those moving at an average rate of 840 bp s^{-1} were effectively stopped; the two scenarios roughly existed in 50:50 ratio (discussed in Chapter 3) (Fig. 6.2A). We next investigated if Rep could release Tus from *Ter* by using a fork containing 19 nt of ssDNA on the leading strand to allow Rep loading, as shown above (Figure 6.1B). Interestingly, we observed now that the majority of the trajectories (80%) displayed a stoppage of DNA synthesis at Tus−*Ter* (Figure 6.2B). This increased stoppage yield is presumably the result of the 4-fold reduction in rate of DNA synthesis in the Rep-associated replisome. Nonetheless, this stoppage was only transient and lasted for ~ 17 s (Figure 6.2B). This experiment revealed important mechanistic information on Tus–*Ter* polar arrest activity. We showed that T7 DNA polymerase-mediated strand-displacement synthesis was more effective than helicase–polymerase leading-strand synthesis in displacing Tus at the NP face[232]. This indicates that the helicase is blocked first at the Tus–*Ter* before the polymerase arrives. In the 50% bypass trajectories, the replisome displaced Tus without even transient pausing, raising an interesting paradox as to how DnaB can pass through the intensive interactions among α6/L3/α7 region on Tus and DNA[264]. Our results show that pulling on the leading strand could prevent the C6-base flipping process and displace Tus. However, this mechanism would still require a transient stoppage (Figure 6.2B). We are able therefore to propose that the fast moving DnaB can sneak through the extensive α6/L3/α7 and DNA interactions and displace Tus in the bypass trajectories.

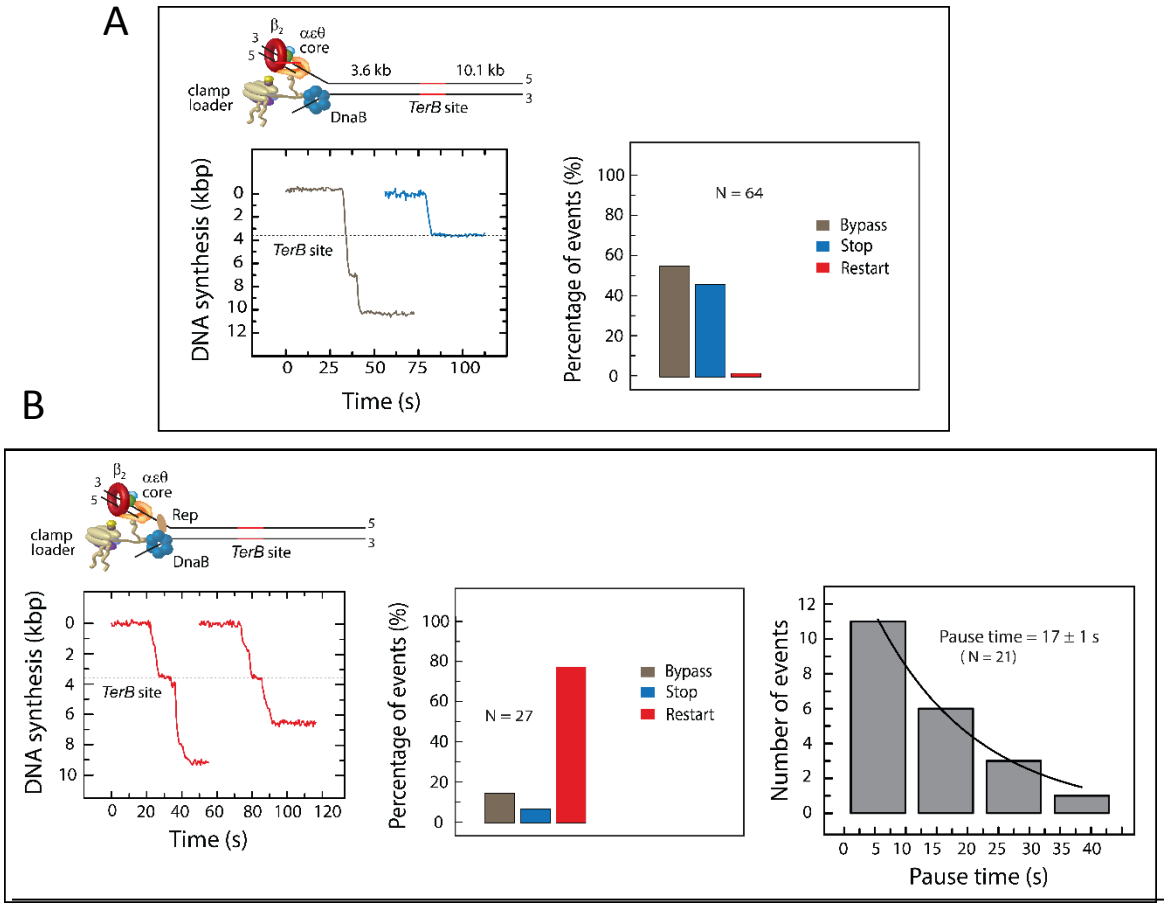

Figure 6.2: Rep-associated *E. coli* replisome releases Tus from the non-permissive face of Tus–*TerB* after a transient pausing of DNA synthesis

A. Top panel: a schematic representation of *E. coli* replisome mediating leading-strand synthesis and encountering Tus–*TerB* complex from the non-permissive face (NP). The design of the forked region of the DNA template prevents Rep loading at the fork. Bottom left panel: Representative trajectories of DNA synthesis upon encountering Tus–*TerB* complexes. The fork bypassed the complex in 50% of the trajectories (left) and fully stopped in the other 50% (right). Trajectories showing unimpeded bypass and permanent stoppage are color coded with brown and red, respectively. The location of *TerB* site is indicated by the dashed line. Bottom right panel: the percentages of molecules that bypassed, stopped or restarted are shown *(N = 64)*.

B. Top panel: increasing the ssDNA gap to 19-nt enables Rep loading at the *E. coli* fork. Bottom left panel: Representative trajectories of DNA synthesis upon encountering Tus–*TerB* complexes. The fork stopped transiently at the complex before resumption of DNA synthesis in 80% of the trajectories. The location of *TerB* site is indicated by the dashed line. The transiently stopped replisomes restarted replication with the same slow rate of DNA synthesis. Bottom middle panel: the percentages of molecules that bypassed, stopped or restarted are shown *(N = 27)*. Bottom right panel: distribution of pause durations was fit to a single exponential decay. The fit line is shown and uncertainty corresponds to the standard error *(N = 21)*.

These results demonstrated that Rep was able to resolve the Tus−*Ter* barrier and supported the replisome to restart its DNA synthesis activity. Interestingly, the restarted replisome after the displacement of Tus still synthesized DNA at a slow rate (Figure 6.2B), suggesting that Rep remained bound at the fork even under conditions where it was actively resolving a strong protein–DNA barrier.

6.4 Future Studies

Our newly reconstituted Rep-containing *E. coli* replisome provides a powerful tool to characterize Rep interaction with the replisome during DNA synthesis. To assign the effect of Rep in attenuating the rate and processivity of the *E. coli* replisome to either Rep interaction with DnaB or Rep helicase activity, we will use a DnaB-interaction defective Rep mutant (Rep lacking the 33 residues at the C-terminal tail)[202,204] and Rep that is helicase deficient. We will also investigate if Rep could be actively recruited at a stalled replisome by firstly stalling the *E. coli* replisome at Tus−*Ter* and investigating if Rep can be recruited from solution to release Tus. Interestingly, our results suggested that Rep was

still associated with the fork even after it releases Tus. We plan to use our reconstituted system to investigate the mechanisms that releases Rep from the replisome and restore its normal rate of DNA synthesis. We propose that a competition between Rep and single-stranded binding protein (SSB) to the ssDNA gap ahead of the leading strand polymerase would take place during the frequent cycling of Rep at the fork. In parallel, we will establish another protein–DNA barrier system using the previously studied multiple *EcoRI* restriction enzyme–DNA barrier approach to stall the replisome[270]. This will be critical to ensure that our findings using the Tus−*Ter* system constitute general concepts in the accessory helicase-mediated restart mechanism.

Chapter 7

Discussion

7. Mechanisms of Tus-mediated Polar Arrest of the *Escherichia coli* Replisome

Clusters of sequence-specific DNA replication termination sites were identified in the terminus regions in several bacterial plasmids and chromosomes[10,20,21,99,100]. Each of these sites consists of a *trans*-acting element (terminator protein) bound to a *cis*-acting element (termination sites) that stops approaching replisomes from one direction (non-permissive face (NP)) but not the other (permissive face (P))[20,23,24,86,128]. In the circular *Escherichia coli* chromosome, two replisomes are assembled at the origin and synthesize DNA in opposite directions to meet nearly halfway in the terminus region[10,19,21,53]. Two clusters of five termination sites (*Ter*) bound to the terminator protein (Tus) create a "replication fork trap" by allowing the first arriving fork to enter but not leave the terminus, while waiting for the late arriving one[101,127,130,135]. This synchronization is achieved by orienting the NP face of Tus−*Ter* sites in each cluster to encounter the replisome copying the opposite replicore[20,23,86]. The *Ter* sites are arranged with progressively enhanced affinity to Tus and efficiency of fork arrest activity in the direction of origin-to-terminus[20,23,86,129,137,138].

Three models were proposed for the mechanism of Tus−*Ter* polar arrest activity. In the dynamic clamp model[101,127], the intrinsic asymmetry of Tus interactions that specifically embrace the *Ter* sites through protruding helical structure at the NP face blocks forks at this face while approaching of forks from the P face leads to facile dissociation of Tus. In

the helicase interaction model[135,145], a physical interaction between the replicative DnaB helicase, which unwinds the parental DNA strands, and the NP face of Tus blocks the advancing helicase. In the mousetrap model[130], strand separation activity of DnaB engineers a highly stable Tus−*Ter* structure that blocks DnaB movement by flipping a strictly conserved cytosine residue (C6) at the NP face to interact with a cytosine-binding pocket on Tus.

Each one of these models cannot alone explain the conflicting results in the literature (reviewed in [24,86,128]). Furthermore, the polarity of Tus−*Ter* disscociation could act in reverse with some motors[142] and more unexpectedly arrest them at the P and NP faces with comparable efficiencies[141]. Finally, the efficiency at any Tus−*Ter* site in reporter plasmids *in vivo* does not exceed 50%, even when Tus is overexpressed[137,208], despite their ability to halt replication forks permanently *in vitro*[232,264]. This low efficiency explains why the terminus site contains redundant *Ter* sequences but it leaves us with an interesting paradox regarding the discrepancy between the *in vitro* and *in vivo* work.

Intensive research over the past three decades left us with a highly complex mechanistic picture of Tus−*Ter* that is also controversial. This thesis work utilized complementary experimental approaches to show that Tus−*Ter* polar arrest activity is mediated by its differential response to strand separation through an intrinsic multistep mechanism that consists of at least two steps[264]. The operation and relevance of these mechanisms are determined by how far the helicase unwinds the *Ter* site before Tus is able to stop it. Maintaining the clasping on the lagging strand to prevent DnaB from advancing farther

into Tus−*Ter* central interactions is the key step that determines the efficiency of a Tus−*Ter* site and it is mediated by a C6-mousetrap independent mechanism. However, the interactions that impose this clasping are first established upon Tus binding to the duplex form of *Ter* and need to be rearranged in response to *Ter* unwinding by the helicase[264]. The strength of the clasping is progressively weakened as DnaB breaks into Tus−*Ter* interactions and is able therefore to stop the fork either permanently or temporarily, depending on the rate of strand separation. Escaping the clasping mechanisms by faster moving forks leads to breaking into Tus−*Ter* central interactions and facile dissociation of Tus[264]. The mechanism of Tus−*Ter* polar arrest activity is further complicated by what appears to be an overlapping function between the clasping interactions by the C6-moustrap independent mechanism and the C6-base flipping process itself[145]. The triggering of the C6-mousetrap is inefficient process and requires at least a transient stoppage by the clasping interactions. This multistep response of Tus−*Ter* to strand separation is an intrinsic phenomenon since it operates when Tus−*Ter* encounters the heterologous bacteriophage T7 system[232,264]. This thesis work left us with a mechanistic model of Tus−*Ter* polar arrest activity that is best described by a composite of both dynamic clasping and C6-mousetrap mechanisms[232,264]. Finally, studying the responses of the P and NP faces of Tus−*Ter* to the T7 DNA polymerase, T7 helicase and their concerted leading-strand synthesis activity[232], reveal that the intrinsic asymmetric interactions between Tus and the two strands, that is extensive on the lagging strand at the NP and P faces[23,127,232], explains why motors translocating on the lagging- or leading-strands are preferentially blocked by the NP and P faces, respectively (reviewed in [23]).

7.1 Mechanisms of *E. coli* Replication Fork Arrest

7.1.1 C6-mousetrap Model

The role of the C6-mousetrap mechanism in Tus–*Ter* polar arrest activity has been debated since its first description in 2006[130]. Firstly, the relevance of the C6-base flipping mechanism had not been directly tested under physiological conditions of double-stranded (ds) DNA unwinding by a helicase or a replisome. Secondly, studying the contribution of C6- flipping to the kinetic stability of Tus–*Ter* complex requires the use of high salt concentrations (250 mM KCl) since it is masked by the strong electrostatic interactions of Tus and *Ter* at lower salt concentrations. These high salt concentrations are not physiological and would be inhibitory for most of the cellular and molecular processes including DNA replication[209,210]. Thirdly, the Tus–*Ter* complex displays some specificity in blocking helicases such as DnaB, PriA, and simian virus 40 (SV40) large T-antigen but not others such as PcrA, Rep, and UvrD *in vitro*[118,136,140-142,214]. This helicase specificity however is disputed between various studies (reviewed in [23]). Furthermore, the leading-strand specificity of the C6-base flipping process makes it difficult to interpret its role without functional studies that consider the orientation of the helicase-translocating strands (3'–5' or 5'–3'). Fourthly, the Tus–*Ter* complex blocks DnaB translocating on dsDNA in a polar manner under conditions where the C6 is altered or its melting is prevented by DNA cross-linking[145]. This assay however does not report on the encounter of DnaB and Tus–*Ter* under replication-relevant conditions where the helicase translocates on the lagging strand while actively melting the parental dsDNA[145]. Fifthly, several old studies in the literature downplayed the role of C6 base on the binding affinity

to Tus as well as fork arrest activity[100,131]. Lastly, a recent study shows that polarity of blockage by Tus–*Ter* is maintained in yeast MCM2–7 complex[211] although it translocates at the C6-containing strand in the 3'–5' direction and is believed therefore to inhibit C6-flipping[212,213]. The same study also showed that F140A mutation in the cytosine-binding pocket in Tus do not abolish the Tus–*Ter* polar arrest activity of the MCM2–7 complex *in vivo*[211].

7.1.2 Operation of the C6-mousetrap Under Physiological Conditions

In this research, we reveled a role for the C6-mousetrap model in Tus–*Ter* fork arrest activity within the context of a functional replisome encountering the Tus–*Ter* complex[232,264]. In the first study[232], transient state bulk-kinetics and single-molecule DNA replication assays were used to characterize the responses of the P and NP faces of Tus–*Ter* to the heterologous bacteriophage T7 replisome. Only three proteins mediate the mechanism that couples the DNA unwinding activity of the helicase and copying the exposed single-stranded (ss) DNA template by the polymerase[14,182,183] in contrast to 14 proteins in the *E. coli* replisome[47,55]. T7 helicase encircles the lagging strand as a hexamer and uses the energy of nucleotide hydrolysis to translocate on it in the 5'–3' direction, similar to the *E. coli* DnaB helicase, and displaces the complementary leading strand[15,268]. The T7 polymerase copies the excluded leading strand ssDNA template and coordinates its activities with the helicase *via* protein-protein interactions[183,271]. This coordination involves the cooperation of both the polymerase and helicase in melting the DNA and copying it through a tight one-nucleotide stepping mechanism[248,272]. The complex synthesizes DNA in a highly processeive manner and at rates approaching 100-200 base

pairs/s (bp s^{-1})[248,249]. Unlike the *E. coli* system, the T7 leading-strand synthesis complex can be assembled at a forked structure with very high efficiency[249,253,255]. This enables the synchronization and monitoring of its activity on short DNA templates with a single-base spatial and millisecond temporal resolutions, using a rapid reaction-quenched flow assay[248,249,252,253,272].

The 23-bp *TerB* sequence was introduced in either the P or NP orientation by inserting it at a specific position in the middle of a 60-bp dsDNA region of synthetic replication fork substrates (Figures 4.4 and 4.5A)[232]. In the absence of Tus, the helicase/polymerase complex completed the synthesis of the 60 bp DNA without any significant pausing at a specific site (Figure 4.5B). Similar results were observed in the presence of Tus that was bound to *TerB* to encounter the fork through its P face, except for a minor percentage of molecules displaying transient pausing at the Tus–*TerB* site, presumably due to the high affinity of the Tus–*TerB* complex (Figures 4.9 and 4.10). When the fork encountered the NP face of Tus–*TerB*, nearly 90% of the replisomes were stopped permanently after the incorporation of the third nucleotide and as the fourth nucleotide is being incorporated. A run-off DNA synthesis was observed in the remaining 10% of the molecules with no intermediates between the fifth nucleotide of *TerB* site and the run-off products (Figures 4.5B,C and 4.6)[232]. These results demonstrate that the highest energy barrier for the strand separation activity of the replisomes is within two to three nucleotides from the GC6 bp. The ability of Tus–*Ter* to stop the T7 replisome in a polar manner similar to the *E. coli* system suggests that Tus–*Ter* polar arrest activity is an intrinsic phenomenon that is system independent, arguing against the DnaB/Tus interaction model[135,145].

Altering the C6 base to G6 compromised the C6 lock formation as shown by surface plasmon resonance (SPR) binding studies (Figure 3.10)[264]. This was further supported by the crystal structure of a Tus complex with a forked *Ter* containing an unpaired G replacing C6, which showed the substituted G6 base neither bound in the cytosine pocket nor formed any new specific interaction with Tus (Figure 3.7)[264]. Surprisingly, Tus bound to the NP face of AT6- or CG6-altered *TerB* was still able to stop the fork with similar efficiency and a slow-incorporation rate of the third and fourth nucleotides to that in the case of wild-type *TerB* sequence, but the run-off DNA synthesis increased to 70% (Figure 4.12A,B)[232]. These results demonstrate that Tus–*Ter* has an intrinsic ability to transiently stop the replication fork by a C6-lock-independent mechanism. The similar fork stoppage efficiency, either permanently or transiently in the case of wild-type *TerB* or when the GC6 bp is altered, respectively[232], demonstrates that this C6-lock independent mechanism is what determine the efficiency of Tus–*Ter* fork arrest activity.

The 10% run-off DNA synthesis at the NP face of *TerB* that continues over the course of several minutes suggests that either the C6-mousetrap mechanism is not triggered in these molecules or it has been overcome by the replisome[232]. These two scenarios were distinguished by studying the encounter of the fork with a preformed C6-locked complex, which was achieved by incubating Tus with a *TerB* site containing a bubble structure up to the GC6 bp. This preformed C6-locked complex eliminated the 10% run-off DNA synthesis, providing evidence that the C6-mousetrap is operational under physiological conditions and is able to permanently stop the fork once formed (Figure 4.12A,B)[232]. Furthermore, it demonstrates that the 10% run-off DNA synthesis in the case of wild-type

TerB must have resulted from molecules where C6-flipping is not triggered. This strongly suggests that the triggering of C6-mousetrap mechanism is indeed an inefficient process.

In another study[264], the fate of the *E. coli* leading-strand DNA synthesis upon encountering the P or NP faces of Tus–*TerB* was investigated using single-molecule DNA replication assays[14,55,182]. A 13.7 kilobase (kb) substrate containing a single copy of *TerB* that was inserted 3.6 kb-away from a forked region and followed by a 10.1 kb-DNA was used in these assays: *TerB* was oriented in the P or NP orientations or contained altered sequences at the NP face (Figure 3.2A,B). Location of the inserted *TerB* site can be defined with an accuracy of 0.1 kb at the used DNA stretching forces[264]. This assay established that the rate of DNA synthesis varies among individual replisomes, reflecting the *in vivo* situation (Figure 3.3). Our newly reconstituted *E. coli* replisome in these assays approaches the *in vivo* rate of ~ 900 bp s^{-1} with a processivity of 10 kb[55].

In the absence of Tus, only 5% of the replication forks observed to each *TerB site* stopped at 3.6 ± 0.1 kb as a result of random collapse of the fork due to processivity limitation, while the other 95% replicated past the inserted *TerB* site (Figure 3.1E and Table 3.1)[264]. In the presence of Tus that was bound to *TerB* to encounter the fork through its P face, 11% of the forks stopped permanently, presumably due to forks encountering the strong protein–DNA roadblock (Figure 3.1E and Table 3.1). Transient stoppage followed by resumption of synthesis occurred in 5% of trajectories. The fork in the remaining 84% of trajectories displaced Tus and continued synthesis beyond *TerB* without stopping, even transiently (Figure 3.1E and Table 3.1)[264]. When the fork encountered the NP face of Tus–

TerB, only 45% of the trajectories displayed permanent stoppage (9.7 ± 1 min on average in our assay), while in 52% of trajectories the replisome displaced Tus without stopping even transiently as observed in the case of the P face (Figure 4.1D,E and Table 3.1)[264]. This ~ 50% fork arrest efficiency by Tus–*TerB* is in perfect agreement with that reported from *in vivo* studies on reporter plasmids[137,208], demonstrating that the reconstituted encounter of the *E. coli* fork and Tus–*TerB* at the single-molecule level is a true mimic of the *in vivo* conditions.

The yield of run-off DNA synthesis in the T7 system at the NP face of Tus–*TerB* from the reaction-quenched flow assays was remarkably less than that observed in *E. coli* (Figure 4.12B *cf.* 3.1E)[232,264]. Reconstituting the encounter of the T7 fork with the P or NP faces of Tus–*TerB* in a similar single-molecule replication assays to those used in the *E. coli* system showed high efficiency of fork arrest activity and results that were in agreement with those from the quenched flow experiments (Figure 4.1D *cf*. 4.12B)[232,264]. The 52% run-off DNA synthesis without pausing in the case of *E. coli* was caused by the inefficient triggering of the C6-moustrap, as evident by the increase in the percentage of fork permanent stoppage to ~ 90% when the C6-locked structure was preformed prior to replication using a *TerB* containing bubble-DNA structure in place of bps 3–7 while keeping the C6 base unpaired (Figure 3.1H and Table 3.1)[264].

Interestingly, NP *TerB* with swapped GC6 to CG6 had similar effect on Tus-mediated polar arrest activity upon encountering the *E. coli* fork to that seen in the case of the T7 fork[232,264]; the efficiency of fork stoppage remained similar to that in the wild-type *TerB*,

but the stopped forks were able to resume DNA synthesis after a short pause (Figures 3.3C and 3.6A,B)[264]. These results supports the conclusion derived from the quenched flow experiments with the T7 system[232], which postulates that the efficiency of Tus–*Ter* is determined by a step preceding the C6-lock formation. Nevertheless, the induction of this intrinsic step is significantly much less efficient in the *E. coli* system.

7.1.3 Fork Arrest Efficiency is a Kinetically Controlled Process

The K_D of the C6-locked complex is only 3-fold lower than Tus–ds*TerB*, while its lifetime is much longer[130]. This prompted the hypothesis that efficiency of C6-lock formation is kinetically rather than thermodynamically controlled. The results from the T7 and *E. coli* systems established that such kinetic control is determined by a step preceding the triggering of the C6-moustrap mechanism[232,264]. Previous *in vivo* studies shows that DNA supercoiling attenuates fork arrest efficiency at Tus–*Ter* in a way that suggests that the rate of strand separation might influence polar arrest activity[208]. The ability of the single-molecule DNA replication assays to measure rates of individual replisomes approaching the NP face of Tus–*TerB* enabled the direct investigation of this kinetic competition hypothesis. A positive correlation was observed between the rate of DNA synthesis and fork bypass, where forks moving at an average rate of 840 bp s^{-1} were effectively stopped and those at 1700 bp s^{-1} displaced Tus and continued synthesis (Figure 3.1G and Table 3.1)[264]. This observation demonstrates that fork arrest efficiency is indeed controlled kinetically by a competition between rate of strand separation and rate of induction of the C6-lock independent transient stoppage[264]. The nearly 10-fold slower moving T7 replication fork is therefore arrested more efficiently than the *E. coli* replisome.

We demonstrated previously that reconstituted replication forks assembled using a preformed 1:1 complex of DnaB and its loader DnaC approaches the *in vivo* rate of DNA synthesis (~ 900 bp s^{-1})[55]. This rate is twice that reported with the commonly used 1:1 mixture of DnaB and DnaC[47], underscoring the importance of our ability to restore the *in vivo* rate of DNA synthesis in reproducing the 50% efficiency reported here *in vivo* for Tus–*TerB*[137,208] for the first time in an *in vitro* assay[264].

In the Tus–ds*Ter* or Tus–forked-*TerB* crystal structures, the α6/L3/α7 region has extensive interactions with the lagging strand (Figure 1.10A) before and after C6-lock formation[127,264]. This raises and interesting paradox as to how the fast moving DnaB can selectively disrupt these interactions without even pausing. We showed that T7 DNA polymerase-mediated strand-displacement synthesis was more effective than leading-strand synthesis in displacing Tus at the NP face since it advances farther into the Tus–*Ter* central interactions, demonstrating that DnaB arrives and is blocked at Tus–*Ter* before Pol III[232]. We sought therefore to determine from which strand the fast moving forks break into the central Tus–*Ter* interactions. We included Rep helicase (3'−5') to selectively release Tus from the Pol III direction. Rep interacts with DnaB adding another motor at the fork[204] and has been shown on its own to release Tus oriented at the NP face[118,140]. Rep moved with the fork and decreased the rate of *E. coli* leading-strand synthesis to 250 bp s^{-1} (Figure 6.1B) in a mechanism that is currently under investigation (discussed in Chapter 6). This reduction in rate increased the efficiency of fork stoppage to 80% (Figure 6.2B), indicating that efficient fork stoppage occurs at forks moving at rates below 300 bp s^{-1}. However, this stoppage was transient (Figure 6.2B). Rep-containing forks also

displaced Tus from a preformed Tus–*TerB* locked complex after a similar duration of transient stoppage (data not shown). This experiment demonstrated that pulling on the leading strand could release the flipped C6 and displace Tus. However, this mechanism would still require a transient stoppage. We propose therefore that fast moving DnaB is able to sneak through the extensive α6/L3/α7 DNA interactions on the lagging strand[264].

The main sequence-specific contacts α6/L3/α7 makes with the first 6 bps of ds*Ter* are *via* Arg198 in L3 with the A5 and G6 bases on the lagging strand, and also with T5 on the leading strand (Figures 3.7E and 4.19)[130,264]. In the C6-locked complex however, Arg198 switches from these base-specific contacts to make a new salt bridge with the phosphate backbone between nucleotides 6 and 7 on the lagging strand (Figure 3.7A)[264]. The side chain of Arg198 therefore makes multiple transient interactions with G6, TA5 and the lagging strand phosphate backbone that is likely to contribute to the sealing of the two DNA strands together before strand separation at the GC6 bp[264]. The rearrangement of Arg198 interactions during strand separation provides a window of opportunity for the fast-moving DnaB to break into the Tus–*Ter* central interactions before Arg198 rearrangement or C6 flipping occurs[264]. Allowing Arg198 to rearrange its interaction prior to replication by incubating Tus with a substrate containing a *TerB* bubble-DNA structure in place of bps 3–7, but this time with altered C6 to eliminate Tus–*Ter* lock formation, resulted in highly efficient fork stoppage but this stoppage was not permanent (77% transient and 8% permanent) (Figure 3.6E and Table 3.1)[264]. These results demonstrate that head-to-head kinetic competition between the rate of strand separation and the rate of rearrangement of Tus–*Ter* interactions during the separation of the first 6 bp of *Ter* is

what determines the fork arrest efficiency[264]. It also shows that strand separation beyond GC6 in the absence of the C6 lock would impose only transient fork stoppage; *i.e.* imposing permanent stoppage after separation of the GC6 bp would therefore necessitate triggering of the C6-mousetrap.

Extensive alterations of the first five bps of *TerB* showed that the interactions of A5 and/or T5 are the primary contributors in this region for the rate-dependent fork arrest activity (Figure 3.7E)[264]. In fact the average rate of DNA synthesis by stopped replisomes when altering AT5 bp was 2-fold slower than that in the case of wild-type *TerB* (Figure 3.9A and Table 3.1). Substitution of wild-type GC6 with a CG had a modest effect on Tus binding to ds*TerB* in comparison to an AT or TA[100]. Comparison of the effect of substituting GC6 with CG6 versus AT6 showed that both substitutions abolished the permanent fork stoppage but the efficiency of fork arrest activity in the case of AT6 was markedly reduced and the average rate of the stopped forks was also shifted to a 2-fold slower range relative to the wild-type *TerB* (Figure 3.6B *cf.* 3.9D and Table 3.1)[264]. This demonstrates an important role for the interaction of Arg198 with G6 in the rate-dependent fork arrest activity. The differential effect of CG6 versus AT6 substitutions was also observed in the case of the T7 system (Figure 4.12)[232].

Tus(R198A) interacts with ds*TerB* with a 140-fold reduction in K_D, but only a two-fold shorter half-life[101] and was also able to form the locked complex as shown by SPR (Figure 3.10D)[264]. Interestingly, Tus(R198A) stopped the replication fork but only transiently and with significantly reduced efficiency, with the average rate of forks that it stopped shifting

to a 2-fold slower range relative to the wild-type Tus (Table 3.1)[264]. Nevertheless, preforming the locked complex with Tus(R198A) and a *TerB* site containing a bubble-DNA structure between bps 3–7 with intact C6 resulted in very efficient (86%) induction of permanent stoppage (Table 3.1)[264]. The interactions of Arg198 are therefore required for both the rate-dependent fork arrest activity and enabling the inefficient C6-flipping process by slowing down or transiently halting the fork.

These sets of experiments established a model for triggering the C6-mousetrap through a 2-step mechanism (Figure 3.12)[264]. The interactions of Arg198 with G6, A5 and/or T5 clasp the lagging strand to protect the Tus–*Ter* central interactions from the first arriving DnaB. These interactions are dynamic during the separation of the first 6 bps changing from base-specific to phosphate backbone-mediated interactions. Faster moving forks would have a higher chance of melting the GC6 bp before R198 succeeds in rearranging its contacts leading to facile dissociation of Tus without even transient pausing (Figure 3.12). Slower moving forks on the other hands are stopped transiently if the GC6 bp is melted and Arg198 managed to rearrange its interactions (Figure 3.12). This transient pausing enables the triggering of the inefficient C6-mousetrap that acts as a terminal step in imposing permanent fork arrest (Figure 3.12)[264].

7.1.4 Permanent Fork Arrest by a C6-mousetrap-independent Mechanism

Several experiments hinted at the operation of an uncharacterized C6-lock independent mechanism[100,145]. We showed using data from *in vitro* single-molecule replication experiments and *in vivo* replication assays that mutating various residues in the cytosine-binding pocket of Tus do not necessarily abrogate fork arrest activity (Figure 5.2 and Table 5.2), despite their substantial influence in reducing binding to C6-locked complexes (Table 5.1) (discussed in Chapter 5). These results clearly suggest the operation of additional mechanisms that are independent of the C6-mousetrap and able to impose permanent fork arrest.

The complete failure of Tus(R198A) to impose permanent fork arrest activity reveals an important role for the interactions of R198 with G6, A5 and/or T5 in such a mechanism[264]. These interactions must hold the replication fork before the GC6 bp is melted since permanent fork arrest is not achieved under a scenario where the GC6 bp is melted and the C6-locked mechanism is deactivated (Figure 3.6E and Table 3.1)[264]. To explore whether the interactions of R198 with AT5 and G6 contribute directly to the C6-lock independent mechanism, these interactions were maintained using the wild-type *TerB* sequence but the formation of the C6-locked complex was deactivated by mutating the key H144 residue in the cytosine pocket to alanine[130]. This mutation completely eliminated lock formation as shown by SPR and it was confirmed by X-ray crystallography that showed the C6 was not flipped in a Tus complex with a *Ter* site containing a forked structure with unpaired C6 (Figures 3.7D and 3.10F)[264]. The efficiency of fork arrest and its rate dependence was maintained in the case of Tus(H144A) (Figure 3.11 and Table 3.1),

supporting that fork arrest efficiency is in part determined by a C6-lock independent mechanism[264]. Surprisingly, half of the stopped forks were permanently arrested by Tus(H144A), confirming the existence of the C6-lock independent mechanism leading to permanent fork stoppage. In the remaining half, the fork resumed DNA synthesis after short pauses of 33 s (Table 3.1)[264]. This short pausing must have resulted from a mechanism additional to permanent arrest, since restarts would otherwise be randomly distributed over the full 10 min period of observing full stoppage. These results demonstrate that the C6-lock dependent mechanism contributes to nearly half of the total fork arrest activity of Tus–*Ter*. This provides an explanation why, in helicase assays, the slowly moving DnaB (35−390 bp s^{-1})[233,234] is efficiently stopped at the NP face without requiring C6-flipping[145].

Collectively, these experiments unraveled the identity of the C6-lock independent mechanism to be mediated mainly by R198. The interactions of R198 with G6, A5 and/or T5 therefore play overlapping roles with the C6-lock dependent mechanism. These interactions could permanently stop the slower moving forks before the GC6 bp is melted in a C6-lock independent manner or transiently if the GC6 bp is melted to enable the inefficient C6-flipping process (Figure 3.12)[264]. The C6-lock independent mechanisms revealed from the single-molecule experiments using the *E. coli* fork, in principle, should be sufficient to block replication forks moving at low rates such as in the T7 system. The contribution of the C6-lock independent mechanisms to permanent arrest activity of the T7 fork could therefore be significantly higher than that in the case of the *E. coli* system.

7.1.5 C6-mousetrap is Invoked in the Absence of DnaB

A recent single-molecule study employed magnetic tweezers to mimic the action of the helicase by applying force to unwind a DNA-hairpin structure containing a *TerB* site that is oriented in either the P or NP direction[267]. At low regime forces, Tus–*TerB* blocks the unzipping force in a polar manner, arguing against the requirement of a physical interaction between Tus and DnaB in mediating Tus–*Ter* fork arrest activity. High force regimes that far exceed those exerted by the replisome release Tus at the NP face and therefore enable the characterization of its mechanism. Applying high force regimes (~ 60 pN) unravel a 3-steps mechanism during the release of Tus at the NP face[267]. Swapping the orientation of GC6 to CG6 or mutations of the residues in or around the cytosine-binding pocket influence either the probability and/or the lifetime of the three states at appropriate forces. On the other hand, a mutation in the DNA binding domain of Tus did not produce any effect on these states, suggesting that they are all influenced by the interaction of Tus with C6. The blockage shows a progressive strengthening over the three states of different stochastic dwell-time scales. Varying the force attenuates the probability of these states with the longest-lived state being the only one observed at higher force regimes[267]. This force dependency of the three states also suggests that they are all influenced by the interaction of Tus with C6, with the longest lived-state being assigned to the full C6-lock conformer. It has been suggested that the three states are independent of each other and the timescale of their exponential decays reflect the dissociation of Tus from each state. Consequently, an assumption has been made that the full C6-lock state would dominate over the other two states at lower force regimes.

Furthermore, the first and the second states were arbitrarily assigned to be different forms of the C6-lock state just based on the fact that weakening the interactions in the cytosine-binding pocket influence their probabilities/lifetimes[267].

Surprisingly, the fork arrest efficiency of Tus–*TerB* in the magnetic tweezers experiments exceeds those reported from *in vivo* studies and our *in vitro* single-molecule replication assays[137,208,232,264]. It has been proposed therefore that protein–protein interaction would hinder rather than promote fork arrest efficiency[267]. The inefficient triggering of the C6-lock however is system independent as shown by the 10% run-off DNA synthesis at the NP face of Tus–*Ter* in the case of the T7 system (Figure 4.12E)[232] and the fact that different helicases are also able to displace Tus to different degrees[118,140,264]. It is also difficult to imagine from an evolutionary perspective as to why the *E. coli* Tus–*Ter* system would develop and/or conserve an interaction with the helicase to attenuate its primary function of blocking the fork.

Explaining the results on some of the Tus mutants by solely relying on their deficiency in the formation of three C6-lock states appears to be inconsistent with the *in vivo* fork arrest activity studies[23,143,144]. Furthermore, some of the C6-lock kinetics derived from these assays, particularly Tus(H144A) and CG6-swapped *TerB*, are also inconsistent with the SPR binding studies and crystallography that showed that they cannot form the C6-locked complex (Figures 3.7D and 3.10F)[264]. It is possible therefore that the extremely high forces applied in this study or the unusual geometry of fork opening, that would be nearly 180° in the magnetic tweezers experiments, might have helped the C6-lock to

move into the cytosine pocket and/or maintain its interaction with the pocket[267]. We found that recruitment of Rep helicase that translocates on the C6-containing leading strand in front of the polymerase, into the reconstituted single-molecule *E. coli* DNA replication assay was able to displace Tus from a pre-formed C6-locked complex after a short pause of only ~ 16 s (date not shown). This experiment clearly suggests that the C6-locked complex can be released by the operation of two helicases acting simultaneously on the leading- and lagging-strands and therefore argues against the ultimate sustainability of the C6-lock in the magnetic tweezers experiments. This result also suggest that the orientation of pulling on the leading strand could make a significant difference and is likely to be in favor of the C6-flipping process when the DNA is unzipped by magnetic tweezers[267].

In our opinion, the magnetic tweezers experiments establish the presence of three Tus–*Ter* conformers that involve the interactions of the C6 base with the cytosine-binding pocket and E49 outside this pocket[267]. The nature of the interactions in these conformers however is unknown but at least the longest-lived state should correspond to the fully flipped C6-locked complex; this would be the equivalent conformer that we refer to as the C6-locked complex. All three conformers are able to impose a significant barrier to strand-separation activity[267]. The interesting question therefore would be whether any of these conformers correspond to the clasping interactions. We propose that the first or second, or both conformers report on interactions that could be mediated by the clasping mechanism, particularly *via* Arg198, in addition to those mediated by the C6 base. Testing Tus(R198A) in the magnetic tweezers experiments would be highly informative. We

anticipate that it would specifically influence one or both of the first two states but will form a C6-locked complex, agreeing with its ability to form a C6-locked complex in SPR binding studies (Figure 3.10D)[264]. In fact, the formation of the first and second states were more defective in the combination of wild-type Tus and CG6-swapped *TerB* than Tus(H144A) and wild-type *TerB* in the magnetic tweezers experiments[267]. This was explained by a decreased ability of G6 to form the lock. If the G6 is not able to form the lock, as proposed, then one would anticipate that the combination of Tus(H144A) and CG6-swapped *TerB* should not differ from wild-type Tus and CG6-swapped *TerB*. On the contrary, Tus(H144A) and CG6-swapped *TerB* display a dramatic accumulative effect in the magnetic tweezers experiments[267]. We propose that these results strongly indicate a role of the interactions of Arg198 with G6 in the formation of the first and/or second states, in addition to the interactions of the C6 with the cytosine-binding pocket and E49 outside the pocket. Interestingly, we observed a relatively minor effect of some of the tested cytosine-pocket mutants on the rate-dependent fork arrest activity in our replication assays (Table 5.2) (discussed in Chapter 5). This suggests that the C6-lock independent mechanism might involve some minor contribution from the interactions of the C6 base with the cytosine pocket and E49, perhaps from the conformers in the first or both first and second states[267], while the main contribution is mediated by the interactions of Arg198 with AT5 and G6[264].

7.2 Tus/DnaB Physical Interaction Model

Several experiments established the line of thinking of a model where a possible physical interaction between Tus and DnaB at the NP face could mediate Tus–*Ter* polar arrest

activity[135,144,145]. This was first suggested by the assessment of binding of Tus to *Ter* sites that shows that the DNA binding affinity is not always correlated with the blockage activity[144]. The same observation is demonstrated in the cognate *B. subtilis* replication termination system that is mediated by the dimeric replication terminator protein (RTP) binding to *B. subtilis Ter*[122]. A hydrophobic patch was identified at the NP face of RTP and mutations in two of its residues (E30 and Y33) markedly reduced the RTP fork arrest activity *in vitro* without altering its binding affinity to DNA or its dimerization[123]. Furthermore, fusion of tag peptides at the NP face of RTP in an attempt to hinder its putative interaction with the advancing replisome also reduces its fork arrest activity without affecting its DNA binding affinity[126].

In *E. coli*, there are several lines of evidence supporting a direct physical interaction between DnaB and the L1 loop at the NP face of Tus[135]. This loop is proposed to be the first region on Tus to encounter the advancing DnaB on the lagging strand (Figure 1.11A). The physical interaction between L1 and DnaB was first demonstrated *in vivo* using the yeast two-hybrid system and subsequently *in vitro* using enzyme-linked immunosorbent and glutathione *S*-transferase pull down assays[135]. The interaction site on L1 was narrowed down to a specific residue E49. The Tus(E49K) mutant had significantly reduced *in vivo* fork arrest activity and polar helicase stoppage *in vitro*, without altering Tus binding to ds*Ter*[135]. In principle, a physical interaction between Tus and DnaB appears to be consistent with the observation of helicase specificity of the Tus–*Ter* complex (reviewed in [23]). For instance, fork arrest activity of *E. coli* Tus–*TerB* was diminished upon being encountered by the *B. subtilis* fork[124]. However, the RTP–*Ter* complex was able to impose

polar arrest activity on the *E. coli* forks but with a 3-fold reduced activity as compared to the native *B. subtilis* fork[125]. It is noteworthy that the literature on the issue of system specificity of Tus–*Ter* polar arrest activity is rather conflicting[118,136,140-142].

The ability of the heterologous bacteriophage T7 system to block the Tus–*Ter* complex in a polar manner like the *E. coli* system[232] argues against the detail of Tus/DnaB interaction being an indispensable requirement for imposing fork arrest activity. It would be very unlikely that the T7 helicase evolved to develop a physical interaction with Tus since T7 genomic DNA does not contain *Ter* sites. Nonetheless, the structure of the T7 helicase and DnaB are related, raising the possibility that some conserved structural features between the two helicases could exist and facilitate a Tus/T7 helicase interaction[232]. The Tus–*Ter* polar arrest activity with the heterologous T7 system therefore could not conclusively refute an auxiliary role of Tus/DnaB interaction. A recent study however showed that a Tus–*TerB* site introduced into the yeast genome is able to form a feeble but still polar fork barrier against the MCM2–7 complex[211], providing another argument that Tus–*Ter* polar arrest activity is an intrinsic process that is system independent. This intrinsic mechanism manifested itself in the remarkable similarities of its actions in both T7 and *E. coli* systems including the induction of a transient pausing step prior to C6-lock formation and the inefficiency of the C6-mousetrap mechanism[264]. The strongest argument against a role of Tus/DnaB interaction is shown by the ability of the NP face of Tus–*TerB* to impose polar arrest blockage in the absence of DnaB in the mechanical DNA unzipping experiments by magnetic tweezers[267].

Thus the longest-lasting support of the Tus/DnaB interaction model is based on the results from the Tus(E49K) mutant that reported a significantly reduced binding to DnaB and marked reduction in fork arrest activity, without altering DNA binding[135]. This particular residue is also shown to form a water-mediated hydrogen bond with the 5'-phosphate of the displaced A7 base in the C6-locked structure and therefore contributes to the C6-lock formation[130]. Assessment of the binding parameters of Tus(E49K) to ds*TerB* and locked *TerB* sequences by SPR showed a modest effect on its binding to ds*TerB* but marked reduction in forming the C6-locked structure (Table 5.1). The measured fork arrest efficiency of Tus(E49K) using the *in vitro* single-molecule replication and *in vivo* replication arrest assays was clearly weaker than mutants with comparable binding affinities to the ds*TerB* and C6-locked *TerB* sequences such as Tus(E49A), Tus(I79A), and Tus(F140A) (Figure 5.2 and Table 5.2) (discussed in Chapter 5). These results suggested an additional plausible mechanism mediated by E49 in reducing Tus–*Ter* fork arrest efficiency. The crystal structure of Tus(E49K)–*TerB*-locked complex shows that the C6 is flipped into the cytosine-binding pocket, demonstrating that the reduced ability of Tus(E49K) to form a C6-locked complex cannot account for its defect in polar arrest activity (unpublished results from Professor Nicholas Dixon's lab (University of Wollongong)). Although disrupting the interaction with DnaB appears to be a resilient candidate for the role of E49, the crystal structure showed that part of the α6/L3/α7 region including the key residue Arg198 was unstructured. This suggests that this structural defect could be an additional factor that contributes to the reduced arrest activity of Tus(E49K). It is therefore difficult to utilize this mutant to argue for or against a Tus/DnaB interaction.

Collectively, the recent experiments provide several lines of evidence that argue against the Tus/DnaB interaction model but none of them could conclusively refute this mechanism. More experiments will be needed that should be aimed to first establish the putative Tus interaction with DnaB under various conditions and signify its exact role in the Tus–*Ter* fork arrest activity, in particular provide an answer as to why Tus(E49K) considerably decreases the fork arrest efficiency.

7.3 Tus–*Ter* Blocks Motors in a Strand Specific Manner

Characterizing the ability of the Tus–*Ter* complex to block the unwinding activity of range of helicases and DNA and RNA polymerases served as a fundamental approach in describing the mechanisms controlling the Tus–*Ter* polar arrest activity. Most of these studies however reported rather conflicting results, making it difficult to utilize them to derive mechanistic information (reviewed in [23]). Early studies show that NP face of Tus–*Ter* blocks the activity of the helicases DnaB, UvrD, PriA, and Rep[136] as well as the RNA polymerases from *E. coli*, T7 and SP6[261,273]. Other studies found that NP face of Tus–*Ter* blocks the helicases DnaB and PriA but not UvrD[118,140] and fails to block helicases involved in DNA repair and plasmid rolling-circle replication such as Rep, UvrD, TraI and Dda[274]. Similarly, RTP–*Ter* complex in *B. subtilis* system fails to block helicases involved in plasmid rolling-circle replication (Rep and UvrD)[118,123]. The helicases involved in rolling-circle replication are classified as 3'–5' helicases, unlike the 5'–3' replicative DnaB and the non-replicative helicase PriA[275,276]. Interestingly, Tus–*TerB* blocks SV40 large T-antigen that translocates in the 3'–5' direction, but with a reversed polarity where the blockage is favored at its P face[142]. More paradoxically, strand displacement synthesis by three DNA

polymerases (T7, T5, and DNA polymerase I) is blocked at both the P and NP faces with comparable efficiencies[141].

The structure of Tus–ds*Ter* shows the α6/L3/α7 region at the NP face makes asymmetric contacts with DNA, where the helicase-translocating lagging strand is heavily contacted, while the polymerase-translocating leading strand is widely exposed[23,127,130]. These asymmetric interactions are maintained at the P face, where the extensive interactions are also concentrated on the lagging strand (Figures 1.9B and 4.18)[127,232]. This asymmetric arrangement of Tus–*Ter* interactions is believed to modulate the polarity of blockage in view of the orientation of the approaching helicase (3'–5 or 5'–3'). Thus, it is important to consider the orientation as well as the structure and relative power of the helicase motor in interpreting results from assays studying Tus-mediated counter-helicase activity.

Our results appear consistent with the observation of modulating the polarity of Tus–*Ter* in view of the orientation of the traveling motor. Strand displacement synthesis by an isolated T7 DNA polymerase (3'–5') was blocked at the P face, but not at the NP face. The opposite was found to be true for an isolated T7 helicase (5'–3') (Figures 4.14, 4.15, 4.16C,D)[232]. The extensive Tus-mediated interactions at the 5' end of the P face will compel the traveling polymerase to be less effective in breaking the interactions that are preferentially concentrated at that strand. On the other hand, the 5'–3' traveling helicase would disrupt Tus interactions at the 5' strand of the P face. The preferential extensive interactions of Tus at the 5' end of the NP face are clasping the DNA (Figure 4.18)[127,232], which is typically involved in either full blockage or slowing the progression of the T7

replisome. The latter would enable the inefficient C6-base flipping process in order to impose full fork stoppage. The same interactions at the lagging strand of the NP face are believed to slow the 3'–5' traveling polymerase, which in turn sequesters the C6 within its template channel and hence prevents C6-lock formation. Thus, only the pre-melted fork was able to block the strand displacement activity of T7 polymerase at the NP face (Figures 4.14 and 4.15)[232].

We showed that introducing Rep helicase (3'–5') to an *E. coli* replisome-mediated leading-strand synthesis reaction released Tus from the NP face after a transient pausing of DNA synthesis (Figure 6.2B) (discussed in Chapter 6). Also, Rep was able to release Tus from a preformed lock structure after nearly equivalent pause duration (data not shown). These results argue against the notion of the extreme stability of the C6-locked complex[267]. The ability of Rep and DnaB to cooperate in displacing Tus even from a pre-formed C6-locked complex in contrast to the inability of helicase–polymerase leading-strand synthesis demonstrates that considering the relative power of the motors is an important factor when studying their fates upon encountering the Tus–*Ter* complex. Finally, this experiment also supports the findings that motors translocating in the 3'–5' direction on the widely exposed C6-containing leading strand at the NP face are effective in releasing Tus, indicating an important contribution from the orientation of DNA pulling in Tus–*Ter* arrest activity.

7.4 Concluding Remarks

In summary, our study offered valuable insights into understanding the fascinating process of polar fork arrest by Tus–*Ter* and contributed significantly in building a continuous timing mechanism that controls and modulates the efficiency of the process[232,264]. The results clearly showed for the first time the operation of the C6-mousetrap model under physiological conditions, nonetheless it suggested the operation of additional mechanism(s) that function autonomously or combined with the mousetrap to impose replication arrest. Our work reproduces the *in vivo* efficiency of Tus-mediated fork arrest for the first time *in vitro* and provides an explanation for the paradox of discrepancy between the *in vivo* and *in vitro* data. Additionally, these studies resolve the controversy between various conflicting studies, where most of the results can now be reconciled with the operation of a dynamic clamp and/or C6-mousetrap mechanism and relative power and orientation of the helicase motor, besides the experimental conditions of the particular assay.

Thus, we refine the mousetrap model and redefine the efficiency of Tus–*Ter* polar arrest to depend on collective contributions of *(i)* intrinsic affinity of Tus for *Ter*, *(ii)* stability of the flipped C6 in its binding pocket, and *(iii)* rate-dependent induction of fork stoppage that fully or temporarily protects Tus–*Ter* central interactions from DnaB.

The consequences of the arrested two replication forks at the terminus region involves a multistep process that implicates repair synthesis of the melted helix, generation of two catenated DNA molecules, decatenation of the two linked DNA molecules by DNA

topoisomerase IV, XerCD mediated recombination, and resolution of DNA oligomers. Nonetheless the molecular details of all these steps remain poorly understood[158,277-282]. Future studies should be devoted to study the final stages of termination of DNA replication that involves unlinking and repairing of the DNA oligomers and chromosomal segregation.

BIBLIOGRAPHY

1 Benkovic, S. J., Valentine, A. M. & Salinas, F. Replisome-mediated DNA replication. *Annu Rev Biochem* **70**, 181-208, doi:10.1146/annurev.biochem.70.1.181 (2001).

2 Davey, M. J. & O'Donnell, M. Mechanisms of DNA replication. *Curr Opin Chem Biol* **4**, 581-586 (2000).

3 Baker, T. A. & Bell, S. P. Polymerases and the replisome: machines within machines. *Cell* **92**, 295-305 (1998).

4 Langston, L. D., Indiani, C. & O'Donnell, M. Whither the replisome: emerging perspectives on the dynamic nature of the DNA replication machinery. *Cell Cycle* **8**, 2686-2691 (2009).

5 Matson, S. W. DNA helicases of Escherichia coli. *Prog Nucleic Acid Res Mol Biol* **40**, 289-326 (1991).

6 Matson, S. W. & Kaiser-Rogers, K. A. DNA helicases. *Annu Rev Biochem* **59**, 289-329, doi:10.1146/annurev.bi.59.070190.001445 (1990).

7 Lohman, T. M. Helicase-catalyzed DNA unwinding. *J Biol Chem* **268**, 2269-2272 (1993).

8 Pomerantz, R. T. & O'Donnell, M. Replisome mechanics: insights into a twin DNA polymerase machine. *Trends Microbiol* **15**, 156-164, doi:10.1016/j.tim.2007.02.007 (2007).

9 Johansson, E. & Dixon, N. Replicative DNA polymerases. *Cold Spring Harb Perspect Biol* **5**, doi:10.1101/cshperspect.a012799 (2013).

10 Alberts, B. M. Prokaryotic DNA replication mechanisms. *Philos Trans R Soc Lond B Biol Sci* **317**, 395-420 (1987).

11 Langston, L. D. & O'Donnell, M. DNA replication: keep moving and don't mind the gap. *Mol Cell* **23**, 155-160, doi:10.1016/j.molcel.2006.05.034 (2006).

12 McHenry, C. S. DNA replicases from a bacterial perspective. *Annu Rev Biochem* **80**, 403-436, doi:10.1146/annurev-biochem-061208-091655 (2011).

13 MacNeill, S. A. DNA replication: partners in the Okazaki two-step. *Curr Biol* **11**, R842-844 (2001).

14 Hamdan, S. M., Loparo, J. J., Takahashi, M., Richardson, C. C. & van Oijen, A. M. Dynamics of DNA replication loops reveal temporal control of lagging-strand synthesis. *Nature* **457**, 336-339, doi:10.1038/nature07512 (2009).

15 Hamdan, S. M. & van Oijen, A. M. Timing, coordination, and rhythm: acrobatics at the DNA replication fork. *J Biol Chem* **285**, 18979-18983, doi:10.1074/jbc.R109.022939 (2010).

16 Kurth, I. & O'Donnell, M. New insights into replisome fluidity during chromosome replication. *Trends Biochem Sci* **38**, 195-203, doi:10.1016/j.tibs.2012.10.003 (2013).

17 Chandler, M., Bird, R. E. & Caro, L. The replication time of the Escherichia coli K12 chromosome as a function of cell doubling time. *J Mol Biol* **94**, 127-132 (1975).

18 Drake, J. W., Allen, E. F., Forsberg, S. A., Preparata, R. M. & Greening, E. O. Genetic control of mutation rates in bacteriophageT4. *Nature* **221**, 1128-1132 (1969).

19 Beattie, T. R. & Reyes-Lamothe, R. A Replisome's journey through the bacterial chromosome. *Front Microbiol* **6**, 562, doi:10.3389/fmicb.2015.00562 (2015).

20 Bussiere, D. E. & Bastia, D. Termination of DNA replication of bacterial and plasmid chromosomes. *Mol Microbiol* **31**, 1611-1618 (1999).

21 Reyes-Lamothe, R., Wang, X. & Sherratt, D. Escherichia coli and its chromosome. *Trends Microbiol* **16**, 238-245, doi:10.1016/j.tim.2008.02.003 (2008).

22 Barre, F. X. *et al.* Circles: the replication-recombination-chromosome segregation connection. *Proc Natl Acad Sci U S A* **98**, 8189-8195, doi:10.1073/pnas.111008998 (2001).

23 Neylon, C., Kralicek, A. V., Hill, T. M. & Dixon, N. E. Replication Termination in Escherichia coli: Structure and Antihelicase Activity of the Tus-Ter Complex. *Microbiology and Molecular Biology Reviews* **69**, 501-526, doi:10.1128/mmbr.69.3.501-526.2005 (2005).

24 Kaplan, D. L. & Bastia, D. Mechanisms of polar arrest of a replication fork. *Mol Microbiol* **72**, 279-285, doi:10.1111/j.1365-2958.2009.06656.x (2009).

25 Davey, M. J., Jeruzalmi, D., Kuriyan, J. & O'Donnell, M. Motors and switches: AAA+ machines within the replisome. *Nat Rev Mol Cell Biol* **3**, 826-835, doi:10.1038/nrm949 (2002).

26 Fang, L., Davey, M. J. & O'Donnell, M. Replisome assembly at oriC, the replication origin of E. coli, reveals an explanation for initiation sites outside an origin. *Mol Cell* **4**, 541-553 (1999).

27 Erzberger, J. P., Pirruccello, M. M. & Berger, J. M. The structure of bacterial DnaA: implications for general mechanisms underlying DNA replication initiation. *EMBO J* **21**, 4763-4773 (2002).

28 Felczak, M. M. & Kaguni, J. M. The box VII motif of Escherichia coli DnaA protein is required for DnaA oligomerization at the E. coli replication origin. *J Biol Chem* **279**, 51156-51162, doi:10.1074/jbc.M409695200 (2004).

29 Seufert, W., Dobrinski, B., Lurz, R. & Messer, W. Functionality of the dnaA protein binding site in DNA replication is orientation-dependent. *J Biol Chem* **263**, 2719-2723 (1988).

30 Seufert, W. & Messer, W. Start sites for bidirectional in vitro DNA replication inside the replication origin, oriC, of Escherichia coli. *EMBO J* **6**, 2469-2472 (1987).

31 Baker, T. A., Funnell, B. E. & Kornberg, A. Helicase action of dnaB protein during replication from the Escherichia coli chromosomal origin in vitro. *J Biol Chem* **262**, 6877-6885 (1987).

32 LeBowitz, J. H. & McMacken, R. The Escherichia coli dnaB replication protein is a DNA helicase. *J Biol Chem* **261**, 4738-4748 (1986).

33 Davey, M. J., Fang, L., McInerney, P., Georgescu, R. E. & O'Donnell, M. The DnaC helicase loader is a dual ATP/ADP switch protein. *EMBO J* **21**, 3148-3159, doi:10.1093/emboj/cdf308 (2002).

34 Costa, A., Hood, I. V. & Berger, J. M. Mechanisms for initiating cellular DNA replication. *Annu Rev Biochem* **82**, 25-54, doi:10.1146/annurev-biochem-052610-094414 (2013).

35 Duderstadt, K. E. & Berger, J. M. AAA+ ATPases in the initiation of DNA replication. *Crit Rev Biochem Mol Biol* **43**, 163-187, doi:10.1080/10409230802058296 (2008).

36 Arias-Palomo, E., O'Shea, V. L., Hood, I. V. & Berger, J. M. The bacterial DnaC helicase loader is a DnaB ring breaker. *Cell* **153**, 438-448, doi:10.1016/j.cell.2013.03.006 (2013).

37 Mott, M. L., Erzberger, J. P., Coons, M. M. & Berger, J. M. Structural synergy and molecular crosstalk between bacterial helicase loaders and replication initiators. *Cell* **135**, 623-634, doi:10.1016/j.cell.2008.09.058 (2008).

38 Duderstadt, K. E. & Berger, J. M. A structural framework for replication origin opening by AAA+ initiation factors. *Curr Opin Struct Biol* **23**, 144-153, doi:10.1016/j.sbi.2012.11.012 (2013).

39 O'Shea, V. L. & Berger, J. M. Loading strategies of ring-shaped nucleic acid translocases and helicases. *Curr Opin Struct Biol* **25**, 16-24, doi:10.1016/j.sbi.2013.11.006 (2014).

40 Cunningham, E. L. & Berger, J. M. Unraveling the early steps of prokaryotic replication. *Curr Opin Struct Biol* **15**, 68-76, doi:10.1016/j.sbi.2005.01.003 (2005).

41 Schaeffer, P. M., Headlam, M. J. & Dixon, N. E. Protein--protein interactions in the eubacterial replisome. *IUBMB Life* **57**, 5-12, doi:10.1080/15216540500058956 (2005).

42 Chodavarapu, S., Jones, A. D., Feig, M. & Kaguni, J. M. DnaC traps DnaB as an open ring and remodels the domain that binds primase. *Nucleic Acids Res*, doi:10.1093/nar/gkv961 (2015).

43 Mitkova, A. V., Khopde, S. M. & Biswas, S. B. Mechanism and stoichiometry of interaction of DnaG primase with DnaB helicase of Escherichia coli in RNA primer synthesis. *J Biol Chem* **278**, 52253-52261, doi:10.1074/jbc.M308956200 (2003).

44 Griep, M. A. Primase structure and function. *Indian J Biochem Biophys* **32**, 171-178 (1995).

45 Corn, J. E. & Berger, J. M. Regulation of bacterial priming and daughter strand synthesis through helicase-primase interactions. *Nucleic Acids Res* **34**, 4082-4088, doi:10.1093/nar/gkl363 (2006).

46 Kuchta, R. D. & Stengel, G. Mechanism and evolution of DNA primases. *Biochim Biophys Acta* **1804**, 1180-1189, doi:10.1016/j.bbapap.2009.06.011 (2010).

47 Tanner, N. A. *et al.* Single-molecule studies of fork dynamics in Escherichia coli DNA replication. *Nat Struct Mol Biol* **15**, 170-176, doi:10.1038/nsmb.1381 (2008).

48 McHenry, C. S. Bacterial replicases and related polymerases. *Curr Opin Chem Biol* **15**, 587-594, doi:10.1016/j.cbpa.2011.07.018 (2011).

49 Johnson, A. & O'Donnell, M. Cellular DNA replicases: components and dynamics at the replication fork. *Annu Rev Biochem* **74**, 283-315, doi:10.1146/annurev.biochem.73.011303.073859 (2005).

50 Kelman, Z. & O'Donnell, M. DNA polymerase III holoenzyme: structure and function of a chromosomal replicating machine. *Annu Rev Biochem* **64**, 171-200, doi:10.1146/annurev.bi.64.070195.001131 (1995).

51 Georgescu, R. E., Kurth, I. & O'Donnell, M. E. Single-molecule studies reveal the function of a third polymerase in the replisome. *Nat Struct Mol Biol* **19**, 113-116, doi:10.1038/nsmb.2179 (2012).

52 McInerney, P., Johnson, A., Katz, F. & O'Donnell, M. Characterization of a triple DNA polymerase replisome. *Mol Cell* **27**, 527-538, doi:10.1016/j.molcel.2007.06.019 (2007).

53 Reyes-Lamothe, R., Sherratt, D. J. & Leake, M. C. Stoichiometry and architecture of active DNA replication machinery in Escherichia coli. *Science* **328**, 498-501, doi:10.1126/science.1185757 (2010).

54 Kim, D. R. & McHenry, C. S. Identification of the beta-binding domain of the alpha subunit of Escherichia coli polymerase III holoenzyme. *J Biol Chem* **271**, 20699-20704 (1996).

55 Jergic, S. *et al.* A direct proofreader-clamp interaction stabilizes the Pol III replicase in the polymerization mode. *EMBO J* **32**, 1322-1333, doi:10.1038/emboj.2012.347 (2013).

56 Fang, J., Engen, J. R. & Beuning, P. J. Escherichia coli processivity clamp beta from DNA polymerase III is dynamic in solution. *Biochemistry* **50**, 5958-5968, doi:10.1021/bi200580b (2011).

57 Heltzel, J. M. *et al.* Sliding clamp-DNA interactions are required for viability and contribute to DNA polymerase management in Escherichia coli. *J Mol Biol* **387**, 74-91, doi:10.1016/j.jmb.2009.01.050 (2009).

58 Wing, R. A., Bailey, S. & Steitz, T. A. Insights into the replisome from the structure of a ternary complex of the DNA polymerase III alpha-subunit. *J Mol Biol* **382**, 859-869, doi:10.1016/j.jmb.2008.07.058 (2008).

59 Georgescu, R. E. *et al.* Structure of a sliding clamp on DNA. *Cell* **132**, 43-54, doi:10.1016/j.cell.2007.11.045 (2008).

60 Bloom, L. B. Dynamics of loading the Escherichia coli DNA polymerase processivity clamp. *Crit Rev Biochem Mol Biol* **41**, 179-208, doi:10.1080/10409230600648751 (2006).

61 Jeruzalmi, D. *et al.* Mechanism of processivity clamp opening by the delta subunit wrench of the clamp loader complex of E. coli DNA polymerase III. *Cell* **106**, 417-428 (2001).

62 Jeruzalmi, D., O'Donnell, M. & Kuriyan, J. Crystal structure of the processivity clamp loader gamma (gamma) complex of E. coli DNA polymerase III. *Cell* **106**, 429-441 (2001).

63 O'Donnell, M., Jeruzalmi, D. & Kuriyan, J. Clamp loader structure predicts the architecture of DNA polymerase III holoenzyme and RFC. *Curr Biol* **11**, R935-946 (2001).

64 Dallmann, H. G., Kim, S., Pritchard, A. E., Marians, K. J. & McHenry, C. S. Characterization of the unique C terminus of the Escherichia coli tau DnaX protein. Monomeric C-tau binds alpha AND DnaB and can partially replace tau in reconstituted replication forks. *J Biol Chem* **275**, 15512-15519, doi:10.1074/jbc.M909257199 (2000).

65 Gao, D. & McHenry, C. S. tau binds and organizes Escherichia coli replication proteins through distinct domains. Domain IV, located within the unique C terminus of tau, binds the replication fork, helicase, DnaB. *J Biol Chem* **276**, 4441-4446, doi:10.1074/jbc.M009830200 (2001).

66 Jeruzalmi, D. The opened processivity clamp slides into view. *Proc Natl Acad Sci U S A* **102**, 14939-14940, doi:10.1073/pnas.0507120102 (2005).

67 El Houry Mignan, S., Witte, G., Naue, N. & Curth, U. Characterization of the chipsi subcomplex of Pseudomonas aeruginosa DNA polymerase III. *BMC Mol Biol* **12**, 43, doi:10.1186/1471-2199-12-43 (2011).

68 Xiao, H., Dong, Z. & O'Donnell, M. DNA polymerase III accessory proteins. IV. Characterization of chi and psi. *J Biol Chem* **268**, 11779-11784 (1993).

69 Kelman, Z., Yuzhakov, A., Andjelkovic, J. & O'Donnell, M. Devoted to the lagging strand-the subunit of DNA polymerase III holoenzyme contacts SSB to promote processive elongation and sliding clamp assembly. *EMBO J* **17**, 2436-2449, doi:10.1093/emboj/17.8.2436 (1998).

70 Yuzhakov, A., Kelman, Z. & O'Donnell, M. Trading places on DNA--a three-point switch underlies primer handoff from primase to the replicative DNA polymerase. *Cell* **96**, 153-163 (1999).

71 Meyer, R. R. & Laine, P. S. The single-stranded DNA-binding protein of Escherichia coli. *Microbiol Rev* **54**, 342-380 (1990).

72 Curth, U., Genschel, J., Urbanke, C. & Greipel, J. In vitro and in vivo function of the C-terminus of Escherichia coli single-stranded DNA binding protein. *Nucleic Acids Res* **24**, 2706-2711 (1996).

73 Kuznetsov, S. V., Kozlov, A. G., Lohman, T. M. & Ansari, A. Microsecond dynamics of protein-DNA interactions: direct observation of the wrapping/unwrapping kinetics of

single-stranded DNA around the E. coli SSB tetramer. *J Mol Biol* **359**, 55-65, doi:10.1016/j.jmb.2006.02.070 (2006).

74 Raghunathan, S., Kozlov, A. G., Lohman, T. M. & Waksman, G. Structure of the DNA binding domain of E. coli SSB bound to ssDNA. *Nat Struct Biol* **7**, 648-652, doi:10.1038/77943 (2000).

75 Antony, E. *et al.* Multiple C-terminal tails within a single E. coli SSB homotetramer coordinate DNA replication and repair. *J Mol Biol* **425**, 4802-4819, doi:10.1016/j.jmb.2013.08.021 (2013).

76 Savvides, S. N. *et al.* The C-terminal domain of full-length E. coli SSB is disordered even when bound to DNA. *Protein Sci* **13**, 1942-1947, doi:10.1110/ps.04661904 (2004).

77 Lohman, T. M. & Ferrari, M. E. Escherichia coli single-stranded DNA-binding protein: multiple DNA-binding modes and cooperativities. *Annu Rev Biochem* **63**, 527-570, doi:10.1146/annurev.bi.63.070194.002523 (1994).

78 Ferrari, M. E., Bujalowski, W. & Lohman, T. M. Co-operative binding of Escherichia coli SSB tetramers to single-stranded DNA in the (SSB)35 binding mode. *J Mol Biol* **236**, 106-123, doi:10.1006/jmbi.1994.1122 (1994).

79 Ferrari, M. E. & Lohman, T. M. Apparent heat capacity change accompanying a nonspecific protein-DNA interaction. Escherichia coli SSB tetramer binding to oligodeoxyadenylates. *Biochemistry* **33**, 12896-12910 (1994).

80 Cadman, C. J. & McGlynn, P. PriA helicase and SSB interact physically and functionally. *Nucleic Acids Res* **32**, 6378-6387, doi:10.1093/nar/gkh980 (2004).

81 Witte, G., Urbanke, C. & Curth, U. DNA polymerase III chi subunit ties single-stranded DNA binding protein to the bacterial replication machinery. *Nucleic Acids Res* **31**, 4434-4440 (2003).

82 Wessel, S. R. *et al.* PriC-mediated DNA replication restart requires PriC complex formation with the single-stranded DNA-binding protein. *J Biol Chem* **288**, 17569-17578, doi:10.1074/jbc.M113.478156 (2013).

83 Rigler, M. N. & Romano, L. J. Differences in the mechanism of stimulation of T7 DNA polymerase by two binding modes of Escherichia coli single-stranded DNA-binding protein. *J Biol Chem* **270**, 8910-8919 (1995).

84 Roy, R., Kozlov, A. G., Lohman, T. M. & Ha, T. SSB protein diffusion on single-stranded DNA stimulates RecA filament formation. *Nature* **461**, 1092-1097, doi:10.1038/nature08442 (2009).

85 Dalgaard, J. Z. *et al.* Random and site-specific replication termination. *Methods Mol Biol* **521**, 35-53, doi:10.1007/978-1-60327-815-7_3 (2009).

86 Bastia, D. & Zaman, S. Mechanism and physiological significance of programmed replication termination. *Semin Cell Dev Biol* **30**, 165-173, doi:10.1016/j.semcdb.2014.04.030 (2014).

87 Helmstetter, C. E. Origin and sequence of chromosome replication in Escherichia coli B-r. *J Bacteriol* **95**, 1634-1641 (1968).

88 Jonasson, J. Evidence for bidirectional chromosome replication in Escherichia coli C based on marker-frequency analysis by DNA-DNA hybridization with P2 and lambda prophages. *Mol Gen Genet* **120**, 68-90 (1973).

89 Crosa, J. H., Luttropp, L. K. & Falkow, S. Mode of replication of the conjugative R-plasmid RSF1040 in Escherichia coli. *J Bacteriol* **126**, 454-466 (1976).

90 Abhyankar, M. M., Reddy, J. M., Sharma, R., Bullesbach, E. & Bastia, D. Biochemical investigations of control of replication initiation of plasmid R6K. *J Biol Chem* **279**, 6711-6719, doi:10.1074/jbc.M312052200 (2004).

91 Abhyankar, M. M., Zzaman, S. & Bastia, D. Reconstitution of R6K DNA replication in vitro using 22 purified proteins. *J Biol Chem* **278**, 45476-45484, doi:10.1074/jbc.M308516200 (2003).

92 Louarn, J., Patte, J. & Louarn, J. M. Evidence for a fixed termination site of chromosome replication in Escherichia coli K12. *J Mol Biol* **115**, 295-314 (1977).

93 Messer, W. The bacterial replication initiator DnaA. DnaA and oriC, the bacterial mode to initiate DNA replication. *FEMS Microbiol Rev* **26**, 355-374 (2002).

94 Kuempel, P. L., Duerr, S. A. & Maglothin, P. D. Chromosome replication in an Escherichia coli dnaA mutant integratively suppressed by prophage P2. *J Bacteriol* **134**, 902-912 (1978).

95 Kuempel, P. L., Duerr, S. A. & Seeley, N. R. Terminus region of the chromosome in Escherichia coli inhibits replication forks. *Proc Natl Acad Sci U S A* **74**, 3927-3931 (1977).

96 Bastia, D., Germino, J., Crosa, J. H. & Ram, J. The nucleotide sequence surrounding the replication terminus of R6K. *Proc Natl Acad Sci U S A* **78**, 2095-2099 (1981).

97 Hill, T. M., Kopp, B. J. & Kuempel, P. L. Termination of DNA replication in Escherichia coli requires a trans-acting factor. *J Bacteriol* **170**, 662-668 (1988).

98 Hill, T. M., Tecklenburg, M. L., Pelletier, A. J. & Kuempel, P. L. tus, the trans-acting gene required for termination of DNA replication in Escherichia coli, encodes a DNA-binding protein. *Proc Natl Acad Sci U S A* **86**, 1593-1597 (1989).

99 Sista, P. R., Mukherjee, S., Patel, P., Khatri, G. S. & Bastia, D. A host-encoded DNA-binding protein promotes termination of plasmid replication at a sequence-specific replication terminus. *Proc Natl Acad Sci U S A* **86**, 3026-3030 (1989).

100 Coskun-Ari, F. F. & Hill, T. M. Sequence-specific Interactions in the Tus-Ter Complex and the Effect of Base Pair Substitutions on Arrest of DNA Replication in Escherichia coli. *Journal of Biological Chemistry* **272**, 26448-26456, doi:10.1074/jbc.272.42.26448 (1997).

101 Neylon, C. *et al.* Interaction of the Escherichia coli replication terminator protein (Tus) with DNA: a model derived from DNA-binding studies of mutant proteins by surface plasmon resonance. *Biochemistry* **39**, 11989-11999 (2000).

102 Mehta, P. P., Bussiere, D. E., Hoffman, D. W., Bastia, D. & White, S. W. Crystallization and preliminary structural analysis of the replication terminator protein of Bacillus subtilis. *J Biol Chem* **267**, 18885-18889 (1992).

103 Hastings, A. F. *et al.* Interaction of the replication terminator protein of Bacillus subtilis with DNA probed by NMR spectroscopy. *Biochem Biophys Res Commun* **335**, 361-366, doi:10.1016/j.bbrc.2005.07.082 (2005).

104 de Massy, B., Bejar, S., Louarn, J., Louarn, J. M. & Bouche, J. P. Inhibition of replication forks exiting the terminus region of the Escherichia coli chromosome occurs at two loci separated by 5 min. *Proc Natl Acad Sci U S A* **84**, 1759-1763 (1987).

105 Pelletier, A. J., Hill, T. M. & Kuempel, P. L. Location of sites that inhibit progression of replication forks in the terminus region of Escherichia coli. *J Bacteriol* **170**, 4293-4298 (1988).

106 Pelletier, A. J., Hill, T. M. & Kuempel, P. L. Termination sites T1 and T2 from the Escherichia coli chromosome inhibit DNA replication in ColE1-derived plasmids. *J Bacteriol* **171**, 1739-1741 (1989).

107 Francois, V., Louarn, J., Patte, J., Rebollo, J. E. & Louarn, J. M. Constraints in chromosomal inversions in Escherichia coli are not explained by replication pausing at inverted terminator-like sequences. *Mol Microbiol* **4**, 537-542 (1990).

108 Iismaa, T. P. & Wake, R. G. The normal replication terminus of the Bacillus subtilis chromosome, terC, is dispensable for vegetative growth and sporulation. *J Mol Biol* **195**, 299-310 (1987).

109 Roecklein, B., Pelletier, A. & Kuempel, P. The tus gene of Escherichia coli: autoregulation, analysis of flanking sequences and identification of a complementary system in Salmonella typhimurium. *Res Microbiol* **142**, 169-175 (1991).

110 Lemon, K. P., Kurtser, I. & Grossman, A. D. Effects of replication termination mutants on chromosome partitioning in Bacillus subtilis. *Proc Natl Acad Sci U S A* **98**, 212-217, doi:10.1073/pnas.011506098 (2001).

111 Markovitz, A. A new in vivo termination function for DNA polymerase I of Escherichia coli K12. *Mol Microbiol* **55**, 1867-1882, doi:10.1111/j.1365-2958.2005.04513.x (2005).

112 Duggin, I. G., Wake, R. G., Bell, S. D. & Hill, T. M. The replication fork trap and termination of chromosome replication. *Mol Microbiol* **70**, 1323-1333, doi:10.1111/j.1365-2958.2008.06500.x (2008).

113 Krabbe, M., Zabielski, J., Bernander, R. & Nordstrom, K. Inactivation of the replication-termination system affects the replication mode and causes unstable maintenance of plasmid R1. *Mol Microbiol* **24**, 723-735 (1997).

114 Wake, R. G. Replication fork arrest and termination of chromosome replication in Bacillus subtilis. *FEMS Microbiol Lett* **153**, 247-254 (1997).

115 Bastia, D., Manna, A. C. & Sahoo, T. Termination of DNA replication in prokaryotic chromosomes. *Genet Eng (N Y)* **19**, 101-119 (1997).

116 Vivian, J. P., Porter, C. J., Wilce, J. A. & Wilce, M. C. An asymmetric structure of the Bacillus subtilis replication terminator protein in complex with DNA. *J Mol Biol* **370**, 481-491, doi:10.1016/j.jmb.2007.02.067 (2007).

117 Wilce, J. A. *et al.* Structure of the RTP-DNA complex and the mechanism of polar replication fork arrest. *Nat Struct Biol* **8**, 206-210, doi:10.1038/84934 (2001).

118 Sahoo, T., Mohanty, B. K., Lobert, M., Manna, A. C. & Bastia, D. The contrahelicase activities of the replication terminator proteins of Escherichia coli and Bacillus subtilis are helicase-specific and impede both helicase translocation and authentic DNA unwinding. *J Biol Chem* **270**, 29138-29144 (1995).

119 Manna, A. C., Pai, K. S., Bussiere, D. E., White, S. W. & Bastia, D. The dimer-dimer interaction surface of the replication terminator protein of Bacillus subtilis and termination of DNA replication. *Proc Natl Acad Sci U S A* **93**, 3253-3258 (1996).

120 Kralicek, A. V., Wilson, P. K., Ralston, G. B., Wake, R. G. & King, G. F. Reorganization of terminator DNA upon binding replication terminator protein: implications for the functional replication fork arrest complex. *Nucleic Acids Res* **25**, 590-596 (1997).

121 Bussiere, D. E., Bastia, D. & White, S. W. Crystal structure of the replication terminator protein from B. subtilis at 2.6 A. *Cell* **80**, 651-660 (1995).

122 Duggin, I. G., Matthews, J. M., Dixon, N. E., Wake, R. G. & Mackay, J. P. A complex mechanism determines polarity of DNA replication fork arrest by the replication terminator complex of Bacillus subtilis. *J Biol Chem* **280**, 13105-13113, doi:10.1074/jbc.M414187200 (2005).

123 Manna, A. C. *et al.* Helicase-contrahelicase interaction and the mechanism of termination of DNA replication. *Cell* **87**, 881-891 (1996).

124 Andersen, P. A., Griffiths, A. A., Duggin, I. G. & Wake, R. G. Functional specificity of the replication fork-arrest complexes of Bacillus subtilis and Escherichia coli: significant specificity for Tus-Ter functioning in E. coli. *Mol Microbiol* **36**, 1327-1335 (2000).

125 Kaul, S. *et al.* The replication terminator protein of the gram-positive bacterium Bacillus subtilis functions as a polar contrahelicase in gram-negative Escherichia coli. *Proc Natl Acad Sci U S A* **91**, 11143-11147 (1994).

126 Duggin, I. G. DNA replication fork arrest by the Bacillus subtilis RTP-DNA complex involves a mechanism that is independent of the affinity of RTP-DNA binding. *J Mol Biol* **361**, 1-6, doi:10.1016/j.jmb.2006.06.013 (2006).

127 Kamada, K., Horiuchi, T., Ohsumi, K., Shimamoto, N. & Morikawa, K. Structure of a replication-terminator protein complexed with DNA. *Nature* **383**, 598-603, doi:10.1038/383598a0 (1996).

128 Duggin, I. G., Wake, R. G., Bell, S. D. & Hill, T. M. The replication fork trap and termination of chromosome replication. *Molecular Microbiology* **70**, 1323-1333, doi:10.1111/j.1365-2958.2008.06500.x (2008).

129 Moreau, M. J. & Schaeffer, P. M. Differential Tus-Ter binding and lock formation: implications for DNA replication termination in Escherichia coli. *Mol Biosyst* **8**, 2783-2791, doi:10.1039/c2mb25281c (2012).

130 Mulcair, M. D. *et al.* A molecular mousetrap determines polarity of termination of DNA replication in E. coli. *Cell* **125**, 1309-1319, doi:10.1016/j.cell.2006.04.040 (2006).

131 Sista, P. R., Hutchinson, C. A., 3rd & Bastia, D. DNA-protein interaction at the replication termini of plasmid R6K. *Genes Dev* **5**, 74-82 (1991).

132 Coskun-Ari, F. F., Skokotas, A., Moe, G. R. & Hill, T. M. Biophysical characteristics of Tus, the replication arrest protein of Escherichia coli. *J Biol Chem* **269**, 4027-4034 (1994).

133 Morin, I., Dixon, N. E. & Schaeffer, P. M. Ultrasensitive detection of antibodies using a new Tus-Ter-lock immunoPCR system. *Mol Biosyst* **6**, 1173-1175, doi:10.1039/c002163f (2010).

134 Morin, I., Askin, S. P. & Schaeffer, P. M. IgG-detection devices for the Tus-Ter-lock immuno-PCR diagnostic platform. *Analyst* **136**, 4815-4821, doi:10.1039/c1an15731k (2011).

135 Mulugu, S. *et al.* Mechanism of termination of DNA replication of Escherichia coli involves helicase-contrahelicase interaction. *Proc Natl Acad Sci U S A* **98**, 9569-9574, doi:10.1073/pnas.171065898 (2001).

136 Lee, E. H., Kornberg, A., Hidaka, M., Kobayashi, T. & Horiuchi, T. Escherichia coli replication termination protein impedes the action of helicases. *Proc Natl Acad Sci U S A* **86**, 9104-9108 (1989).

137 Duggin, I. G. & Bell, S. D. Termination structures in the Escherichia coli chromosome replication fork trap. *J Mol Biol* **387**, 532-539, doi:10.1016/j.jmb.2009.02.027 (2009).

138 Moreau, M. J. & Schaeffer, P. M. Dissecting the salt dependence of the Tus-Ter protein-DNA complexes by high-throughput differential scanning fluorimetry of a GFP-tagged Tus. *Mol Biosyst* **9**, 3146-3154, doi:10.1039/c3mb70426b (2013).

139 Natarajan, S., Kelley, W. L. & Bastia, D. Replication terminator protein of Escherichia coli is a transcriptional repressor of its own synthesis. *Proc Natl Acad Sci U S A* **88**, 3867-3871 (1991).

140 Khatri, G. S., MacAllister, T., Sista, P. R. & Bastia, D. The replication terminator protein of E. coli is a DNA sequence-specific contra-helicase. *Cell* **59**, 667-674 (1989).

141 Lee, E. H. & Kornberg, A. Features of replication fork blockage by the Escherichia coli terminus-binding protein. *J Biol Chem* **267**, 8778-8784 (1992).

142 Bedrosian, C. L. & Bastia, D. Escherichia coli replication terminator protein impedes simian virus 40 (SV40) DNA replication fork movement and SV40 large tumor antigen helicase activity in vitro at a prokaryotic terminus sequence. *Proc Natl Acad Sci U S A* **88**, 2618-2622 (1991).

143 Skokotas, A., Wrobleski, M. & Hill, T. M. Isolation and characterization of mutants of Tus, the replication arrest protein of Escherichia coli. *J Biol Chem* **269**, 20446-20455 (1994).

144 Skokotas, A., Hiasa, H., Marians, K. J., O'Donnell, L. & Hill, T. M. Mutations in the Escherichia coli Tus protein define a domain positioned close to the DNA in the Tus-Ter complex. *J Biol Chem* **270**, 30941-30948 (1995).

145 Bastia, D. *et al.* Replication termination mechanism as revealed by Tus-mediated polar arrest of a sliding helicase. *Proc Natl Acad Sci U S A* **105**, 12831-12836, doi:10.1073/pnas.0805898105 (2008).

146 Kaplan, D. L. The 3'-tail of a forked-duplex sterically determines whether one or two DNA strands pass through the central channel of a replication-fork helicase. *J Mol Biol* **301**, 285-299, doi:10.1006/jmbi.2000.3965 (2000).

147 Aussel, L. *et al.* FtsK Is a DNA motor protein that activates chromosome dimer resolution by switching the catalytic state of the XerC and XerD recombinases. *Cell* **108**, 195-205 (2002).

148 Crozat, E., Rousseau, P., Fournes, F. & Cornet, F. The FtsK family of DNA translocases finds the ends of circles. *J Mol Microbiol Biotechnol* **24**, 396-408, doi:10.1159/000369213 (2014).

149 Grainge, I. Simple topology: FtsK-directed recombination at the dif site. *Biochem Soc Trans* **41**, 595-600, doi:10.1042/BST20120299 (2013).

150 Crozat, E. & Grainge, I. FtsK DNA translocase: the fast motor that knows where it's going. *Chembiochem* **11**, 2232-2243, doi:10.1002/cbic.201000347 (2010).

151 Recchia, G. D., Aroyo, M., Wolf, D., Blakely, G. & Sherratt, D. J. FtsK-dependent and -independent pathways of Xer site-specific recombination. *EMBO J* **18**, 5724-5734, doi:10.1093/emboj/18.20.5724 (1999).

152 Yates, J., Aroyo, M., Sherratt, D. J. & Barre, F. X. Species specificity in the activation of Xer recombination at dif by FtsK. *Mol Microbiol* **49**, 241-249 (2003).

153 Bonne, L., Bigot, S., Chevalier, F., Allemand, J. F. & Barre, F. X. Asymmetric DNA requirements in Xer recombination activation by FtsK. *Nucleic Acids Res* **37**, 2371-2380, doi:10.1093/nar/gkp104 (2009).

154 Hendrickson, H. & Lawrence, J. G. Mutational bias suggests that replication termination occurs near the dif site, not at Ter sites. *Mol Microbiol* **64**, 42-56, doi:10.1111/j.1365-2958.2007.05596.x (2007).

155 Grigoriev, A. Analyzing genomes with cumulative skew diagrams. *Nucleic Acids Res* **26**, 2286-2290 (1998).

156 Arakawa, K. & Tomita, M. The GC skew index: a measure of genomic compositional asymmetry and the degree of replicational selection. *Evol Bioinform Online* **3**, 159-168 (2007).

157 Kono, N., Arakawa, K. & Tomita, M. Validation of bacterial replication termination models using simulation of genomic mutations. *PLoS One* **7**, e34526, doi:10.1371/journal.pone.0034526 (2012).

158 Zechiedrich, E. L. & Cozzarelli, N. R. Roles of topoisomerase IV and DNA gyrase in DNA unlinking during replication in Escherichia coli. *Genes Dev* **9**, 2859-2869 (1995).
159 Levine, C., Hiasa, H. & Marians, K. J. DNA gyrase and topoisomerase IV: biochemical activities, physiological roles during chromosome replication, and drug sensitivities. *Biochim Biophys Acta* **1400**, 29-43 (1998).
160 Wang, X., Reyes-Lamothe, R. & Sherratt, D. J. Modulation of Escherichia coli sister chromosome cohesion by topoisomerase IV. *Genes Dev* **22**, 2426-2433, doi:10.1101/gad.487508 (2008).
161 Espeli, O., Lee, C. & Marians, K. J. A physical and functional interaction between Escherichia coli FtsK and topoisomerase IV. *J Biol Chem* **278**, 44639-44644, doi:10.1074/jbc.M308926200 (2003).
162 Suski, C. & Marians, K. J. Resolution of converging replication forks by RecQ and topoisomerase III. *Mol Cell* **30**, 779-789, doi:10.1016/j.molcel.2008.04.020 (2008).
163 Greenleaf, W. J., Woodside, M. T. & Block, S. M. High-resolution, single-molecule measurements of biomolecular motion. *Annu Rev Biophys Biomol Struct* **36**, 171-190, doi:10.1146/annurev.biophys.36.101106.101451 (2007).
164 Perumal, S. K., Yue, H., Hu, Z., Spiering, M. M. & Benkovic, S. J. Single-molecule studies of DNA replisome function. *Biochim Biophys Acta* **1804**, 1094-1112, doi:10.1016/j.bbapap.2009.07.022 (2010).
165 Perez, C. E. & Gonzalez, R. L., Jr. In vitro and in vivo single-molecule fluorescence imaging of ribosome-catalyzed protein synthesis. *Curr Opin Chem Biol* **15**, 853-863, doi:10.1016/j.cbpa.2011.11.002 (2011).
166 Castoreno, A. B. & Eggert, U. S. Small molecule probes of cellular pathways and networks. *ACS Chem Biol* **6**, 86-94, doi:10.1021/cb1002976 (2011).
167 van Oijen, A. M. & Loparo, J. J. Single-molecule studies of the replisome. *Annu Rev Biophys* **39**, 429-448, doi:10.1146/annurev.biophys.093008.131327 (2010).
168 Geertsema, H. J. & van Oijen, A. M. A single-molecule view of DNA replication: the dynamic nature of multi-protein complexes revealed. *Curr Opin Struct Biol* **23**, 788-793, doi:10.1016/j.sbi.2013.06.018 (2013).
169 van Oijen, A. M. Single-molecule studies of complex systems: the replisome. *Mol Biosyst* **3**, 117-125, doi:10.1039/b612545j (2007).
170 Lu, H. P. Sizing up single-molecule enzymatic conformational dynamics. *Chem Soc Rev* **43**, 1118-1143, doi:10.1039/c3cs60191a (2014).
171 Robison, A. D. & Finkelstein, I. J. High-throughput single-molecule studies of protein-DNA interactions. *FEBS Lett* **588**, 3539-3546, doi:10.1016/j.febslet.2014.05.021 (2014).
172 Juette, M. F. *et al.* The bright future of single-molecule fluorescence imaging. *Curr Opin Chem Biol* **20**, 103-111, doi:10.1016/j.cbpa.2014.05.010 (2014).
173 Chiu, S. W. & Leake, M. C. Functioning nanomachines seen in real-time in living bacteria using single-molecule and super-resolution fluorescence imaging. *Int J Mol Sci* **12**, 2518-2542, doi:10.3390/ijms12042518 (2011).
174 Comstock, M. J. *et al.* Protein structure. Direct observation of structure-function relationship in a nucleic acid-processing enzyme. *Science* **348**, 352-354, doi:10.1126/science.aaa0130 (2015).
175 Smiley, R. D., Zhuang, Z., Benkovic, S. J. & Hammes, G. G. Single-molecule investigation of the T4 bacteriophage DNA polymerase holoenzyme: multiple pathways of holoenzyme formation. *Biochemistry* **45**, 7990-7997, doi:10.1021/bi0603322 (2006).

176 Xi, J. *et al.* Interaction between the T4 helicase loading protein (gp59) and the DNA polymerase (gp43): unlocking of the gp59-gp43-DNA complex to initiate assembly of a fully functional replisome. *Biochemistry* **44**, 7747-7756, doi:10.1021/bi047296w (2005).
177 Dessinges, M. N., Lionnet, T., Xi, X. G., Bensimon, D. & Croquette, V. Single-molecule assay reveals strand switching and enhanced processivity of UvrD. *Proc Natl Acad Sci U S A* **101**, 6439-6444, doi:10.1073/pnas.0306713101 (2004).
178 Manosas, M., Spiering, M. M., Zhuang, Z., Benkovic, S. J. & Croquette, V. Coupling DNA unwinding activity with primer synthesis in the bacteriophage T4 primosome. *Nat Chem Biol* **5**, 904-912, doi:10.1038/nchembio.236 (2009).
179 Manosas, M., Perumal, S. K., Croquette, V. & Benkovic, S. J. Direct observation of stalled fork restart via fork regression in the T4 replication system. *Science* **338**, 1217-1220, doi:10.1126/science.1225437 (2012).
180 Dohoney, K. M. & Gelles, J. Chi-sequence recognition and DNA translocation by single RecBCD helicase/nuclease molecules. *Nature* **409**, 370-374, doi:10.1038/35053124 (2001).
181 Bianco, P. R. *et al.* Processive translocation and DNA unwinding by individual RecBCD enzyme molecules. *Nature* **409**, 374-378, doi:10.1038/35053131 (2001).
182 Lee, J. B. *et al.* DNA primase acts as a molecular brake in DNA replication. *Nature* **439**, 621-624, doi:10.1038/nature04317 (2006).
183 Hamdan, S. M. *et al.* Dynamic DNA helicase-DNA polymerase interactions assure processive replication fork movement. *Mol Cell* **27**, 539-549, doi:10.1016/j.molcel.2007.06.020 (2007).
184 Johnson, D. E., Takahashi, M., Hamdan, S. M., Lee, S. J. & Richardson, C. C. Exchange of DNA polymerases at the replication fork of bacteriophage T7. *Proc Natl Acad Sci U S A* **104**, 5312-5317, doi:10.1073/pnas.0701062104 (2007).
185 Yao, N. Y., Georgescu, R. E., Finkelstein, J. & O'Donnell, M. E. Single-molecule analysis reveals that the lagging strand increases replisome processivity but slows replication fork progression. *Proc Natl Acad Sci U S A* **106**, 13236-13241, doi:10.1073/pnas.0906157106 (2009).
186 Pomerantz, R. T. & O'Donnell, M. What happens when replication and transcription complexes collide? *Cell Cycle* **9**, 2537-2543, doi:10.4161/cc.9.13.12122 (2010).
187 Leman, A. R. & Noguchi, E. The replication fork: understanding the eukaryotic replication machinery and the challenges to genome duplication. *Genes (Basel)* **4**, 1-32, doi:10.3390/genes4010001 (2013).
188 Labib, K. & Hodgson, B. Replication fork barriers: pausing for a break or stalling for time? *EMBO Rep* **8**, 346-353, doi:10.1038/sj.embor.7400940 (2007).
189 Gupta, M. K. *et al.* Protein-DNA complexes are the primary sources of replication fork pausing in Escherichia coli. *Proc Natl Acad Sci U S A* **110**, 7252-7257, doi:10.1073/pnas.1303890110 (2013).
190 Merrikh, H., Zhang, Y., Grossman, A. D. & Wang, J. D. Replication-transcription conflicts in bacteria. *Nat Rev Microbiol* **10**, 449-458, doi:10.1038/nrmicro2800 (2012).
191 Merrikh, H., Machon, C., Grainger, W. H., Grossman, A. D. & Soultanas, P. Co-directional replication-transcription conflicts lead to replication restart. *Nature* **470**, 554-557, doi:10.1038/nature09758 (2011).
192 McGlynn, P., Savery, N. J. & Dillingham, M. S. The conflict between DNA replication and transcription. *Mol Microbiol* **85**, 12-20, doi:10.1111/j.1365-2958.2012.08102.x (2012).

193 Rudolph, C. J., Dhillon, P., Moore, T. & Lloyd, R. G. Avoiding and resolving conflicts between DNA replication and transcription. *DNA Repair (Amst)* **6**, 981-993, doi:10.1016/j.dnarep.2007.02.017 (2007).

194 Bruning, J. G., Howard, J. L. & McGlynn, P. Accessory replicative helicases and the replication of protein-bound DNA. *J Mol Biol* **426**, 3917-3928, doi:10.1016/j.jmb.2014.10.001 (2014).

195 Yeeles, J. T. Discontinuous leading-strand synthesis: a stop-start story. *Biochem Soc Trans* **42**, 25-34, doi:10.1042/BST20130262 (2014).

196 Yeeles, J. T., Poli, J., Marians, K. J. & Pasero, P. Rescuing stalled or damaged replication forks. *Cold Spring Harb Perspect Biol* **5**, a012815, doi:10.1101/cshperspect.a012815 (2013).

197 Marians, K. J. Mechanisms of replication fork restart in Escherichia coli. *Philos Trans R Soc Lond B Biol Sci* **359**, 71-77, doi:10.1098/rstb.2003.1366 (2004).

198 Heller, R. C. & Marians, K. J. Unwinding of the nascent lagging strand by Rep and PriA enables the direct restart of stalled replication forks. *J Biol Chem* **280**, 34143-34151, doi:10.1074/jbc.M507224200 (2005).

199 Heller, R. C. & Marians, K. J. Replisome assembly and the direct restart of stalled replication forks. *Nat Rev Mol Cell Biol* **7**, 932-943, doi:10.1038/nrm2058 (2006).

200 McGlynn, P. Helicases at the replication fork. *Adv Exp Med Biol* **767**, 97-121, doi:10.1007/978-1-4614-5037-5_5 (2013).

201 Lane, H. E. & Denhardt, D. T. The rep mutation. IV. Slower movement of replication forks in Escherichia coli rep strains. *J Mol Biol* **97**, 99-112 (1975).

202 Atkinson, J., Gupta, M. K. & McGlynn, P. Interaction of Rep and DnaB on DNA. *Nucleic Acids Res* **39**, 1351-1359, doi:10.1093/nar/gkq975 (2011).

203 Boubakri, H., de Septenville, A. L., Viguera, E. & Michel, B. The helicases DinG, Rep and UvrD cooperate to promote replication across transcription units in vivo. *EMBO J* **29**, 145-157, doi:10.1038/emboj.2009.308 (2010).

204 Guy, C. P. *et al.* Rep provides a second motor at the replisome to promote duplication of protein-bound DNA. *Mol Cell* **36**, 654-666, doi:10.1016/j.molcel.2009.11.009 (2009).

205 Cheng, W., Hsieh, J., Brendza, K. M. & Lohman, T. M. E. coli Rep oligomers are required to initiate DNA unwinding in vitro. *J Mol Biol* **310**, 327-350, doi:10.1006/jmbi.2001.4758 (2001).

206 Korolev, S., Hsieh, J., Gauss, G. H., Lohman, T. M. & Waksman, G. Major domain swiveling revealed by the crystal structures of complexes of E. coli Rep helicase bound to single-stranded DNA and ADP. *Cell* **90**, 635-647 (1997).

207 Atkinson, J. *et al.* Localization of an accessory helicase at the replisome is critical in sustaining efficient genome duplication. *Nucleic Acids Res* **39**, 949-957, doi:10.1093/nar/gkq889 (2011).

208 Valjavec-Gratian, M., Henderson, T. A. & Hill, T. M. Tus-mediated arrest of DNA replication in Escherichia coli is modulated by DNA supercoiling. *Mol Microbiol* **58**, 758-773, doi:10.1111/j.1365-2958.2005.04860.x (2005).

209 Fuchse, Millette, R. L., Zillig, W. & Walter, G. Influence of salts on RNA synthesis by DNA-dependent RNA-polymerase from Escherichia coli. *Eur J Biochem* **3**, 183-193 (1967).

210 Griep, M. A. & McHenry, C. S. Glutamate overcomes the salt inhibition of DNA polymerase III holoenzyme. *J Biol Chem* **264**, 11294-11301 (1989).

211 Larsen, N. B., Sass, E., Suski, C., Mankouri, H. W. & Hickson, I. D. The Escherichia coli Tus-Ter replication fork barrier causes site-specific DNA replication perturbation in yeast. *Nat Commun* **5**, 3574, doi:10.1038/ncomms4574 (2014).

212 McGeoch, A. T., Trakselis, M. A., Laskey, R. A. & Bell, S. D. Organization of the archaeal MCM complex on DNA and implications for the helicase mechanism. *Nat Struct Mol Biol* **12**, 756-762, doi:10.1038/nsmb974 (2005).

213 Rothenberg, E., Trakselis, M. A., Bell, S. D. & Ha, T. MCM forked substrate specificity involves dynamic interaction with the 5'-tail. *J Biol Chem* **282**, 34229-34234, doi:10.1074/jbc.M706300200 (2007).

214 Amin, A. A. & Hurwitz, J. Polar arrest of the simian virus 40 tumor antigen-mediated replication fork movement in vitro by the tus protein-terB complex of Escherichia coli. *J Biol Chem* **267**, 18612-18622 (1992).

215 Oakley, A. J. *et al.* Flexibility revealed by the 1.85 A crystal structure of the beta sliding-clamp subunit of Escherichia coli DNA polymerase III. *Acta Crystallogr D Biol Crystallogr* **59**, 1192-1199 (2003).

216 Marians, K. J. Phi X174-type primosomal proteins: purification and assay. *Methods Enzymol* **262**, 507-521 (1995).

217 Notarnicola, S. M., Mulcahy, H. L., Lee, J. & Richardson, C. C. The acidic carboxyl terminus of the bacteriophage T7 gene 4 helicase/primase interacts with T7 DNA polymerase. *J Biol Chem* **272**, 18425-18433 (1997).

218 Patel, S. S., Rosenberg, A. H., Studier, F. W. & Johnson, K. A. Large scale purification and biochemical characterization of T7 primase/helicase proteins. Evidence for homodimer and heterodimer formation. *J Biol Chem* **267**, 15013-15021 (1992).

219 Patel, S. S., Wong, I. & Johnson, K. A. Pre-steady-state kinetic analysis of processive DNA replication including complete characterization of an exonuclease-deficient mutant. *Biochemistry* **30**, 511-525 (1991).

220 Tabor, S., Huber, H. E. & Richardson, C. C. Escherichia coli thioredoxin confers processivity on the DNA polymerase activity of the gene 5 protein of bacteriophage T7. *J Biol Chem* **262**, 16212-16223 (1987).

221 Henderson, T. A., Nilles, A. F., Valjavec-Gratian, M. & Hill, T. M. Site-directed mutagenesis and phylogenetic comparisons of the Escherichia coli Tus protein: DNA-protein interactions alone can not account for Tus activity. *Mol Genet Genomics* **265**, 941-953 (2001).

222 Kulczyk, A. W., Tanner, N. A., Loparo, J. J., Richardson, C. C. & van Oijen, A. M. Direct observation of enzymes replicating DNA using a single-molecule DNA stretching assay. *J Vis Exp*, doi:10.3791/1689 (2010).

223 Tanner, N. A. & van Oijen, A. M. Visualizing DNA replication at the single-molecule level. *Methods Enzymol* **475**, 259-278, doi:10.1016/S0076-6879(10)75011-4 (2010).

224 Tanner, N. A. & van Oijen, A. M. Single-molecule observation of prokaryotic DNA replication. *Methods Mol Biol* **521**, 397-410, doi:10.1007/978-1-60327-815-7_22 (2009).

225 Bustamante, C., Marko, J. F., Siggia, E. D. & Smith, S. Entropic elasticity of lambda-phage DNA. *Science* **265**, 1599-1600 (1994).

226 van Oijen, A. M. *et al.* Single-molecule kinetics of lambda exonuclease reveal base dependence and dynamic disorder. *Science* **301**, 1235-1238, doi:10.1126/science.1084387 (2003).

227 Tanner, N. A. *et al.* Real-time single-molecule observation of rolling-circle DNA replication. *Nucleic Acids Res* **37**, e27, doi:10.1093/nar/gkp006 (2009).

228 Tanner, N. A., Loparo, J. J. & van Oijen, A. M. Visualizing Single-molecule DNA Replication with Fluorescence Microscopy. *J Vis Exp*, doi:10.3791/1529 (2009).
229 Sobhy, M. A. *et al.* Versatile single-molecule multi-color excitation and detection fluorescence setup for studying biomolecular dynamics. *Rev Sci Instrum* **82**, 113702, doi:10.1063/1.3657153 (2011).
230 Hill, T. M., Henson, J. M. & Kuempel, P. L. The terminus region of the Escherichia coli chromosome contains two separate loci that exhibit polar inhibition of replication. *Proc Natl Acad Sci U S A* **84**, 1754-1758 (1987).
231 Pham, T. M. *et al.* A single-molecule approach to DNA replication in Escherichia coli cells demonstrated that DNA polymerase III is a major determinant of fork speed. *Mol Microbiol* **90**, 584-596, doi:10.1111/mmi.12386 (2013).
232 Pandey, M. *et al.* Two mechanisms coordinate replication termination by the Escherichia coli Tus-Ter complex. *Nucleic Acids Res* **43**, 5924-5935, doi:10.1093/nar/gkv527 (2015).
233 Kim, S., Dallmann, H. G., McHenry, C. S. & Marians, K. J. Coupling of a replicative polymerase and helicase: a tau-DnaB interaction mediates rapid replication fork movement. *Cell* **84**, 643-650 (1996).
234 Ribeck, N., Kaplan, D. L., Bruck, I. & Saleh, O. A. DnaB helicase activity is modulated by DNA geometry and force. *Biophys J* **99**, 2170-2179, doi:10.1016/j.bpj.2010.07.039 (2010).
235 Finkelstein, I. J. & Greene, E. C. Molecular traffic jams on DNA. *Annu Rev Biophys* **42**, 241-263, doi:10.1146/annurev-biophys-083012-130304 (2013).
236 McPhillips, T. M. *et al.* Blu-Ice and the Distributed Control System: software for data acquisition and instrument control at macromolecular crystallography beamlines. *J Synchrotron Radiat* **9**, 401-406 (2002).
237 Otwinowski, Z. & Minor, W. Processing of X-ray diffraction data collected in oscillation mode. *Macromolecular Crystallography, Pt A* **276**, 307-326, doi:10.1016/s0076-6879(97)76066-x (1997).
238 Vagin, A. & Teplyakov, A. MOLREP: an Automated Program for Molecular Replacement. *Journal of Applied Crystallography* **30**, 1022-1025, doi:doi:10.1107/S0021889897006766 (1997).
239 Murshudov, G. N., Vagin, A. A. & Dodson, E. J. Refinement of macromolecular structures by the maximum-likelihood method. *Acta Crystallogr D Biol Crystallogr* **53**, 240-255, doi:10.1107/S0907444996012255 (1997).
240 Winn, M. D., Isupov, M. N. & Murshudov, G. N. Use of TLS parameters to model anisotropic displacements in macromolecular refinement. *Acta Crystallogr D Biol Crystallogr* **57**, 122-133 (2001).
241 Emsley, P., Lohkamp, B., Scott, W. G. & Cowtan, K. Features and development of Coot. *Acta Crystallogr D Biol Crystallogr* **66**, 486-501, doi:10.1107/S0907444910007493 (2010).
242 Hiasa, H. & Marians, K. J. Tus prevents overreplication of oriC plasmid DNA. *J Biol Chem* **269**, 26959-26968 (1994).
243 Neylon, C., Kralicek, A. V., Hill, T. M. & Dixon, N. E. Replication termination in Escherichia coli: structure and antihelicase activity of the Tus-Ter complex. *Microbiol Mol Biol Rev* **69**, 501-526, doi:10.1128/MMBR.69.3.501-526.2005 (2005).
244 Gottlieb, P. A. *et al.* Equilibrium, kinetic, and footprinting studies of the Tus-Ter protein-DNA interaction. *J Biol Chem* **267**, 7434-7443 (1992).

245 Moreau, M. J., Morin, I. & Schaeffer, P. M. Quantitative determination of protein stability and ligand binding using a green fluorescent protein reporter system. *Mol Biosyst* **6**, 1285-1292, doi:10.1039/c002001j (2010).

246 Bastia, D. *et al.* Replication termination mechanism as revealed by Tus-mediated polar arrest of a sliding helicase. *Proceedings of the National Academy of Sciences* **105**, 12831-12836, doi:10.1073/pnas.0805898105 (2008).

247 Khatri, G. S., Macallister, T., Sista, P. R. & Bastia, D. THE REPLICATION TERMINATOR PROTEIN OF ESCHERICHIA-COLI IS A DNA SEQUENCE-SPECIFIC CONTRA-HELICASE. *Cell* **59**, 667-674, doi:10.1016/0092-8674(89)90012-3 (1989).

248 Pandey, M. & Patel, S. S. Helicase and polymerase move together close to the fork junction and copy DNA in one-nucleotide steps. *Cell Rep* **6**, 1129-1138, doi:10.1016/j.celrep.2014.02.025 (2014).

249 Pandey, M. *et al.* Coordinating DNA replication by means of priming loop and differential synthesis rate. *Nature* **462**, 940-943, doi:10.1038/nature08611 (2009).

250 Patel, S. S. & Donmez, I. Mechanisms of helicases. *J Biol Chem* **281**, 18265-18268, doi:10.1074/jbc.R600008200 (2006).

251 Patel, S. S., Pandey, M. & Nandakumar, D. Dynamic coupling between the motors of DNA replication: hexameric helicase, DNA polymerase, and primase. *Current Opinion in Chemical Biology* **15**, 595-605, doi:http://dx.doi.org/10.1016/j.cbpa.2011.08.003 (2011).

252 Syed, S., Pandey, M., Patel, S. S. & Ha, T. Single-molecule fluorescence reveals the unwinding stepping mechanism of replicative helicase. *Cell Rep* **6**, 1037-1045, doi:10.1016/j.celrep.2014.02.022 (2014).

253 Donmez, I. & Patel, S. S. Coupling of DNA unwinding to nucleotide hydrolysis in a ring-shaped helicase. *EMBO J* **27**, 1718-1726, doi:10.1038/emboj.2008.100 (2008).

254 Hacker, K. J. & Johnson, K. A. A hexameric helicase encircles one DNA strand and excludes the other during DNA unwinding. *Biochemistry* **36**, 14080-14087, doi:10.1021/bi971644v (1997).

255 Stano, N. M. *et al.* DNA synthesis provides the driving force to accelerate DNA unwinding by a helicase. *Nature* **435**, 370-373, doi:10.1038/nature03615 (2005).

256 Pandey, M., Levin, M. K. & Patel, S. S. Experimental and computational analysis of DNA unwinding and polymerization kinetics. *Methods Mol Biol* **587**, 57-83, doi:10.1007/978-1-60327-355-8_5 (2010).

257 Coskun-Ari, F. F. & Hill, T. M. Sequence-specific interactions in the Tus-Ter complex and the effect of base pair substitutions on arrest of DNA replication in Escherichia coli. *J Biol Chem* **272**, 26448-26456 (1997).

258 Donmez, I., Rajagopal, V., Jeong, Y. J. & Patel, S. S. Nucleic acid unwinding by hepatitis C virus and bacteriophage t7 helicases is sensitive to base pair stability. *J Biol Chem* **282**, 21116-21123, doi:10.1074/jbc.M702136200 (2007).

259 Doublie, S., Tabor, S., Long, A. M., Richardson, C. C. & Ellenberger, T. Crystal structure of a bacteriophage T7 DNA replication complex at 2.2 angstrom resolution. *Nature* **391**, 251-258 (1998).

260 Hill, T. M. & Marians, K. J. Escherichia coli Tus protein acts to arrest the progression of DNA replication forks in vitro. *Proc Natl Acad Sci U S A* **87**, 2481-2485 (1990).

261 Mohanty, B. K., Sahoo, T. & Bastia, D. Mechanistic studies on the impact of transcription on sequence-specific termination of DNA replication and vice versa. *J Biol Chem* **273**, 3051-3059 (1998).

262 Cavaluzzi, M. J. & Borer, P. N. Revised UV extinction coefficients for nucleoside-5'-monophosphates and unpaired DNA and RNA. *Nucleic Acids Res* **32**, e13, doi:10.1093/nar/gnh015 (2004).

263 Kallansrud, G. & Ward, B. A comparison of measured and calculated single- and double-stranded oligodeoxynucleotide extinction coefficients. *Anal Biochem* **236**, 134-138, doi:10.1006/abio.1996.0141 (1996).

264 Elshenawy, M. M. *et al.* Replisome speed determines the efficiency of the Tus-Ter replication termination barrier. *Nature*, doi:10.1038/nature14866 (2015).

265 Kaplan, D. L. & O'Donnell, M. Twin DNA pumps of a hexameric helicase provide power to simultaneously melt two duplexes. *Mol Cell* **15**, 453-465, doi:10.1016/j.molcel.2004.06.039 (2004).

266 Fu, Y. V. *et al.* Selective bypass of a lagging strand roadblock by the eukaryotic replicative DNA helicase. *Cell* **146**, 931-941, doi:10.1016/j.cell.2011.07.045 (2011).

267 Berghuis, B. A. *et al.* Strand separation establishes a sustained lock at the Tus-Ter replication fork barrier. *Nat Chem Biol* **11**, 579-585, doi:10.1038/nchembio.1857 (2015).

268 Hamdan, S. M. & Richardson, C. C. Motors, switches, and contacts in the replisome. *Annu Rev Biochem* **78**, 205-243, doi:10.1146/annurev.biochem.78.072407.103248 (2009).

269 McGlynn, P. Helicases that underpin replication of protein-bound DNA in Escherichia coli. *Biochem Soc Trans* **39**, 606-610, doi:10.1042/BST0390606 (2011).

270 Finkelstein, I. J., Visnapuu, M. L. & Greene, E. C. Single-molecule imaging reveals mechanisms of protein disruption by a DNA translocase. *Nature* **468**, 983-987, doi:10.1038/nature09561 (2010).

271 Hamdan, S. M. *et al.* A unique loop in T7 DNA polymerase mediates the binding of helicase-primase, DNA binding protein, and processivity factor. *Proc Natl Acad Sci U S A* **102**, 5096-5101, doi:10.1073/pnas.0501637102 (2005).

272 Nandakumar, D., Pandey, M. & Patel, S. S. Cooperative base pair melting by helicase and polymerase positioned one nucleotide from each other. *Elife* **4**, doi:10.7554/eLife.06562 (2015).

273 Mohanty, B. K., Sahoo, T. & Bastia, D. The relationship between sequence-specific termination of DNA replication and transcription. *EMBO J* **15**, 2530-2539 (1996).

274 Hiasa, H. & Marians, K. J. Differential inhibition of the DNA translocation and DNA unwinding activities of DNA helicases by the Escherichia coli Tus protein. *J Biol Chem* **267**, 11379-11385 (1992).

275 Bailey, S., Eliason, W. K. & Steitz, T. A. Structure of hexameric DnaB helicase and its complex with a domain of DnaG primase. *Science* **318**, 459-463, doi:10.1126/science.1147353 (2007).

276 Strycharska, M. S. *et al.* Nucleotide and partner-protein control of bacterial replicative helicase structure and function. *Mol Cell* **52**, 844-854, doi:10.1016/j.molcel.2013.11.016 (2013).

277 Blakely, G., Colloms, S., May, G., Burke, M. & Sherratt, D. Escherichia coli XerC recombinase is required for chromosomal segregation at cell division. *New Biol* **3**, 789-798 (1991).

278 Deibler, R. W., Rahmati, S. & Zechiedrich, E. L. Topoisomerase IV, alone, unknots DNA in E. coli. *Genes Dev* **15**, 748-761, doi:10.1101/gad.872301 (2001).

279 Hiraga, S. Chromosome partition in Escherichia coli. *Curr Opin Genet Dev* **3**, 789-801 (1993).

280 Kuempel, P. L., Henson, J. M., Dircks, L., Tecklenburg, M. & Lim, D. F. dif, a recA-independent recombination site in the terminus region of the chromosome of Escherichia coli. *New Biol* **3**, 799-811 (1991).

281 Nielsen, H. J., Youngren, B., Hansen, F. G. & Austin, S. Dynamics of Escherichia coli chromosome segregation during multifork replication. *J Bacteriol* **189**, 8660-8666, doi:10.1128/JB.01212-07 (2007).

282 Youngren, B., Nielsen, H. J., Jun, S. & Austin, S. The multifork Escherichia coli chromosome is a self-duplicating and self-segregating thermodynamic ring polymer. *Genes Dev* **28**, 71-84, doi:10.1101/gad.231050.113 (2014).

Statement of authors' contributions

Professor Nicholas Dixon's and Prof Aaron Oakley's labs (University of Wollongong):

Dr. Slobodan Jergic: purified the *E. coli* replication proteins, purified Tus protein and conducted the SPR binding studies. Figures contributed by Dr. Jergic: Chapter 3 (Figure 3.10); Chapter 5 (Table 5.1)

Dr. Zhi-Qiang Xu: purified mutant derivatives of Tus protein, crystallized Tus–*Ter* complexes, collected X-ray data and refined crystal structures. Figures contributed by Dr. Xu: Chapter 3 (Figures 3.6D, 3.7 and Table 3.2).

Dr. Simon Brown: conducted the *in vivo* fork arrest activity by *E. coli* growth assays. Figures contributed by Dr. Brwon: Chapters 5 (Figure 5.4)

Professor Smita Patel's lab (Rutgers University):

Dr. Manjula Pandey: Conducted rapid reaction-quenched DNA-synthesis flow assay. Figures contributed by Dr. Pandey: Chapter 4 (Figures 4.4, 4.5, 4.6, 4.7. 4.8, 4.9, 4.10, 4.11, 4.12A,B, 4.13, 4.14, 4.15, 4.16, 4.17).

Accomplishments

List of publications:

- Mohamed M. Elshenawy, Slobodan Jergic, Zhi-Qiang Xu, Mohamed A. Sobhy, Masateru Takahashi, Aaron J. Oakley, Nicholas E. Dixon, and Samir M. Hamdan. "Replisome speed determines the efficiency of the Tus−*Ter* replication termination barrier"*: Nature* (June 2015), doi: 10.1038/nature14866.

- Pandey M, Elshenawy MM, Jergic S, Takahashi M, Dixon NE, Hamdan SM, and Patel SS. *"Two mechanisms coordinate replication termination by the Escherichia coli Tus-Ter complex": Nucleic Acids Research* (May 2015), doi: 10.1093/nar/gkv527.

- S. Jergic, N.P. Horan, M.M. Elshenawy, C.E. Mason, T. Urathamakul, K. Ozawa, A. Robinson, J.M. Goudsmits, Y. Wang, X. Pan, J.L. Beck, A.M. van Oijen, T. Huber, S.M. Hamdan, and N.E. Dixon. *"A direct proofreader-clamp interaction stabilizes the Pol III replicase in the polymerization mode": EMBO Journal* (May 2013), doi: 10.1038/emboj.2012.347.

- M. A. Sobhy, M. M. Elshenawy, M. Takahashi, B. H. Whitman, N. G. Walter, and S. M. Hamdan. *"Versatile single-molecule multi-color excitation and detection fluorescence setup for studying biomolecular dynamics": Review of Scientific instruments* (November 2011), doi:10.1063/1.3657153.

List of presentations in international conferences:

- "Towards studying Termination of DNA replication at the single molecule level": 2011 Keystone symposium on DNA replication and recombination from February 27th to 4th March 2011: Keystone, Colorado, USA, (poster presentation).
- "How a nimble mouse avoid replication termination trap":2012 Tubingen conference on Single-molecule imaging and related spectroscopies from August 27th to 30th 2012: Tubingen, Germany, (poster presentation).
- "How a nimble mouse avoid replication termination trap": The 38th Lorne conference on protein structure and function from February 5th to 9th 2013: Lorne, Victoria, Australia, (poster presentation).
- "Heterogeneity of rate of *E.coli* replisome determines the efficiency of replication termination": 2013 Keystone symposium on DNA replication and recombination from March 3rd to 8th 2013: Banff, Alberta, Canada, (poster presentation).
- "Heterogeneity of rate of *E.coli* replisome determines the efficiency of replication termination": 2014 Fusion conference on dynamic structures in DNA damage responses and cancer from February 12th to 15th 2014: Cancun, Mexico, (poster presentation).
- "Replisome speed influences termination of DNA replication by Tus-*Ter* complex": 2014 FASEB conference on machines on genes: Nucleic Acid enzymes from June 22th to 27th 2014: Snowmass, Colorado, USA, (poster presentation).

- "Replisome speed influences termination of DNA replication by Tus-*Ter* complex": 2015 Keystone symposium on DNA replication and recombination from March 1st to 6th 2013: Whistler, British Columbia, Canada, (poster presentation).

- "How fast *E.coli* replisomes avoid the termination trap": 2015 FASEB conference on genetic recombination and genome rearrangements from July 19th to 24th 2015: Steamboat Springs, Colorado, USA, (poster presentation).

- "How fast *E.coli* replisomes avoid the termination trap": EMBO conference on DNA replication, chromosome segregation and cell division from July 27th to 31st 2015: Egham, UK, (Oral presentation).